Cape Peninsula
University of Technology

MULTILEVEL INVERTERS USING FINITE SET- MODEL PREDICTIVE CURRENT CONTROL FOR RENEWABLE ENERGY SYSTEMS APPLICATIONS

by

ALI MUSTAFA ALI ALMAKTOOF

Thesis submitted in fulfilment of the requirements for the degree

Doctor of Technology: Electrical Engineering

in the Faculty of Engineering

at the Cape Peninsula University of Technology

Supervisor: Prof. MTE Kahn

Co-supervisor: Dr. AK Raji

Bellville
March 2015

DECLARATION

I, Ali Mustafa Ali Almaktoof, declare that the contents of this thesis represent my own unaided work, and that the thesis has not previously been submitted for academic examination towards any qualification. Furthermore, it represents my own opinions and not necessarily those of the Cape Peninsula University of Technology.

Signed

Date

ABSTRACT

This research focuses on the predictive current control of multilevel converters with the aim of providing an optimized system for three-phase, multilevel inverters (MLIs) so that the load current and the voltage of the capacitors can be controlled. A model predictive current control algorithm is proposed, specifically directed at the utilisation of power obtained from renewable energy systems (RESs). The model was developed for three-phase, multilevel voltage source inverters (MLVSIs), three-phase, three-level diode-clamped converters (DCCs) and flying capacitor converters (FCCs). In this study the renewable energy systems model is used to investigate system performance when power is supplied to a resistive-inductive load (RL-load).

The proposed control method was split into two different control algorithms. Firstly, a finite set-model predictive current control (FS-MPCC) method was developed to control the output current of three-phase, MLIs. This control method was selected to reduce the calculation effort for model predictive control (MPC) and to increase the possible prediction horizon. Secondly, to solve the flying capacitor voltage balance problem in an FCC, as well as to solve the DC-link capacitor voltage balance problem in a DCC, a hysteresis-voltage balancing algorithm based on predictive control, was designed—this algorithm was used to keep the flying capacitor voltages and DC-link capacitor voltages within their hysteresis bands.

Finally, for some classes of power converters, a performance evaluation of the FS-MPCC method for three-phase, three-level MLIs was investigated in terms of power quality and dynamic response. The improvement was assessed in terms of total harmonic distortion (THD) of the output voltage for the RL-load. The modelling and co-simulation were carried out using MATLAB/Simulink with PSIM software. The co-simulation results indicated that the proposed control algorithms achieved both high performance and a high degree of robustness in RESs applications.

ACKNOWLEDGEMENTS

First and foremost, all praise be to ALLAH who has guided me to be who I am, and all thanks to HIM for his guidance and mercy that he bestowed on me, giving me the strength to complete this study successfully.

My sincere gratitude and appreciation to my supervisor, Professor MTE Kahn, for his invaluable guidance, enthusiastic help, and consistent encouragement throughout the entire research project. I am also thankful to Dr Atanda Raji, the co-supervisor, for his fruitful discussions, encouragement, support and time spent to make this study successful.

Also, I thank Libyan Embassy and Azawia University for their support.

I am grateful to Dr. M Adonis for his help and encouragement throughout this journey. Thanks to all my friends and colleagues in the Department of Electrical Electronic and Computer Engineering, especially the Centre for Distributed Power and Electronic Systems (CDPES) for their academic exchange, support and encouragement during my study.

Special thanks to Mr Kalim-u-llah Mohamed and Mr. Christopher Wills, for their technical support. I appreciate the support provided by Mrs Julie Medhurst and Mrs Cindy Engel. I acknowledge Mr. Niels Wieffering; his intensive editing work is highly appreciated. And also, I thank our family friend, Ms. Helen Lambrechts for her support during our stay in South Africa.

I cannot forget to mention my Masters' programme supervisor Prof Mohamed Ali Ekhlat for establishing me well in the research arena and his continuous moral and technical supports.

For all the unconditional love and support and patience, for all the encouragement and sacrifices, I thank my parents Mustafa and Khadija, my wife Faten, my brothers and sisters and my in-laws Elhadi and Fathia; may ALLAH bless them and reward them abundantly in this life and in the hereafter.

Ali
March 2015

DEDICATION

This thesis is dedicted to my parents, my wife and my three angels Khadija, Aisha and Fatima—may they see in this work the fruit of their love and support.

TABLE OF CONTENTS

APPENDICES

LIST OF FIGURES

LIST OF TABLES

ABBREVIATIONS & ACRONYMS

a, b, c	phase sequence (coordinates)
AC	alternating current
AFE	active-front-end
ARCP	auxiliary resonant commutated pole
C	capacitance
CHBC	cascaded H-bridge converter
CHBMLI	cascaded H-bridge multilevel inverter
CM	common-mode
DC	direct current
D_c	clamping diode
DCC	diode-clamped converter
DCMLI	diode-clamped multilevel inverter
DG	distributed generation
DTC	direct torque control
EMC	electromagnetic compatibility
EMI	electromagnetic interference
FACTS	flexible AC transmission system
FC	fuel cell
FCC	flying capacitor converter
FCMLI	flying capacitor multilevel inverter
FS-MPCC	finite set-model predictive current control
g	cost function
GTO	gate turn-off thyristor
i	measured current
i_L	load current

$i(k)$	measured current at time (k)
i_{max}	maximum allowed current
i_{ref}	reference current
$i_x(k)$	phase current at time (k)
$i^*_{\alpha,\beta,x,y}$	reference currents of a multi-phase VSI
$i^p_{\alpha,\beta,x,y}$	predicted currents of a multi-phase VSI
$i^*_{\alpha,\beta}$	reference currents of $\alpha\beta$ fram
$i^p_{\alpha,\beta}$	predicted currents of $\alpha\beta$ fram
i^*_α	real part of the reference current vector
i^p_α	real part of the predicted load current vector
i^*_β	imaginary part of the reference current vector
i^p_β	imaginary part of the predicted load current vector
IGBT	insulated-gate bipolar transistors
L1-norm	simple cost function
L_f	AC filter
L-RPC	long-range predictive control
MC	matrix converters
MIMO	multiple-input-multiple-output
$m(k)$	modulation index
MLC	multilevel converter
MLI	multilevel inverter
MLVSI	multilevel voltage source inverter
MPC	model predictive control
NPC	neutral-point-clamped
n	neutral/middle point
PID	proportional-integral-derivative
PV	photovoltaic

PWM	pulse width modulation
P^*	reference active power
P^p	predicted active power
Q^p	predicted reactive power
r	trajectory
RES	renewable energy system
RL-load	resistive-inductive load
S	switching state
SISO	single-input-single-output
SSI	software simulation integration
t	time
THD	total harmonic distortion
$\mathrm{T_S}$	sampling period
TWh	terawatt-hours
T_e^*	reference torque
T_e^p	predicted torque
U	number of possible switching states
UPS	uninterruptible power supply
$\mathrm{V_0}$	zero-voltage vector
v_{an}	leg voltage
v_c	capacitor voltage
v_{DC}	DC voltage
$v(k)$	inverter voltage at time (k)
V_m	peak value of the voltage
n_{sw}^p	number of commutations to reach the next state
$v_{c\alpha,\beta}^*$	reference output capacitor voltages
$v_{c\alpha,\beta}^p$	predicted output capacitor voltages

υ_{on}	star point voltage
υ_{ref}	reference voltage
υ_{xn}	output voltage
υ_{xo}	yield phase voltage
VSI	voltage source inverter
$\bar{\upsilon}_s$	space vector
WT	wind turbine
X(k)	measured variables at time k
X(k+1)	predicted values at time $(k+1)$
X_{ref}	reference value
x	number of possible states of each leg or phase
y	number of phases or legs
ZVT	zero-voltage transition
$d\upsilon/dt$	voltage stresses
$\alpha\beta$	stationary reference frames
λ	weighting factor
ΔV	maximum flying capacitor voltage ripple
$\left\|\Delta V_c^p\right\|$	absolute error of predicted capacitor voltage
$\|\psi_s\|^*$	reference stator flux
$\|\psi_s\|^p$	predicted stator flux

CHAPTER ONE

INTRODUCTION

1.1 Introduction

In recent years the use of renewable energy systems (RESs) has become very important due to environmental concerns and the increased demand for energy. Using RESs can substantially reduce harmful emissions from polluting the environment while also offering inexhaustible resources of primary energy. Renewable energy resources like solar, wind and tidal energy can be used with maximum efficiency by utilizing appropriate power converters. As the availability of these energy resources is greatly uncertain, the power conversion system must rely on a suitable power converter and controller unit such that they deliver a constant output voltage having constant frequency (Bueno et al. 2008; Tolbert & Peng 2000). The urge to increase the energy efficiency of all energy related systems in combination with the need to support emerging technologies like sustainable energy sources, promotes the development of highly efficient, high-power converters. To achieve these goals, new topologies for power electronic converters have been developed (Busquets-Monge et al. 2008; Tolbert & Peng 2000). The purpose of multilevel topology development is to increase the power rating of converters in an efficient way. The three most promising multilevel topologies are diode-clamped multilevel inverters (DCMLIs), flying capacitor multilevel inverters (FCMLIs) and cascaded H-bridge multilevel inverters (CHBMLIs).

Multilevel converters (MLCs) have been extensively studied over the last few decades in most industrial sectors for many applications. Considering that demands for energy continue are set to increase, power quality and efficiency are necessary; this is why in RESs applications today the control and power conversion processes using power electronics, have become important topics (Bueno et al. 2008; Carrasco et al. 2006; Tolbert & Peng 2000). Research of modern voltage source MLCs began in 1981 with the introduction of the three-level diode-clamped converter (DCC)—also known as the neutral-point-clamped converter (Nabae et al. 1981). The flying capacitor converter (FCC) was first presented by Meynard and Foch in the 1990s as an alternative to the DCC (Meynard & Foch 1992). Recently the DCC and FCC topologies have attracted a lot of interest in the literature (Cortés et al. 2008; Defay et al. 2010; Huang & Corzine 2006; Ruderman & Reznikov 2009; Vargas et al. 2007). These topologies and their derivations are the focus of several studies (Huang & Corzine 2006:144; Ruderman & Reznikov 2009:87; Stolze et al. 2011), most of them related to capacitor voltage control.

Predictive control for power electronics has been researched since the early 1980s (Kennel & Schroeder 1983). Predictive control requires a high number of calculations as compared to classic control methods, but the fast microprocessors available today have made it possible to viably implement predictive control coupled with multilevel

voltage source inverters (MLVSIs). Furthermore, model predictive control (MPC) has distinct advantages when compared to the traditional pulse width modulation (PWM) methods (Rodríguez & Cortés 2012:59).

Predictive control strategies have been applied to power converters in general and to MLCs in particular. Some research has been presented on the use of an MPC scheme for current control for a three-phase inverter (Abu-Rub et al. 2004) and in a study by Rodríguez et al. (2004) a control algorithm for matrix converters was presented. Furthermore, a study by Muller et al. (2005) presented a study on torque control for an induction machine.

Since power converters have a finite number of switching states, the MPC optimization problem can be simplified by limiting the prediction of the system behaviour to only those switching states that are permissible. Following this simplification process, each prediction is used to evaluate a cost function (also known as a quality or decision function), and the state with the minimum cost is then selected and generated. This control method is known as a finite set-model predictive current control (FS-MPCC) since the possible control actions (switching states) are finite. FS-MPCC has been successfully applied to a wide range of power converter and drive applications (Rodríguez & Cortés 2012; Vargas et al. 2007), and it is the control method used in this study.

Another subject increasingly studied in recent years involves controlling balancing problems of the DC-link capacitor voltages in DCCs, and of the flying capacitor voltages in FCCs (Bendre et al. 2006; Defay 2010:2241; Huang & Corzine 2006; Ruderman & Reznikov 2009:87; Stolze et al. 2011; Tallam et al. 2005; Yaramasu et al. 2013). Recent studies indicate that modern microprocessor systems allow for a reduction in the control complexity of power converter systems (Texas Instruments 1995; Xilinx 2014). Such advances highlight the need to control balancing problems in the DC-link capacitor and flying capacitor voltages, thus avoiding distortion from the output phase voltages and a decrease in current quality. If the switching control signals are not optimally selected and applied to power devices, the problems of unbalanced voltages in the DC-link and flying capacitor will result in output with a poor current quality. The natural balancing control strategy of the capacitor voltages of FCCs fails in certain circumstances, and there is a trend towards an independent control strategy (Clos et al. 2005; Defay et al. 2010; Escalante et al. 2002; Feng et al. 2007; Khazraei et al. 2010, 2012). In the independent voltage control technique, the capacitor voltages are measured and a control strategy uses these measurements along with the values of reference signals and knowledge about the system, to define the switching logics which are subsequently applied. As pointed out in Srikanthan et al. (2009), the different control strategies have evolved in parallel with the

development of the multilevel power converter topologies. This evolution resulted in an increased complexity of the controllers used to achieve capacitor voltage balancing, where voltage control is often implemented in addition to current control, by a multilevel power converter. However, these kinds of multiple-input-multiple-output (MIMO) systems generally benefit from a true multivariable controller. It is widely known that a combination of several single-input-single-output (SISO) controllers form an MIMO system such as an FCC; this results in complex, but inferior control systems. Multivariable controllers offer better performance and simpler implementation for MIMO systems. In the case of an FCC, a truly multivariable control also inherently accounts for capacitor voltage variations without additional and complex compensation schemes; this was put forward by Naumanen et al. (2010).

In this research, a model predictive current control strategy is proposed, specifically for three-phase MLVSIs, diode-clamped converter and flying capacitor converter inverters for RESs applications. The proposed control was split into two different control algorithms. Firstly, an FS-MPCC method was presented to control the output current of the three-phase, multilevel inverters (MLIs). This control method was selected to reduce the calculation effort required for the MPC method and increase the possible prediction horizon. Secondly, to solve the flying capacitor voltage and DC-link capacitor voltage balance problems, a hysteresis-voltage balancing algorithm based on predictive control was presented; this algorithm was used to keep the flying capacitor voltages and DC-link capacitor voltages within their hysteresis band. Finally, a performance evaluation of the proposed algorithms for three-phase, three-level MLIs was investigated in terms of power quality and dynamic response.

1.2 Control of power converters

To adjust the electrical characteristics of the power source, modern power converters use semiconductor solid-state switches to synthesize the desired output voltage to be applied to an electrical load. The electrical power quality generated by the power converter depends on the electrical topology and the commutation scheme used to handle the semiconductor power switches.

The high need for improved power converters has ensured their continued development, not only in order to obtain new advantageous architectures, but also to improve the control techniques used. (Bose 2009; Holtz 2011; Kouro et al. 2010). The control of power converters is extensively studied, and new control schemes are presented every year. Several control schemes have been proposed for the control of power converters and drives; some of these are shown in Figure 1.1.

From the literature it has been determined that of these control schemes, hysteresis and linear controls (both with PWM), are the most popular (Kazmierkowski et al. 2002; Linder 2005; Mohan et al. 1995).

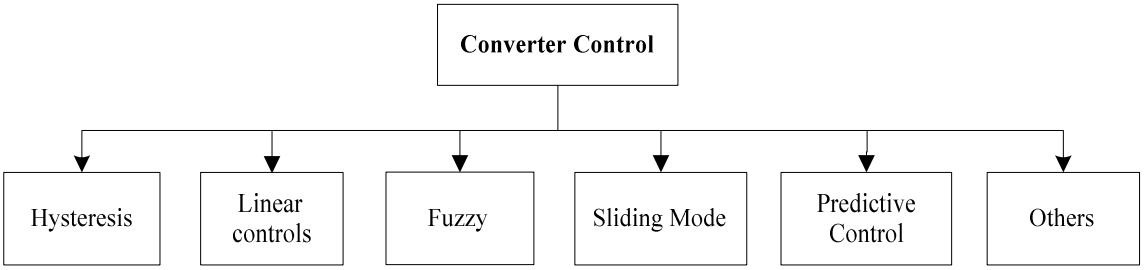

Figure 1.1: Basic methods of converter control

1.2.1 Traditional control of power converters

When providing the power required by a load, the power converter is normally expected to deliver only a limited number of voltage levels. In this process the power converter, as the driver of the load, delivers the required voltage level subject to input it receives from the controller. To improve the quality, the output voltage from the inverter usually has to be processed via a modulation unit before being supplied to the load. Figure 1.2 illustrates a common control loop for a power system converter that includes modulation. The PWM method is the most popular switching procedure applied to deliver the required output voltage, $v(k)$, from a converter (Holmes & Lipo 2003; Kaźmierkowski et al. 2002). In this technique the controller provides a modulation index, $m(k)$, which is used by the modulator to handle the converter switches, $S(k)$, in order to obtain an average value of the required voltage, $v(k)$, in a particular switching period; this is illustrated in Figure 1.2.

Classic approaches such as fuzzy logic, sliding mode, and predictive control (Bose 2000, 2007; Cortés et al. 2008(a); Raviraj & Sen 1997; Tan et al. 2006) as presented in Figure 1.1 have been proposed to handle power converters to improve the performance achieved.

PWM strategies used in a conventional inverter can be modified for use in MLCs. The two multilevel PWM methods discussed most frequently in the literature are the multilevel carrier-based PWM and the multilevel space vector PWM; both are extensions of traditional two-level PWM strategies to more than two levels (Geyer 2011; Holmes & Lipo 2003; Tan et al. 2006). Investigators have proposed carrier-based multilevel sine-triangle PWM schemes for the control of a DCMLI used as a motor-drive or static var compensator (Agelidis & Calais 1998; Carrara et al. 1992; Chen et al. 1997; Choi et al. 1991, 1993; Menzies et al. 1994; Menzies & Zhuang

1995; Steinke 1988), and for control of an FCMLI (Feng et al. 2007; Ghias et al. 2012; Lee et al. 2001; Thielemans et al. 2012). Others advocate a generalized space vector PWM theory for use with MLIs (Fracchia et al. 1992; Liu & Cho 1994; Sinha & Lipo 1996). A third PWM method used to control MLCs is with selective harmonic elimination (Carrara et al. 1993; Jingang et al. 2007; Konstantinou et al. 2013; Lie & Agelidis 2005; Ohsato et al. 1991).

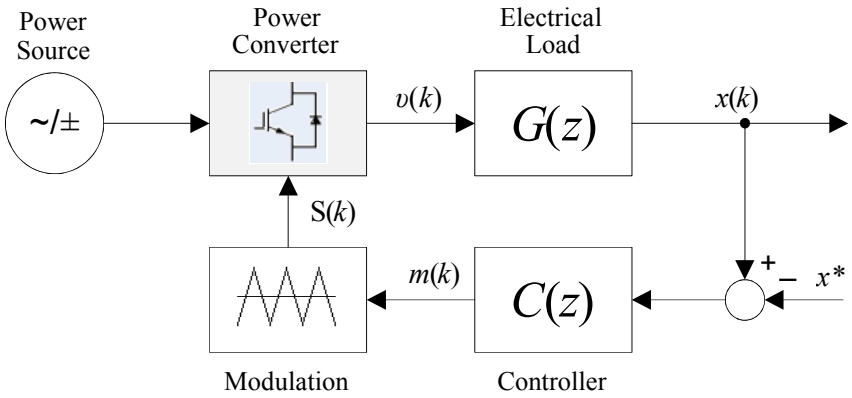

Figure 1.2: Standard modulation-based control scheme for power converters

1.2.2 Model predictive control

Predictive control encompasses a very wide class of controllers that has of late found applications in power converters. Predictive control can be considered any algorithm that uses a model of the system to predict its future behaviour and selects the most appropriate control action based on an optimal criterion (Abu-Rub et al. 2004; Cortés et al. 2008:4312). When compared to classic control methods, the model predictive control algorithm requires a high number of calculations, but the fast microprocessors available today make it possible to implement predictive control for MLCs. A different approach is taken for MPC (Camacho & Bordons 1999; Cortés et al. 2008; Kouro et al. 2009) where a model of the system is considered in order to predict the future behaviour of the variables over a time frame; the time frame is a integer multiple of the sample time. These predictions are evaluated, based on a cost function, and the sequence that minimizes the cost function is then chosen; in this way the future control actions are obtained. Only the first value of the sequence is applied, and the algorithm is calculated again after every sampling period. This approach is known as the continuous set MPC method (Geyer et al. 2009; Vazquez et al. 2011). The FS-MPCC approach takes advantage of the limited number of switching states of the power converter, for solving the optimization problem. A discrete model is used to predict the behaviour of the system for every admissible actuation sequence up to the prediction horizon. The switching action that minimizes a predefined cost function is

finally selected to be applied in the next sampling instant. The main advantage of the FS-MPCC approach lies in the direct application of the control action to the converter without requiring a modulation stage.

In several studies an FS-MPCC scheme has been successfully applied for current control in MLCs (Cortés et al. 2008(b); Rodríguez & Cortés 2012; Stolze et al. 2011; Vargas et al. 2007). The typical structure of a predictive current controller is shown in Figure 1.3; the classification for MPC methods is shown in Figure 1.4.

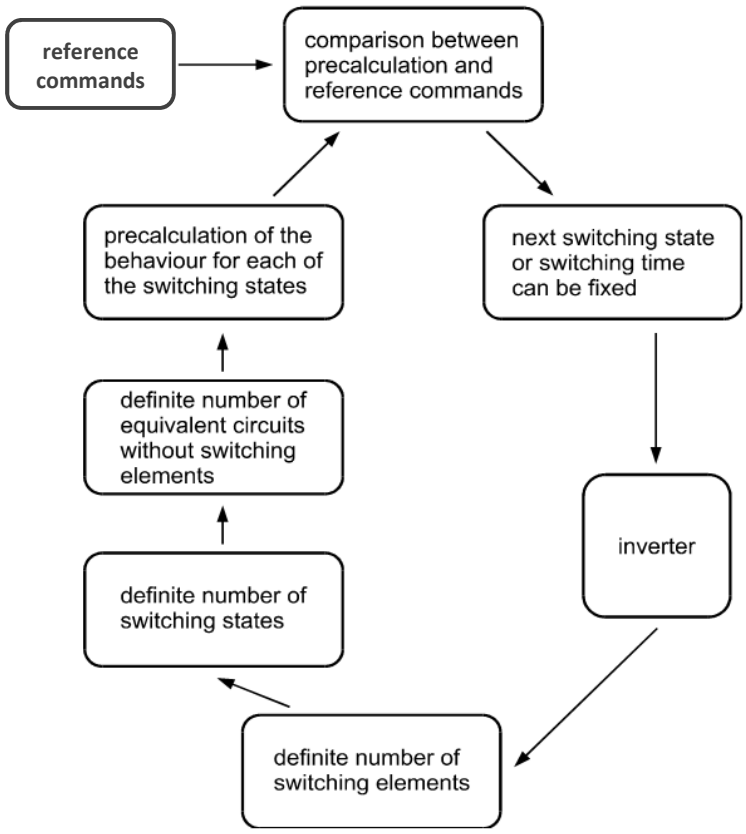

Figure 1.3: Structure of typical model predictive controller

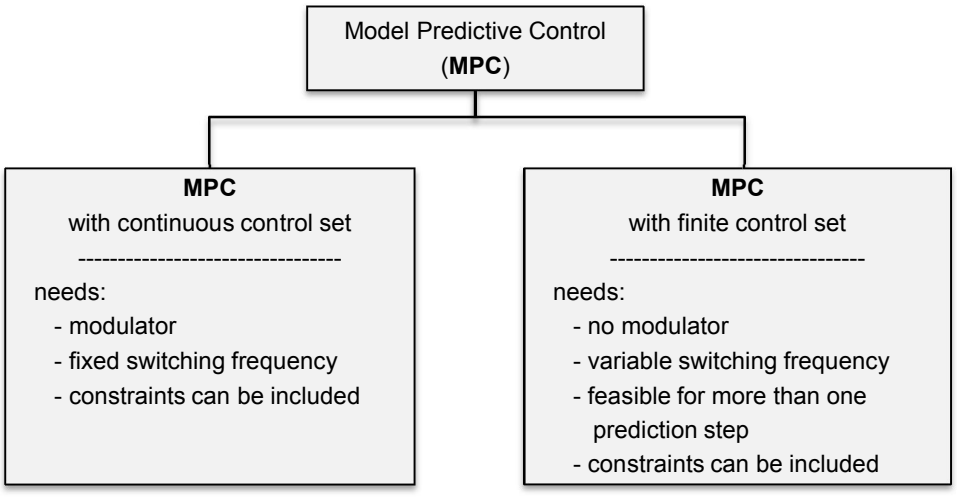

Figure 1.4: Classification of MPC methods

1.3 Statement of research problems

MPC is based largely on fast microprocessor calculations. The research problem that this thesis addressed was how to reduce the enormous volume of calculations required when an inverter is controlled directly without a modulator, since the number of calculation cycles increases exponentially with the prediction horizon. This has been a major problem to overcome in MPC, as the control task is not feasible for prediction horizons greater than one prediction step.

A research sub-problem that arose, involved the flying capacitor voltage and DC-link capacitor voltage balance problems. The main challenge here was to ensure that the correct operation of the inverter kept the correct voltage across the flying capacitor and DC-link capacitor voltage at all times during the operation of the converters.
Another sub-problem to overcome in both cases above was how to reduce the total harmonic distortion (THD) in the output stage of the inverters.

1.4 Study objectives

The first research objective was to increase the prediction horizon, by reducing the calculation effort required by the MPC method when a DCC and an FCC are to be controlled.

The second research objective was to balance the flying capacitor voltages of the FCC, as well as the DC-link capacitor voltages of the DCC in terms of excellent reference current tracking and a minimal harmonic content in the load current. The main challenge was to ensure that the correct operation of the inverter maintained the correct voltage across the flying capacitors. The balancing of the flying capacitor and DC-link capacitor voltages must be guaranteed at all times during the operation of the converters.

To achieve the objectives stated above, the following steps were carried out:

1. Literature study of MPC methods with a particular focus on MLCs were carried out.
2. An RES model was developed to investigate the system performance when power is supplied to a resistive-inductive load (RL-load).
3. A proposal was made for a predictive current control strategy for three-phase, three-level DCC and FCC inverters in which an FS-MPCC strategy was applied to control the load current and the voltage of the capacitors associated with DCC and FCC.
4. A control algorithm that exhibits high dynamic performance for MLCs was proposed. This algorithm is required to reduce the complexity of calculations

and the number of possible combinations for MPC. It is also needed to increase the prediction horizon, which is applied to the proposed algorithm for three-phase, three-level DCC and FCC inverters.

5. A proposal was put forward for a hysteresis-based voltage balancing algorithm to control the DC-link and flying capacitor voltages in the DCC and FCC respectively. The purpose of this algorithm is to keep the DC-link capacitor voltages and flying capacitor voltages within the hysteresis band.
6. A performance evaluation of the FS-MPCC strategy for MLIs under different conditions, in terms of the THD in the output stage of the inverters, was undertaken.
7. The detailed simulation results were presented to demonstrate the performance of the predictive current control strategy in comparison with a conventional PWM control technique.
9. Several modelling and simulation tools were used in this project. The simulation, co-simulation and mathematical models were done in: MATLAB/Simulink and PSIM.

1.5 Contribution of the research

This thesis introduced a novel approach to use an FS-MPCC and hysteresis based on MPC using a singular cost function in the control of a power electronic converter. This method reduces the bulky hardware of PWM modulation electronics and driver circuits as used in a software-driven, multicore processor solution. The technical and theoretical issues regarding the use of an FS-MPCC approach in power electronics have been thoroughly explored and improved upon. The study illustrated and provided a benchmark on how to implement predictive control techniques to improve the performance in some classes of power converters in terms of power quality and dynamic response. This has huge benefits for future micro-power generation and will contribute to improved efficiency in power electronic drives and electronic vehicle developments.

In particular, two algorithms have been developed. The purpose of the first algorithm is to reduce the calculation effort for the MPC and increase the prediction horizon, making higher prediction horizons possible. The second algorithm balances the DC-link capacitor voltages and flying capacitor voltages in the DCC and FCC respectively; this algorithm keeps the DC-link capacitor voltages and flying capacitor voltages within the hysteresis band.

These two algorithms offer the following contributions to the research area:

1. No need to use any modulation.
2. Can be applied to different kinds of MLI.
3. Suitable for any type of load.
4. Suitable for RES applications.

1.6 Organization of the thesis

This thesis is comprised of three major parts which are summarized as follows:

Part I. This part gives an overview and general introduction to power converter control, common MLC topologies highlighting their pros and cons, industrial applications, and control methodology of model predictive control as applied in this thesis.

Chapter one presents an introduction to control of power converters in general with specific reference to the state-of-the-art as published in the literature. This chapter further describes the scope of this thesis and formulates the problems that are discussed in the manuscript.

Chapter two gives an overview of the most common MLC topologies, introducing the nomenclature used and the operational basis of this type of converter. This chapter introduces the manner of switching for MLCs and depending on the chosen converter topology, it makes available the possible output voltages that can be achieved. An overview of existing multilevel topologies with their respective strengths and weaknesses is presented. The importance and methods of voltage balancing of the capacitors as related to particular converter topologies, are then discussed, and software simulation integration (SSI) for enhancing the engineering design during power conversion feasibility studies, is presented. The chapter concludes with a discussion of the modern and more practical industrial applications of MLCs for RESs. The objective of this chapter is to provide a general background to readers who are interested in multilevel power converters and their applications.

Chapter three begins with an introduction to predictive current control techniques for power conversion. Different predictive control methods are discussed, hysteresis-based, trajectory-based, dead-beat and model-based predictive control schemes are all considered. Next, the terminology used in the proposed MPC is presented. The modelling of a system and approximations for the derivatives of differential equations are given. While the Euler forward method is used in this study, the Euler backward and the fourth-order Runge-Kutta approximations are also mentioned. The chapter concludes with a discussion of the cost function classifications in terms of weighting factors, delay compensation, reference frames, and the natural abc and $\alpha\beta$ frames.

Part II. The study of MPC techniques for three-phase, three-level inverters of different topologies are presented in this section in terms of current tracking behaviour and capacitor voltages balancing.

In Chapter four a finite control set-model predictive strategy to handle the output current, as well as the balancing of the DC-link capacitor voltages for the three-phase, three-level DCC inverter with an RL-load, is proposed. This strategy allows for fast load current control while maintaining the balance of the DC-link capacitor voltages. The problems of balancing the DC-link voltage and output current reference tracking are examined by means of co-simulation using MATLAB and PSIM software. The hysteresis-based voltage balancing algorithm is then presented; this algorithm is applied to control the DC-link capacitor voltages and keep them within the hysteresis band. An assessment is given of the robustness of the control strategy under variable DC-link voltages, and as required for RESs applications, by measuring the THD and tracking behaviour of the reference currents; this was done for all DC-link voltage values. System performance was investigated in terms of tracking behaviour and the dynamic response of the system, by applying step changes in the amplitude of different waveforms; a square waveform in orthogonal coordinates, a constant reference steps and a sawtooth waveform as a reference current. Lastly, the system robustness was studied by comparing the model with the actual system parameters of the proposed control algorithm. A summary is presented in the last section.

Chapter five presents a new direct model predictive control strategy for a three-phase, three-level FCC. Additionally a hysteresis-based algorithm is presented for balancing the flying capacitor voltage and keeping the flying capacitor voltage within the hysteresis boundaries in compliance with the FS-MPCC algorithm. An MPC strategy can produce only 19 different voltage vectors to handle the output current as well as the balancing of the flying capacitor voltages for the three-phase, three-level FCC inverter with an RL-load. Presented in the first step is the time-continuous model which is then discretized to obtain the output currents and flying capacitor voltages; this is followed by the determination of the optimum voltage vector. In the next step, the optimum switching state that produces this optimum voltage vector is selected. In this chapter a predictive current control technique for an FCC inverter when the power converter model is used, is presented. Thereafter the control scheme was developed in the subsection of the system that is used to control the power converter model. The improvement in performance was assessed by measuring the THD of the output voltage for RL-load. In this chapter the FS-MPCC algorithm was evaluated under three different conditions by means of co-simulation; this involved measuring of reference current tracking and flying capacitor voltage balance. First of all, the

robustness of control strategy under variable DC-link voltages for use in RESs applications was done in terms of the THD. Secondly, sinusoidal waveform current reference tracking and the step change in the amplitude of the reference current were investigated. In order to check the dynamic response, the control algorithm was then tested by using different waveforms; a square waveform in orthogonal coordinates, constant reference steps and a sawtooth waveform as a reference current. Lastly, the performance of the proposed control was assessed by the level of mismatching that occurs between the model and the actual system parameters. A summary is presented in the last section of the chapter.

Part III. Conclusions drawn from previous chapters are expressed and future work related to this thesis is proposed. The appendix attached hereafter contains mathematical derivations, data and parameters of the system model, as well as useful MATLAB and PSIM scripts developed for this thesis.

Chapter six is the final chapter and presents a brief summary of the research work undertaken for this thesis. The chapter highlights significant contributions made as a result this study, including a comparative analysis of the control method studied and an evaluation of the proposed control technique for MLIs. The chapter concludes with a discussion of possible future research work identified in the production of this thesis.

Appendices:

Appendix A: Coordinate transformations

Appendix B: Switching states and voltage vectors

Appendix C: Total harmonic distortion factor

Appendix D: Modelling and co-simulation models

1.7 Publications

The following list presents the author's contributions to the body of literature in the field of power electronics as a result of the research carried out to produce this thesis.

Conferences proceedings:

1. A. M. Almaktoof, A. K. Raji and M. T. E. Kahn, “Finite Set-Model Predictive Current control of three-phase voltage source inverter for Renewable Energy Systems (RES) applications” 12th International Conference on Sustainable Energy Technologies (SET 2013), pp. 2369–2376. Hong Kong 26–29 Aug. 2013.
2. A. M. Almaktoof, A. K. Raji and M. T. E. Kahn, “Modeling and simulation of Three-Phase Voltage Source Inverter using a Model Predictive Current Control” 2013 the 2nd International Conference on Information and Digital Engineering (ICIDE 2013), Hong Kong 26-27 Oct. 2013.
3. A. M. Almaktoof, A. K. Raji and M. T. E. Kahn, “Performance Evaluation and Improvement of an FS-MPC for Two-Level VSI” The International Conference on Electrical and Electronics Engineering, Clean Energy and Green Computing (EEECEGC 2013), United Arab Emirates, pp. 120–126. December 11–13, 2013.
4. A. M. Almaktoof, A. K. Raji, M. T. E. Kahn and M. Ali Ekhlat, “Sizing and Evaluation of A Battery-less PV System-Driven Desalination with RO for Rural Areas-Case Study” 2014 Proceeding of the 22nd Domestic Use of Energy, pp. 173–180. 31 March–2 April 2014 in Cape Town, South Africa.
5. A.M. Almaktoof, A.K. Raji and M.T.E. Kahn, “Robust Current Control Technique for Variable DC-link Voltage Source Inverters for Renewable Energy Systems” 11th Industrial and Commercial Use of Energy Conference (ICUE2014), pp. 353–360. 18–20 August 2014 in Cape Town, South Africa.
6. A.M. Almaktoof, A.K. Raji and M.T.E. Kahn, “Finite-Set Model Predictive Control and DC-Link Capacitor Voltages Balancing for Three-Level NPC Inverters” 16th International Power Electronics and Motion Control Conference and Exposition (PEMC 2014), pp. 305–310, on 21–24 September, 2014, Antalya-Turkey.
7. A. M. Almaktoof, A. K. Raji, M. T. E. Kahn, “Software Simulation Integration in Enhancing Engineering Design in Power Conversion Studies” Proceedings of the 23rd Southern African Universities Power Engineering Conference (SAUPEC 2015), pp. 63–68, on 28–30 January 2015, University of Johannesburg, Johannesburg, South Africa

8. A. K. Raji, A. M. Almaktoof and M. T. E. Kahn, “Synergy of small-scale wind energy system with energy efficient appliances and reticulation system” 12th International Conference on Sustainable Energy Technologies (SET 2013), pp. 2425–2433. Hong Kong 26–29 Aug. 2013.
9. Christian Alexandra, Ali M. Almaktoof and AK Raji, “Development of a Proportional + Resonant (PR) Controller for a Three-Phase AC Micro-Grid System” The International Conference on Electrical and Electronics Engineering, Clean Energy and Green Computing (EEECEGC 2013), United Arab Emirates, pp. 107–112. December 11–13, 2013.

International Journals:

10. A. M. Almaktoof, A. K. Raji and M. T. E. Kahn, “Modeling and simulation of Three-Phase Voltage Source Inverter using a Model Predictive Current Control” International Journal of Innovation, Management and Technology (IJIMT), vol. 5, no. 1, pp. 9–13, 2014.
11. A. M. Almaktoof, A. K. Raji and M. T. E. Kahn, “Finite Set-Model Predictive Current control of three-phase voltage source inverter for Renewable Energy Systems (RES) applications”, Journal of Energy and Power Engineering, USA, 8 (2014), pp 748–755, 2014.
12. A. M. Almaktoof, A. K. Raji, M. T. E. Kahn,” Finite Set-Model Predictive Current Control of Three-phase Three-Level Neutral-Point-Clamped Inverters for Renewable Energy Systems Applications”, Control Engineering and Applied Informatics Journal, DHET’s accredited journal, submitted in May 2014, ID: 2536.
13. A. M. Almaktoof, A. K. Raji, M. T. E. Kahn and M. Ali Ekhlat, “Batteryless PV Desalination System for Rural Areas－A Case Study”, Journal of Energy in South Africa, JESA, DHET’s accredited journal, submitted in Jan. 2015.
14. A. M. Almaktoof, A. K. Raji, M. T. E. Kahn,” Predictive Control Techniques of a Multilevel Inverter for Renewable Energy Systems Applications”, IET Renewable Power Generation Journal, DHET’s accredited journal, submitted in Feb 2015, ID: RPG-2015-0066.
15. A. M. Almaktoof, A. K. Raji, M. T. E. Kahn,” An improved finite state-model predictive current control and voltage balancing techniques-based for multilevel converter”, Journal of Electrical Engineering & Technology (JEET), DHET’s accredited journal, submitted in March 2015, ID: J-15-03-265.

CPUT Conferences:

16. A. M. Almaktoof, A. K. Raji and M. T. E. Kahn, “Performance Evaluation of Model Predictive Control Strategy for a Three-phase Voltage Source Converters”, CPUT Postgraduate Research Conference 2013, 5 November 2013, Centre for Postgraduate Studies (CPGS), Bellville campus, (power point presentation).
17. A. M. Almaktoof, A. K. Raji and M. T. E. Kahn, “Model Predictive Current Control of Voltage Source Inverter for Renewable Energy Systems Applications”, CPUT Research Day 2013, 29 November 2013, Cape Town Campus, (Poster presentation).
18. A. M. Almaktoof, A. K. Raji and M. T. E. Kahn, “Multi-level inverters using Finite-Set Model Predictive Current Control for Renewable Energy Systems applications”, Engineering Postgraduate Seminars 2014, 28 August 2014, Bellville campus, (power point presentation).
19. A. M. Almaktoof, A. K. Raji and M. T. E. Kahn, “Co-Simulation in Improving Engineering Design in Static Power Conversion Studies”, CPUT Research Day 2014, 27 November 2014, Mowbray Campus, (Poster presentation).
20. A. M. Almaktoof, A. K. Raji and M. T. E. Kahn, “Multi-Loop Control Strategy for A Flying Capacitor Converter for Renewable Energy Systems Applications”, CPUT Postgraduate Research Conference 2014, 5 November 2014, Centre for Postgraduate Studies (CPGS), Bellville campus, (Oral and Poster presentations).

CHAPTER TWO

MULTILEVEL CONVERTERS FOR RENEWABLE ENERGY SYSTEMS APPLICATIONS

2.1 Introduction

This thesis is focused on a combination of MLCs with predictive current control to improve some specific characteristics and performance in some classes of power converters, such as of power quality and dynamic response. This chapter introduces the switching manner for MLCs and, presents the possible output voltages that could be achieved, which depends on the chosen converter topology. Comparison of different topologies in terms of both the number of components, and isolated DC sources, is presented. The importance and methods of voltage balancing of the capacitors in relation to the converter topology, are discussed. Software simulation integration for enhancing engineering design of power conversion systems is then presented. This chapter also focuses on the modern and more practical industrial applications of MLCs as required for RESs. The main objective of this chapter is to provide a general overview for readers who are interested in MLCs and their applications.

2.2 Power electronic converters

Power Electronic converters technology used in a wide range of applications such as energy generation, transmission, distribution. The essential characteristic of power electronic converters is that the switches are operated only in one of two states—either 'on' or 'off'—unlike other types of electrical circuits where the control elements are operated in a linear or near-linear active region. Power electronics industry has developed, various categories of power electronic converters, these are linked by power level, switching devices and topological origins. Figure 2.1 presents a categorization of power electronic converters into groups according to their type of electrical conversion.

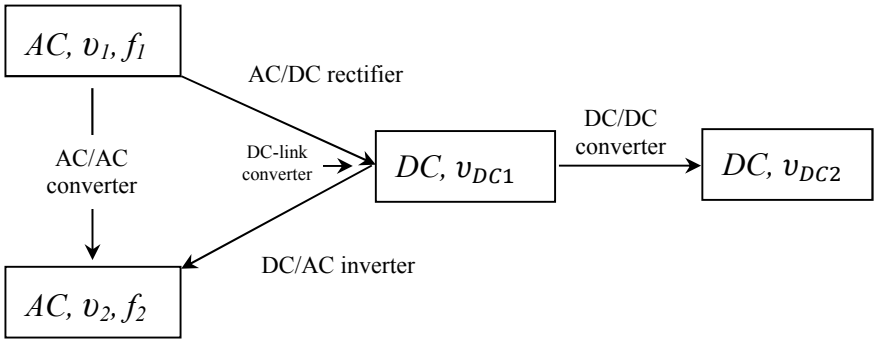

Figure 2.1: Groupings of solid-state power converters categorized according to their conversion function

In the last decade, applications of MLVSIs found in most industrial sectors have been extensively studied. Today, increasing energy demands coupled with the requirements for power quality and efficiency have resulted in the use of power

electronics for control and power conversion becoming an important topic. Power converters interfaced with renewable and distributed energy resources have been studied with great interest this because with MLC, the power from these resources can be connected to a load or to the utility grid (Alepuz et al. 2006; Carrasco et al. 2006; Tolbert & Peng 2000). Examples of such renewable and distributed energy resources are: battery banks; photovoltaic (PV) systems (Alonso et al. 2003; Blaabjerg et al. 2006; Busquets-Monge et al. 2008; Myrzik & Calais 2003); wind turbines (Bueno et al. 2008; Nami & Zare 2009); fuel cells (Sharma & Gao 2006); and micro turbines (Alepuz et al. 2006; Carrasco et al. 2006). Figure 2.2 depicts a scheme in which the different power converters available for electrical conversion as applicable in RESs, are grouped according to their function.

In RESs, sources can be either alternating current (AC) or direct current (DC), such as wind turbines or PV systems respectively. The power requirements of the load may however, make it necessary to convert AC to DC or vice versa. Based on the particular application, a properly selected and controlled combination of power converters can supply the required power for a load. The AC–DC, DC–DC and/or DC–AC converters may be needed in residential application (see Figure 2.2(a)), or grid-connected systems where the variable voltage of RESs should be converted to achieve the desired AC voltage and frequency. On the other hand, when the input voltage is a variable DC source, such as PV or fuel cell systems as shown in Figure 2.2(b), a DC–DC converter combined with a DC–AC converter may be used to yield a regulated AC waveform suitable for residential application or grid-connected systems.

One of the most common converter topologies found in industry is the three-phase, two-level voltage source inverter, which today, is mostly used to generate an AC voltage from a DC voltage (v_{DC}). The two-level inverter, when fed with v_{DC}, can only create one of two discrete output voltages for the load: $v_{DC}/2$ or $-v_{DC}/2$.

MLCs represent the latest development in power electronic converter circuitry and have opened up applications which hitherto, had impractically high power requirements (Rodríguez et al. 2002).

MLCs present substantial advantages over conventional two-level converters; they were developed to overcome some of the limitations imposed by those conventional converters. Research of modern MLVSIs began in 1981 with the introduction of DCC three-level inverters (Nabae et al. 1981). Subsequently, the flying capacitor multilevel converter (Meynard & Foch 1992) and the cascaded H-bridge converter (CHBC) multilevel inverter (Peng & Lai 1995; Franquelo et al. 2008) have been introduced.

Electronic control of very high-power, variable-speed drive systems and power conditioning systems for enhancing the quality of existing high-voltage power distribution networks, are the two main application areas where MLCs will play a

significant role in the future. The integration of alternative renewable energy sources within the power distribution infrastructure will also be aided by these newer forms of power converters.

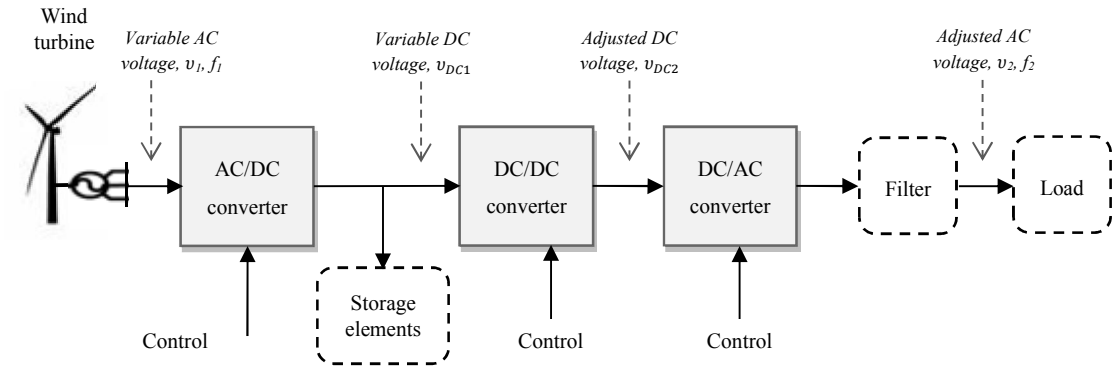

(a)

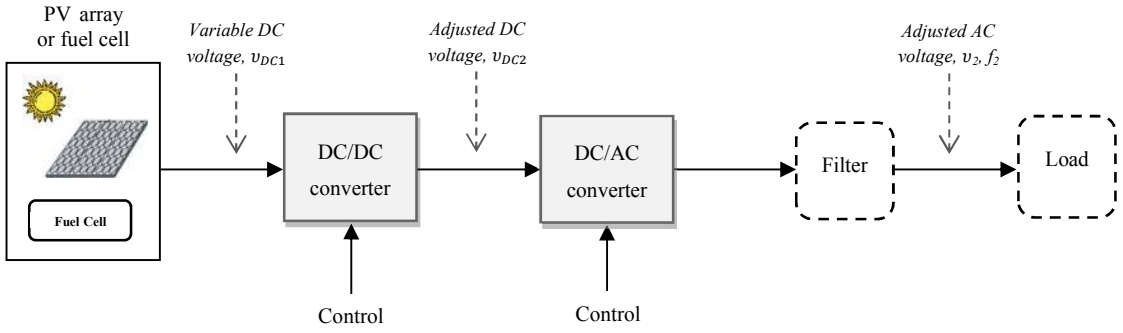

(b)

Figure 2.2: Families of power converters categorized according to their energy conversion in RESs

2.3 The concept of MLCs for RESs

In the current global climate, demand for RESs has increased due to environmental issues and limited energy from fossil resources. PV and wind turbine systems have become the most common source type for residential applications or grid-connected RESs (Bueno et al. 2008; Carrasco 2006; Nami & Zare 2009). Energy from renewable sources is growing throughout the world. Siemens (2012) predicts that energy from renewable sources will account for exceed 28% of the global power in 2030 and estimates that global power consumption will increase from 22.1 TWh in 2010 to 37.1 TWh in 2030. Figure 2.3 depicts recent and future data concerning the world electricity generation from renewable energy sources.

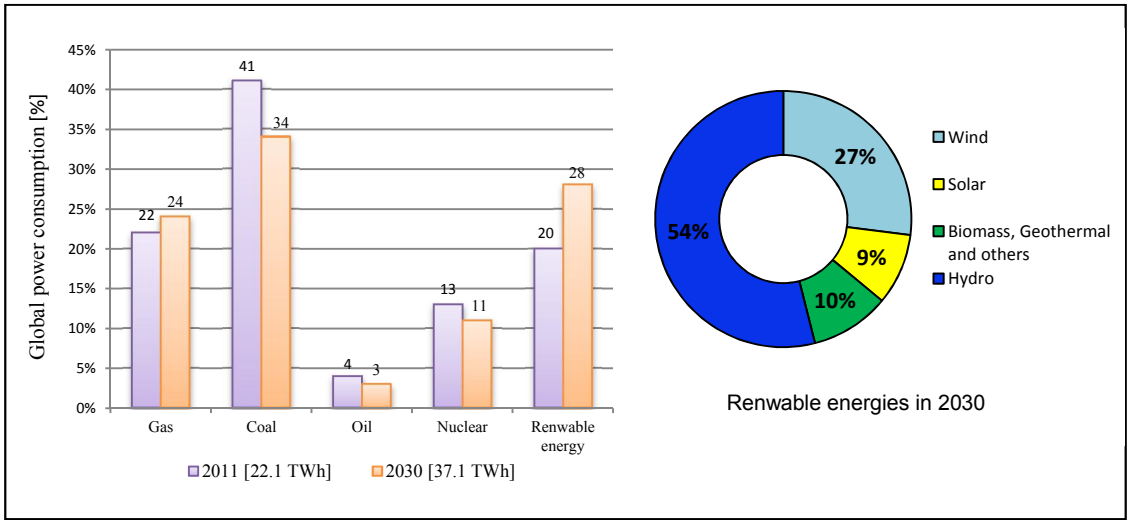

Figure 2.3: World electricity generation

In connecting these systems to different kinds of load and applications, or utility grids, the main challenge relates to issues of manipulating the output voltage and frequency. MLCs like AC–DC, DC–AC, AC–AC and DC–DC converters can be used to interface with renewable energy sources to supply a load, as illustrated earlier in Figure 2.2.

With MLIs, the output voltage can be increased without increasing the voltage rating of switching components, so that an MLI offers a direct connection of the output voltage from an RES to the load or grid without using expensive, bulky and heavy transformers. In addition, MLIs synthesize a staircase output voltage, which is closer to sinusoidal voltage using DC-link voltages, unlike the voltage required by a two-level inverter. Synthesising a stepped output voltage allows reduction in the harmonic content of voltage and current waveforms and ultimately a reduction in the size of the output filter.

MLIs contain several power switches and capacitors. Output voltages of MLIs are the sum of the voltages resulting from the commutation of the switches. In Figure 2.4, a schematic diagram of one-phase leg of inverters with different level numbers is shown. A two-level inverter, as shown in Figure 2.4(a), generates an output voltage with two levels relative to the negative terminal of the capacitor.

The three-level inverter shown in Figure 2.4(b) generates a three-level voltage, and an m-level inverter shown in Figure 2.4(c) generates an m-level voltage. Thus, MLIs are available with output voltages that can have several levels. Moreover, they can also reach a high voltage, while the power semiconductors are only capable of withstanding reduced voltages. As mentioned earlier, three different multilevel topologies have been proposed in current literature. Among the more serious drawbacks affecting the DCMLI are limitations of the DC-link voltage imbalance, indirect clamping of the inner devices, and multiple blocking voltages of the clamping diodes (Lai & Peng 1996).

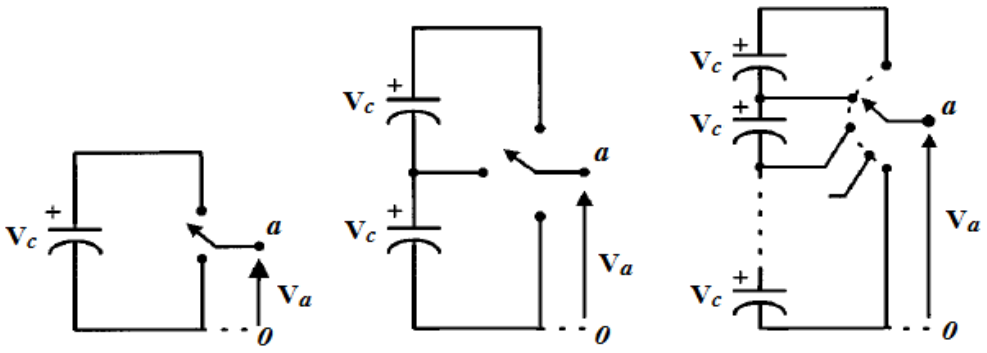

(a) (b) (c)

Figure 2.4: One-phase leg of an inverter: (a) two-level, (b) three-level and (c) m-level

The main limitation of the CHBMLI is in the required provision of an isolated power supply for each individual H-bridge cell, when real power transfer is demanded. For flexible AC transmission system (FACTS) applications where the isolated power supplies are not required, the power pulsation at twice the output frequency occurring within the DC-link of each H-bridge cell necessitates an over-sizing of the DC-link capacitors. The FCMLI structure attempts to address some of the limitations imposed by the conventional two-level inverters and by the two above-mentioned MLI types. The use of capacitors for voltage clamping, as opposed to using diodes as in DCMLIs, permits several switch combinations for a particular level of voltage generation; these combinations may be used for preferential charging and

discharging of capacitors in order to achieve voltage balance. The classification of DC–AC inverters is illustrated in Figure 2.5. The different DC–AC inverter types were grouped according to their sources.

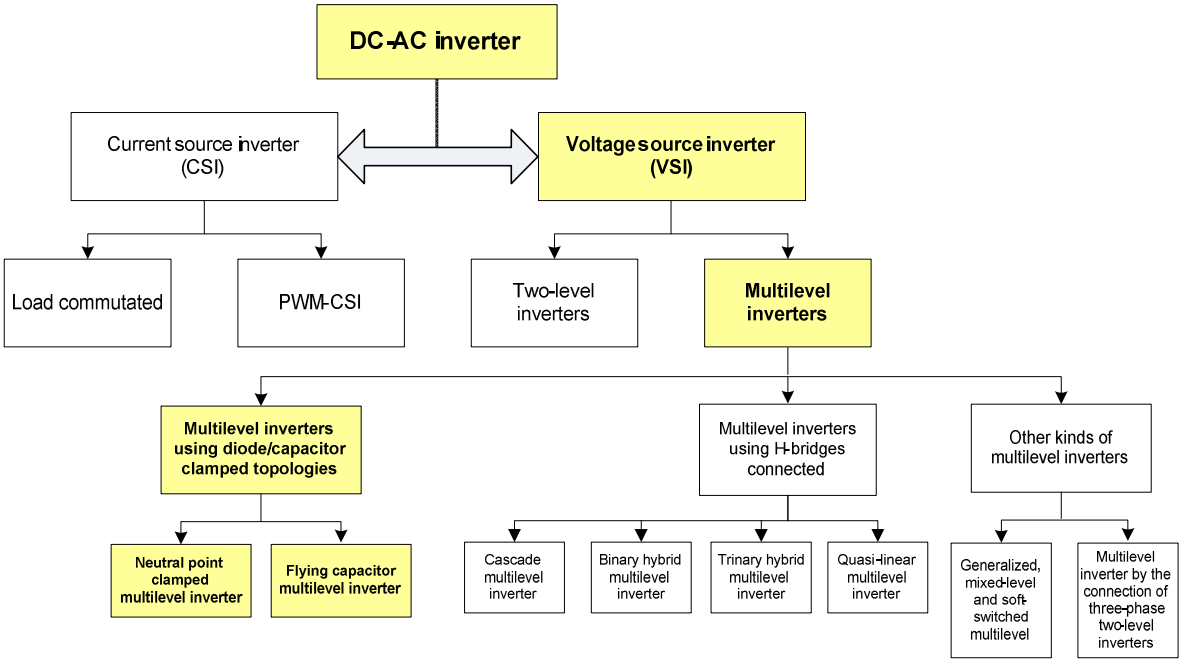

Figure 2.5: Family tree of the DC–AC inverters

2.4 Multilevel voltage source inverter

MLIs have gained increasing attention in recent decades due to their many attractive features. When high switching frequency PWM (Lai & Peng 1996; Teodorescu et al. 1999) is used with MLIs, these inverters offer significant advantages compared with conventional two-level converters (Shakweh 2001). These advantages are fundamentally focused on improvements in the quality of the output signals and a nominal power increase in the converter. These properties make MLIs very attractive to the industry. Currently researchers all over the world are expending great effort in trying to improve the performance of these inverters with regard to control simplification and the performance of the different optimization algorithms. Their aim is to enhance, among others, the THD of the output signals, the balancing of the DC-link capacitors voltage, and the ripple of the load currents (Chiasson et al. 2005; Du et al. 2006; Kimura et al. 2002; Vassallo et al. 2003). Figure 2.6 shows a comparison of the differences in the output voltage waveform and frequency spectra between a standard two-level inverter and a three-level inverter when the number of switching transitions is the same for each power switch. As seen in the spectra, the three-level effectively doubles the switching frequency and reduces the harmonic content in the output voltage. In a motor-drive system, this will reduce the harmonic content in the

winding current and lessen the torque ripple at the shaft. The size of any additional filtering required, between the load and the inverter will also be reduced.

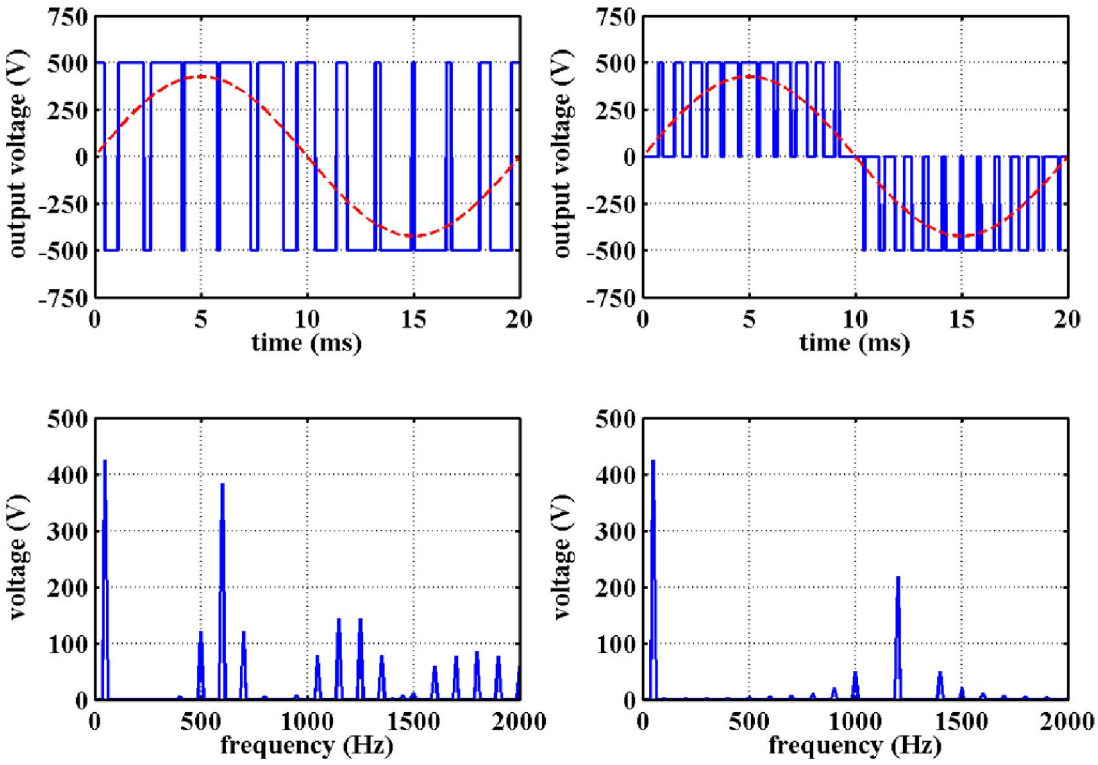

(a) Two-level inverter (b) Three-level inverter

Figure 2.6: Time and frequency domain comparison between two- and three-level inverters

The attractive features of an MLC can be briefly summarized as follows:

1. **Staircase waveform quality:** not only can MLCs generate the output voltages with very low distortion, but they also reduce the voltage stress (dv/dt), thereby reducing electromagnetic compatibility (EMC) problems.
2. **Common-mode (CM) voltage:** MLCs produce a small CM voltage, thereby reducing the stress in the bearings of a motor connected to a multilevel motor-drive. Furthermore, the CM voltage can be eliminated by using advanced modulation strategies, such as that proposed by Cengelci et al. (1998).
3. **Input current:** MLCs are capable of drawing an input current which has a low distortion.
4. **Switching frequency:** MLCs can operate at both fundamental switching frequency and a high switching frequency PWM. It should be noted that a lower switching frequency usually means a lower switching loss and higher efficiency.

Unfortunately, MLCs do have some disadvantages; a major one is the increased probability of failure due to the larger number of required devices (Richardeau et al. 2002; Turpin et al. 2002). Although lower-rated voltage switches can be utilized in an MLC, each switch requires an isolated gate drive circuit. This may cause the overall system to be more expensive and complex. There are three main promising types of MLI topology: the DCMLI, the FCMLI and the CHBMLI converters (Fang & Ye 2013:581; Franquelo et al. 2008; Meynard & Foch 1992; Nabae et al. 1981; Peng & Lai 1995; Teodorescu et al. 1999).

2.4.1 Diode-clamped inverter

The concept of a diode-clamped topology was proposed by Nabae et al. (1981). This topology, has high efficiency operation, and used in high voltage applications. One phase leg of a three-level DCC is shown in Figure 2.7(a). It consists of two pairs of switches and two diodes. Each switch pair works in complementary mode with the other pair in order to avoid short-circuiting the DC source, and the diodes are used to provide access to the mid-point voltage. In this representation the label 'S' is used to identify the switches, and switch logic is: 1 = 'on', 0 = 'off'; the switches are insulated-gate bipolar transistors (IGBTs). The DC-link voltage is split into three voltage levels by using a two-series connection of DC capacitors, C_1 and C_2. The two capacitors are supposed to have identical DC voltage ratings, and each voltage stress is limited to one capacitor level through the clamping diodes (D_{c1} and D_{c2}). If it is assumed that the total DC-link voltage is v_{DC}, and that the mid-point is regulated at half the DC-link voltage; then the voltage across each capacitor is $v_{DC}/2$ where $v_{C1} = v_{C2} = v_{DC}/2$. Based on the structure of the DCC, there are three different possible switching states which apply the staircase voltage on the output load relating to the DC-link capacitor voltage value. The switching states of the three-level converter are summarized in Table 2.1. To study the effect of the number of output voltage levels in a diode-clamped topology, the phase legs of a four- and five-level inverter are shown in Figures 2.7(b) and (c) respectively.

Table 2.1: Switching states in one leg of the three-level DCC

Voltage Level	complementary pair no. 1		complementary pair no. 2		Leg voltage (v_{an})
	S_1	S'_1	S_2	S'_2	
1	1	0	1	0	$v_{DC}/2$
2	0	1	1	0	0
3	0	1	0	1	$-v_{DC}/2$

In the case of the five-level inverter, if it is operating at a balanced condition, the DC-link voltage is split in four equal values by the series capacitors, with $v_{C1} = v_{C2} = v_{C3} = v_{C4} = {}^{v_{DC}}/_{4}$. There are five different switching combinations shown in Table 2.2 that can generate five different voltage levels in output leg voltage (v_{an}).

Table 2.2: Switching states in one leg of the five-level DCC

Voltage Level	complementary pair no. 1		complementary pair no. 2		complementary pair no. 3		complementary pair no. 4		Leg voltage (v_{an})
	S_1	S'_1	S_2	S'_2	S_3	S'_3	S_4	S'_4	
1	1	0	1	0	1	0	1	0	${}^{v_{DC}}/_{2}$
2	0	1	1	0	1	0	1	0	${}^{v_{DC}}/_{4}$
3	0	1	0	1	1	0	1	0	0
4	0	1	0	1	0	1	1	0	${}^{-v_{DC}}/_{4}$
5	0	1	0	1	0	1	1	0	${}^{-v_{DC}}/_{2}$

2.4.1.1 Advantages and disadvantages of DCC topology

The primary merits of the DCC topology are the following:

1. The number of capacitors is low compared with other topologies; this reduces the high cost of these reactive devices. Furthermore the capacitors can be pre-charged as a group.
2. This topology does not require a transformer.
3. There is only one DC-link voltage.
4. The change between adjacent states is done, changing only the state of two transistors.

The main negative aspects of DCC topology are the following:

1. The possibilities of controlling the balance of the DC-link capacitors voltage are limited. In fact other topologies, such as the flying capacitor topology, present more possibilities to achieve the balance.
2. The number of clamping diodes required is quadratically related to the number of levels, which can be cumbersome for units with a high number of levels.

DCC topology has become very popular among researchers all over the world, and this has led to the development of other hybrid topologies in the quest to improve converter attributes (Kai et al. 2004; Xiaoming & Barbi 2000; Zhiguo et al. 2004).

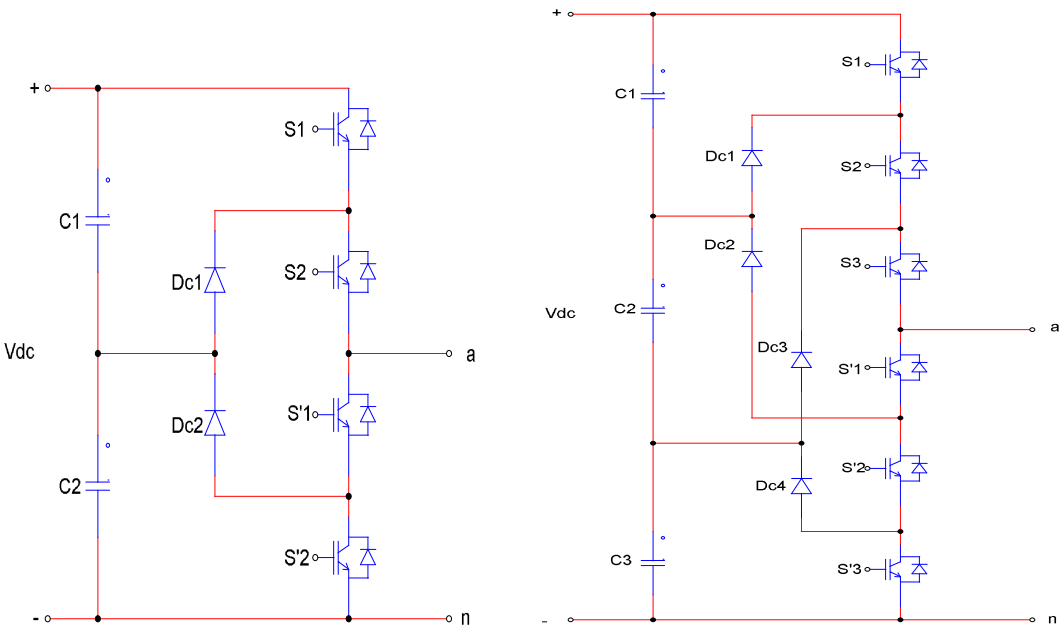

(a) three-level (b) four-level

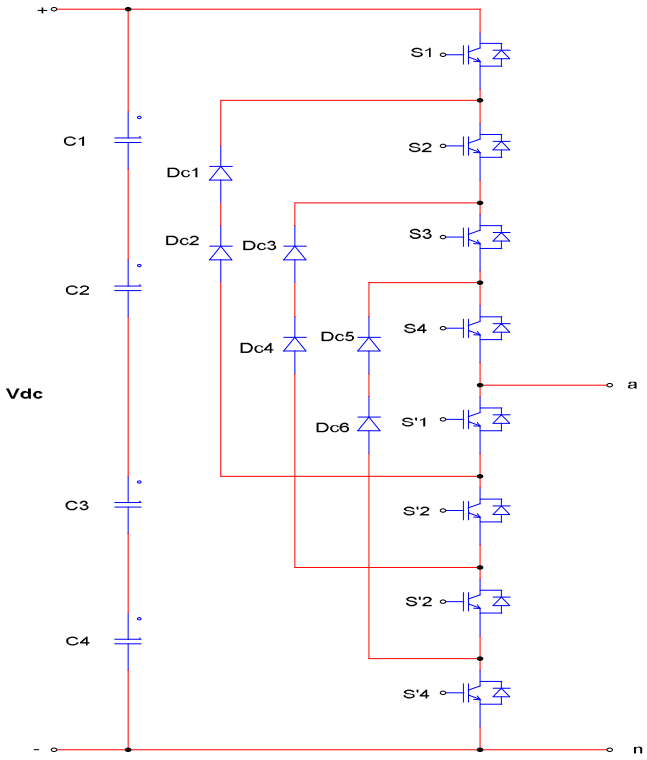

(c) five-level

Figure 2.7: One leg of diode-clamped converter

2.4.2 Flying capacitor inverter

FCMLIs are also called capacitor-clamped inverters. Figure 2.8 shows one leg structure of an FCC inverter. This configuration is an alternative to the DCC; in an FCMLI however, the voltage across an open switch is constrained by clamping capacitors instead of by clamping diodes as in a DCC (Meynard & Foch 1992). Therefore in an FCMLI the use of multiple diodes at the higher voltage levels can be avoided.

By increasing the number of levels, more capacitors are needed (Bum-Seok et al. 1998). If the input DC-link voltage is v_{DC} and the flying capacitor works in balance-condition mode, then in order to have equal step voltages as the output, the clamped capacitor should be regulated at $v_{C1} = {}^{v_{DC}}/_{2}$ in the three-level inverter, and at $v_{C2} = 2v_{C1} = {}^{2v_{DC}}/_{3}$ in the four-level inverter. For an m-level converter the voltage rating of the capacitors in an FCC is ${}^{v_{DC}}/_{\mathrm{m}-1}$. An m-level FCC will consist of $(\mathrm{m}-1)$ DC-link capacitors, with $\frac{(\mathrm{m}-1)\times(\mathrm{m}-2)}{2}$ flying capacitors in each phase leg.

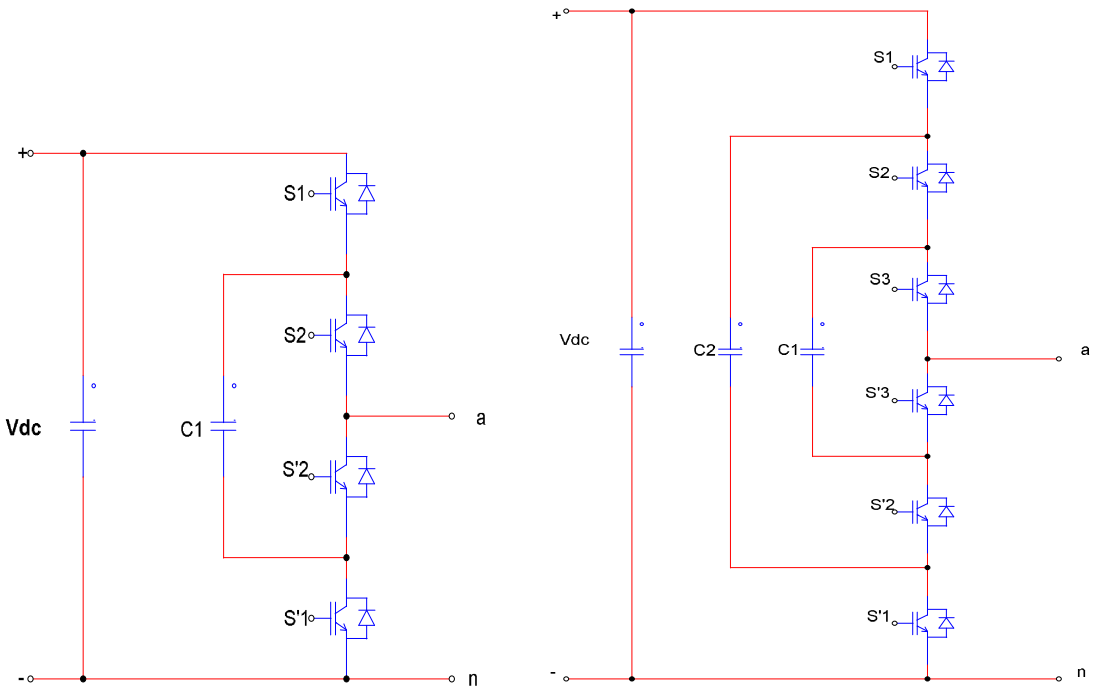

(a) three-level (b) four-level

Figure 2.8: One leg of a flying capacitor converter

Different leg voltage levels, associated with different switching states for respectively three- and four-level FCCs are given in Tables 2.3 and 2.4. It is clear that an additional voltage level is available in the four-level inverter. Although the output voltage levels in an FCC inverter are similar to those in a DCC, there is more than one switching state to achieve a specific level; these are called redundant switching states. These redundant switching vectors give freedom to balance the flying capacitor voltages because they provide different current loops through the capacitors.

Table 2.3: Switching states in one leg of the three-level FCC

Voltage Level	complementary pair no. 1		complementary pair no 2		Leg voltage (v_{an})
	S_1	S'_1	S_2	S'_2	
1	1	0	1	0	$v_{DC}/_2$
2	1	0	1	0	0
	0	1	0	1	
3	0	1	0	1	$-v_{DC}/_2$

Table 2.4: Switching states in one leg of the four-level FCC

Voltage Level	complementary pair no. 1		complementary pair no. 2		complementary pair no. 3		Leg voltage (v_{an})
	S_1	S'_1	S_2	S'_2	S_3	S'_3	
1	1	0	1	0	1	0	$v_{DC}/_2$
2	1	0	1	0	0	1	$v_{DC}/_6$
	1	0	0	1	1	0	
	0	1	1	0	1	0	
3	1	0	0	1	0	1	$-v_{DC}/_6$
	0	1	1	0	0	1	
	0	1	0	1	1	0	
4	0	1	0	1	0	1	$-v_{DC}/_2$

Although this type of converter shares the merits of all MLIs, it does have some problems. One of the main problems is the requirement of a complicated control strategy in order to enable regulation of the floating capacitor voltages (Zare & Ledwich 2008).

2.4.2.1 Advantages and disadvantages of FCC topology

The main benefits of the FCC topology are the following:

1. Using redundant switching configurations, this topology presents more possibilities to control the voltage of DC-link capacitors in comparison to other multilevel topologies.
2. Both real and reactive power flow can be controlled.

3. The large number of capacitors enables the inverter to ride through short duration outages and deep voltage sags.
4. This topology does not require a transformer.

The main drawbacks of FCC topology are the following:

1. The number of capacitors is high compared with other topologies such as the DCC; a very important fact considering the cost of these reactive devices.
2. The change between the state of adjacent switches is achieved by changing the state of one of several transistors. This change increases the number of commutations in the transistors and consequently, the power losses in the converter.
3. The clamping capacitors must be set up at the required voltage levels, so that an initialization of the converter is necessary.

2.4.3 Cascaded H-bridge multilevel inverter

The third topology for the MLC is the cascaded H-bridge inverter, which can be synthesized by a series of single-phase, full-bridge converters. Assuming that the DC voltage of each full-bridge cell is the same and equal to $v_{DC}/2$, then each full-bridge inverter can switch between $-v_{DC}/2$, 0 and $v_{DC}/2$. Therefore, by adding and subtracting the output voltage levels of the two cascaded, full-bridge converter cells, five different levels can be achieved in the output voltage; this is depicted in figure 2.9(a). Switching states associated with different output voltage levels for the cascaded inverter with two full-bridge inverter cells are illustrated in Table 2.5. A three-phase configuration can be easily implemented by the application of three single-phase structures. CHBC configurations have been used for medium and high-voltage RESs applications, such as PV installations (Alonso et al. 2003). A higher level can easily be implemented by adding classical H-bridge cells to this configuration. However, this higher level configuration needs an additional DC voltage source, as well as switching devices, all of which can increase the cost of the system. Every cell added means that two more voltage levels can be achieved in the output voltage, which in turn, can reduce the harmonic distortion. In Figure 2.9(b), a CHBC inverter with three full-bridge inverter cells is illustrated; each cell provides $v_{DC}/3$ of the total input DC voltage, v_{DC}. To achieve two more voltage levels at the output and to reduce the voltage stress on each cell in a cascaded inverter topology, four extra switches and one isolated DC source need to be added. In general, the cascaded converter with n-full-bridge inverter cells can synthesize $(2n + 1)$ voltage levels at the output voltage of each phase structure.

Table 2.5: Switching states of the five-level CHBC

Voltage Level	complementary pair no. 1		complementary pair no. 2		complementary pair no. 3		complementary pair no. 4		Leg voltage (v_{an})
	S_1	S_2	S_3	S_4	S_5	S_6	S_7	S_8	
1	1	0	0	1	1	0	0	1	v_{DC}
2	0	1	0	1	1	0	0	1	$v_{DC}/2$
	1	0	0	1	0	1	0	1	
	1	0	0	1	1	0	1	0	
	1	0	1	0	1	0	0	1	
3	0	1	0	1	0	1	0	1	0
	0	1	0	1	1	0	1	0	
	0	1	1	0	1	0	0	1	
	1	0	0	1	0	1	1	0	
	1	0	1	0	0	1	0	1	
	1	0	1	0	1	0	1	0	
4	0	1	0	1	0	1	1	0	$-v_{DC}/2$
	0	1	1	0	0	1	0	1	
	0	1	1	0	1	0	1	0	
	1	0	1	0	0	1	1	0	
5	0	1	1	0	0	1	1	0	$-v_{DC}$

2.4.3.1 Advantages and disadvantages of cascaded converter topology

The main advantages of the CHBC converter topology are the following:

1. This topology is based on basic cells (full-bridge converters) connected to each other, so it is modular, facilitating easy expansion, and the controller can be distributed, which makes for a simpler controller structure than either of the two previously discussed topologies.
2. This type of converter is commercially produced by companies such as ABB and Semikron. Therefore, the cost of using this type of converter is lower compared to other topologies that are completely custom made.

The main drawback of the CHBC converter topology is that:

1. To date this topology has not been applied at low power levels because of the need to provide separate, isolated DC supplies for each full-bridge converter element.

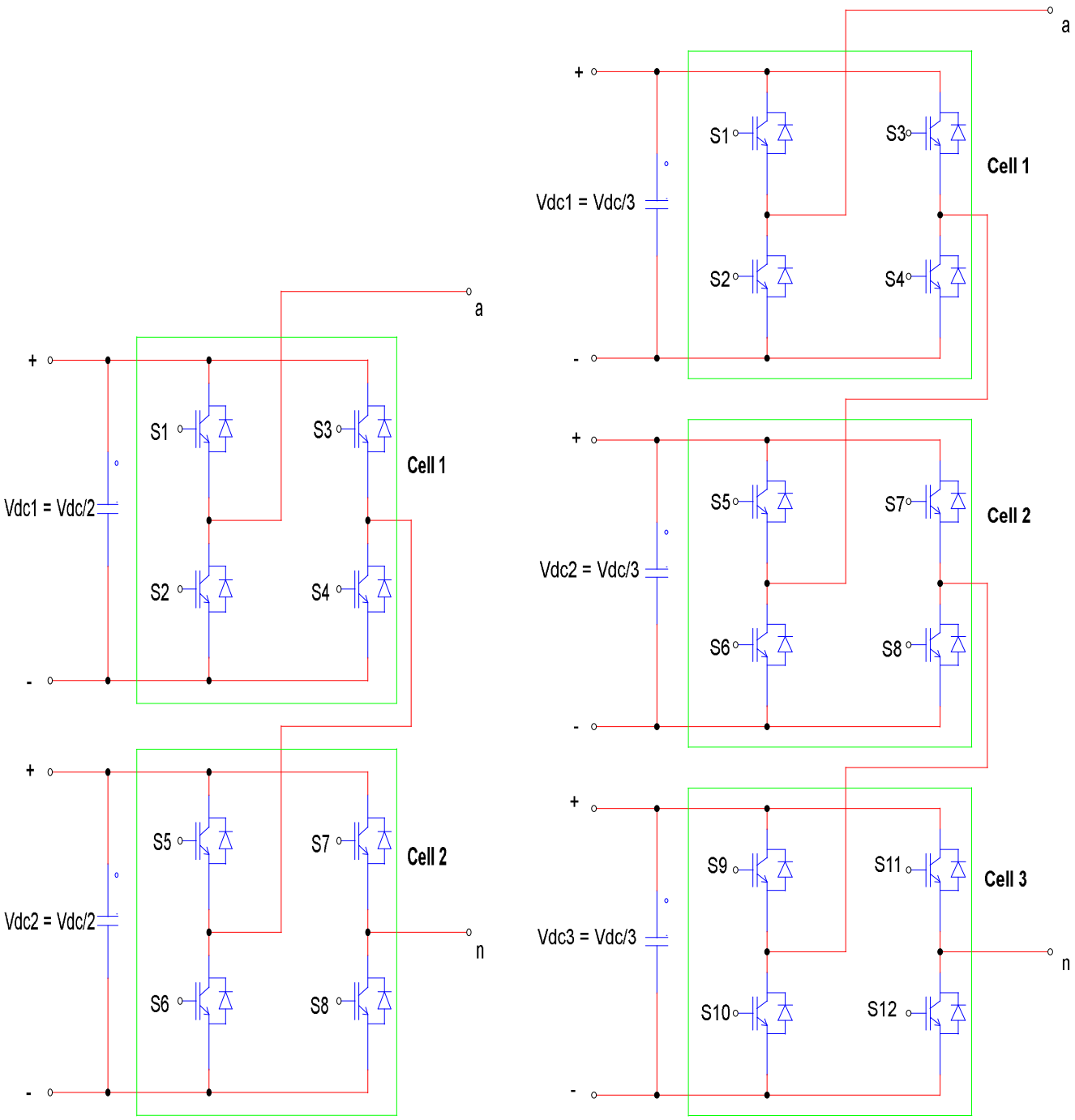

(a) five-level

(b) seven-level

Figure 2.9: One leg of cascaded H-bridge multilevel inverter

2.4.4 Generalized multilevel topology

Existing MLCs, such as diode-clamped and capacitor-clamped MLCs, can be derived from the generalized converter topology called P2 topology, as proposed by Peng (2001) and illustrated in Figure 2.10. For any number of levels, the generalized MLC topology can automatically balance each voltage level, regardless of load characteristics, whether active or reactive power conversion occurs, and without any assistance from other circuits. Thus, the topology provides a complete multilevel topology that in principle embraces the existing MLCs.

The P2 MLC structure per phase leg is shown in Figure 2.10. The voltage of each switching device, diode, and capacitor is $1v_{DC}$. Any converter with any number of levels, including the conventional bi-level converter, can be obtained using this generalized topology (Peng 2001; Rodríguez et al. 2002).

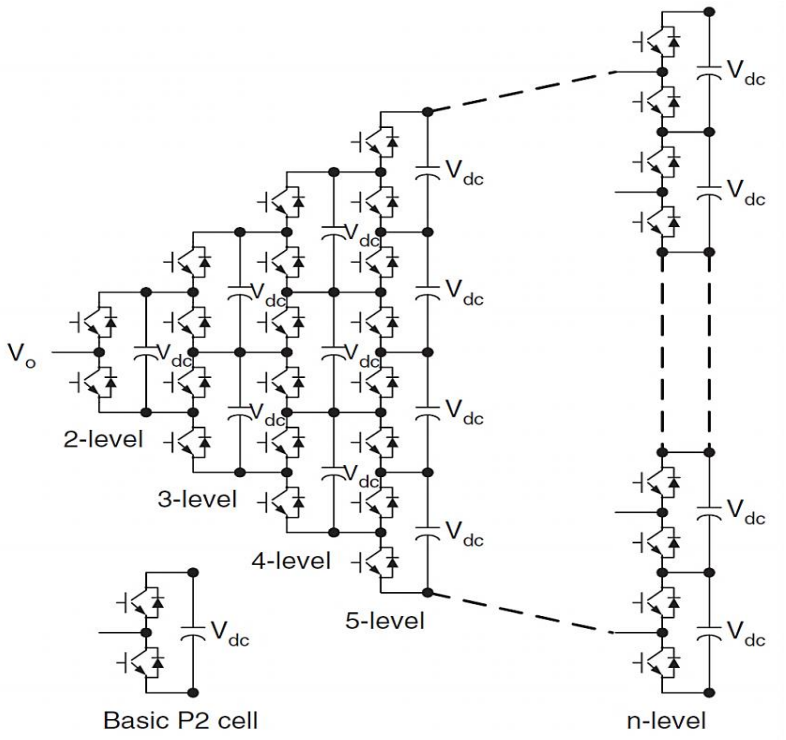

Figure 2.10: Generalized P2 MLC topology for one phase leg

2.4.5 Mixed-level hybrid MLC

Replacing the full-bridge cell in a CHBC with MLCs, diode-clamped converters, or flying capacitor converters, is an option for reducing the number of individual DC sources as used in high-voltage, high-power applications; this according to Hill and Harbourt (1999). A typical mixed-level hybrid topology to increase the voltage levels, is shown in Figure 2.11; the nine-level CHBC incorporates a three-level DCC as the cell. Four individual DC sources for one-phase leg, and twelve such sources for a

three-phase converter were needed in the basic CHBMLIs; the voltage level is effectively doubled for each cell when a five-level converter is substituted for a full-bridge cell. Therefore, one-phase leg requires just two individual DC sources, and a three-phase converter requires six for such sources, so as to also produce nine voltage levels per phase. Because the converter incorporates multilevel cells as its basic unit, the structure of the CHBC has mixed-level, hybrid multilevel units. Although this topology has an advantage in that it requires fewer independent DC sources. It also has a disadvantage as it requires complicated control because of its compound configuration.

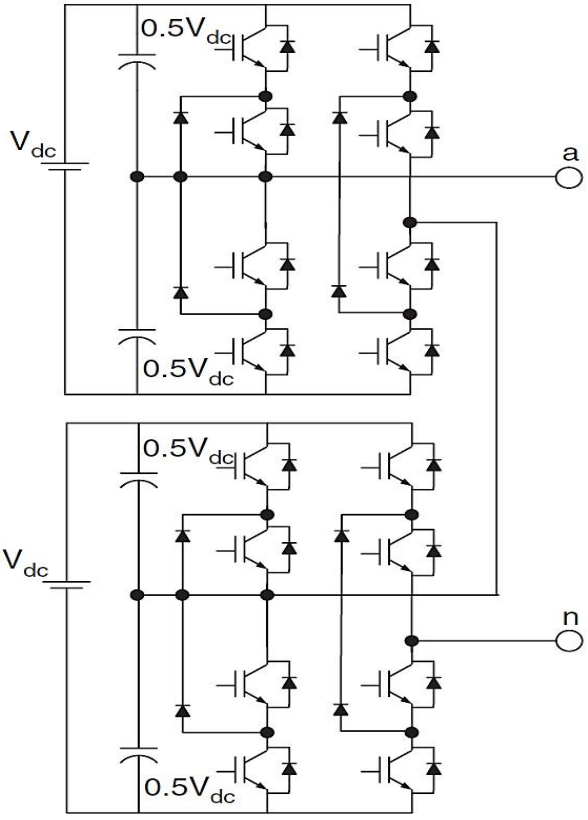

Figure 2.11: Mixed-level hybrid unit configuration using a three-level DCC

2.4.6 Soft-switched MLC

Some soft-switching methods can be incorporated in different MLCs to reduce switching loss and increase efficiency. For the CHBC, because each converter cell is a bi-level circuit, the implementation of soft switching is not all different from that of conventional bi-level converters. For capacitor-clamped or diode-clamped converters, soft-switching circuits have been proposed with different circuit combinations. One

such circuit combination is a zero-voltage soft-switching circuit which includes an auxiliary resonant commutated pole (ARCP), a coupled inductor with zero-voltage transition (ZVT) and their combinations (Fang & Ye 2013:581; Rodríguez et al. 2002; Song & Lai 2001); a zero-voltage switching circuit incorporated in a capacitor-clamped converter is shown in Figure 2.12.

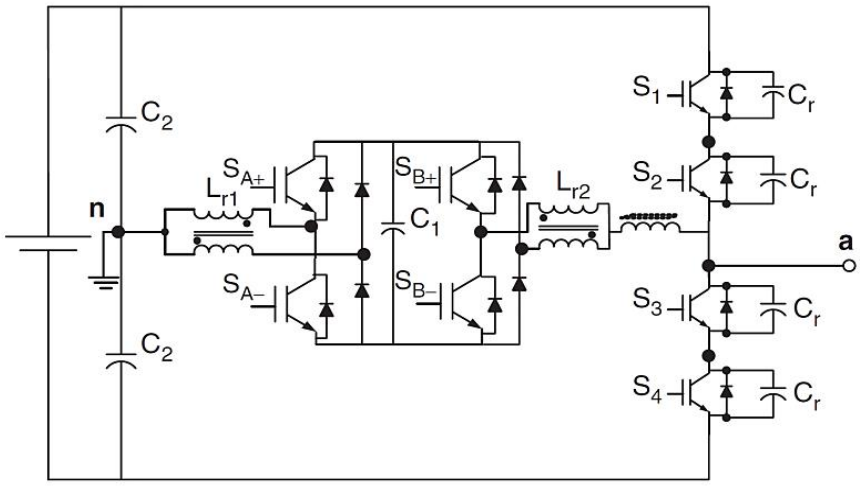

Figure 2.12: Zero-voltage soft-switching capacitor-clamped converter circuit

2.4.7 Back-to-back diode-clamped converter

Two MLCs are connected in a back-to-back configuration, thereby constructing a back-to-back DCC; the combination is then incorporated into the electrical system in the series–parallel assembly shown in Figure 2.13. The voltage supplied to the load and the current required by the utility, can be controlled concurrently. For applications in electrical distribution systems, the series–parallel active power filter has been hailed as a generally-applicable power conditioner in several literature sources (Fujita & Akagi 1998; Jeon & Cho 1997; Kamran & Habetler 1995, 1998; Moran & Joos 1998; Muthu & Kim 1997; van Zyl et al. 1996). Likewise, applied at the transmission level, it has also been acclaimed as a universal power flow controller (Chen et al. 1997(a); Enslin et al. 1996; Fujita et al. 1998; Gyugyi 1994; Gyugyi et al. 1995). Earlier, it had been suggested that the back-to-back diode-clamped topology, shown in Figure 2.14, is suitable for application as a high-voltage DC interconnection linking two asynchronous AC systems or in high-voltage motors as a rectifier/inverter for an adjustable-speed drive (Lai and Peng 1996).

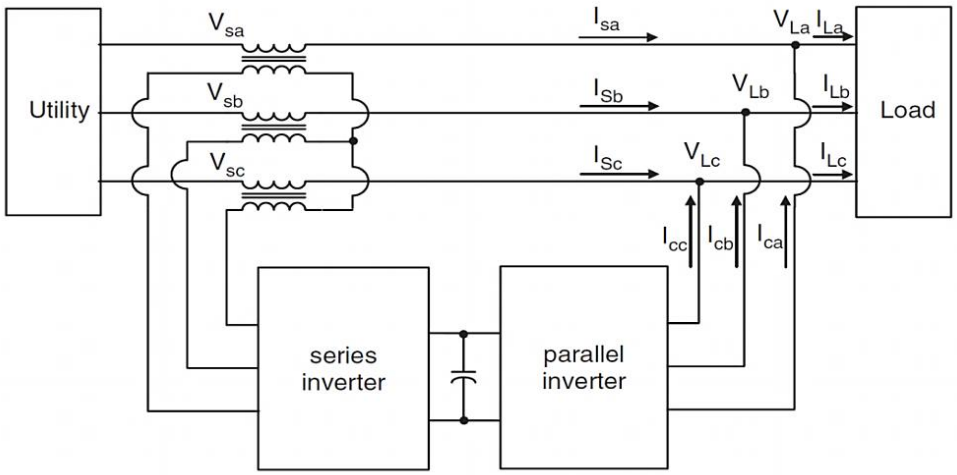

Figure 2.13: Series–parallel connection to electrical system of two back-to-back inverters

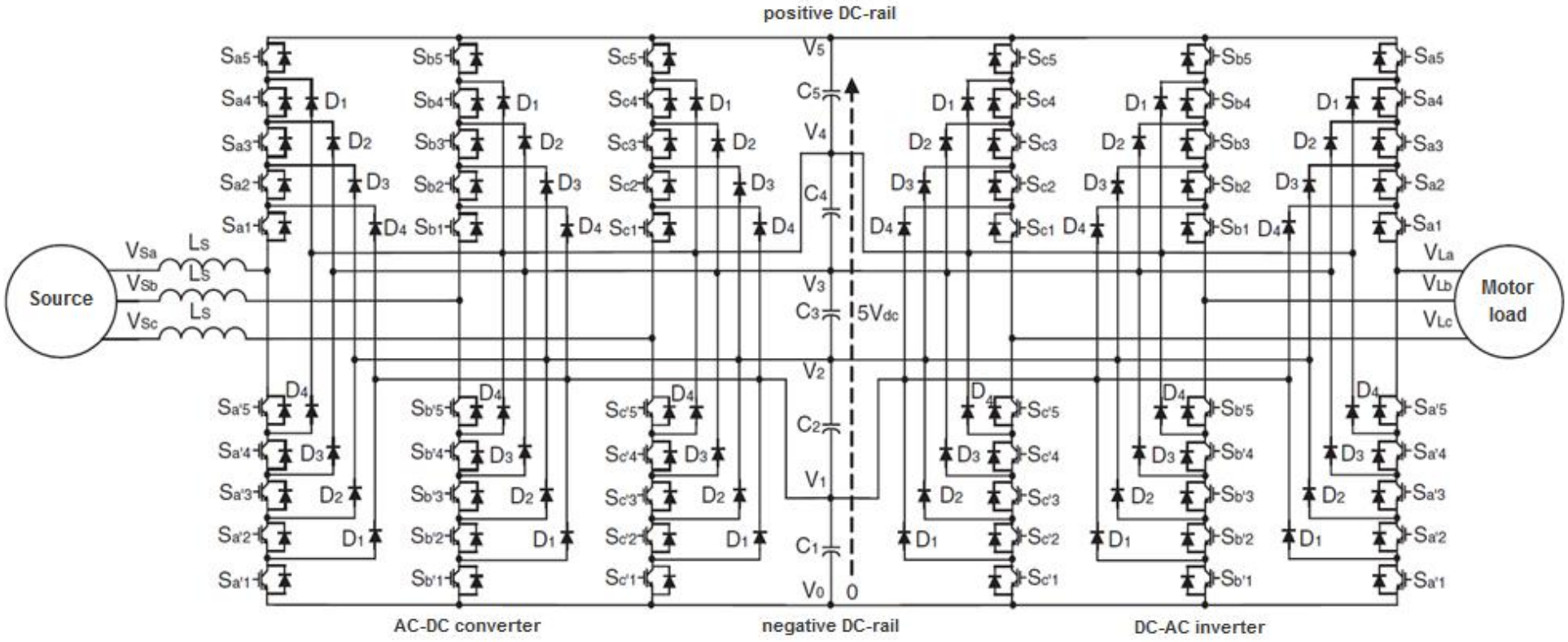

Figure 2.14: Six-level diode-clamped back-to-back converter structure

2.5 Comparison of multilevel topologies

Despite the choice of a multilevel topology being governed by the application and the specifications, usually a reduction in the number of components plays the most important role in minimizing power losses, unit size and costs. Therefore, to provide some guidelines for selecting the applicable multilevel topology, the number of semiconductors and passive components required by the most promising topologies is summarized in Table 2.6.

For a three-level approach, the analysis shows that the DCC, FCC and CHBC all require the 12 switches; however, they differ in the number of clamping elements and DC sources needed. For applications where only one DC source is available, the DCC and FCC topologies have advantages over the cascaded H-bridge system, which requires a complex transformer to provide the various independent DC sources. On the other hand, when multiple DC sources are available, the CHBC topology might be considered a reasonable solution since it requires the least number of components.

The high number of clamping elements adds to the complexity of balancing the DC-link and the flying capacitors. In this case it limits the use of DCC and FCC converters to more than three levels.

Table 2.6: Comparison of the multilevel topologies in terms of numbers of components and isolated DC sources

Topology	Levels	Switches[1]	Clamping Diodes[2]	Floating Capacitors	DC-link Capacitors	Isolated DC sources
Diode clamped converter (DCC)	3	12	6	0	2	1
	5	24	36	0	4	1
	m	$6(m-1)$	$3(m-1)(m-2)$	0	$m-1$	1
Flying capacitor converter (FCC)	3	12	0	3	2	1
	5	24	0	18	4	1
	m	$6(m-1)$	0	$\frac{3}{2}(m-1)(m-2)$	$m-1$	1
Symmetric cascaded h-bridge converter (CHBC)	3	12	0	0	3	3
	5	24	0	0	6	6
	m	$6(m-1)$	0	0	$\frac{3}{2}(m-1)$	$\frac{3}{2}(m-1)$

[1] Switches with anti-parallel diodes.
[2] Series connection for same blocking voltage stress.

2.6 Voltage balancing depending on the MLC topology

MLCs present several advantages when compared to classical two-level converters (Lai & Peng 1996; Teodorescu et al. 1999). They improve the harmonic content of the output signals, and they accept a power increase in the DC-link due to its voltage that can be shared between more transistors. The disadvantages of MLCs are an increase in control and implementation complexity. Recently the control complexity has been reduced by the availability of new and powerful microprocessor systems (Rodríguez & Cortés 2012; Texas Instruments 1995; Xilinx 2014). The balance of the voltage of the DC-link capacitors is one of the most important drawbacks of this type of converter topology. If any imbalance in the voltage of DC-link capacitors appears, the output phase voltages show distortion, and the increased harmonic content of the output signals will cause a decrease in power quality. In fact, if the switching controls are not selected with care, and a suitable control algorithm is not implemented, the problem immediately appears and the voltage of the DC-link capacitors will be unbalanced. In this study, control strategies to balance the voltage of the capacitors of MLCs are presented. The balancing control algorithms proposed in this thesis have been developed to prevent a voltage imbalance in the current that flows through either the DC-link of the DCC, or the flying capacitors of FCC, should such an imbalance threaten. To solve the voltage balancing problems for both the DCC and FCC, a hysteresis-based, voltage balancing algorithm is presented. Hysteresis-based predictive control aims to keep the capacitor voltages of the capacitors within the desired boundaries. It is important to note that the proposed methods are completely generalized, and as a result they are independent of the load and the number of levels of the converter.

2.6.1 Diode-clamped converter topology

In a multilevel DCC configuration, and depending on the topology of the MLC, the voltage values of the DC capacitors will change; it is required that the DC-link capacitors equally share the DC-link voltage (Nabae et al. 1981). In Figure 2.15 a three-level DCC topology is shown with capacitors C_1 and C_2 sharing the DC-link voltage. Different methods of balancing DC voltages have been developed, some of which have been presented by Grzesiak and Tomasik (2007), Pan and Peng (2009) and Peng et al. (1995). A simple, albeit expensive, solution to the voltage imbalance problem is to use a back-to-back topology and then to control the switching angles of the rectifier and inverter independently (Pan et al. 2005). This approach depends on the operation of a symmetrical back-to-back converter, where the rectifier and inverter compensate each other when a specific voltage level of the DC-link is overcharged.

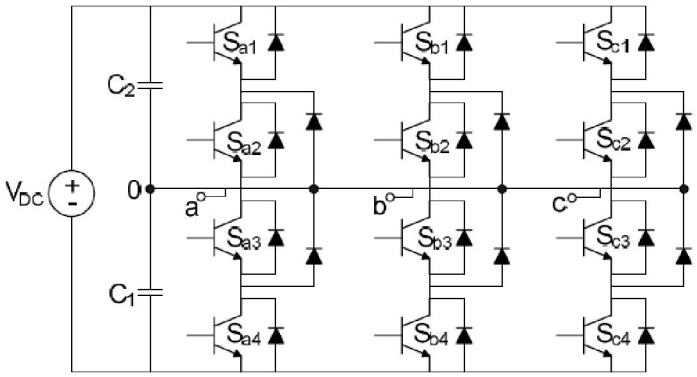

Figure 2.15: Three-level diode-clamped converter

For instance if the rectifier overcharges a predetermined voltage level, the inverter will discharge that level. The resultant charging and discharging for each voltage level can be regulated to be zero; this is effected by controlling the switching angles, θ_1 and θ_2, by which the output and input voltage levels are changed. The switching angles are shown in Figure 2.16. Both the rectifier and inverter voltages are in part defined by these angles, and they can be monitored and adjusted.

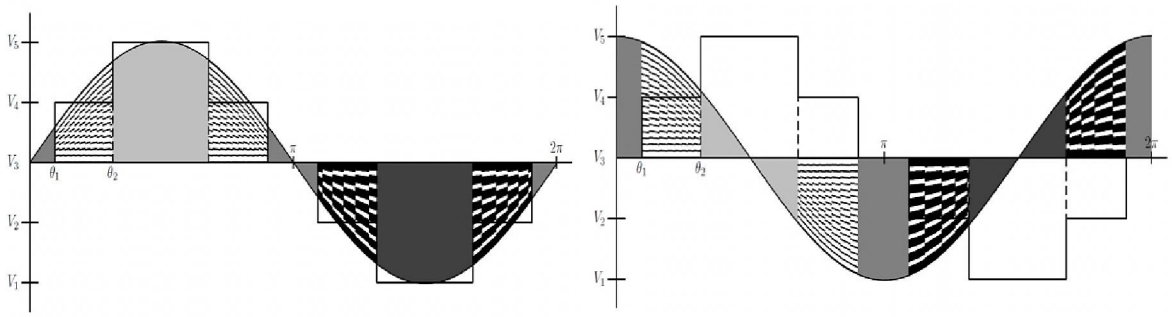

(a) Current in phase with voltage (b) Current 90° leading with respect to the voltage

Figure 2.16: Currents flowing into capacitor junctions

To balance the DC-link capacitor voltage of a three-level DCC, a hysteresis-based, voltage balancing algorithm is presented in this thesis. Hysteresis-based predictive control aims to keep the capacitor voltages within the desired boundaries. The proposed control predicts the outcome of the capacitor voltages for all the possible control inputs and then selects the cost function that will keep the controlled variables within the desired boundaries for the longest possible time. After the optimum voltage vector for the next sampling cycle has been determined, the optimum switching state, which produces this voltage vector, has to be found and applied. The two capacitor voltages of the DC-link have to stay within a certain hysteresis band with boundaries

on either side of $^{v_{DC}}/_{2}$. Chapter four presents an in-depth study of the calculation of these steps.

2.6.2 Flying capacitor converter topology

In multilevel FCC topology, each flying capacitor voltage value is different (Meynard & Foch 1992). For instance, a three-phase, three-level FCC is represented in Figure 2.17, showing the flying capacitor voltages. The structure of an FCC does not require a split DC–link voltage, such as a DCC does. Therefore, there are no junction currents between the DC-link capacitors that will unbalance their respective voltages. However, for the three-level converter it is very important that the voltages across the flying capacitors be half the DC-link voltage. Different level converters will have differing numbers of flying capacitors, each at a different voltage. If these voltages become unbalanced, the clamping mechanism will not function correctly and the danger of exposing some switches to over-voltage arises. As was explained in Section 2.4.2, some of the voltage levels that need to be produced can be generated by more than one switching state.

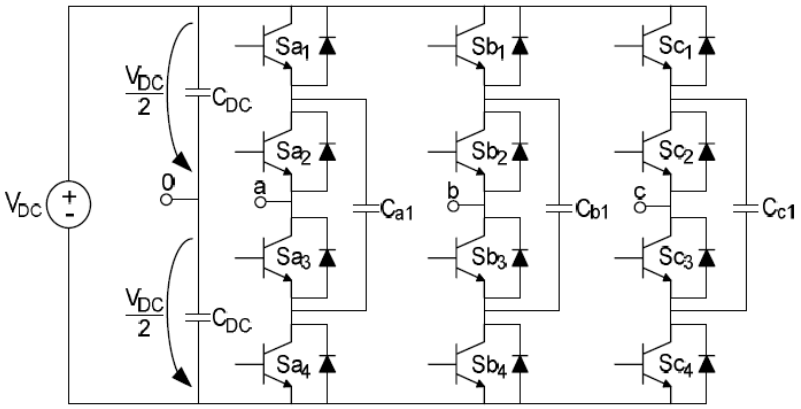

Figure 2.17: Three-phase, three-level FCC

In FCCs, failure of a natural balance control of the capacitor voltages under certain conditions (Defay et al. 2010; Feng et al. 2007; Khazraei et al. 2012), has created a move toward an autonomous control method (Clos et al. 2005; Defay et al. 2010; Escalante et al. 2002; Feng et al. 2007; Khazraei et al. 2010). In this autonomous voltage control strategy, the capacitor voltages are measured, and a control strategy uses these measurements, as well as the values of the reference signals and knowledge about the system, to define the switching logics that are subsequently applied. As pointed out in Srikanthan et al. (2009), the different control strategies have evolved alongside with the development of the multilevel power converter

topologies. Various independent control mechanisms exist, and these can be divided into two groups. The one group uses separate controllers for each controlled system variable, mostly with an inner loop for the control of the voltages of the flying capacitors. The other group uses a single controller for all the controlled system variables at the same time. Some representative examples of these types of control systems are represented as follows:

i. First group of controllers

A typical example of the first group of control strategies is a system where a proportional-integral-derivative (PID) controller controls the load current (or another load parameter) and generates an input for a PWM scheme in the form of a voltage command. An inner loop controller uses the obtained output voltage level from the PWM, together with the voltage measurements of the flying capacitors, to select an appropriate switch state; this is done in an attempt to bring the capacitor voltages to a more balanced state.

One such way to choose between the redundant switching states was presented by Shukla et al. (2007); their control scheme is shown in Figure 2.18. The desired PWM technique is input at the carrier and the reference; for example, a sinusoidal wave is input at reference. For each flying capacitor, a reference exists from which the measured voltage is subtracted.

The comparators determine whether the voltage of the flying capacitors should either be increased or decreased. The control law receives the switching state input from the reference and carrier comparison and uses the flying capacitor voltage comparisons to choose between the appropriate redundant switching states. The corresponding switching signals are then produced by the gating circuit.

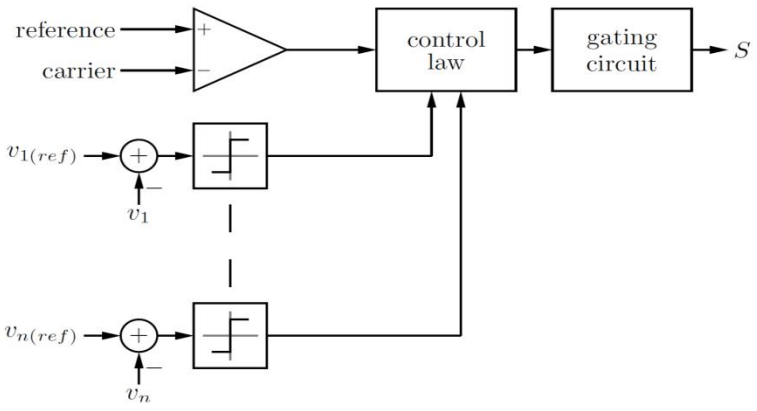

Figure 2.18: Control strategy for voltage balancing of flying capacitor voltages

ii. Second group of controllers

The second group of control strategies attempts to control all the system variables at once. This strategy permits decision on a future switch state using all information available. Predictive controllers are a typical example of such controllers. The influence of all possible future switch states on the system variables is predicted. The controllers using a model for the predictions are referred to as model predictive controllers, and they incorporate an MPC system. A cost function, which describes the cost corresponding to the predicted values of the system variables, is used to evaluate the possible future switch states and select the best option. This selected switch state is then applied to the converter, and a new iteration of the prediction method is started.

An alternative to the PWM scheme is to use a hysteresis-based predictive control scheme (Shukla et al. 2008). The controller selects the n possible voltage levels that the inverter can produce in order to attempt to force the output current error to zero. When the current error exceeds the defined hysteresis limit, the next higher (or lower) voltage level should be selected.

The hysteresis-based predictive control scheme is used in this thesis. This algorithm is proposed for DC-link capacitor and flying capacitor voltages and an in-depth study of this control scheme is presented in Chapter four and Chapter five respectively. This algorithm will keep the DC-link capacitor voltage and flying capacitor voltage within acceptable limits in relation to their reference values. The proposed control algorithms are based on the calculation of the currents that flow through floating capacitors; these currents depend on the instantaneous state vector applied to the MLC. The knowledge of the expressions of these currents and the voltages of the unbalanced capacitors form the basis of the balancing control algorithms.

2.7 Software simulation integration in enhancing engineering design in power conversion studies

There are various software applications available to analyse power electronic devices and circuits. These programs enable the designer to view and assess semiconductor switching characteristics, and they provide accurate information on the behaviour of power electronic circuits with regard to properties like voltage, current and harmonic distortion. Many studies mainly use languages like SPICE (Simulation Program with Integrated Circuit Emphasis) and ACSL (Advanced Continuous Simulation Language). These programs are useful in detailed design studies where time-domain

analysis is necessary for predicting circuit performances in detail (Bose 1997; PSPICE 1996).

In the last two decades, simulation tools have made a significant contribution to the rapid progress in the development of power electronic systems. Computer simulation can greatly aid in analysis, design and education in the field of power electronics and its applications. PSIM and MATLAB are the most commonly used software packages available for the simulation of power electronic systems (Almaktoof et al. 2014; Rodríguez & Cortés 2012). PSIM is a simulation software application specifically designed for power electronic systems (Boscaino & Capponi 2011; PSIM® User's Guide 2014). With fast simulation and a user-friendly interface, PSIM provides a powerful simulation environment for studies in power electronics, control systems, and motor-drive systems (Boscaino & Capponi 2011; PSIM Software 2006). MATLAB is one of the most popular software packages used in control systems, and MATLAB/Simulink is highly suited for dynamic system simulation because of the many toolboxes and modules available for use within the platform. In using MATLAB/Simulink to simulate electric circuits, the program was found to be awkward and cumbersome; this was especially so for power electronic circuits using Simulink (Boscaino & Capponi 2011).

The SimCoupler module allows designers of power electronics to simulate control in the MATLAB/Simulink environment (Boscaino & Capponi 2011; PSIM Software 2006); it thus further enhances the control simulation capability of PSIM by providing access to numerous Simulink toolboxes for various applications. For example, one can achieve automatic code generation with the PSIM-MATLAB/Simulink for SSI. First, the power circuit is simulated in PSIM, and the control algorithm is simulated in MATLAB/Simulink. Then Simulink toolbox and supporting resources can be used to generate production quality code automatically for a target platform. Figure 2.19 depicts how the SimCoupler module provides an interface between PSIM and MATLAB/Simulink for SSI.

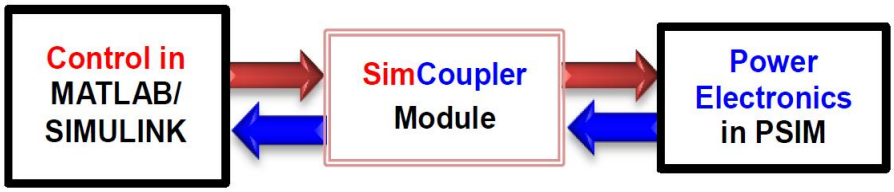

Figure 2.19: The SimCoupler module provides interface between PSIM and MATLAB/Simulink

2.8 Application of MLCs in RESs

Nowadays, the electrical power generation from renewable energy sources has become a focal point in research because of environmental problems and a reduction of the availability of sufficient traditional energy sources in the not too distant future. Since the last decade, researchers have been working on electrical systems for variable wind turbines. The major merits of variable-speed turbines are noise reduction, maximum power tracking, and proper controlled torque. With variable wind turbines, it becomes possible to dampen resonance and to avoid speeds causing resonance. Several electrical systems have been presented for the connection of a wind turbine with variable speed and frequency, to the constant voltage and frequency of a network. The main aspects of these topologies are: an increased efficiency and robustness, a decrease in the size and maintenance of the system, and eventually a reduction of the whole system cost.

It is increasingly recognized worldwide that grid-connected PV systems, which are currently mainly single-phase PV systems, are making a growing contribution to clean power generation. The main advantages of PV systems are their long lifespan, high efficiency and environmentally-friendly footprint. The most important issues for the wide acceptance of grid-connected PV systems are reliability and low cost. There are two approaches to achieve a high voltage and high efficiency. One approach is to connect the cells in series to generate high-voltage DC and then to use a high-voltage DC–AC inverter circuit. However, this configuration needs a high voltage rating for the inverter. The other approach is to use low voltage devices for the inverter, and then to step up the voltage using transformers; this can increase the losses and cost of the system. Using transformerless concepts is beneficial because of the high efficiency and the resulting benefits of a reduction in cost, size, weight, and complexity when using an inverter as opposed to a transformer.

Another renewable energy source is fuel cells, which are considered attractive for distributed generation (DG) applications. Fuel cells are electrochemical devices that convert the chemical energy of fuel and an oxidant, directly to electrical energy and heat. In fuel cell powered applications, a low-power fuel cell will supply the system. The low voltage from the fuel cell is boosted to a high voltage via a DC–DC converter, and this high voltage is then supplied to the DC-link. Thereafter a DC–AC inverter is used to obtain an AC voltage to feed the load.

In some high-voltage, high-power wind turbine or PV systems, if protection is not a big issue, MLIs are a suitable configuration in transformerless, grid-connected systems (Lopez et al. 2006). MLCs synthesize a higher output voltage than the voltage rating of each switching device, so that they can provide a direct connection of RESs applications to the grid. Even in grid-connected systems with a transformer,

MLIs are suitable topologies due to low THD and low voltage stress, which minimise electromagnetic interference (EMI); also, switching losses in MLI topologies are greatly reduced when compared to traditional converters. In addition, the above advantages will lead to a reduction in the cost and size of the output filter in the systems based on MLCs. The attractive features of MLC applications in wind turbine and PV systems are explained in the following sections.

2.8.1 Variable-speed wind turbine systems

A wind-driven generator is the power source in this topology; the generator is essentially a synchronous or an induction machine. The topology for processing and delivery of the power from the source, consists of a rectifier fed by the generator, which is connected to a DC-link, which in turn is connected to an inverter outputting to the load or grid; this is depicted in Figure 2.20.

The two primary aims of this type of system are to extract the maximum amount of power from the wind available and to transfer high quality electricity to the load or grid. A power electronic converter in this topology can be constructed in one of two ways: a diode rectifier with a boost chopper converter connected to a PWM inverter, or two bidirectional PWM-Voltage source inverters (VSIs) connected back-to-back (Carrasco et al. 2006). Aligned with its aims, this type of system facilitates control of active and reactive powers of the power source, while processing by the power converter results in the harmonics of current waveform being reduced. To reap the benefits of MLIs in such a scheme, Beuno et al. (2008) suggested that inverters at the front- and back-end be utilised, based on the DCC converter because it shares the DC-link in its structure.

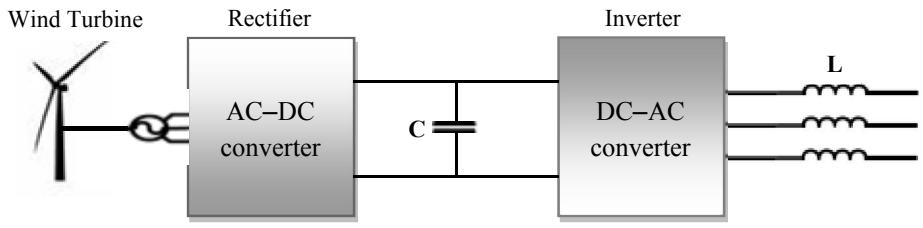

Figure 2.20: Power conversion in wind turbine systems using back-to-back configuration

An alternative to the power conversion system for a wind turbine using an induction machine, is to use a synchronous or permanent magnet generator as shown in Figure 2.21. The power converter on the generator side is replaced by an AC–DC rectifier connected to a step-up DC–DC converter. This is a low cost configuration when

compared with the back-to-back topology. As the wind energy is variable, the step-up converter is responsible to increase the rectifier voltage to the DC-link voltage of the inverter. Also, this structure can provide transformerless connection systems due to the regulation of the DC level voltage using a boost converter. Based on back-to-back configuration, using MLCs for medium- and high-voltage applications has favouarable aspects, considering that MLCs can increase the voltage without increaseing the voltage rating of the switching components (Alepuz et al. 2006).

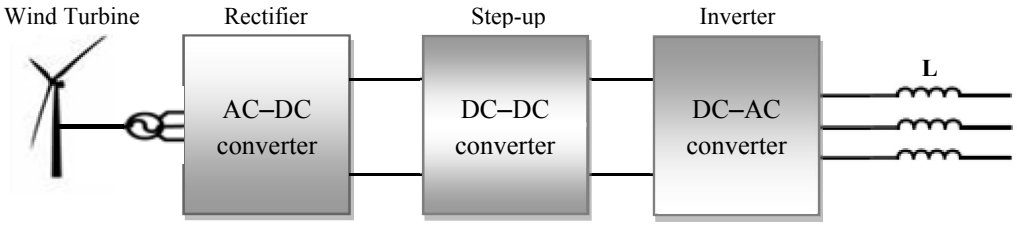

Figure 2.21: Power conversion in wind turbine systems using a rectifier and step-up converter

2.8.2 Photovoltaic systems

PV systems are mostly used in single-phase residential applications, with or without grid connection systems. The main advantages of these systems are their long lifespan, high efficiency, and low environmental impact. As the output voltage of PV panels is a low DC voltage, one approach to power conversion in this type of system, is to use a low voltage inverter and then increase the AC voltage using transformers. However, this approach can increase losses and also the cost of the system.

An alternative power connection topology illustrated in Figure 2.22, utilises a DC–DC boost converter to generate a high DC voltage for an inverter DC-link, which necessitates a high-voltage DC–AC inverter. This imposes the requirement of a high voltage rating for switching devices. To address this problem, MLCs such as DCC and FCC are good candidates for this configuration because they can increase the number of voltage levels without increasing the voltage rating of power components in a DC–AC inverter (Myrzik 2003; Sharma & Hongwei 2006). A configuration consisting of a single-phase PV system with a CHBC is shown in Figure 2.23. The DC–DC converters are responsible for boosting the low input voltage and a CHBC can synthesize a high AC voltage by adding inverter cell output voltages. As mentioned before, a CHBC is a suitable topology for this kind of application, as it needs a separate DC voltage. However, DCC and FCC structures can be utilised in this configuration only if DC-link capacitor voltage and flying capacitor voltage imbalances can be solved (Nami et al. 2008; Pulikanti 2012; Warszawska 2012).

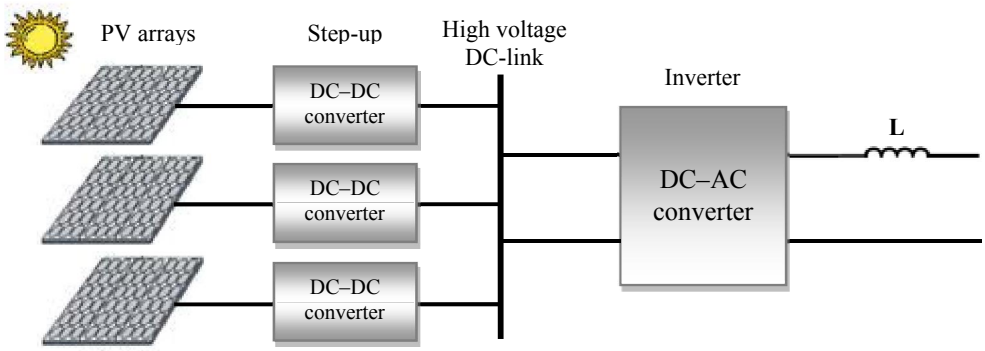

Figure 2.22: Power conversion in transformerless PV systems

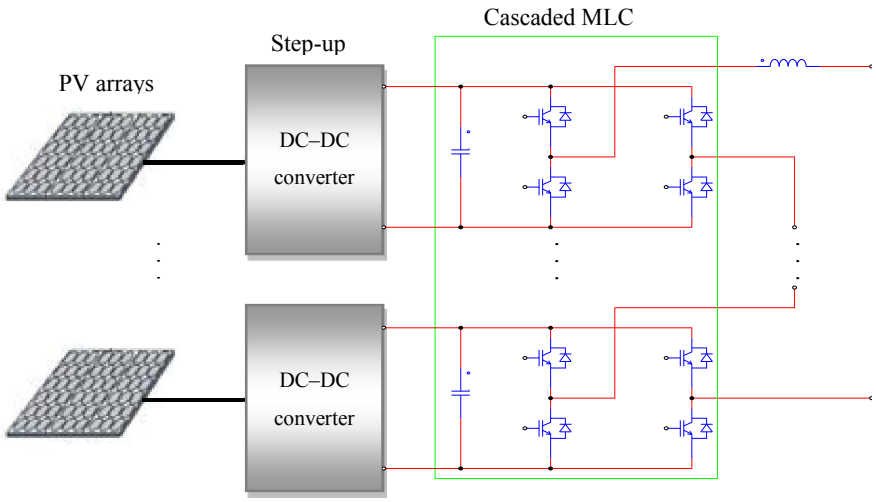

Figure 2.23: MLC in transformerless PV systems

2.9 Summary

In this chapter the state-of-the-art of MLC technology and its applications, were expounded on. At the start of the chapter, an introduction to power electronic converters was presented. The fundamentals and concepts of MLC structures were outlined, as well as the advantages and disadvantages of each type of converter. Next, a comparison of the most promising multilevel topologies was presented in terms of the number of components and isolated DC sources. Following this section, voltage balancing problems as related to the MLC topology, were highlighted. In this chapter, current and more practical industrial applications of MLCs as used in RESs, were addressed with specific emphasis on the use of MLCs to interface with PV and/or wind turbine resources. It should be noted that not all multilevel power converter related applications could be covered in this chapter; however, the basic principles of the different MLCs have been methodically discussed.

CHAPTER THREE

PREDICTIVE CURRENT CONTROL TECHNIQUES FOR POWER CONVERSION

3.1 Introduction

Initially, the linear PID-controllers used in electric drive technology, were mostly built with analog operational amplifiers and used the control deviation in order to generate an actuating signal. With the availability of inexpensive microcomputers and the development of digital control techniques in drive technology, the idea originated to pre-calculate the behaviour of a plant by means of a mathematical model, and determine optimum values for the actuating variables from these pre-calculated values (Linder et al. 2010:17).

The first predictive controllers could only be applied to relatively slow processes such as those in the chemical (Emeljanov 1969) and process engineering fields (Antwerp & Braatz 2000; Eaton & Rawlings 1992); because these controllers were slow and not very powerful. However, the development of digital controllers in recent years has made them more efficient and powerful enough for implementation in accelerated, more complex production schemes. Furthermore, power electronic converters are well adapted for predictive control methods because of their discrete nature which is the result of their individual switching states. The first ideas for predictive control methods were published in the 1960s by Emeljanov (1969).

Many predictive control algorithms that are fundamental for drive technology, like direct torque control (DTC) (Aaltonen et al. 1995; Takahashi & Noguchi 1985), and predictive current control (Holtz & Stadtfeld 1983), were developed in the decades following the 60s. However, further publications relating to the control of the armature current of DC drives with the help of line-commutated converters (Holtz & Schwellenberg 1982; Kennel 1984) decreased significantly. More publications about predictive drive control appeared in the late 1990s. For instance, Purcell and Acarnley (1998) published extensions and improvements of known control methods, while other authors (e.g., Flach 1999; Trzynadlowski et al. 1999) published completely new control strategies. But ultimately most of these methods turned out to be only further enhancements or combinations of already-published fundamental predictive control strategies. Hence, it makes sense to point out the basic functional and fundamental principles of predictive control strategies first.

The main characteristic of predictive control is the use of a model of the system for predicting future behaviour of the controlled variables. This information is used by the controller in order to obtain the optimal actuation, according to a predefined optimization criterion.

Section 3.2 of this chapter presents an introduction to predictive control techniques for power conversion, and also discusses the functional principles of the different control methods based on predictive control. An FS-MPCC approach for the control of a power converter is presented in Section 3.4. Next, the parameters used in model

predictive control are presented. The modelling parameters of the system and approximations for the derivatives of the differential equations used are given; the Euler forward method is used in this study. The cost function classifications are discussed in terms of weighting factors, delay compensation and reference frames. Simulation results of a two-level, three-phase VSI using FS-MPCC are carried out to demonstrate the influence of some system parameters, such as the predictive current control operation, with and without delay compensation.

3.2 Predictive control techniques for power conversion.

Converter control can be divided into a number of categories, one of these is predictive control. One of the earlier predictive control methods used in power converters is the dead-beat control, which replaced the classic linear controller. Dead-beat control is used to calculate the required reference voltage in order to achieve the desired reference value for a certain variable (usually the current); the method requires a modulator. This method has been applied to the current control of inverters (Abu-Rub et al. 2004), rectifiers (Zhang et al. 2003), active filters (Jeong & Woo 1997) and uninterruptible power supplies (UPSs) (Stolze et al. 2011).

Hysteresis-based predictive control aims to keep the controlled variables within the boundaries of a defined band, while in the trajectory-based control method, the variables are forced to follow a predefined trajectory. However, predictive control was unsuitable for controlling power electronic converters because of limited availability of digital controllers. Calculation speed is of utmost importance when using predictive control and the high switching frequencies as required by some converters, rendered available digital controllers too slow. Figure 3.1 displays a breakdown of the different control techniques and the classification for MPC methods used in power electronics.

A different approach is model predictive control in which a model of the system is considered in order to predict the future behaviour of the variables over a time frame (Camacho & Bordons 1999). These predictions are evaluated, based on a cost function, and then the sequence that minimizes the cost function is chosen. This whole process is repeated again for each sampling instant, by considering the new measured data.

Early applications of the MPC in power electronics can be found in the 1980s high-power systems where a low-switching frequency was considered (Holtz & Stadtfeld 1983). The use of higher switching frequencies was not possible at that time due to the large calculation time required for the control algorithm. However, with the development of fast and powerful microprocessors, interest in the application of MPC using power electronics has increased considerably over the last decade.

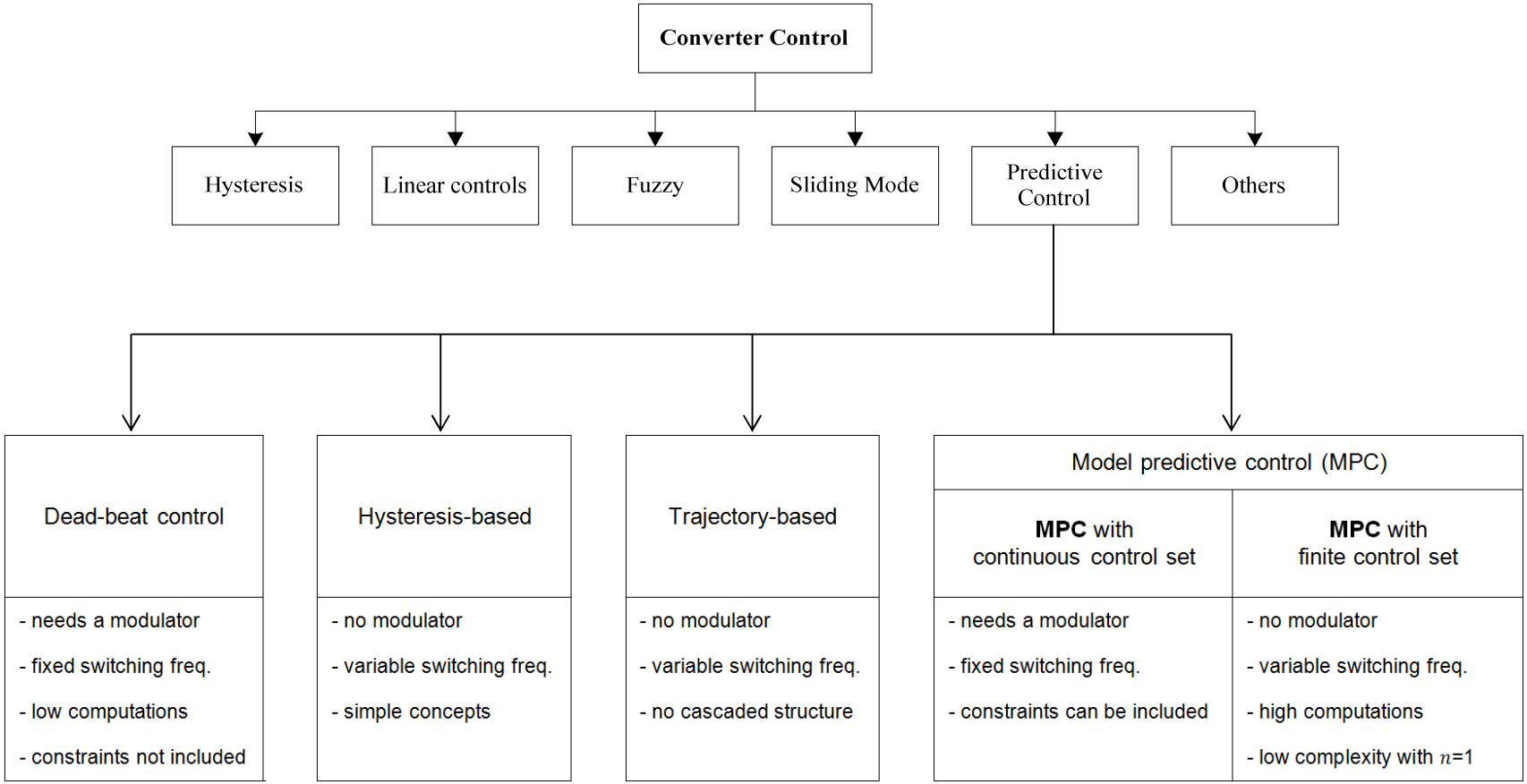

Figure 3.1: Breakdown of different control techniques and classification of predictive control methods used in power electronics

Figure 3.2 shows the typical structure of a predictive controller. An example of a converter under predictive control is chosen. The measured variables, namely the converter current, voltage and load are processed simultaneously in a model of the drive in a block converter and load. In this model, i_{ref} is the reference current and i is the measurement taken at time k; therefore, the future values of the load current, $i(k+1)$, are predicted for all permissible switching states to bring the controlled currents closer to their reference. Exact information of the prevailing system state can be obtained, and then transferred into a block called 'prediction and calculation' for processing. This functional block can be regarded as the heart of a predictive control system as it determines an optimum value for the actuating variable by comparing the prevailing converter state with the desired behaviour. By applying this actuating value to the plant via the actuator, the control loop is closed. Calculation of the optimum value for the actuating variable is done in the block 'prediction and calculation', subject to the desired optimum condition, and issues like minimum current error, and minimum current distortion among others, are considered. An evaluation of the effects of changing the values of the actuating variables can be done too.

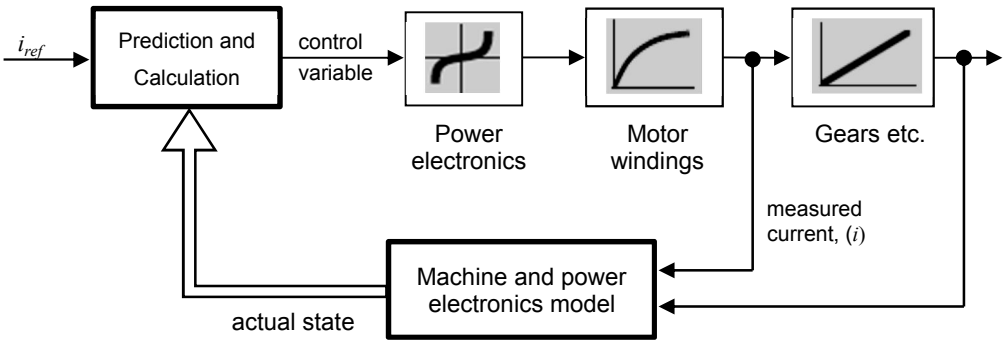

Figure 3.2: Typical structure of a predictive controller

The basic principle described above is common to all predictive control strategies applied in power conversions; the only differences occur in the functionality of the block 'prediction and calculation'. Because of these differences in prediction and optimization, predictive algorithms can be classified according to different criteria, namely: the basic functional principle, the prediction horizon and the inverter control.

3.2.1 Classification based on operational principle of predictive control

Considering the functional principles of the different predictive control algorithms, it can be seen that these can be classified into four main groups—a decision can be made between hysteresis-based, trajectory-based, dead-beat and model-based

strategies. There is no clear-cut boundary between these groups; the transition between them can be quite blurred.

3.2.1.1 Hysteresis-based

Hysteresis-based control aims to keep the controlled variables within boundaries of a specified band. Hysteresis-based predictive control will predict the outcome of the controlled variables for all the possible control inputs and then select the input that will keep the controlled variables within the boundaries for the longest time. This will also automatically reduce the switching frequency to a minimum. It is an improvement on simple 'bang-bang' control (Holtz & Stadtfeld 1983).

Figure 3.3 showing the reference vector and boundary of a current controller. Assume that the power electronic converter being used to control the current has three possible switching states. At the instant that the load current, i_L reaches the boundary, three trajectories are calculated, one for each of the three switching states; these trajectories, r_1, r_2 and r_3, have their origin at the contact point of i_L with the boundary. The switching state that will keep i_L inside the boundary for the longest time will be chosen; r_3 would be chosen. A zero-sized hysteresis band will result in an infinite switching frequency. This is because the current will always be on or outside the hysteresis band. The switching state will therefore constantly be changed.

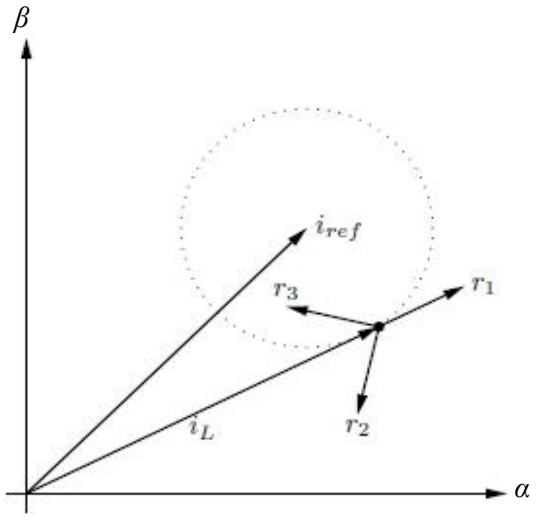

Figure 3.3: Hysteresis-based predictive control

3.2.1.2 Trajectory-based

The model of the system is based on offline calculation of all the permissible trajectories that the controlled variables can follow. When the system becomes active, the shortest route from the initial state via the available trajectories can be determined and thus the sequence of control inputs. The system can then be steered to reach the required state. Varieties of trajectory control are direct self-control (Depenbrock 1988), direct torque-control (Takahashi & Noguchi 1986) and direct speed-control (Mutschler 1998).

With reference to Figure 3.4, a descriptive example of direct predictive speed control follows. The trajectories relating to the acceleration of the system and speed error are parabolas. The route to get to the origin at e = 0, can be determined, and the system can be steered to reach that point. The final value does, however, require a positive and a negative tolerance, effectively creating a tolerance band; this is necessary to allow a limited switching frequency. A zero tolerance will result in an infinite switching frequency because the controller will attempt to keep the state at the final value. In the adjoining figure it is depicted how the trajectory to reach a zero error must be selected; a tolerance band for zero error is, however, not shown. The trajectory that the system selects will be the one that yields the shortest path from the starting to the required state.

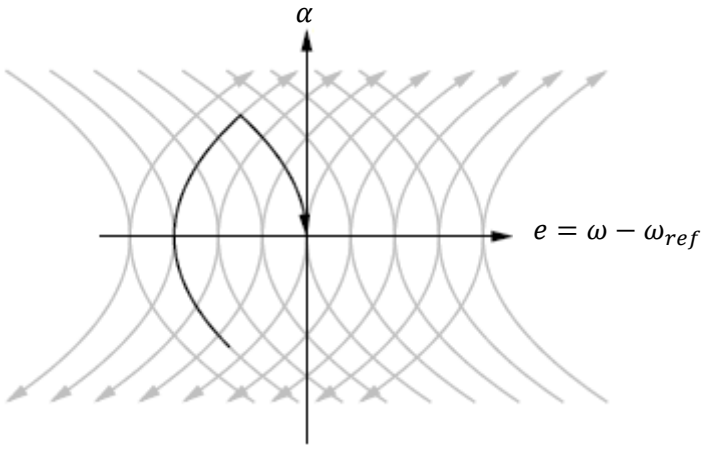

Figure 3.4: Trajectory-based predictive control

3.2.1.3 Dead-beat

At each sampling instance the model of the system is used to calculate the reference that will result in a zero error at the next sampling instant. For a power electronic converter under pulse width modulation control, the PID controller will be replaced by a dead-beat controller; this is shown in Figure 3.5. The references, v_{ref} and i_{ref}, are calculated and compared to the triangular carrier in order to determine the switching

signals for the converter. Errors in the model of the system severely degrade the performance of the controller and could render the system unstable. Moreover, it is difficult to accommodate non-linearities in the controller. This type of controller has been used for inverters (Chen et al. 2003; Le-Huy et al. 1994; Springob & Holtz 1998), rectifiers (Malesani et al. 1999), active filters (Jeong & Woo 1997; Mossoba & Lehn 2003), UPS applications (Buso et al. 2001; Mattavelli 2005; Nasiri 2007), DC-DC converters (Saggini et al. 2007) and torque control of induction motors (Correa et al. 2007). Kukrer (1996) investigated the effects of the control delay on the controlled current of PWM inverters.

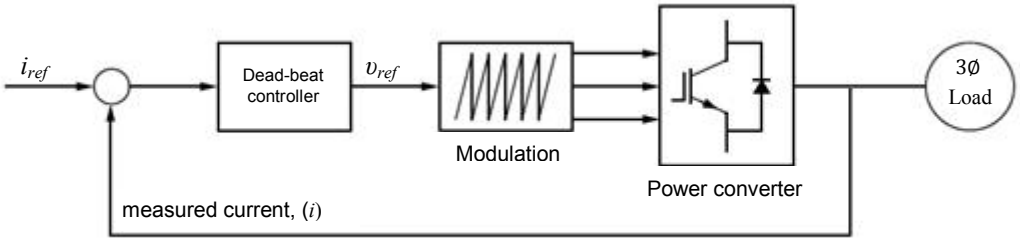

Figure 3.5: Dead-beat predictive control

3.2.1.4 Model-based

Among the more advanced control techniques, as compared to standard PID control, model-based predictive control is one that has been successfully used in industrial applications in the past decades (Camacho & Bordons 1999; Goodwin et al. 2005; Maciejowski 2002). MPC allows for non-linear models and can handle general system constraints, which are required to protect components against excess voltages or currents. MPC can be divided into two subsets: infinite and finite control set MPC. The classification of MPC methods is shown in Figure 3.1.

Several works have reported the use of the MPC technique in power converters such as the three-level DCC, FCC inverters, active-front-end (AFE) rectifiers, cascaded H-bridge MLCs and matrix converters (MC) (Garcia et al. 1989; Linder & Kennel 2005; Mayne et al. 2000; Rossiter 2003). A summary of recent implementations of MPC in different power converter topologies is presented in Figure 3.6.

(i) Infinite control set

In an MPC system where the output from the controller is transmitted through a pulse width modulator, the process is referred to as the infinite control set. The converter receives the switching signals from the modulator. Therefore, the feasible reference values transferred to the modulator have to be calculated and a cost function is utilised to select the most suitable reference set.

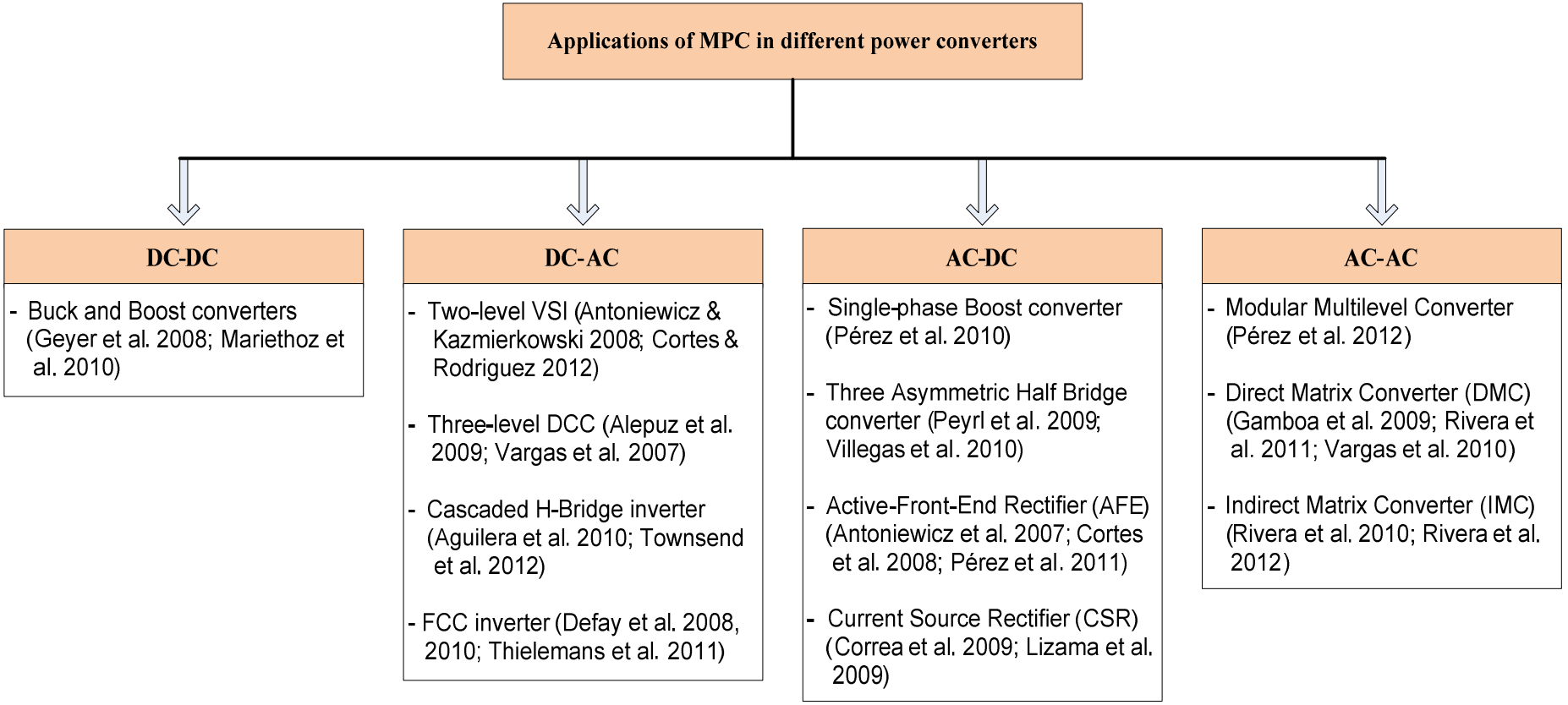

Figure 3.6: Application of MPC in different power converters

(ii) Finite control set

FS-MPCC does not need a modulator to determine the switching signals for the converter. When modelling a power electronic converter, the switches can be modelled as an ideal switch with only two states: 'on' and 'off'. Since power converters have a finite number of switching states, the MPC optimization problem can be simplified and reduced to the prediction of the system behaviour only for those switching states permitted. Each prediction is then used to evaluate a cost function, and subsequently the state with minimum cost is selected and generated. This control method is known as an FS-MPCC approach, since the possible control actions (switching states) are finite. It has been successfully applied to a wide range of power converter and drive applications as a current controller for two-level inverters (Linder & Kennel 2005; Rodríguez et al. 2004, 2004(a); Rodríguez et al. 2007), three-level inverters (Perantzakis et al. 2005(a); Vargas et al. 2007) and four-level inverters (Perantzakis et al. 2005).

In addition the currents of the active and reactive power can also be controlled (Rodríguez et al. 2005). An FS-MPCC approach has also been applied to control more complex converters such as matrix converters (Muller et al. 2005), direct converters (Catucci et al. 2005, 2006; Dang et al. 2006) and FCCs (Silva et al. 2007).

3.2.2 Classification based on prediction horizon and control principle

Another classification method for predictive control algorithms is based on two other criteria. The first distinctive criterion is the depth of the pre-calculation, which is referred to as the prediction horizon. The second criterion relates to the partition that can be made according to the type of inverter control, also called the control principle. While some predictive controllers immediately calculate optimum inverter switching states by controlling the inverter directly. Other strategies determine a value-continuous control signal, which must be synthesized by a modulator before it is passed on to the inverter. Some predictive control methods and their classification into the different families according to the above differentiation criteria are given in Table 3.1.

Table 3.1: Classification of predictive control algorithms

Prediction Horizon	Control principle	
	With modulator	**Direct**
1	Direct control of IM currents Direct flux control	Direct torque-control Direct self-control Direct speed-control
> 1	Generalized predictive control	Direct model predictive control

Most of the control schemes which have been investigated in drive technology so far, have a prediction horizon of only one single sampling cycle. Two well-known examples incorporating a modulator are the direct current control of induction motor currents by Mayerv and Pfaff (1985) and the direct flux control proposed by Asher et al. (2001). The biggest segment of the one-step predictive controllers is made up of the group of the prediction schemes with direct inverter control. Among this group are such prominent controllers as DTC (Aaltonen et al. 1995; Takahashi & Noguchi 1985) and its derivatives, as well as direct self-control (Depenbrock 1985) and direct speed-control (Mutschler 1998). Predictive control strategies with a prediction horizon of more than one single sampling cycle are exclusively model-based predictive controllers. Thus, these schemes are also referred to as long-range predictive control (L-RPC) schemes. The only scheme of this kind used for drive control so far, is a generalized predictive control scheme (Clarke et al. 1987). Its suitability for drive applications has been investigated by Kennel, Linder and Linke (2001).

3.3 Basic principles of an MPC scheme

An MPC scheme encompasses a wide family of control methods (Camacho & Bordons 1999). The common elements of this kind of control strategy are that it uses a model of the system to predict the future behaviour of the variables up to a predefined time horizon and that it selects the optimal actuations by minimizing a cost function. This structure has several important advantages:

a. Concepts are very intuitive and easy to understand.
b. The multivariable case can be easily considered.
c. Dead times can be compensated for.
d. Non-linearities are easily included in the model.
e. Constraints are simple to accommodate.
f. The resulting controller is easy to implement.
g. Depending on specific applications, this control scheme is suitable for the inclusion of modifications and extensions.

Some disadvantages include the larger number of calculations required, when compared to classic controllers. The quality of the model has a direct influence on the quality of the resulting controller, and if the parameters of the system change over time, some adaptation or estimation algorithm has to be considered. The basic ideas present in an MPC method are the following:

1. The use of a model to predict the future behaviour of the variables up to a predefined time horizon.
2. The use of a cost function to represent the desired behaviour of the system.
3. The optimal actuation obtained by minimizing the cost function.

The model used for prediction is a discrete-time model, which can be expressed as a state-space model as follows:

$$\boldsymbol{x}(k+1) = A\boldsymbol{x}(k) + B\boldsymbol{u}(k) \qquad k \in \{0, 1, 2, \dots\} \tag{3.1}$$

$$\boldsymbol{y}(k) = C\boldsymbol{x}(k) + D\boldsymbol{u}(k) \qquad k \in \{0, 1, 2, \dots\} \tag{3.2}$$

where $x(k)$ and $u(k)$ are the state and control input values at time, k and $x(k+1)$ is the predicted state.

A cost function, g that represents the desired behaviour of the system needs to be defined. This function takes into account the references, future states and future actuations:

$$g = f(\boldsymbol{x}(k), \boldsymbol{u}(k), \dots, \boldsymbol{u}(k+N)) \qquad k \in \{0, 1, 2, \dots\} \tag{3.3}$$

MPC is an optimization problem that consists of minimizing the cost function, g for a predefined horizon in time, N, subject to the model of the system and the restrictions of the system. The result is a sequence of N optimal actuations. During each sampling instant, when the optimization problem is solved again the controller will apply only the first element of the sequence using the new measured data and obtaining a new sequence of optimal actuations each time. This is called a *receding horizon* strategy. The working principle of MPC is summarized in Figure 3.7. The future values of the states of the system are predicted until a predefined horizon at time, $(k+N)$ using the system model and the available information (measurements) until time, k. The sequence of optimal actuations is calculated by minimizing the cost function, and the first element of this sequence is applied. This whole process is repeated again for each sampling instant upon consideration of the new measured data.

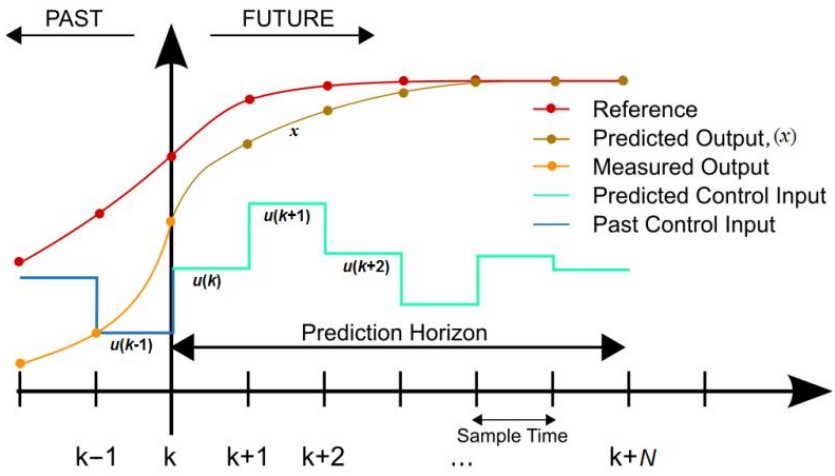

Figure 3.7: Working principle of MPC scheme

3.4 An FS-MPCC approach for the control of a power converter

In the design stage of a finite control set MPC approach for the control of a power converter, the following steps are identified:

1. Model the power converter, identifying all possible switching states and the corresponding input voltages or currents, or the output voltages or currents.
2. Find a cost function representative of the prescribed system behaviour.
3. Derive discrete-time models that allow the prediction of the performance of the variable to be controlled.

In the modelling of a converter, the fundamental component is the power switch; typical switches used are IGBTs, thyristors, and gate turn-off thyristors (GTOs). In an elementary model an ideal switch has only two states: 'on' and 'off '; the total number of switching states of a power converter, therefore, equals the number of different combinations of the two switching states for each switch, keeping in mind that some combinations, however, are not permitted and some are redundant. An example of combinations not permitted, are those that short-circuit the DC-link. As a general rule, the number of possible switching states, U, is given by:

$$U = x^y \tag{3.4}$$

where x is the number of possible states for each leg or phase of the converter, and y is the number of phases or legs of the converter.

Based on Equation 3.4, the possible number of switching states in a three-phase, two-level converter is $U = 2^3 = 8$; in a three-phase, three-level converter $U = 27$; and a five-phase, two-level converter $U = 32$. The number of switching states of the converter, in some multilevel topologies, can be extremely high. For example, in a three-phase, nine-level cascade H-bridge inverter, the number of switching states is in excess of 16 million.

An additional perspective of a converter model is the relationship between the number of switching states and either the voltage levels in the case of single-phase converters, or the voltage vectors in the case of three-phase or multi-phase converters. It can be found that in several cases, the same voltage vector is generated by two or more switching states; an example of this occurs in a three-phase, two-level converter, in which eight switching states produce seven voltage vectors, and two of the switching states generate the zero vector. A three-phase, three-level DCC has 27 possible switching states, of which eight are redundant, and therefore there are only 19 different voltage vectors. Similarly, in a three-phase, three-level FCC with 64 possible switching states, of which 45 are redundant, also leaving only 19 different voltage vectors. Figure 3.8 depicts the relationship between switching states and voltage vectors for three different converter topologies.

The basic principle of FS-MPCC strategies for power conversion is shown in Figure 3.9, where $i(k)_{ref}$ represents the reference currents at time, k for controllable variables, $i(k)$ is the current load measurements taken at time, k, and $i(k+1)$ are the predicted current of the states for n possible switching states at time, $(k+1)$. The error between the reference and predicted current is obtained to minimize the cost function, and then the switching state that minimizes the cost function, is chosen. The switching signals, S, of the chosen state are then applied to the converter.

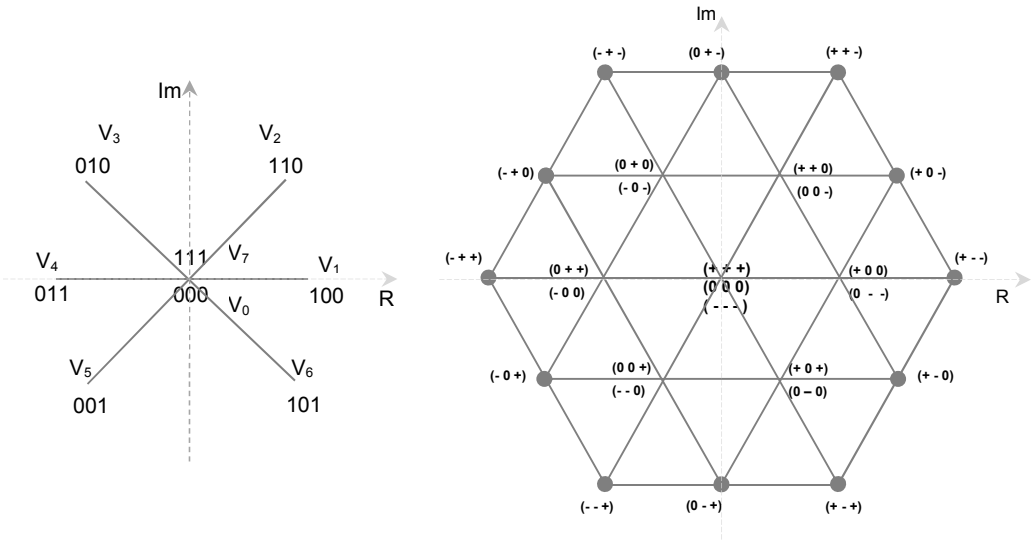

(a) two-level converter (b) three-level converter

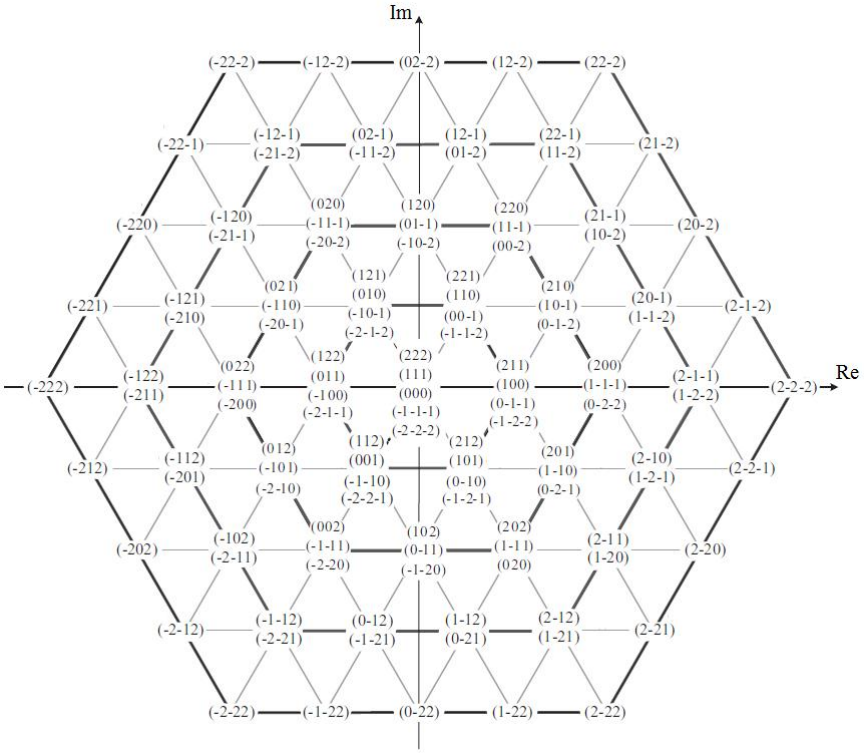

(c) five-level converter

Figure 3.8: Voltage vectors by different converters having different levels

In general, the control algorithm as shown in Figure 3.9 can be summarized by the following steps:

1. Measure the load currents.
2. Initialize the value of the optimum cost function.
3. Predict the load currents for the next sampling instant for all the possible switching states.
4. Evaluate the cost function for each prediction.
5. Select the optimal switching state that minimizes the cost function.
6. Apply the new switching state.

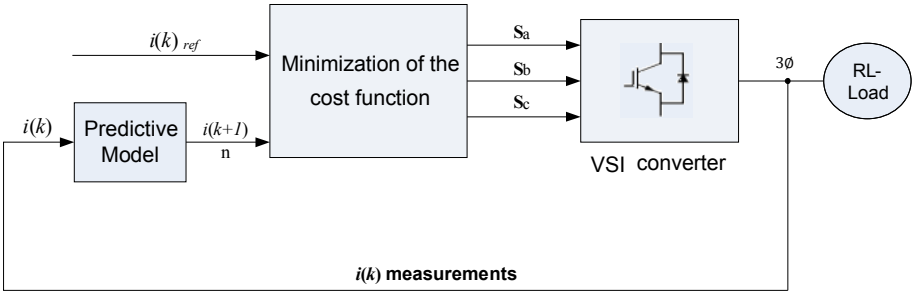

Figure 3.9: FS-MPCC block diagram

3.5 Model predictive control parameters and simulation

The predictive control technique consists of different aspects (Rossiter 2003) working together to control certain variables. These aspects interact with each other and the system to provide the inputs that will drive the system. The terminology most often used in connection with an MPC method is the following: predictions, system model, cost function, receding horizon and computation. Simulation results of a two-level, three-phase VSI using FS-MPCC was carried out in order to show the effects of different approximation methods on the load current and voltage as well as on the predictive current control operation with and without delay compensation.

3.5.1 System modelling

A model is needed to predict the response of the system to a control input. This model should take into account the control inputs as well as the current state of the controllable variables. This model can be linear or non-linear. The modelling of the system to be controlled is an important step. Rossiter (2003) uses the term 'fit for purpose' to qualify the model of a system. Such a model will give sufficiently accurate predictions without further modelling effort. For instance, the 'fit for purpose' model of a non-linear system may be a linearized version.

As stated in Section 3.4, a power electronic converter can be discretised by viewing the power switches as ideal switches with only two states: 'on' and 'off' (Cortés et al. 2008). This means that by only changing the switching combinations at fixed sampling intervals, the measuring and predicting actions of the FS-MPCC need also to be done only at fixed intervals. If $\mathrm{T_S}$ is the sampling period of the controller, then the discretised time will be $t = k\mathrm{T_S}$ with $k \in \{0, 1, 2, \dots\}$ as the sampling instances. The converter can be modelled so that:

$$x(k+1) = f\left(x(k), u(k)\right) \qquad k \in \{0, 1, 2, \dots\} \tag{3.5}$$

where $x(k)$ and $u(k)$ are the state and control input values at time, k, and $x(k+1)$ is the predicted state.

FS-MPCC allows for constraints on both the control inputs and the system states. Therefore, the control inputs can be restricted to

$$u(k) \in \mathrm{U} \leq R^p \qquad k \in \{0, 1, 2, \dots\} \tag{3.6}$$

where U is the set of permitted switching combinations and p is the number of switches.

Consequently, all the switching combinations will be contained in R^p. If, however, a flying-capacitor or diode-clamped converter is used, some of the combinations are not permitted.

Similarly, the states of the converter can be constrained by the control system by applying:

$$x(k) \in X \leq R^n \quad k \in \{0, 1, 2, \dots\} \tag{3.7}$$

The constraints, X, can be used to limit voltages or currents to which components are subjected. Subsequent to predicting the states of the converter using Equation 3.5, a cost function is employed to assess the different switching states and select the best one. The following generic cost function can be applied when a finite horizon of length, N, is used:

$$V\left(x(k),\ u(k)\right) \triangleq \sum_{l=k}^{k+N-1} \lambda(x(l),\ u(l)) \tag{3.8}$$

where

λ is a weighting factor,

$$x(l+1) = f\left(x(l),\ u(l)\right) \qquad l \in \{k, k+1, k+2, \dots\} \tag{3.9}$$

are the predicted states, and

$$u(l) \in \mathrm{U} \quad l \in \{k, k+1, k+2, \dots\} \tag{3.10}$$

are the control inputs.

λ is applied to penalise an unwanted state or control input behaviour. For instance, if the predicted state for a given switching state is $x(k+1) \notin X$, the cost function should penalise that switching state so severely that it will not be chosen as the switching state for the next sampling period.

When the cost functions have been evaluated, a whole series of control inputs, $u(l)$, are available to drive the system. However, the receding horizon dictates that only the first control input is used, and the horizon over which the values are being predicted is shifted one sample period into the future. Thus, at time, $(k+1)$, a measurement will be taken, and the predicted states will be calculated from:

$$x(l+1) = f\left(x(l),\ u(l)\right) \qquad l \in \{k+1,\ k+2,\ k+3, \dots\} \tag{3.11}$$

3.5.2 Approximation methods

Equation 3.5 is not necessarily a linear equation, and this poses a problem because it has to be implemented in a digital controller. Non-linear systems such as exponentials or logarithms are not a problem to implement, but differential and integral equations need special attention. Differential and integral equations need to be approximated by discrete-time equations that can be executed on the digital controller. Three major approximation methods for differentials are the Euler forward, the Euler backward and the Runge-Kutta (Zill & Cullen 2000). Approximations for integrals are not given because they do not form part of the models for the power electronic converters in this thesis.

The state-space representation of a system is:

$$\dot{x}(t) = A\,.\,x(t) + B\,.\,u(t) \tag{3.12}$$

where $x(t)$ and $u(t)$ are the state and the control inputs to the system respectively. Matrices A and B are the transition matrices. It is $\dot{x}(t)$ that needs to be approximated.

The Euler forward, Euler backward and Runge-Kutta approximations have been used for two-level VSI with one prediction step for sampling time, T_S= 25 μs, to control the load current (Rodríguez et al. 2007).

3.5.2.1 Euler forward method

The Euler forward approximation method will approximate a differential equation as:

$$\dot{x} = \frac{dx}{dt} \approx \frac{x(k+1) - x(k)}{T_S} \tag{3.13}$$

Therefore, the state-space representation of a system in discrete time becomes:

$$x(k+1) \approx T_S\,.\,\left(A\,.\,x(k) + B\,.\,u(k)\right) + x(k) \tag{3.14}$$

3.5.2.2 Euler backward method

The Euler backward approximation method will approximate a differential equation as:

$$\dot{x} = \frac{dx}{dt} \approx \frac{x(k) - x(k-1)}{\mathrm{T_S}} \tag{3.15}$$

Therefore, the state-space representation of a system in discrete time becomes:

$$x(k) \approx \mathrm{T_S} \,.\, \big(A \,.\, x(k) + B \,.\, u(k)\big) + x(k-1) \tag{3.16}$$

Shifting time one sample interval yields:

$$x(k+1) \approx \mathrm{T_S} \,.\, \big(A \,.\, x(k+1) + B \,.\, u(k+1)\big) + x(k) \tag{3.17}$$

The difficulty with the backward method is in obtaining an explicit solution for $x(k+1)$. If it is possible to obtain such a solution it will result in a more stable controller for large values of $\mathrm{T_S}$.

3.5.2.3 Runge-Kutta method

The Runge-Kutta approximation uses a fourth-order function to approximate the gradient at time, k. The process approximates the slope, $\dot{x}(t)$, by averaging four slopes obtained from Equation 3.12.

$$\dot{x_0} = A \,.\, x(t) + B \,.\, u(t) \tag{3.18}$$

$$\dot{x_A} = A \,.\, \left[x(t) + \tfrac{1}{2}\mathrm{T_S}\dot{x_0}\right] + B \,.\, u(t) \tag{3.19}$$

$$\dot{x_B} = A \,.\, \left[x(t) + \tfrac{1}{2}\mathrm{T_S}\dot{x_A}\right] + B \,.\, u(t) \tag{3.20}$$

$$\dot{x_C} = A \,.\, [x(t) + \mathrm{T_S}\dot{x_B}] + B \,.\, u(t) \tag{3.21}$$

The four slopes are averaged and the predicted states can then be calculated with:

$$x(k+1) = x(k) + \tfrac{1}{6}\mathrm{T_S} \,.\, (\dot{x_0} + 2\dot{x_A} + 2\dot{x_B} + \dot{x_C}) \tag{3.22}$$

To include the approximation methods, an example of a two-level VSI converter with an RL-load was studied. In Figure 3.10(a) the load currents and the load voltages using the Euler forward approximation are shown, while Figure 3.10(b) shows load currents and load voltages after applying the Runge-Kutta approximation. As can be seen from the simulated results in Figure 3.10, with the output currents tracking their references, the control algorithm has very good tracking characteristics. However, the implementation with Runge-Kutta approximation method shows less ripple than the Euler approximation method. Therefore, because of its simplicity and reduced computation burden, the Euler forward approximation method was used in this study.

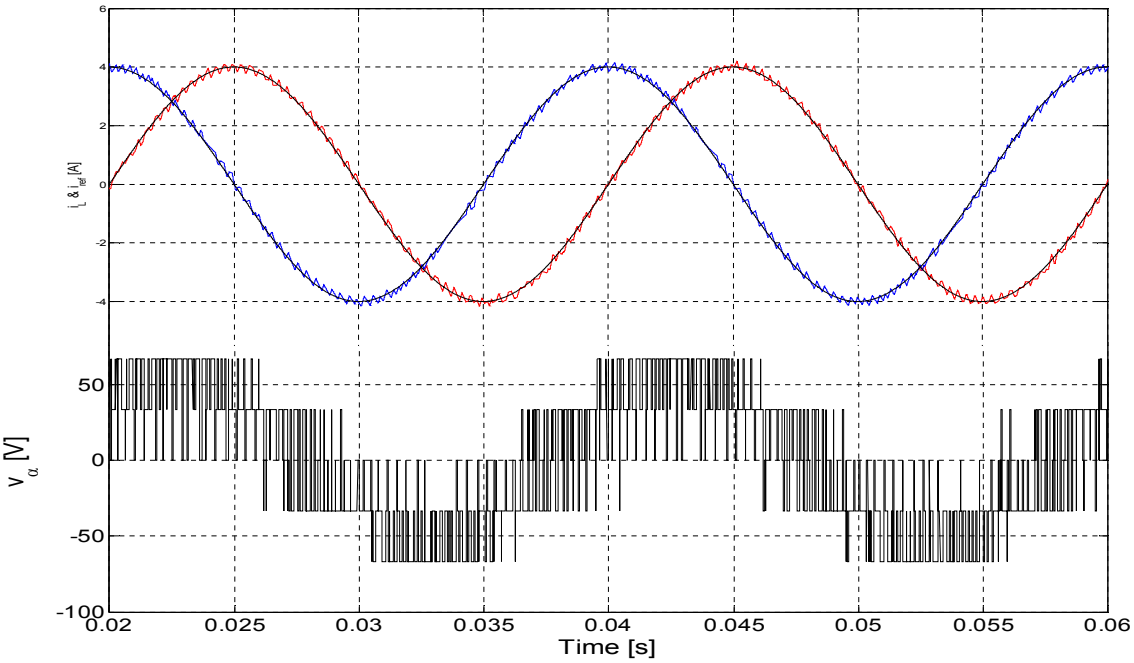

(a)

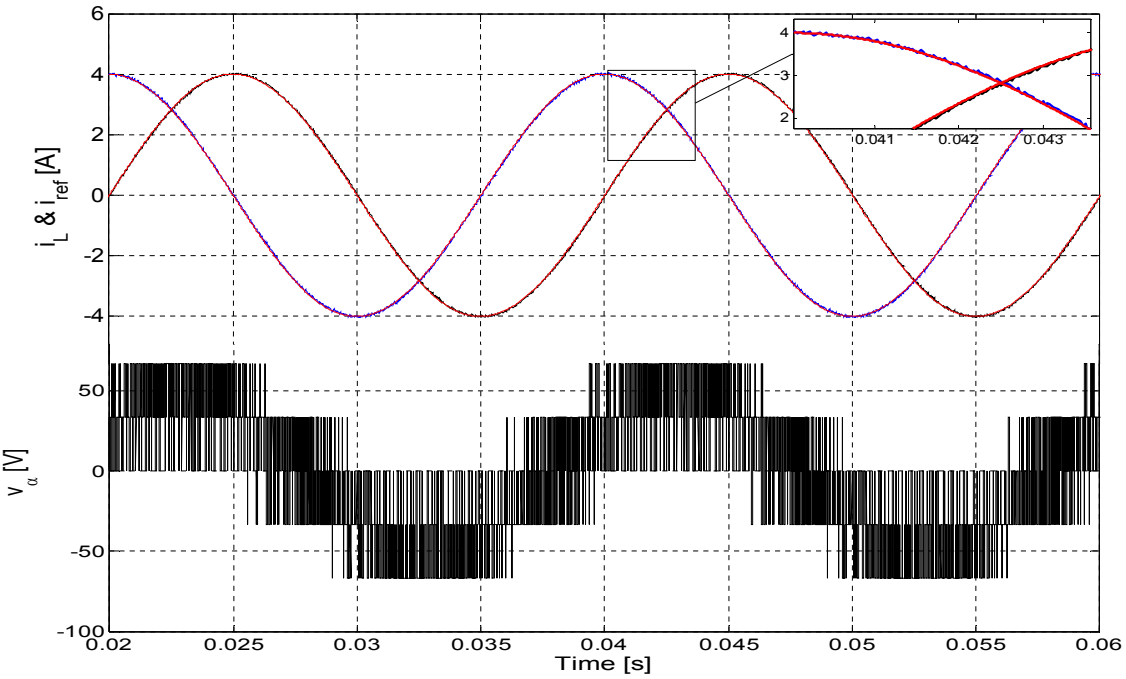

(b)

Figure 3.10: The load currents and voltages for a sampling time Ts = 25 µs using: (a) Euler forward approximation (b) Runge-Kutta approximation

3.5.3 Stability

Consider the discrete state-space model given by Equation 3.12, with an initial condition x_0 and constrained control inputs; then Tsirukis and Morari (1992) proved the following:

1. If λ_i, the eigenvalues of matrix A in Equation 3.12, lie in or on the unit circle, that is $|\lambda_i| \leq 1$, then $x_0 \in X$ can be controlled by a sequence of control inputs, $u(l) \in U$ such that $x(\infty) = x_{ref}$.
2. If at least one λ_i, the eigenvalues of matrix A in Equation 3.12, lies outside the unit circle, that is $|\lambda_i| > 1$, then $x_0 \in X$ cannot be controlled by a sequence of control inputs, $u(l) \in U$ such that $x(\infty) = x_{ref}$.

3.5.4 Cost function classification in terms of weighting factor

After predicting the response of the system to all the different control inputs, the predicted states should be evaluated to enable the selection of the best action. This is done by evaluating a numerical expression that takes the controllable states of the system as its parameters. The control action that minimizes the cost function is chosen, meaning that the optimum outcome of the cost function represents the desired behaviour of the system. Although the main objective of the cost function is to keep track of a particular variable and control the system, it is not limited to this. In fact, one of the main advantages of an MPC is that the cost function admits any necessary term that could represent a prediction for another system variable, system constraint or system requirement. Since these terms most likely can be of a different physical nature (e.g. current, voltage, reactive power, switching losses, torque, flux) their units and magnitudes can also be very different. This issue has been commonly dealt with in MPC by including a weighting coefficient or weighting factor, λ for each term of the cost function:

$$g = \lambda_x \|x^* - x^p\| + \lambda_y \|y^* - y^p\| + \cdots + \lambda_z \|z^* - z^p\| \tag{3.23}$$

Depending on the nature of the different terms involved in the formulation of the cost function, they can be classified in different groups. This classification is necessary in order to facilitate the definition of a weighting factor adjustment procedure that could be applied to similar types of cost functions or terms. Table 3.2 shows the cost functions with and without weighting factors, and with equally important terms.

3.5.4.1 Cost functions without weighting factors

In this kind of cost function, only one variable, or its components are controlled. This is the simplest case, and since only one type of variable is controlled, no weighting factors are necessary. Some representative examples of this type of cost function are found in the predictive current control of a voltage source inverter (Rodríguez et al. 2007), in the predictive power control of an AFE rectifier (Cortés et al. 2008(a)), in the predictive voltage control of a UPS system (Cortés et al. 2009), in the predictive current control with imposed switching frequency (Cortés et al. 2008(b)) and in the predictive current control of multi-phase inverters (Barrero et al. 2009; Cortés et al. 2009(a); Duran et al. 2011). The corresponding cost functions of the examples mentioned are summarized in Table 3.2.

Note that all the terms in a cost function are composed of variables of the same nature (same unit and order of magnitude). Moreover, some variables originate from a single vector that has been broken down into two or more components, therefore no weighting factors or their corresponding tuning processes are necessary.

3.5.4.2 Cost functions with secondary terms

Some systems have a primary goal, or a more important control objective that must be achieved in order to ensure proper system behaviour; additionally there are secondary constraints or requirements that should be accomplished to improve system performance, efficiency, and power quality. In this case, the cost function contains primary and secondary terms and the importance of the secondary terms can vary widely, depending on the application and its specific needs. Some examples are: predictive current control with a reduction in the switching frequency to improve efficiency (Vargas et al. 2007), predictive current control with a reduction in the common-mode voltage to prevent motor damage (Vargas et al. 2008) and predictive current control with reactive power reduction to improve power quality (Muller et al. 2005; Vargas et al. 2008(a)). Cost functions with secondary terms are listed in Table 3.2. The importance of the secondary term (i.e., how much the switching frequency, the common-mode voltage, or the reactive power, is reduced) will depend on the specific requirements of the application and will impose a trade-off with the primary control objective; for cost functions with secondary terms the primary objective is current control. Note that in each cost function, a weighting factor, λ is included with the corresponding secondary term. Hence, balancing the trade-off can be seen as a weighting factor adjustment to the cost function.

Table 3.2: Cost function classification

Application	Cost function	Symbols and nomenclature
1. Cost functions without weighting factors		
Current control of a VSI	$\left\|i_\alpha^* - i_\alpha^p\right\| + \left\|i_\beta^* - i_\beta^p\right\|$	$i_{\alpha,\beta}^*$: reference currents $i_{\alpha,\beta}^p$: predicted currents
Power control of an AFE rectifier	$\|Q^p\| + \|P^* - P^p\|$	P^*: reference active power P^p: predicted active power Q^p: predicted reactive power
Voltage control of a UPS	$(v_{c\alpha}^* - v_{c\alpha}^p)^2 + (v_{c\beta}^* - v_{c\beta}^p)^2$	$v_{c\alpha,\beta}^*$: reference output voltages $v_{c\alpha,\beta}^p$: predicted output voltages
Current control of a multi-phase VSI	$\left\|i_\alpha^* - i_\alpha^p\right\| + \left\|i_\beta^* - i_\beta^p\right\| + \left\|i_x^* - i_x^p\right\| + \left\|i_y^* - i_y^p\right\|$	$i_{\alpha,\beta,x,y}^*$: reference currents $i_{\alpha,\beta,x,y}^p$: predicted currents
2. Cost functions with secondary terms		
Switching frequency reduction	$\left\|i_\alpha^* - i_\alpha^p\right\| + \left\|i_\beta^* - i_\beta^p\right\| + \lambda_{sw} n_{sw}^p$	n_{sw}^p: number of commutations to reach the next state λ_{sw}: weighting factor
Common-mode voltage reduction	$\left\|i_\alpha^* - i_\alpha^p\right\| + \left\|i_\beta^* - i_\beta^p\right\| + \lambda_{cm}\left\|v_{cm}^p\right\|$	λ_{cm}: weighting factor
Reactive power reduction	$\left\|i_\alpha^* - i_\alpha^p\right\| + \left\|i_\beta^* - i_\beta^p\right\| + \lambda_Q\|Q^p\|$	λ_Q: weighting factor
3. Cost functions with equally important terms		
Torque and flux control	$\Big/^{1}_{T_{sn}^2\left(T_e^* - T_e^p\right)^2 + \lambda_\psi / \psi_{sn}^2(\|\psi_s\|^* - \|\psi_s\|^p)^2}$	T_e^*: reference torque T_e^p: predicted torque $\|\psi_s\|^*$: reference stator flux $\|\psi_s\|^p$: predicted stator flux
Capacitor voltage balance	$\Big/^{1}_{i_{sn}\left[\left\|i_\alpha^* - i_\alpha^p\right\| + \left\|i_\beta^* - i_\beta^p\right\|\right] + \lambda_{\Delta V} / V_{cn}\left\|\Delta V_c^p\right\|}$	$\lambda_{\Delta V}$: weighting factor $\left\|\Delta V_c^p\right\|$: absolute error of predicted capacitor voltage

3.5.4.3 Cost functions with equally important terms

Unlike the previous case, there are systems in which several variables with equal importance need to be controlled simultaneously in order to control the system. Here the cost function can include several terms with equal importance, and it is the task of the weighting factors to compensate for the difference in nature of the variables. An example is the torque and flux control of an induction machine, where both variables need to be controlled accurately to achieve proper system performance (Miranda et al. 2009; Rodríguez et al. 2004).

Another example is the current control of a DCC inverter, in which the balance of the DC-link capacitor voltages is essential to reducing voltage distortion and avoiding system damage (should there be a chance that the permitted voltage level of the capacitors could be exceeded, capacitors with a higher rating need to be used) (Vargas et al. 2007). Both cost functions mentioned in the examples above are included in Table 3.2. Note that the two additional terms in each cost function are used to normalize the quantities in relation to their nominal values (denoted by the subscript n).

The following are some examples of converter and drive control applications that are presented to illustrate the use and wide variety of cost functions and weighting factors in predictive control schemes.

(i) Switching frequency reduction

Figure 3.11 was obtained by performing several simulations, starting with λ_{sw} = 0, and gradually increasing this value after each simulation (Rodríguez & Cortés 2012). Figure 3.11 shows comparative results for load current and load voltage with three different values of λ_{sw}, with one of them being the selected value. Note how the load current presents higher distortion for a larger value of λ_{sw}; this is due to the large reduction in the number of commutations.

However, with, $\lambda_{sw} = 0$, the current control works at its best, but at the expense of higher switching losses. Since the DCC is intended for medium-voltage, high-power applications where losses become important, the selection of $\lambda_{sw} = 0.05$, provides a suitable trade-off of efficiency versus performance. A comparison of this predictive method and a traditional PWM-based controller can be found in Vargas et al. (2007).

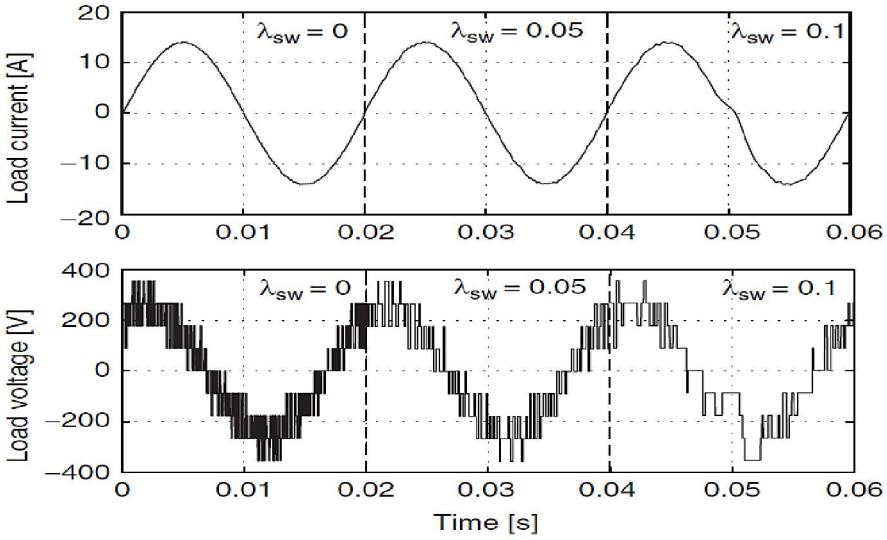

Figure 3.11: Results comparison for different weighting factors

(Permitted/adapted from Rodríguez & Cortés 2012:169)

(ii) Common-mode voltage reduction

The results show that a common-mode voltage is a variable that is more decoupled from the load current than is the switching frequency decoupled from the load current. This occurs because the current error remains very low throughout a wide range of λ_{sw}. Hence, the selection of an appropriate value is easier, and values of $0.05 \leq \lambda_{sw} \leq 0.5$ will perform well. This can be seen in the results shown in Figure 3.12, where a noticeable reduction in the common-mode voltage is clearly achieved without affecting the current control.

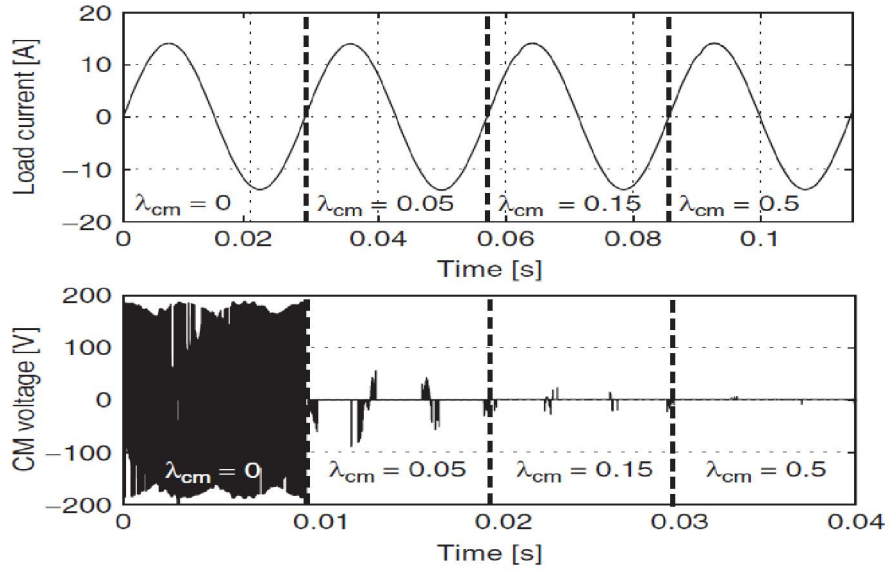

Figure 3.12: Results comparison for different weighting factors

(Permitted/adapted from Rodríguez & Cortés 2012:171)

(iii) Torque and flux control

The objective of the control algorithm is to simultaneously control the electrical torque, T_e, and the magnitude of the stator flux, ψ_s. This objective can be expressed as a cost function with two terms, namely torque error and flux error. Rodríguez et al. (2004) proposed that the weighting factor must handle the difference in magnitude and units between these two terms. A different approach consists of using a normalized cost function, where each term is divided by its rated value, as can be seen in Table 3.2 (Torque and flux control). Using this cost function, the same importance is given to both terms by using $\lambda_\psi = 1$, as proposed by Miranda et al. (2009). However, the optimal value can be different, depending on the defined criteria for optimal operation.

Results for different values of λ_ψ are given in Figure 3.13, showing the performance achieved by the predictive torque and flux control. Note that $\lambda_\psi = 0.85$ yields a very good combination of torque step response, steady-state flux control and load current waveforms.

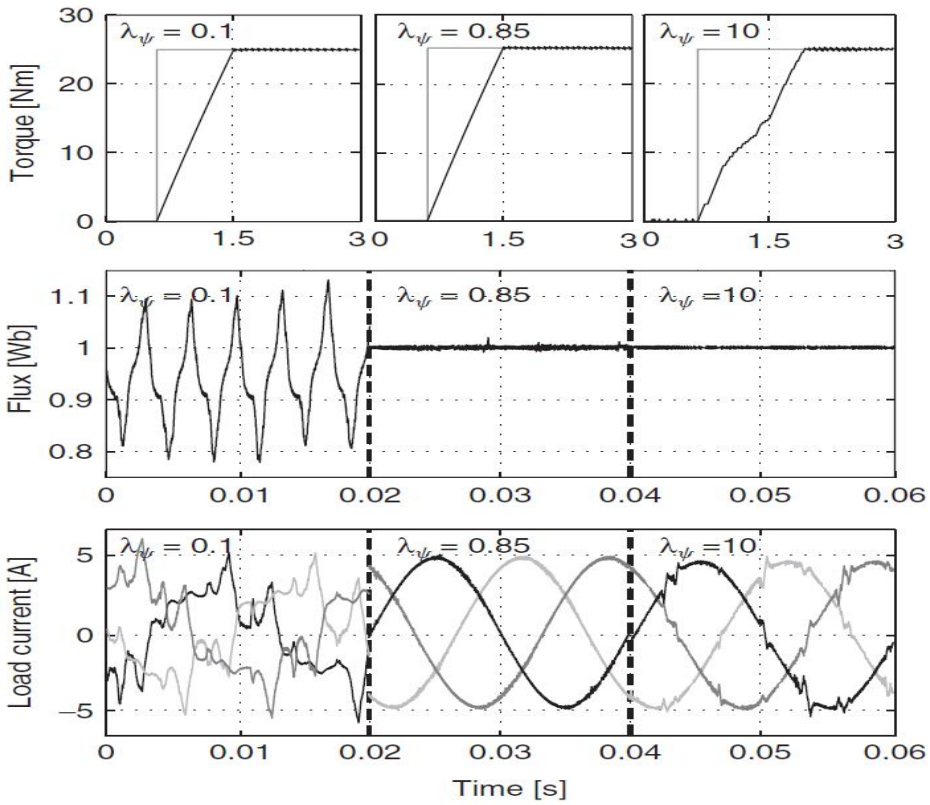

Figure 3.13: Results comparison for different weighting factors

(Permitted/adapted from Rodríguez & Cortés 2012:173)

(iv) Capacitor voltage balancing

Cost functions with equally important terms for capacitor voltage balancing will be studied in detail for the DCC and the FCC in Chapters four and five respectively.

In the case of a DCC, the inverter has two DC-link capacitors, which are required for generating three voltage levels at the output of each phase. These voltages need to be balanced for the proper operation of the inverter. If this balance is not controlled, the DC-link voltages will drift and introduce considerable output voltage distortion, not to mention that the DC-link capacitors, unless they are over-rated, could be damaged by over-voltage. In the case of an FCC, the structure of the converter does not, unlike the DCC, require a split DC-link voltage. There are, therefore, no junction currents between the DC-link capacitors that will unbalance their voltages. However, for the three-level converter it is very important that the voltages across the flying capacitor be half the DC-link voltages. If these voltages are unbalanced, the clamping mechanism will not function correctly, and the danger of exposing some switches to over-voltages arises.

3.5.5 Delay compensation

When control schemes based on an MPC are implemented experimentally, a large number of calculations are required, introducing a considerable time delay in the actuation. This delay can result in deterioration of the performance of a system, if not considered in the design of the controller. In a number of the references consulted, the aspect of compensating for the calculation delay has been dealt with (Arahal et al. 2009; Cortés et al. 2008; Cortés et al. 2008(b); Cortés et al. 2009; Miranda et al. 2009). For other predictive control schemes, such as dead-beat control, comparable compensation methods have been presented (Abu-Rub et al. 2004).

Another source of delay in these types of control schemes appears due to the need for future values of the reference variables in the cost function. Usually the future reference is considered to be the same as the actual reference, which is a good assumption when the reference is a constant value, or the sampling frequency is much higher than the frequency of the reference variable. However, during transients and with sinusoidal references, a delay between the controlled and reference variables appears. In order to eliminate this delay, the future reference variables need to be accurately calculated.

3.5.5.1 Effect of delay due to calculation time

The control of a three-phase inverter with a passive load (resistive–inductive) is used as an example application for explaining both the effects of the delay due to calculation time, as well as the delay compensation method. However, the same ideas are valid for all predictive control schemes.

The predictive current control scheme using MPC is already shown in Figure 3.9 and consists of the:

1. measurement of the load currents,
2. prediction of the load currents for the next sampling instant for all possible switching states,
3. evaluation of the cost function for each prediction,
4. selection of the switching state that minimizes the cost function,
5. application of the new switching state.

In the case of current control, the cost function is defined as the error between the reference current and the predicted currents for a given switching state, and is expressed as:

$$g = \left|i_{\alpha}^{*}(k+1) - i_{\alpha}^{p}(k+1)\right| + \left|i_{\beta}^{*}(k+1) - i_{\beta}^{p}(k+1)\right| \tag{3.24}$$

where i_{α}^{*} and i_{β}^{*} are the real and imaginary parts of the reference current vector, and i_{α}^{p} and i_{β}^{p} are the real and imaginary parts of the predicted load current vector, $i^{p}(k+1)$.

The predicted load current vector is calculated using a discrete-time model of the load, which is a function of the measured currents, $i(k)$ and the inverter voltage (the actuation), $v(k)$ and is expressed as:

$$i^{p}(k+1) = \left(1 - \frac{RT_S}{L}\right) i(k) + \frac{T_S}{L} v(k) \tag{3.25}$$

where R and L are the load resistance and inductance, and T_S is the sampling time.

To graphically illustrate the predictive current control, only i_{β} is shown in Figure 3.14. This simplifies the example as the seven different voltage vectors produce only three different values for their ***β*** component, and hence there are only three possible trajectories for i_{β}. In the figure, the dashed lines represent the predictions for i_{β} as given by Equation 3.25, and the solid line is the actual trajectory given by the application of the optimum voltages obtained by minimization of the cost function from Equation 3.24.

In the ideal case, the time needed for the calculations is negligible, and the predictive control operates as shown in Figure 3.14; this ideal case is shown for comparison. The currents are measured at time, t_k, and the optimal switching state is calculated instantly. The switching state that minimizes the error at time, t_{k+1} is selected and applied at time, t_k, and then the load current reaches the predicted value at t_{k+1}. As the three-phase inverter has seven different voltage vectors, the predicted current from Equation 3.25 and the cost function from Equation 3.24 are calculated seven times. In this way, depending on the sampling frequency and the speed of the microprocessor used for the control, the time between measurement of the load currents and application of the new switching state can be considerable.

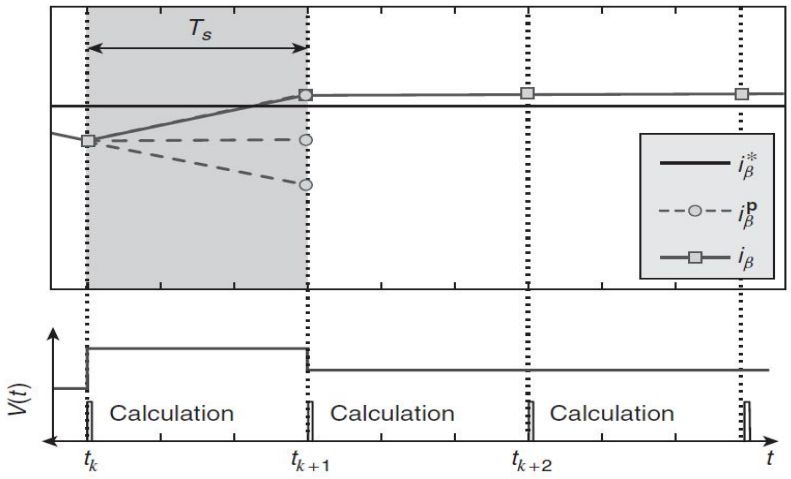

Figure 3.14: Operation of the predictive current control without delay (ideal case)

(Permitted/adapted from Rodríguez & Cortés 2012:180)

If the calculation time is significant compared to the sampling time, there will be a delay between the instant at which the currents are measured and the instant of application of the new switching state; this is shown in Figure 3.15. During the interval between these two instants, the previous switching state will continue to be applied. As can be observed from Figure 3.15, the voltage vector selected using measurements at t_k, will continue being applied after t_{k+1}, causing the load current to move away from the reference. The next actuation will be selected upon consideration of the measurements at t_{k+1} and will be applied near t_{k+2}. As a consequence of this delay, the load current will oscillate around its reference, increasing the current ripple.

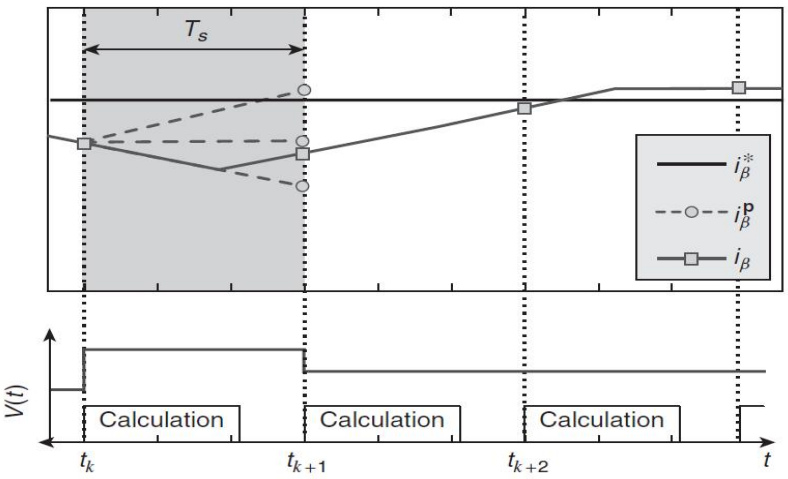

Figure 3.15: Operation of the predictive current control without compensation: long calculation time (real case)

(Permitted/adapted from Rodríguez & Cortés 2012:180)

3.5.5.2 Delay compensation method

A simple solution to compensate this delay is to take into account the calculation time and apply the selected switching state after the next sampling instant. In this way, the control algorithm is modified as follows:

1. The load currents are measured.
2. The switching state (calculated in the previous interval) is applied.
3. The value of the currents at time t_{k+1}, taking into account the applied switching state, are estimated.
4. The load currents for the next sampling instant, occurring at time, t_{k+2}, for all permitted switching states, are predicted.
5. The cost function for each prediction is evaluated.
6. The switching state that minimizes the cost function is selected.

Compared to the original control algorithm mentioned in Section 3.5.5.1, application of the new voltage vector is moved to the beginning, and the estimation of the currents at time, t_{k+1}, is added. Note that the estimation of the currents increases the calculation time, but it only increases marginally because it needs to be calculated only once. The operation of predictive control with compensation delay is shown in Figure 3.16.

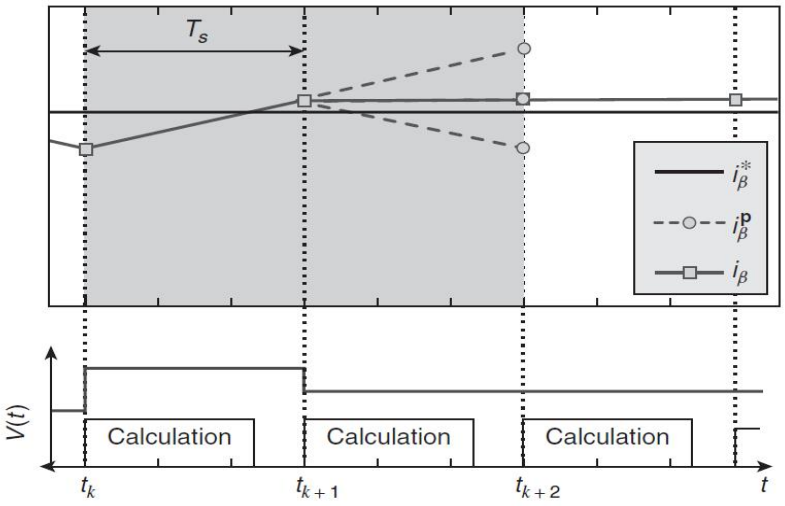

Figure 3.16: Operation of the predictive current control with delay and compensation: long calculation time (real case)

(Permitted/adapted from Rodríguez & Cortés 2012:183)

Here the measured currents and the applied switching state at time t_k are used in Equation 3.25 to estimate the value of the load currents at time, t_{k+1}. This current is then used as a starting point for the predictions for all switching states. These predictions are calculated using the load model, shifted one step forward in time:

$$i^p(k+2) = \left(1 - \frac{R\mathrm{T_S}}{L}\right)\check{\imath}(k+1) + \frac{\mathrm{T_S}}{L}v(k+1) \tag{3.26}$$

where $\check{\imath}$ is the estimated current vector, and $v(k+1)$ is the actuation to be evaluated.

The cost function is modified for evaluation of the predicted currents, $i^p(k+2)$, resulting in:

$$g = \left|i_\alpha^*(k+2) - i_\alpha^p(k+2)\right| + \left|i_\beta^*(k+2) - i_\beta^p(k+2)\right| \tag{3.27}$$

The switching state that minimizes this cost function is selected and stored for application at the next sampling instant. Figure 3.17 illustrates the operation of the predictive current control method with a large delay due to the calculations. It can be seen that the ripple in the load currents is considerable when the delay compensation is not accounted for. The delay compensation method that reduces the ripple and operation is similar to the ideal case. Note that the cost functions in Equations 3.25 and 3.26 require future values of the reference currents, $i^*(k+1)$ and $i^*(k+2)$ respectively. The calculation of these values is discussed in the next section.

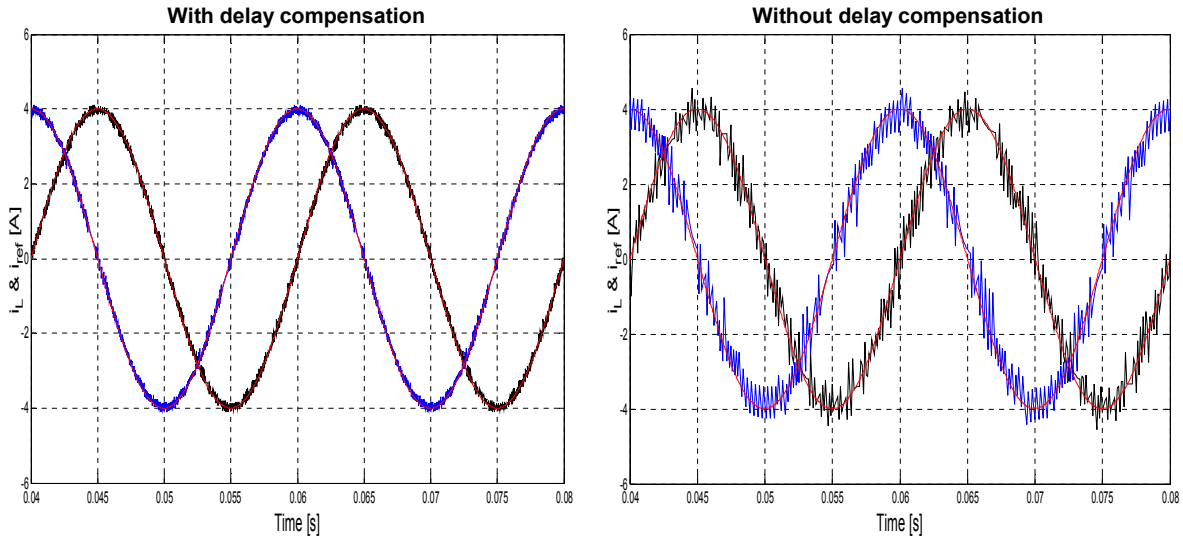

Figure 3.17: Predictive current control operation with and without delay compensation (T_S= 75 µs)

3.5.5.3 Prediction of future references

In the application of the predictive control approaches as stated in this thesis, the cost function depends on the future error. This requires that future references must be known so that the error between the reference and the predicted variable can be calculated at the next sampling instant.

However, future references are unknown, so they need to be estimated. Based on the assumption that the sampling frequency is much higher than the frequency of the reference signal, an uncomplicated way of achieving this is by considering that the future value of the reference is roughly equal to the present value of the reference. For the predictive current control example it can be assumed that $i^*(k+1) = i^*(k)$, which means that the cost function can be rewritten as:

$$g = \left|i_\alpha^*(k+1) - i_\alpha^p(k+1)\right| + \left|i_\beta^*(k+1) - i_\beta^p(k+1)\right| \tag{3.28}$$

This approximation will lead to a one-sample frame delay in the tracking of the reference currents. If compensation for the calculation-time delay (presented in the previous section) is considered, the reference $i^*(k+2)$ is required. Using the same idea, the future reference current can be assumed as $i^*(k+2) = i^*(k)$, resulting in the cost function given by Equation 3.29 below; reference tracking will then be subject to a two-sample frame delay.

$$g = \left|i_\alpha^*(k) - i_\alpha^p(k+2)\right| + \left|i_\beta^*(k) - i_\beta^p(k+2)\right| \tag{3.29}$$

The effect of the delay introduced by this approximation of future references is shown in Figure 3.18. It can be seen that this delay is noticeable for larger sampling times like T_S= 75 µs, but it is not visible when the sampling time is smaller.

It is common to use smaller sampling times in predictive control schemes, so this approach is reasonable in those cases. When the references are constant at a steady-state operation, this approach has no negative effects, and the two-sample delay can be observed only during transience.

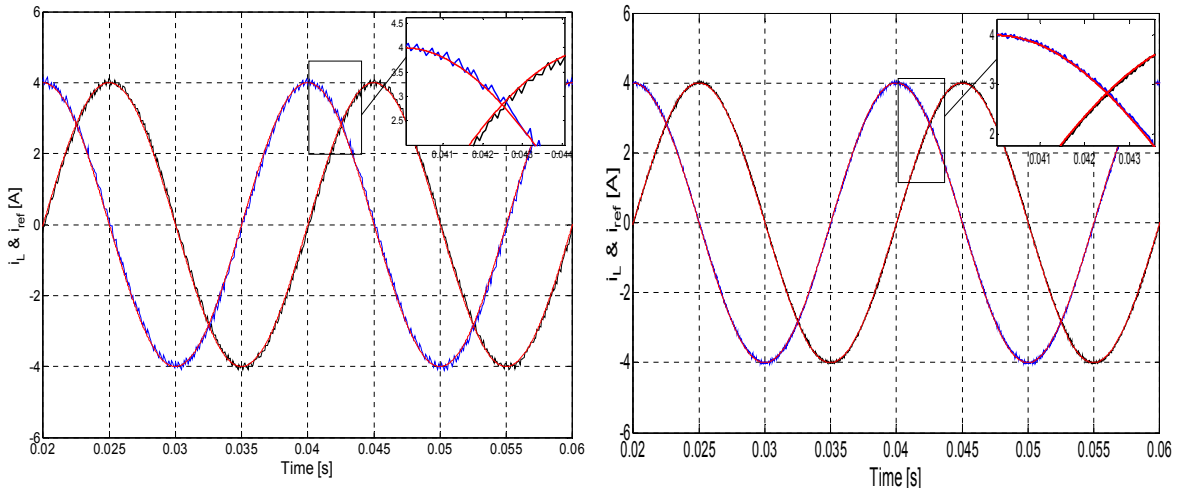

Figure 3.18: The load and reference currents for predictive current control using $\boldsymbol{i^*(k+2) = i^*(k)}$ for a sampling time (a) T_S= 75 µs, (b) T_S= 25 µs

3.5.6 Reference frames

For a three-phase system, the voltages and currents can be described in different reference frames, also called coordinate systems. As a result, the controller can be designed to operate in different coordinate systems. Here, voltages are taken as an example to describe the different reference frames, but the analysis can equally be applied to currents as well—and even to some other quantities (see Bose 2001, 2009). In many applications it is useful to present the system model in a static $\alpha\beta$ or a rotating dq reference frame using the well-known Clarke transformation for the former and the Park transformation for the latter (see Appendix A). The natural abc and stationary reference $\alpha\beta$ frames will be discussed in the subsections immediately following.

3.5.6.1 Natural abc frame

The voltages of a balanced three-phase system in the natural frame, also called the abc frame, can be represented as:

$$\begin{bmatrix} v_a \\ v_b \\ v_c \end{bmatrix} = \begin{bmatrix} V_m \cos(\theta) \\ V_m \cos(\theta - \frac{2\pi}{3}) \\ V_m \cos(\theta + \frac{2\pi}{3}) \end{bmatrix} \tag{3.30}$$

where V_m is the peak value of the voltage; v_a is the voltage of phase a and θ is the phase angle of v_a, which changes with time t.

Hence, the voltages are functions of time, t (and frequency). Note that the phase sequence here is abc. The three phases a, b and c in the natural frame can be regarded as spatially distributed away from each other by $\frac{2\pi}{3}$ rad, as shown in Figure 3.19(a). Also, the three phases are drawn to be consistent with the phase sequence, abc. The three-phase voltages v_a, v_b and v_c at a particular time, t or phase, θ, can be plotted as vectors according to their values, and spatially distributed in accordance with their coordinates, as shown in Figure 3.19(a). Therefore, v_a is on the horizontal line, v_b is in line with the vector $\alpha = e^{-j\frac{2\pi}{3}}$, and v_c is in line with the vector $\alpha^2 = e^{-j\frac{4\pi}{3}}$. The resulting diagrams are referred to as spatial diagrams in the sequel. Note that this is different from the widely used phasor diagrams, where the length of a vector is the amplitude of the voltage, and the angle of the vector is the phase of the voltage; here the length of a vector on a spatial diagram is the instantaneous value of the voltage, and the angle of the vector is fixed as the angle of the coordinate, that is 0 for phase a, $-\frac{2\pi}{3}$ rad for phase b, and $\frac{2\pi}{3}$ rad for phase c; see Figure 3.19(a). Moreover, a phasor diagram is independent of time, but the spatial diagram is dependent on time (and frequency). When θ changes with time, t, the vectors v_a, v_b *and* v_c on the spatial diagram shown in Figure 3.19(a) change their lengths and direction, but do not rotate.

For a balanced system, $v_a + v_b + v_c = 0$, which means that there are only two independent variables and that the three-phase balanced voltages can be expressed in two-dimensional space.

3.5.6.2 Stationary reference $\alpha\beta$ frame

Taking the spatial feature of the voltages in a spatial diagram into account, the vectors representing the instantaneous voltage values in the natural frame, as given in Equation 3.30, can be transformed to a space vector:

$$\bar{v}_s = k(v_a + \alpha v_b + \alpha^2 v_c) \tag{3.31}$$

This space vector, $\bar{v}_s$ can be broken down into a real part, v_α, and an imaginary part, v_β, and therefore $\bar{v}_s = v_\alpha + jv_\beta$; this is shown in Figure 3.19(b).

Note that the instantaneous values of v_a, v_b and v_c, and not their phasors, are used to form the space vector, $\bar{v}_s$. As a result, both v_α and v_β are functions of both time and frequency.

For $\alpha = e^{j\frac{2\pi}{3}}$ and $k = \frac{2}{3}$, the voltage space vector, using Equation 3.31, is:

$$\begin{aligned}\bar{v}_s &= k(v_a + \alpha v_b + \alpha^2 v_c) \\ &= kv_a + k\left(\cos\frac{2\pi}{3} - j\sin\frac{2\pi}{3}\right)v_b + k(\cos\frac{4\pi}{3} - j\sin\frac{4\pi}{3})v_c \\ &= k\left(v_a - \frac{1}{2}v_b - \frac{1}{2}v_c\right) + jk(-\frac{\sqrt{3}}{2}v_b + \frac{\sqrt{3}}{2}v_c)\end{aligned}$$

Hence,

$$\begin{bmatrix} v_\alpha \\ v_\beta \end{bmatrix} = T_{\alpha\beta}\begin{bmatrix} v_a \\ v_b \\ v_c \end{bmatrix} \tag{3.32}$$

with the $abc \rightarrow \alpha\beta$ transformation matrix

$$T_{\alpha\beta} = \frac{2}{3}\begin{bmatrix} 1 & -\frac{1}{2} & -\frac{1}{2} \\ 0 & -\frac{\sqrt{3}}{2} & \frac{\sqrt{3}}{2} \end{bmatrix} \tag{3.33}$$

The reference frame with v_α and v_β as coordinates, is often referred to as the stationary reference frame or the $\alpha\beta$ frame. The transformation in Equation 3.32 is called the Clarke transformation or the $abc \rightarrow \alpha\beta$ transformation. It transforms the voltages in the natural frame into the stationary or $\alpha\beta$ frame.

For balanced systems, $v_a + v_b + v_c = 0$, hence,

$$\begin{bmatrix} v_\alpha \\ v_\beta \end{bmatrix} = \begin{bmatrix} v_a \\ \frac{\sqrt{3}}{2}(-v_b + v_c) \end{bmatrix} \tag{3.34}$$

The α-component in the $\alpha\beta$ frame is always the same as v_a in the abc frame. In other words, v_a remains unchanged and stationary in the $\alpha\beta$ frame. Moreover, according to Equation 3.30,

$$\begin{aligned}v_\beta &= \frac{\sqrt{3}V_m}{3}(\cos\left(\theta + \frac{2\pi}{3}\right) - \cos(\theta - \frac{2\pi}{3})) \\ &= -V_m \sin\theta\end{aligned}$$

Hence, setting these values into Equation 3.31, gives the space vector as:

$$\bar{v}_s = V_m \cos\theta - jV_m \sin\theta = V_m e^{-j\theta} \tag{3.35}$$

When θ changes with time, t, the length of the space vector, $\bar{v}_s$ does not change, but the angle does. As a result, the vector, $\bar{v}_s$ *rotates* clockwise when θ increases with time, t. The direction of the rotation is the same as the spatial order abc, shown in Figure 3.19(a). Note that the $\alpha\beta$ reference frame itself is stationary and does not rotate; hence, the name stationary reference frame. Here, the introduction of the space vector has converted translational movements on a spatial diagram into rotational movements on the $\alpha\beta$ reference frame.

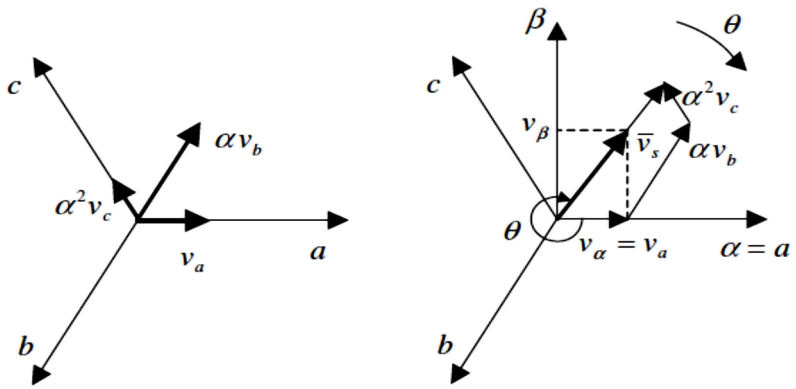

(a) The abc frame (b) The $\alpha\beta$ frame

Figure 3.19: Reference frames for three-phase system

3.6 Summary

Various predictive control methods were introduced in this chapter. It is clear that predictive control has been widely used for the control of power electronic converters and motor drives. This chapter presented an examination of the terminology used in predictive control and described the modelling of a system and the approximations for derivatives of differential equations. The cost function classifications in terms of weighting factors, delay compensation and reference frames were also presented. This chapter further detailed different types of terms that can be included in a wide variety of cost functions and weighting factors. Examples of the procedures discussed were provided to illustrate the wide variety of cost functions and adjusted weighting factors available for use in predictive control applications. Finally, simulation of a three-phase VSI using a finite set-model predictive current control was carried out to obtain results indicating the influence of some system parameters used in predictive control on the load current and load voltage.

CHAPTER FOUR

PREDICTIVE CURRENT CONTROL TECHNIQUES FOR A DCC INVERTER IN RESs APPLICATIONS

4.1 Introduction

Nowadays, PV systems and wind turbines can be used with maximum efficiency by using an appropriate power converter. The increase in the use of power from these resources has led to the need for research on new control strategies and a suitable topology for high-power converters to meet the demands for performance and efficiency. MLCs have been extensively studied in the last few decades. By considering the increasing energy demands and the requirements for power quality and efficiency, power conversion by means of power electronics have become important topics in RESs applications.

Research of modern voltage source MLCs was started with the introduction of diode-clamped, three-level inverters in 1981 (Nabae et al. 1981). Pulse width modulation (Carrara et al. 1992; Holmes & Lipo 2003; McGrath & Holmes 2002) and space vector modulation (Celanovic & Boroyevich 2001) are the most common modulation techniques proposed for controlling this kind of converter. The DC-link balancing problem in this topology is another subject that has been studied in recent years (Bendre et al. 2006; Tallam et al. 2005; Yaramasu et al. 2013).

The application of power electronics for predictive control has been researched since the 1980s (Kennel & Schroeder 1983). This technology requires a high number of calculations compared to classic control methods, but the fast microprocessors available today have made it possible to implement predictive control for voltage source MLCs. Additionally, MPC has distinct advantages when compared to the traditional PWM methods (Najmi et al. 2012; Rodríguez & Cortés 2012).

The inherent discrete nature of power converters sets the stage for implementing MPC in power converters and motor drives. Since power converters have a finite number of switching states, the MPC optimization problem can be easily formulated, simplified and reduced to the prediction of the system behaviour specifically for those possible switching states. Each prediction is used to evaluate a cost function. Consequently, the switching state with the lowest cost is selected, generated and applied in the next switching instant. This control method is known as an FS-MPCC approach, since the possible control actions (switching states) are finite; this is the control strategy used in this study. Many studies have been conducted into the successful application of FS-MPCC schemes incorporated in three-phase MLIs and drive applications (Abu-Rub et al. 2004; Li et al. 2009; Vargas et al. 2007; Yaramasu et al. 2013(a)).

Chapter four outlines a finite set-model predictive current control strategy that is proposed to handle the output current, as well as the balancing of the DC-link capacitor voltages for a three-phase, three-level DCC inverter with an RL-load. This strategy allows for fast load current control, while keeping the DC-link capacitor

voltages balanced. In this chapter the problem of balancing the DC-link voltage and output current reference tracking, are examined through co-simulation of MATLAB and PSIM software. A voltage balancing algorithm to control the DC-link capacitor voltages and keep them within the hysteresis band, is presented. Thereafter, the robustness of a control strategy subject to variable DC-link voltages, as encountered in RESs applications, was investigated. The robustness was assessed in terms of the THD and tracking behaviour of the reference currents applied to all the DC-link voltage values. The system performance in terms of tracking behaviour was investigated, along with the dynamic response of the system with a step change in the amplitude of the sinusoidal wave reference. Additionally the control algorithm was tested with a constant waveform and a square waveform in orthogonal coordinates as the reference current. Lastly, the system robustness of the proposed control algorithm was studied by comparing the model parameters with the actual system parameters.

Chapter four starts with an overview of the SimCoupler module for SSI with PSIM-MATLAB/Simulink, described in Section 4.2. The power converter model that is used in this chapter is presented in Section 4.3. Firstly, the time-continuous model is presented and then discretized to obtain the output currents and DC-link capacitor voltages. The control scheme that is used to control the power converter model and balance the DC-link capacitors is developed in Section 4.4. Results and discussions are presented next, followed by a summary in the last section of the chapter.

4.2 Software simulation integration of two independent software platforms

The software packages available for the simulation of power electronics and drives are PSIM and MATLAB. The link between PSIM and MATLAB/Simulink for SSI/co-simulation is provided by the SimCoupler module. With the SimCoupler module, full use can be made of the power simulation capability of PSIM and the control simulation capability of MATLAB/Simulink, in a complementary way.

One of the objectives of this study is to show how to use the SimCoupler module for a three-phase MLI using a model predictive strategy with an RL-load. In this study the theoretical approach of the system model is explained, and subsequently the simulation results are presented so as to show the effectiveness of the system in the SSI arena.

To validate the feasibility of the proposed control algorithm, MATLAB/Simulink and PSIM modelling for SSI work were carried out for different conditions of the current references and loads implemented for a three-phase, three-level DCC with an RL-load. The SimCoupler module allows the designers of power electronics to simulate control in the MATLAB/Simulink environment. This ability further enhances the control simulation capability of PSIM by providing access to numerous Simulink toolboxes for

various applications. For example, code can automatically be generated with the PSIM-MATLAB/Simulink for SSI. First, the power circuit is simulated in PSIM, and the control algorithm is simulated in MATLAB/Simulink. Then the Simulink toolbox and supporting resources can be used to generate production quality code automatically for a target platform. Figure 4.1 depicts SSI between PSIM and MATLAB/Simulink.

An MPC strategy is applied in a three-phase, three-level DCC inverter with an RL-load; the power converter and the load are implemented in PSIM and the MPC is implemented in MATLAB/Simulink—this is shown in Figure 4.1. The proposed control block and reference current are represented in Simulink, and the SimCoupler model block (highlighted in Figure 4.1(a)), which represents the PSIM calculation, is connected to the rest of the system through input/output ports as shown in Figure 4.1(a). In PSIM, shown in Figure 4.1(b), three-phase load currents, voltages and DC-link capacitor voltages are connected to the output link nodes, so as to pass these variable values to MATLAB/Simulink. To receive values back from Simulink, there are three signals that are connected to the input link nodes, and through which all the switching states can be applied to the inverter.

When the connection of the system model has been completed, there follows the important step in an SSI setup of time synchronization of the two independent software platforms used—in this case, PSIM and MATLAB/Simulink. This step is done by setting the solver type in MATLAB/Simulink to either fixed-step, or variable-step. If the fixed-step type is chosen, the fixed-step size should be the same as, or close to, the time step used in PSIM (in this study, the PSIM time step was 2 μs). The Simulink circuit will resemble that shown in Figure 4.1(a). Alternatively, the variable-step solver option can be used. However, in this case, a zero-order-hold must be inserted to each input port of the SimCoupler model block, and the sampling time of the zero-order-hold must be equal to, or close to, the time step used in PSIM.

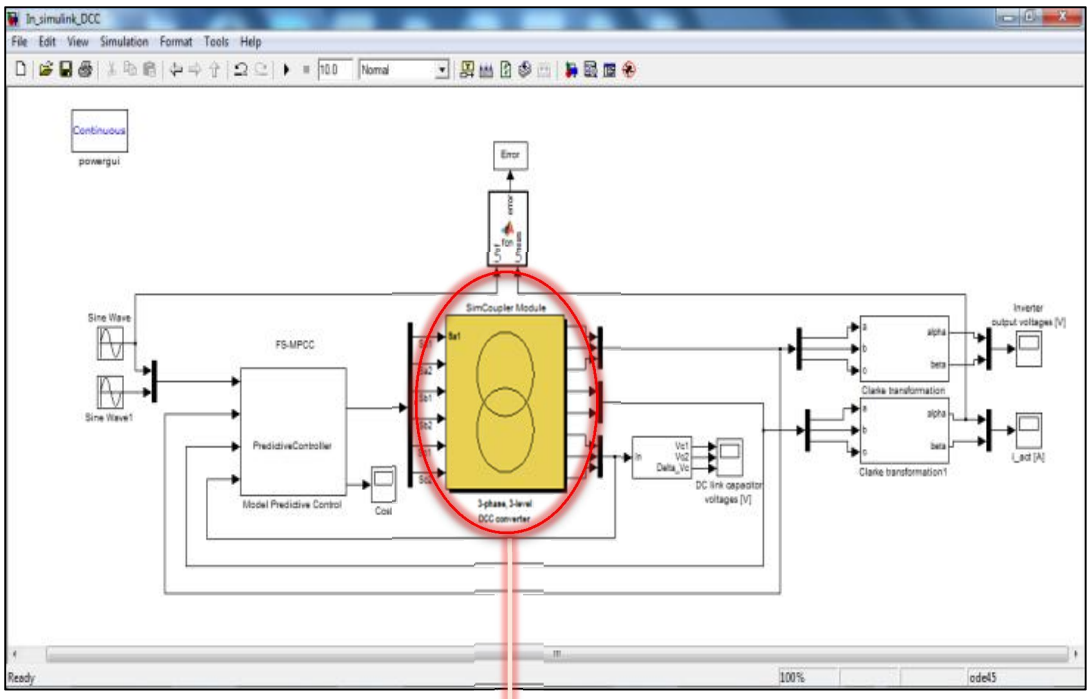

(a) Model predictive current control and SimCoupler model block implemented in MATLAB/Simulink

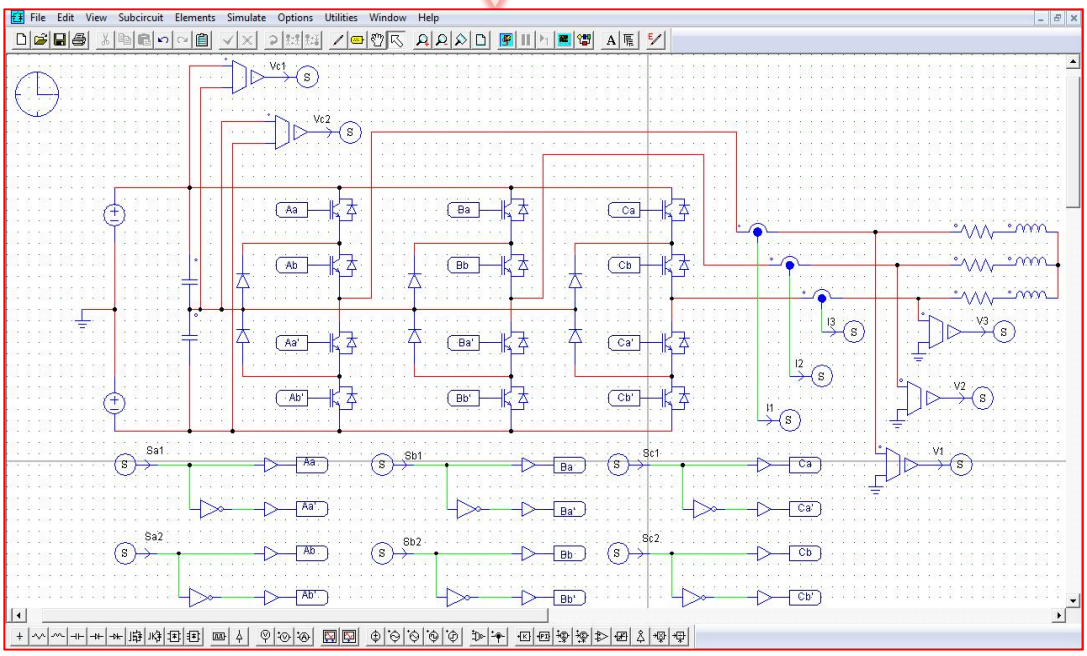

(b) The three-phase, three-level DCC inverter with an RL-load implemented in PSIM

Figure 4.1: The SSI between the PSIM and MATLAB/Simulink

4.3 System description overview

A three-phase DCC with an AC filter is coupled to a resistive-inductive load and powered by a PV system and a wind turbine; this is shown in Figure 4.2. In this chapter, an FS-MPCC scheme for a three-phase DCMLI with an RL-load is discussed. Although the use of a diode-clamped multi-level converter requires quite a large number of active devices, it has the following advantages (Pan & Peng 2009):

- Lower input current harmonics
- Bidirectional power flow
- Ability to control the DC-link voltage
- Ability to control the input power factor

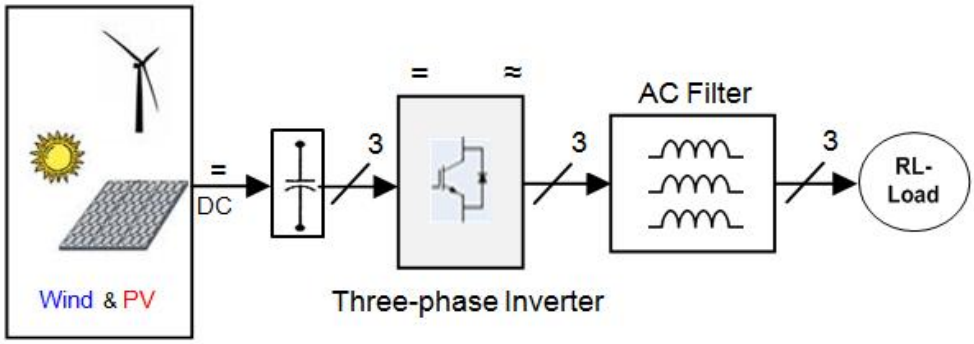

Figure 4.2: Three-phase inverter with AC filter and RL-load for RESs applications

4.3.1 Three-phase, three-level DCC inverter topology

A three-phase, diode-clamped multi-level converter is depicted in Figure 4.3. It includes a three-phase, three-level DCC inverter; a DC-link, which has a DC source, v_{DC}, and capacitors C_1 and C_2. The DCC has twelve switches, and six DCC-diodes referred to as D_{1x} and D_{2x} where $x = a, b, c$. Additionally there is an AC filter connected to the RL-load. The reason for using an RL-load is that it represents one of the most common applications for this kind of converter.

In the DC-link the voltage, v_{DC}, is split into three levels by using two series-connected capacitors, C_1 and C_2. The midpoint, n, is regulated at half the DC-link voltage and is defined as the neutral point. To avoid short-circuiting the DC source, the three-level DCC has two pairs of complementary controlled switches in each phase, (S_{1x}, S_{3x}) and (S_{2x}, S_{4x}), where $x = a, b, c$; this is shown in Figure 4.3. This leads to twenty-seven different, possible combinations of the switching states. The switching states of the three-level DCC inverter are summarized in Table 4.1. Any given output phase of the converter can be connected to the negative point, (S_{1a}= 0, S_{2a}= 0), the neutral point, (S_{1a}= 0, S_{2a}= 1) or the positive point, (S_{1a}= 1, S_{2a}= 1) of the DC-link, which results in

different current paths between the DC-side and AC-side. Figure 4.4 illustrates the allowed switching states.

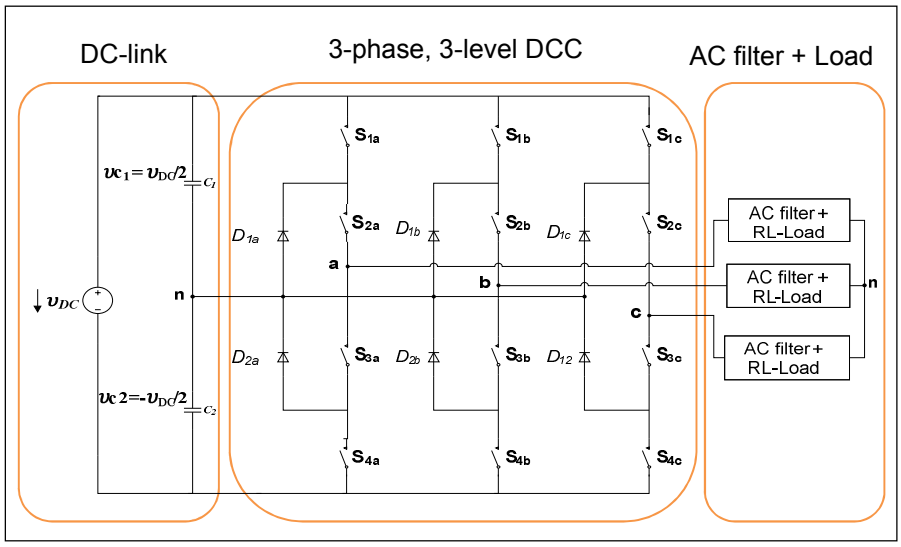

Figure 4.3: Three-level DCC inverter circuit topology

Table 4.1: Switching configurations possible in a three-level DCC

#	complementary pair no. 1		complementary pair no. 2		v_{xn}
	S_{1x}	S_{3x}	S_{2x}	S_{4x}	
1	0	1	0	1	$-v_{DC}/2$
2	0	1	1	0	0
3	1	0	1	0	$v_{DC}/2$

4.3.2 DCC switching vectors: $\alpha\beta$ plane analysis

In a three-phase, three-level DCC inverter there are 27 switching states that generate 19 different voltage vectors on the AC-side of the converter (18 active vectors and one null vector) with eight redundancy states (see Appendix B). Some switching states are redundant, generating the same voltage vector. For example, the zero-voltage vector, V_0 can be generated by three different switching states: (+, +, +), (0, 0, 0) and (−, −, −), as shown in Figure 4.5. The availability of redundancies of different states provides extra degrees of freedom. The 19 voltage vectors, generated from the 27 switching states, as shown in Figure 4.5, can be applied by the inverter to the load.

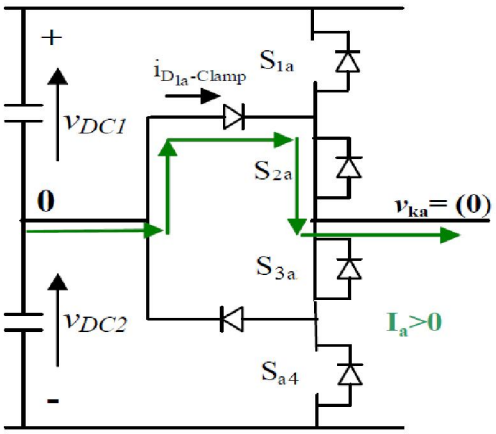

(a) [S_{1a} = 0, S_{2a} = 0] i_a > 0

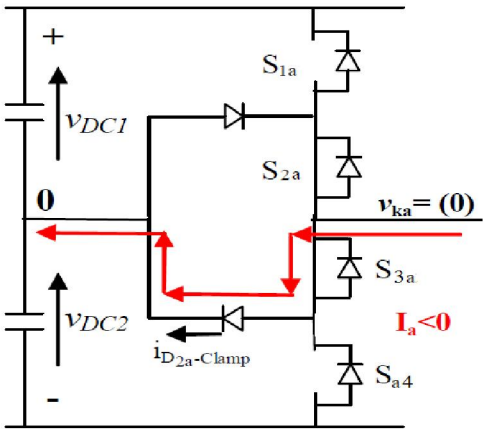

(b) [S_{1a}= 0, S_{2a}= 0] i_a < 0

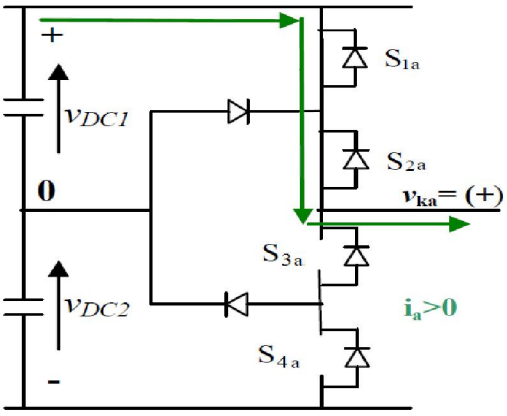

(c) [S_{1a}= 0, S_{a2} =1] i_a > 0

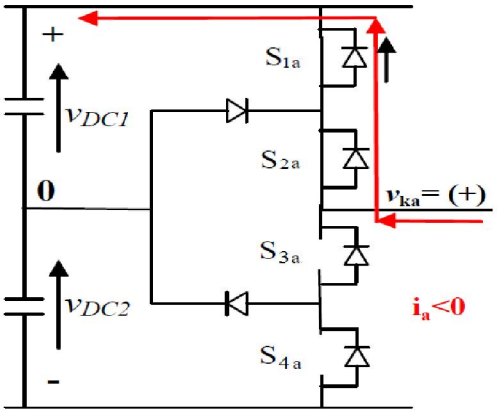

(d) [S_{1a} = 0, S_{2a} = 1] i_a < 0

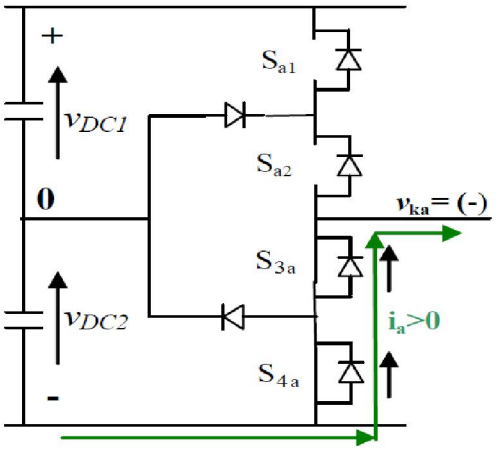

(e) [S_{1a}= 1, S_{2a}= 1] i_a > 0

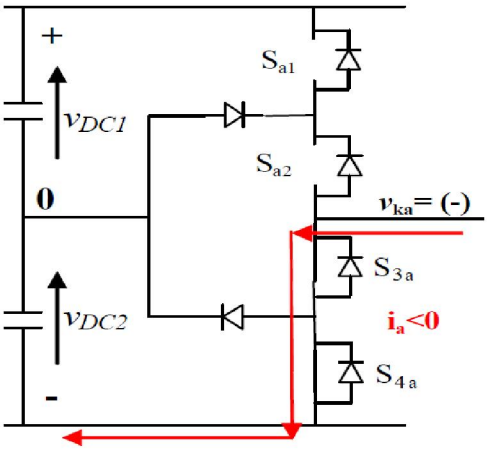

(f) [S_{1a}= 1, S_{2a}= 1] i_a < 0

Figure 4.4: Current flow paths of the three-level DCC

Assuming that the system shown in Figure 4.3 is a balanced, three-phase power system, the following equations per phase can be derived for the converter:

$$\left.\begin{aligned} v_{ka} &= \frac{2S_{1a}-(S_{1b}+S_{1c})}{3}v_{DC1} + \frac{2S_{2a}-(S_{2b}+S_{2c})}{3}v_{DC2} \\ v_{kb} &= \frac{2S_{1b}-(S_{1a}+S_{1c})}{3}v_{DC1} + \frac{2S_{2b}-(S_{2a}+S_{2c})}{3}v_{DC2} \\ v_{kc} &= \frac{2S_{1c}-(S_{1a}+S_{1b})}{3}v_{DC1} + \frac{2S_{2c}-(S_{2a}+S_{2b})}{3}v_{DC2} \end{aligned}\right\} \quad (4.1)$$

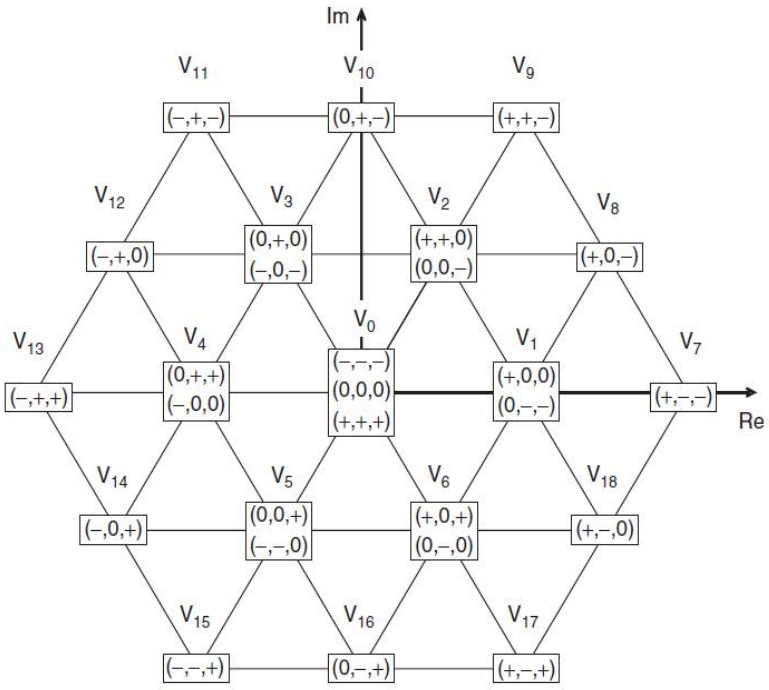

Figure 4.5: Voltage vectors generated by a three-level converter

4.3.3 Load model

To obtain the continuous-time, state-space equations of the load for each phase, the differential equation of the load currents is applied:

$$v_{DC}(t) = \mathrm{R}.i(t) + L\frac{di}{dt} \quad (4.2)$$

When an AC filter is added to the resistive-inductive load, inductance, $\mathrm{L} = \mathrm{L}_f + \mathrm{L}_L$; this is depicted in Figure 4.6.

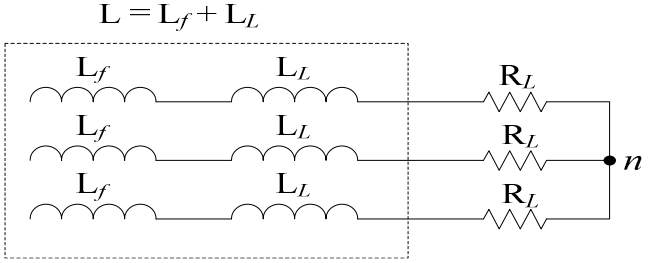

Figure 4.6: Representation of the AC filter with inverter load

Applying the Clarke transformation to the voltages and currents, the load model can be expressed in a simplified coordinate system with linearly independent axes, α and β, as follows:

$$\alpha = 2/3\ (\mathrm{a} - 0.5\ \mathrm{b} - 0.5\ \mathrm{c}) \tag{4.3}$$

$$\beta = 2/3\ (0 + 0.5\sqrt{3}\ \mathrm{b} - 0.5\sqrt{3}\ \mathrm{c}) \tag{4.4}$$

This results in the continuous-time, state-space equation of the load, which is:

$$\begin{bmatrix} i_\alpha \\ \\ i_\beta \end{bmatrix} = \begin{bmatrix} -\frac{R}{L} & 0 \\ \\ 0 & -\frac{R}{L} \end{bmatrix} \begin{bmatrix} i_\alpha \\ \\ i_\beta \end{bmatrix} + \begin{bmatrix} \frac{1}{L} & 0 \\ \\ 0 & \frac{1}{L} \end{bmatrix} \begin{bmatrix} v_\alpha \\ \\ v_\beta \end{bmatrix} \tag{4.5}$$

A discrete-time equation for the future load current is obtained by using the Euler-forward approximation to obtain a discrete-time system representation. The derived approximation is given by:

$$\dot{x} \approx \frac{x(k+1) - x(k)}{\mathrm{T_S}} \tag{4.6}$$

where $\mathrm{T_S}$ is the sampling period, k is the current sampling instant and x is the state variable.

Then, the discrete-time load model can be derived as:

$$\begin{bmatrix} i_\alpha(k+1) \\ \\ i_\beta\ (k+1) \end{bmatrix} = \begin{bmatrix} 1 - \mathrm{T_S}\frac{R}{L} & 0 \\ \\ 0 & 1 - \mathrm{T_S}\frac{R}{L} \end{bmatrix} \begin{bmatrix} i_\alpha(k) \\ \\ i_\beta(k) \end{bmatrix} + \begin{bmatrix} \frac{\mathrm{T_S}}{L} & 0 \\ \\ 0 & \frac{\mathrm{T_S}}{L} \end{bmatrix} \begin{bmatrix} v_\alpha(k) \\ \\ v_\beta(k) \end{bmatrix} \tag{4.7}$$

Equation 4.7 is used to predict the load current for each switching possibility. The cost function, *g*, is evaluated for each of the 19 possible voltage vectors generated by this inverter to calculate the future value of the load current. The voltage vector that minimizes the cost function is selected and applied during the next sampling instant. This is because the current will always be on or outside of the hysteresis band. In this way, the switching state will constantly be changed.

4.4 Finite set-model predictive current control of DCMLIs.

Figure 4.7 shows a DCC converter subject to FS-MPCC where X_{ref} represents the reference values for the predictive control, $\mathrm{X}(k)$ is the measured variable at time, k, and $\mathrm{X}(k+1)$ are the predicted values for n allowed switching states at time, $(k+1)$. The errors between the reference and predicted values are obtained to minimize the cost function, and the switching state that minimizes the cost function, is chosen. The switching signals, S, of the chosen state are then applied to the converter. To reduce the computational effort that arises from the switching possibilities (27 different

switching possibilities for one prediction step), the switching state that delivers the best voltage vector among 19 voltage vectors is determined; this is illustrated in Figure 4.5. The optimal switching state, which is the one that minimizes the simple cost function, is selected and applied at the next sampling instance when the time is (k+1). In the case of the current control mode, the switching signals, S, which are obtained by selecting the (switch) settings that minimize the cost function when the errors between the reference current and predicted current are considered, are then applied to the power converter.

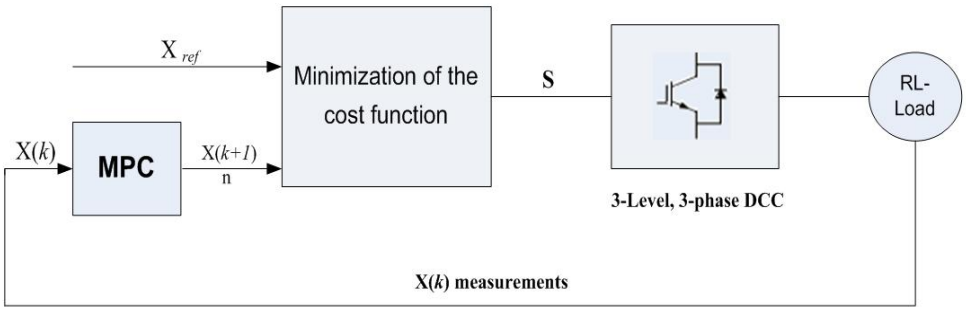

Figure 4.7: FS-MPCC block diagram

With a long prediction horizon, the increase in multiple possibilities raises the calculation effort substantially, and creates the need for very powerful computers with very fast microprocessors and ample RAM capabilities. It is the availability of such computers that makes the SSI technique possible. The specifications of the computer used in this study are presented in Table 4.2.

Table 4.2: The specifications of the computer hardware components needed for co-simulation

Computer hardware components	Specifications
Processor	Intel Core i7-3930K (3.2GHz, 12M Cache, 12x Cores), Overclocked to 4.5GHz Per Core CPU
Memory	32 GB Quad Channel (8x4GB) DDR3 1600MHz
Two Storage Drives	128GB SSD Read: 560MB/s Write:430MB/s Solid-State Drive
	4TB, 6.0Gb/s Hard Drive

4.4.1 DC-link capacitor voltages

To balance the two DC-link capacitors, it is necessary to understand the mechanisms that lead to an imbalance of the two voltages. A hysteresis-based voltage balancing algorithm is used to balance the DC-link capacitor voltage. Hysteresis-based predictive control aims to keep the capacitor voltages within upper and lower boundaries. The proposed control predicts the outcome of the capacitor voltages for all the possible control inputs; the cost function then selects the input that will keep the controlled variables within the boundary for the longest time. After the optimum voltage vector for the next sampling cycle has been determined, the optimum switching state that produces this voltage vector has to be found and applied. The two capacitor voltages have to stay within a certain hysteresis band around their desired voltage of $v_{DC}/2$. The differential equation for the capacitor current is given by Equation 4.8.

$$i_C = C\,\frac{dvc}{dt} \tag{4.8}$$

A discrete-time equation for the DC-link capacitor voltage is obtained by using the Euler forward method (from Equation 4.6) in order to obtain a discrete-time system representation. At this point, the discrete-time DC-link capacitor voltage will be:

$$v_{c1,2}(k+1) = v_c(k) + \frac{1}{C} i_c(k)\,\mathrm{T_S} \tag{4.9}$$

where $v_{c1,2}(k+1)$ are the predicted DC-link capacitor voltages; $i_c(k)$ is the current through the capacitor; $v_c(k)$ is the capacitor voltage; and *C* is the capacitance.

Equation 4.9 is used to predict the DC-link capacitor voltage for each permissible switching possibility. The currents through the capacitors are obtained based on the load currents and the present switching state; no additional measurements are required. Predictions of the future value of the voltage of the capacitor, based on its present current and voltage, can be determined using Equation 4.9.

The proposed control algorithm chooses the switching state that produces the requisite voltage vector and keeps the capacitor voltages within their hysteresis bands. As long as the capacitor voltage is within its limits, a switching combination leading to a zero voltage is allowed. If, however, a capacitor voltage has deviated out of the hysteresis band, only the switching state that drives the voltage back into the hysteresis band is selected and implemented at the next switching instance. The voltage balancing algorithm has to keep both DC-link capacitor voltages equal to each other. Hence, the absolute values of the predicted DC-link capacitor voltages have to be within the hysteresis band for the longest time. The hysteresis band value was chosen to be 0.1% of the v_{DC} value.

4.4.2 Optimization and cost function

As shown in Figure 4.8, the cost function requires predicted output currents, $i(k+1)$, and capacitor voltages, $v_{c1}(k+1)$ and $v_{c2}(k+1)$. In Equations 4.7 and 4.9, the prediction of the load current and capacitor voltages were obtained using an Euler forward approximation based on $i(k)$ and $v_{DC}(k)$ respectively.

The controller, shown in Figure 4.8, can use any permissible output to bring the controlled currents, closer to their reference current and also to balance the DC-link capacitor voltages. The future value of the load current, $i(k+1)$, and capacitor voltages, $v_{c1}(k+1)$ $v_{c2}(k+1)$, are predicted for the 19 permissible switching states generated by the inverter. For this purpose, it is necessary to measure the prevailing load currents, $i(k)$, and DC-link capacitor voltages, $v_{c1}(k)$ and $v_{c2}(k)$. After obtaining the predictions, a cost function, *g*, as given by Equation 4.10, is evaluated for each switching state. The switching state (and therefore the voltage vector generated by the DCC inverter) that minimizes *g*, is selected and applied in the next sampling period.

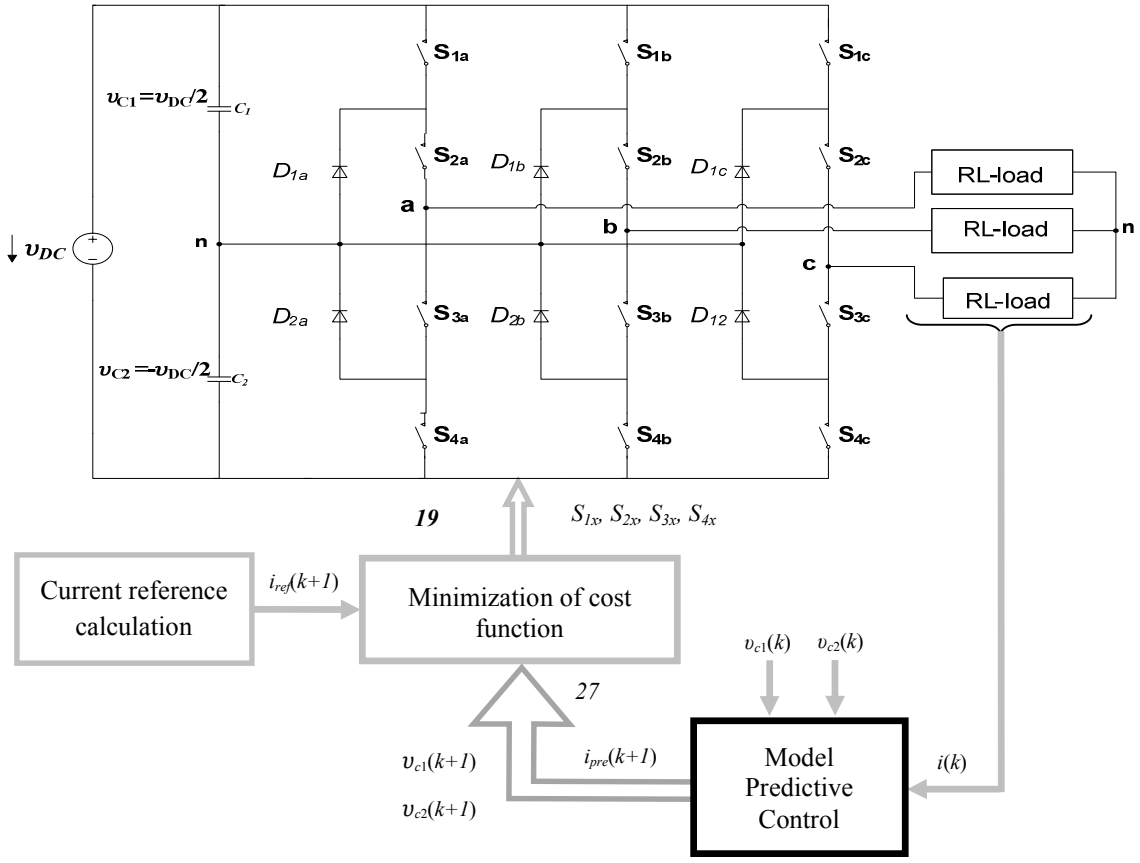

Figure 4.8: DCC topology connected to the load and control block diagram

The proposed cost function, *g*, is defined as

$$g = f\left(i_{ref}(k+1), i(k+1)\right) + \lambda_{DC}|Delta| \tag{4.10}$$

where λ_{DC} is the weighting factor which can be adjusted to handle the relationship between terms dedicated to reference tracking and voltage balance within the cost function.

The objective of the second term, $\lambda_{DC}|Delta|$, in Equation 4.10, is to take advantage of the redundant states of the three-level inverter studied in this work; this advantage stems from the fact that the tracking cost function, *g*, in Equation 4.10, depends only on the voltage vector selected. The proposed composition of the factor $Delta$ is shown in Equation 4.11.

$$Delta = v_{c1}(k+1) - v_{c2}(k+1) \tag{4.11}$$

Equation 4.11 gives the value of the difference between the two predictions of the DC-link capacitor voltage. The redundant switching states of the DCC inverter, which result in smaller differences, are also available for implementation. Within the cost function, the weighting factor, λ_{DC} handles the relationship between the terms dedicated to reference current tracking and those dedicated to voltage balance.

To take advantage of the possibilities offered by this algorithm, it is necessary to adjust the parameter, λ_{DC}. To maintain the DC-link voltage balance by only selecting the appropriate switching state from the redundant states that generate a given voltage vector, a value of λ_{DC} should be selected by taking the average value of *Delta*.

For the DCC inverter, a simple cost function can be defined in absolute value terms by one prediction step, as in Equation 4.12.

$$g = \left|i_{ref\alpha}(k+1) - i_{\alpha}(k+1)\right| + \left|i_{ref\beta}(k+1) - i_{\beta}(k+1)\right| + \lambda_{DC}|v_{c1}(k+1) - v_{c2}(k+1)| \tag{4.12}$$

To simplify the calculations, it can be assumed that the current reference value is constant for the prediction horizon where sampling time, T_S, is small. This approximation is given by Equation 4.13.

$$i_{ref}(k+n) \approx i_{ref}(k) \tag{4.13}$$

For a more accurate approximation, the reference current values, $i_{ref}(k+1)$, as required in Equation 4.12, have to be predicted from the present and previous values of the reference current using a second-order extrapolation technique given by:

$$i_{ref}(k+1) = 3i_{ref}(k) - 3i_{ref}(k-1) + i_{ref}(k-2) \tag{4.14}$$

Equation 4.14 has been obtained from the quadratic Lagrange extrapolation formula (Kukrer 1996).

In Figure 4.9 a flow diagram of how the predictive algorithm is implemented for the three-phase, three-level DCC is illustrated. At the start of the algorithm control loop, the required signals are sampled. Thereafter, the algorithm measures the active component of the load and initializes the value of the optimum cost function, $g_{optimal}$, which it does by making use of Equation 4.5. This optimum cost function is a variable that will contain the lowest cost function value determined by the algorithm up to this point. The algorithm then goes into an internal loop in which, for each permissible switching state, the cost function given by Equation 4.12 is calculated, taking account of the predicted output current obtained from Equation 4.7, and the predicted capacitor voltage obtained from Equation 4.9. If, for a particular switching state, the value of the cost function, g, is less than the value of $g_{optimal}$, that lower value, is then stored as $g_{optimal}$, and the switching state number corresponding to the newly stored cost function value, is stored as $x_{optimal}$. The internal loop is complete after all 27 switching states have been assessed. The value of variable $x_{optimal}$ at that stage identifies the state that produces the optimal value of g, and this state is then activated in the converter during the next sampling period—the control algorithm is then re-run again.

In general, the control algorithm, shown in Figure 4.9, can be summarized by the following steps:

(1) Measure the load currents and DC-link voltage.
(2) Initialize the value of the optimum cost function.
(3) Predict (for all permissible switching states) the load currents and capacitor voltages for the next sampling instant.
(4) Evaluate the cost function for each prediction.
(5) Select the optimal switching state that minimizes the cost function.
(6) Apply the new switching state.

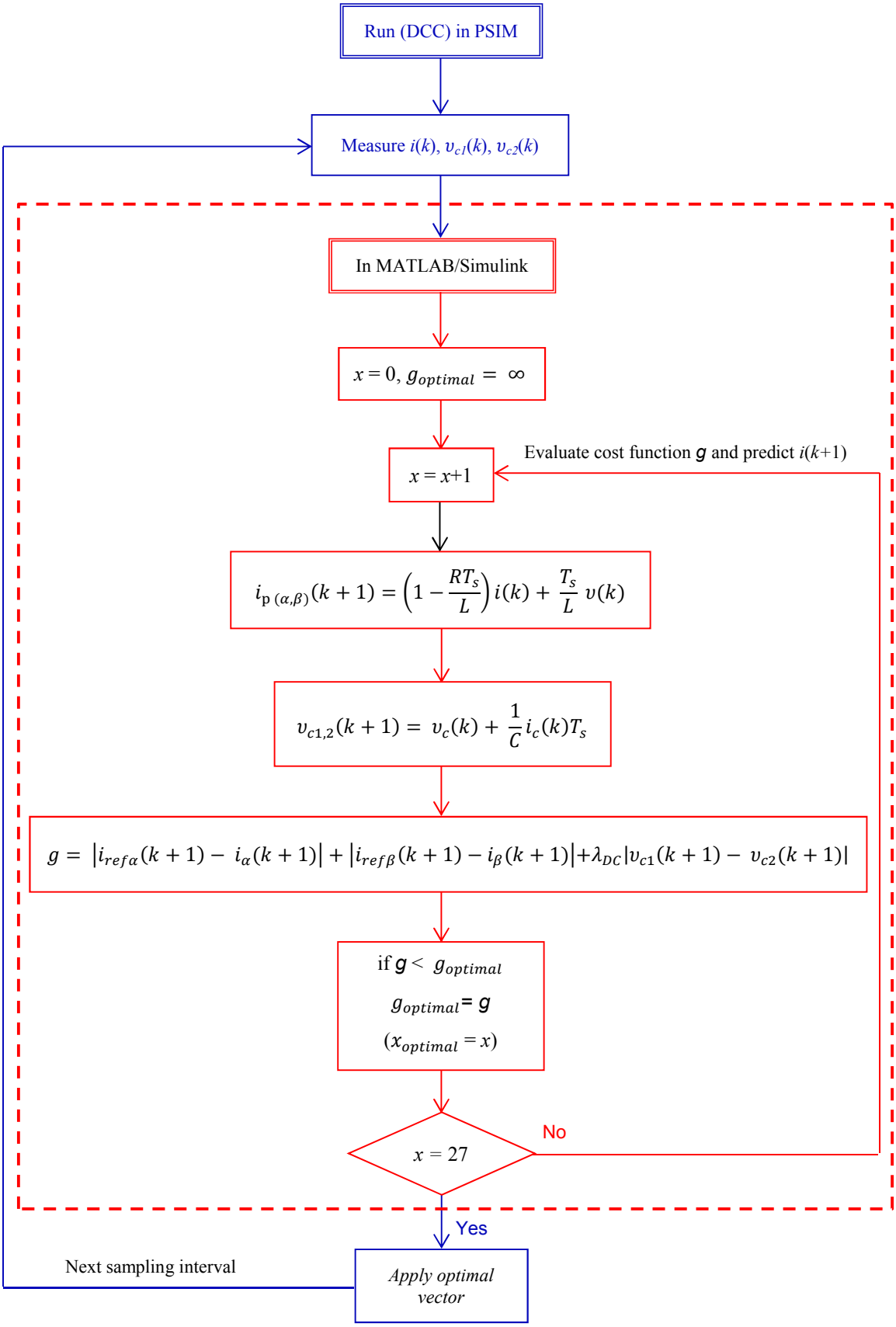

Figure 4.9: Flow diagram of the implemented control algorithm

4.5 Results and discussion

The FS-MPCC strategy for a three-phase, three-level DCC was co-simulated using MATLAB/Simulink together with PSIM to evaluate the performance of the proposed control algorithm and to check the performance and robustness of the proposed predictive control method. A sinusoidal reference current was applied to the system, and the amplitude of the reference current was set to 4 A at a frequency of 50 Hz per phase. An RL-load was then connected to the output of the DCC as shown in Figure 4.8. Table 4.3 shows the parameters used for the simulations.

Table 4.3: Parameters used for the simulations

Parameter	Value
Load resistor, R	10 Ω
Load inductor, L	20 mH
DC-link capacitor	3300 µF
DC-link voltage, v_{DC}	200 V
Reference amplitude current, i_{ref}	4 & 5 A
Hysteresis-band limits relative to v_{DC}	0.1%
Sampling time, T_S	25 and 100 µs

4.5.1 DC-link capacitor voltages balancing

A weighting factor of λ_{DC} = 0.02 was implemented to provide better balanced DC-link capacitor voltages with a smaller steady-state error (Figure 4.10(a)). The selected weighting factor provides: the best performance in terms of the DC-link capacitor voltages balance; excellent current reference tracking; and the lowest harmonics content in the load current. But when only current control is considered in the cost function, the DC-link capacitor voltages are out of control, as is illustrated in Figure 4.10(b). The top two graphs of Figure 4.10(c) show that the DC-link capacitor voltages are kept within the hysteresis band. The band-limited performance of the controller with reduced error is shown in the bottom graph of Figure 4.10(c).

The three-phase load currents with capacitor voltage balancing are depicted in Figure 4.11(a), and the same currents, but without capacitor voltage balancing, are shown in Figure 4.11(b). When only current control is considered in the cost function and the capacitor voltages are not controlled, then λ_{DC} = 0. As is apparent from Figure 4.11(b), when capacitor voltages are not controlled, the load current ripple increases significantly, when compared to that in Figure 4.11(a) where the capacitor voltages have been considered in the cost function.

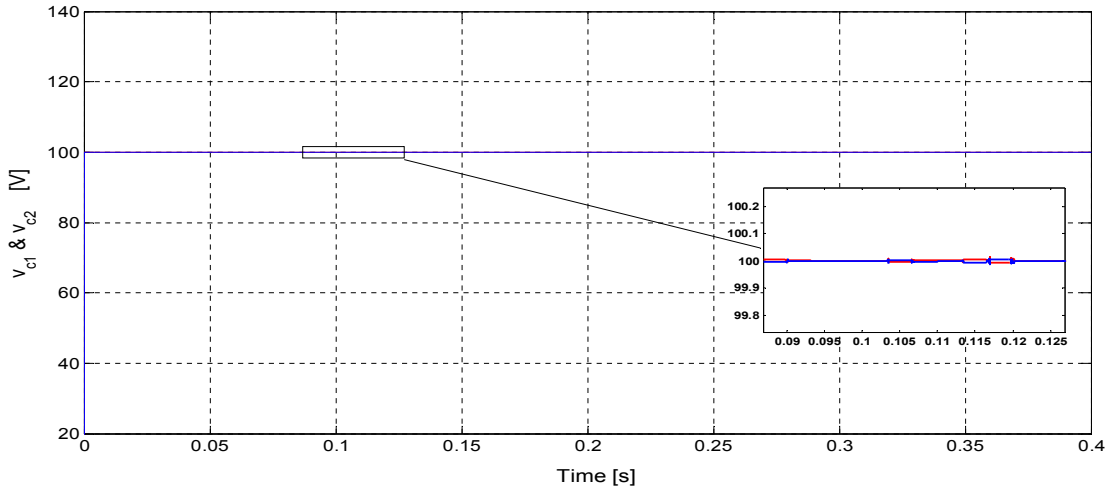

(a)

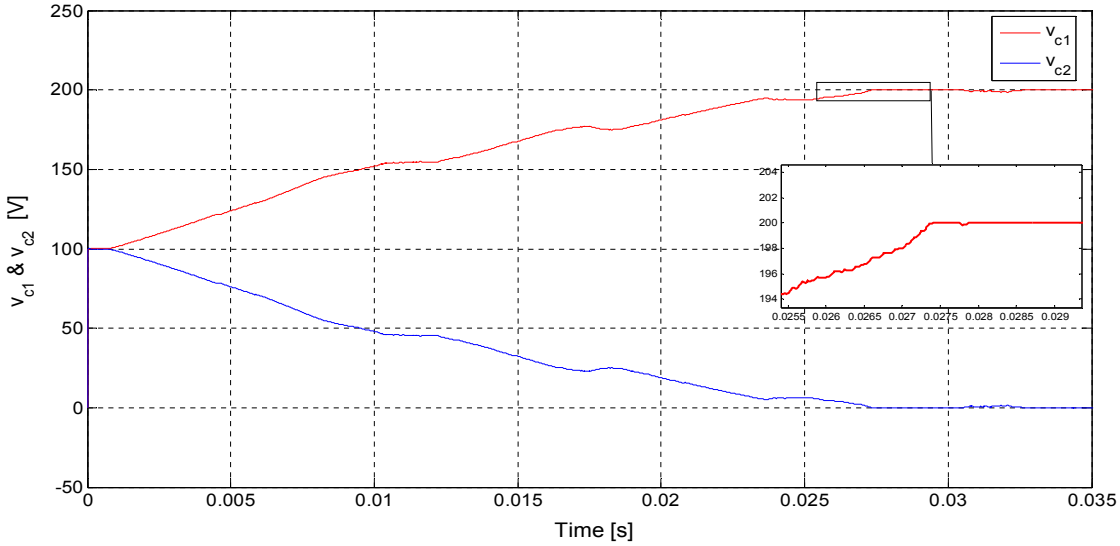

(b)

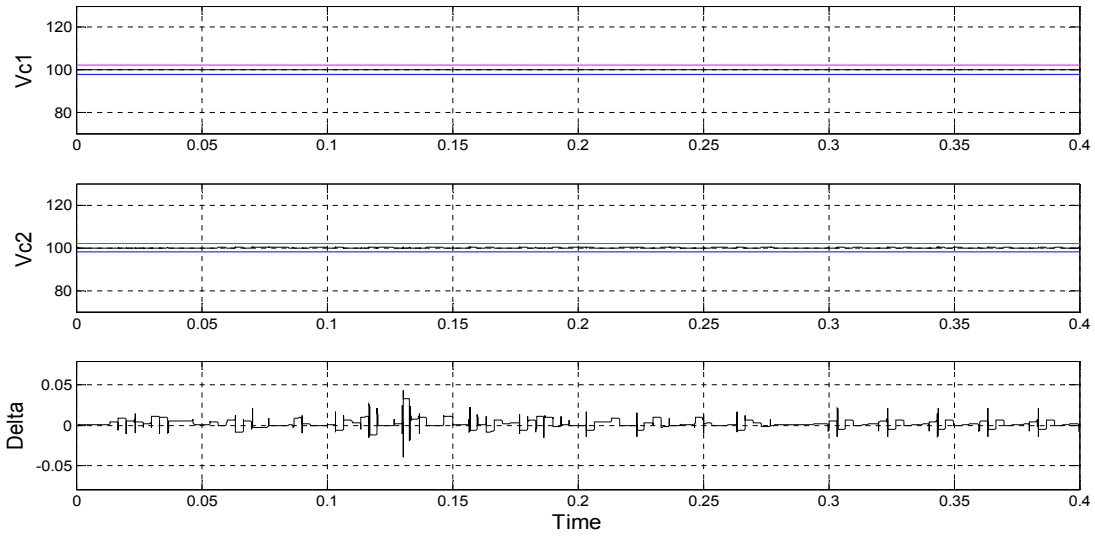

(c)

Figure 4.10: DC-link voltage (a) with capacitor voltages balancing, (b) without capacitor voltages balancing and (c) capacitor voltages υ_{c1} and υ_{c2} around their hysteresis bands and *Delta*

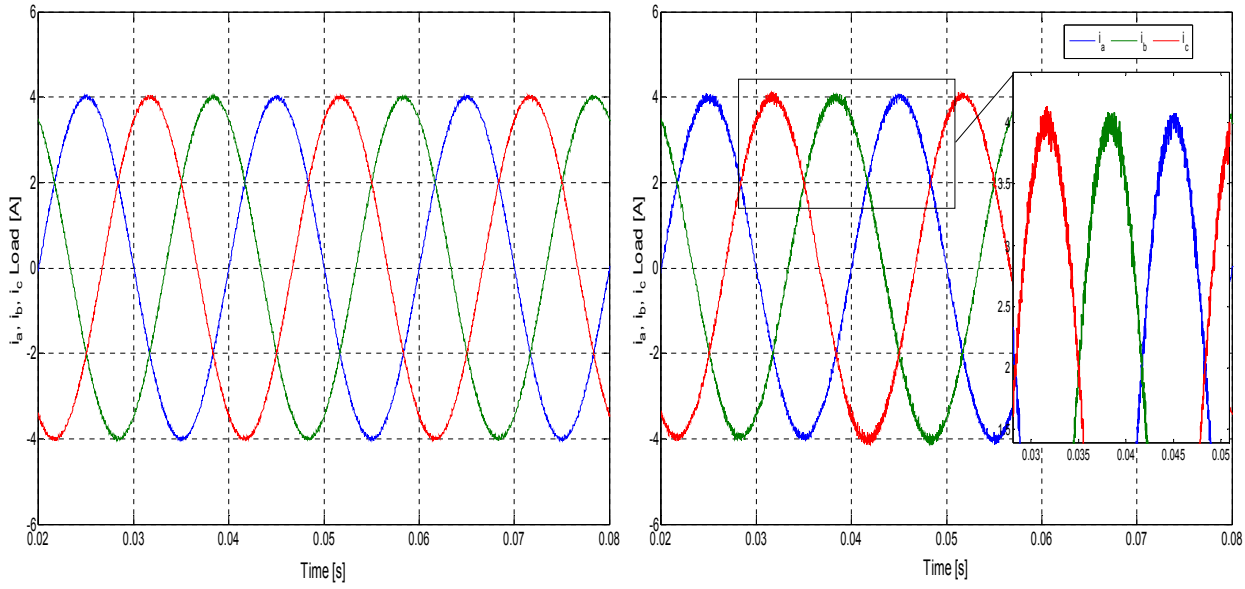

(a) (b)

Figure 4.11: Load current, (a) with capacitor voltage balancing and (b) without capacitor voltage balancing

4.5.2 Stability of the control strategy of a three-level DCC subject to a variable DC-link input

The robustness of the proposed control method of a DCC subject to variable DC-link voltages was investigated in this section; more specifically, when the DC-link voltage was changed from 140 to 280 V for T_S=25 µs. Figure 4.12 shows the output currents for different values of the DC-link voltage. Observe that the proposed control algorithm has the ability to track sinusoidal reference currents irrespective of the DC-link voltage variations around the desired voltage. The results plotted in Figure 4.12 are tabulated in Table 4.4.

In Figure 4.12(a), the DC-link was set to 140 V and the THD was at 0.89%, whereas in (b), the DC-link was set to 180 V and the THD was increased to 1.10%. In Figure 4.12(c), the DC-link was set to 240 V and the THD was increased to 1.47%, while in (d) the DC-link was set to 280 V and the THD was increased to 1.81%.

It was noted that voltages lower than the designed DC-link voltage value of 200 V produced a lower THD, which tracked the reference current with a very small error. On the other hand, DC-link values greater than the designed value, produced higher THD but with a relatively small amplitude error. This simulation confirms that the predictive control method has the ability, even with marginal differences in DC-link values, to track sinusoidal reference currents while showing excellent tracking behaviour with all DC-link voltage values.

Table 4.4: THD and Fundamental output current for variable DC-link voltages

DC-Link voltage value [V]	Fundamental output current at 50 Hz, [A]	THD [%]
140	4.996	0.89
180	4.998	1.10
200	5.000	1.24
240	4.998	1.47
280	4.996	1.81

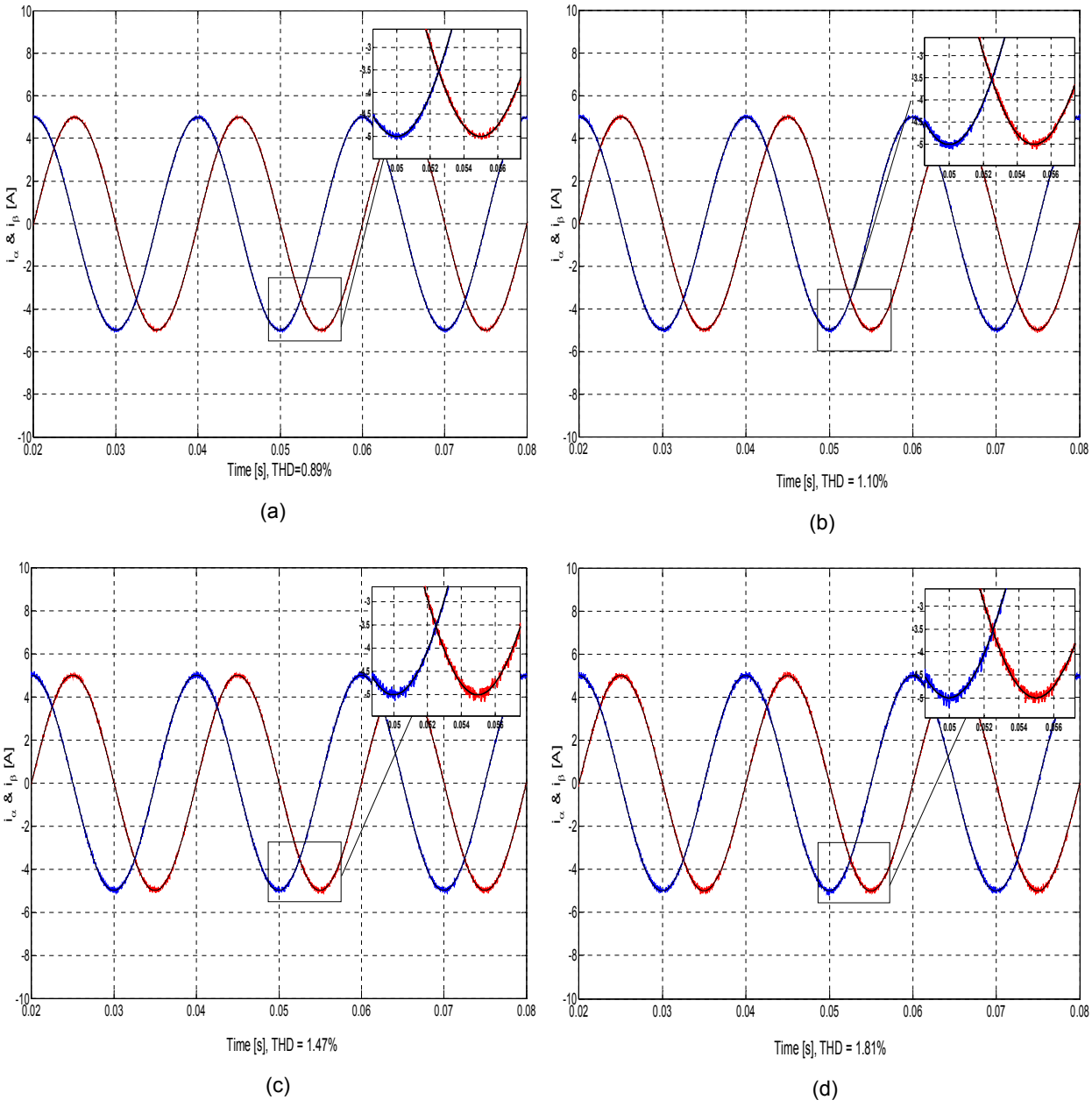

Figure 4.12: Output currents for different values of the DC-link voltage

4.5.3 Reference tracking

The third simulation was to assess the system performance when a step change in the amplitude of the reference and current reference tracking occurs and when the weighting factor is set to 0.02 for T_S = 25 µs with one prediction step.

4.5.3.1 Sinusoidal reference

The system performance with a prediction horizon of one sample time, as shown in Figure 4.13(a), illustrates how the output currents track their references, indicating that the control algorithm shows excellent tracking behaviour. The error between the reference and actual current has been evaluated, and the error has been found to be small, as indicated in Figure 4.13(b).

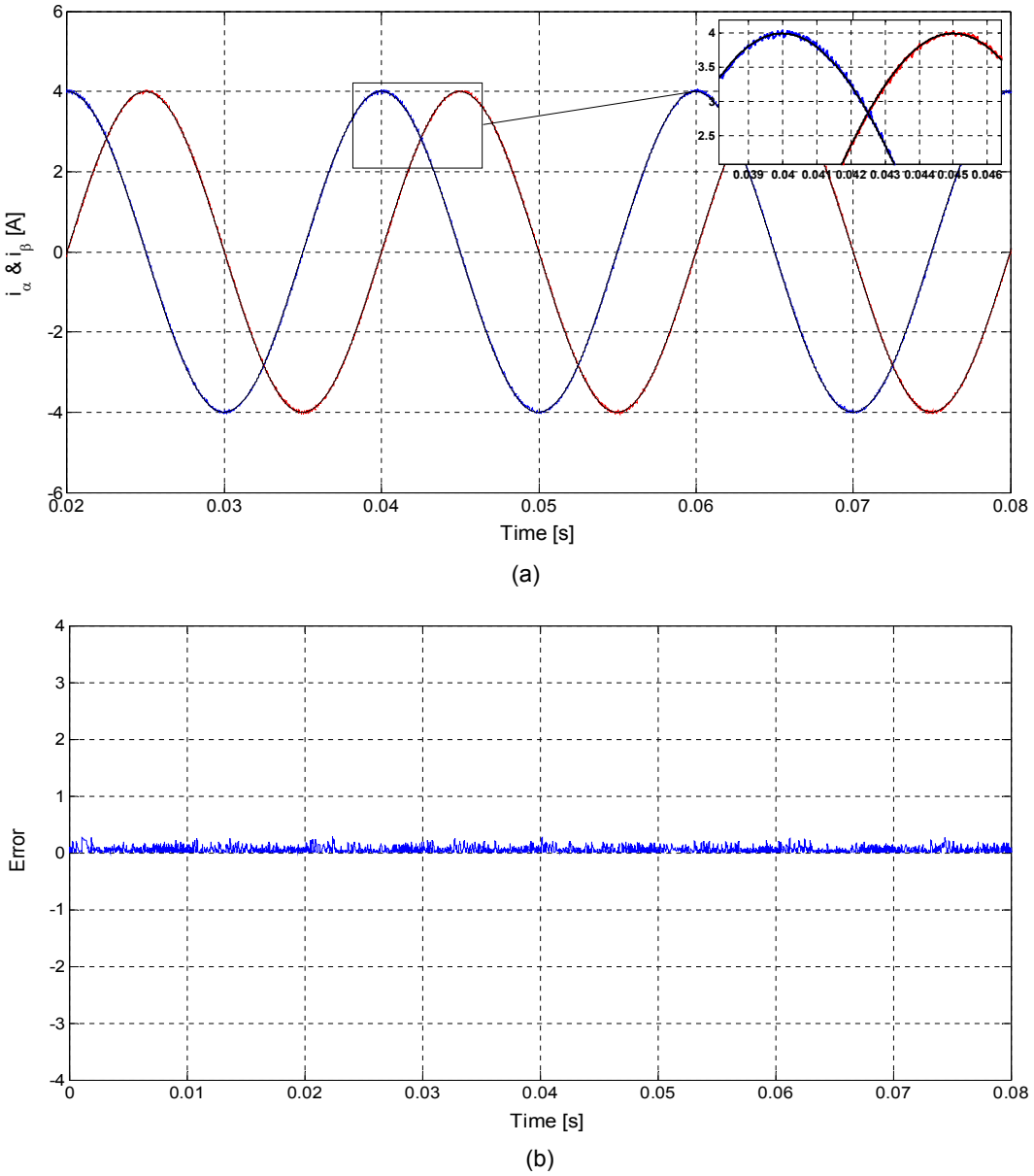

Figure 4.13: (a) Reference tracking for the load current with RL-load and (b) the error between the reference and load currents

4.5.3.2 Sinusoidal reference steps

The result of step changes in the amplitude of the references i_α and i_β were changed from -4 A to -3 A at 0.042 s and 0.05 s respectively, as shown in Figure 4.14(a). As seen in Figure 4.14(b), during the step change of the currents i_α and i_β, the load voltage, v_α, is kept at its maximum value until the reference current, i_α, is achieved. However, the capacitor voltages, shown in Figure 4.14(c), are kept constant with a minimal error.

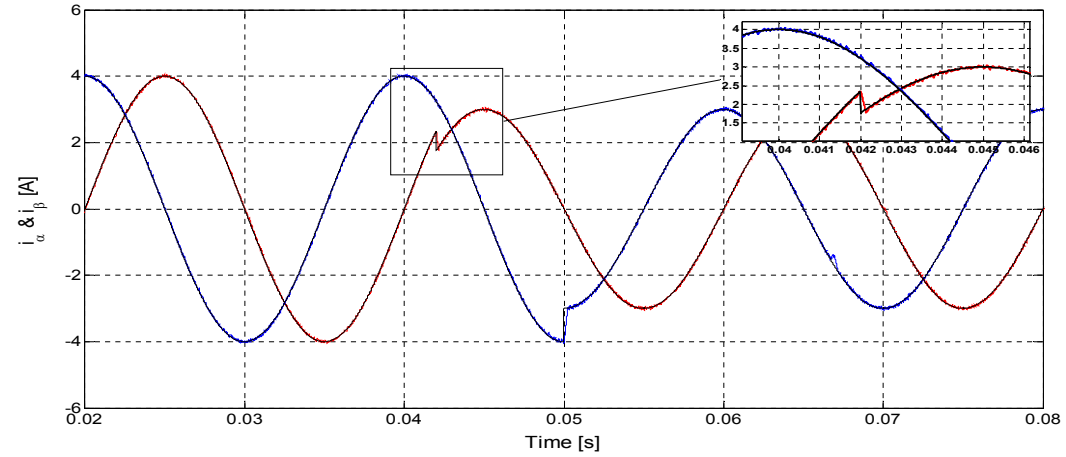

(a)

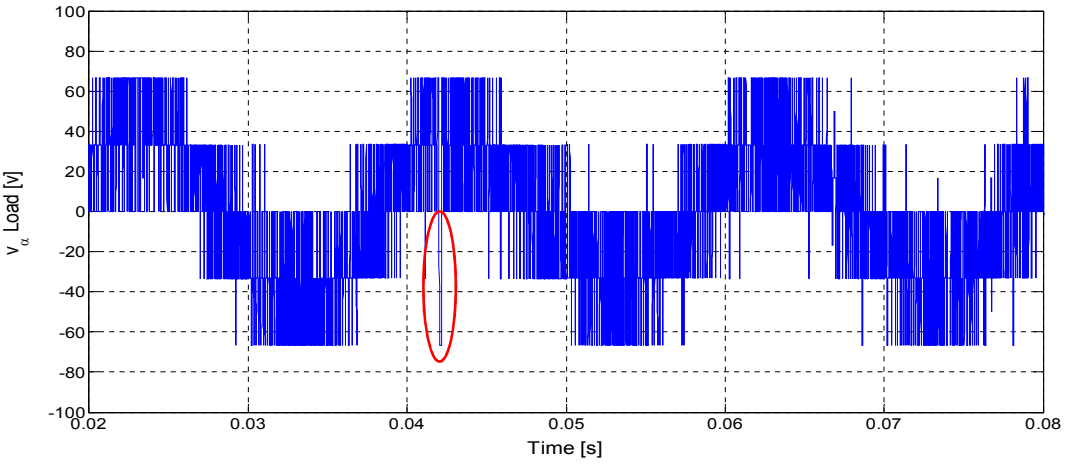

(b)

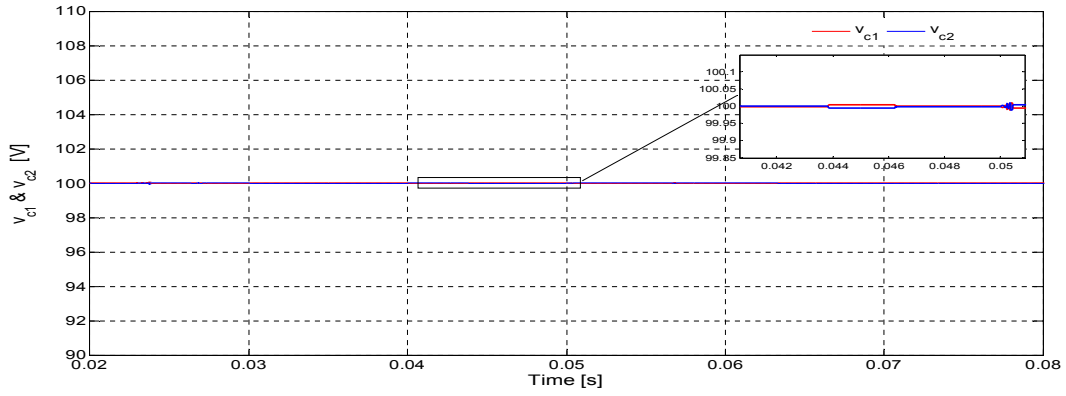

(c)

Figure 4.14: Sinusoidal reference steps for, (a) load current, (b) load voltage v_α and (c) capacitor voltages

This simulation clearly demonstrated the ability of the proposed control algorithm to track sinusoidal reference currents. From this simulation, it was noted that the predictive control method has a fast, dynamic response with inherent decoupling between i_α and i_β. Once again, the proposed algorithm showed excellent tracking behaviour.

The load currents for a three-level DCC inverter were obtained using PID controllers with PWM, and are shown in Figure 4.15 (Rodríguez & Cortés 2012). The same simulation parameters were used by Rodríguez & Cortés as were used for this simulations test. At time t = 0.015, the amplitude of current i_β^* was kept fixed while the amplitude of reference current i_α^* was reduced from 4 to 2 A. These adjustments were performed to assess the decoupling capability of the current control loop. The FS-MPCC method from Figures 4.14 can be compared to the classical control with PWM as shown in Figure 4.15. A noticeable coupling is observable between i_α and i_β, along with a slower response due to the dynamics of the closed current loops; see Figure 4.15. The response of the predictive current control for the same test is shown in Figure 4.14(a). This is a rapid dynamic response with an inherent decoupling between both current components and has been discussed before.

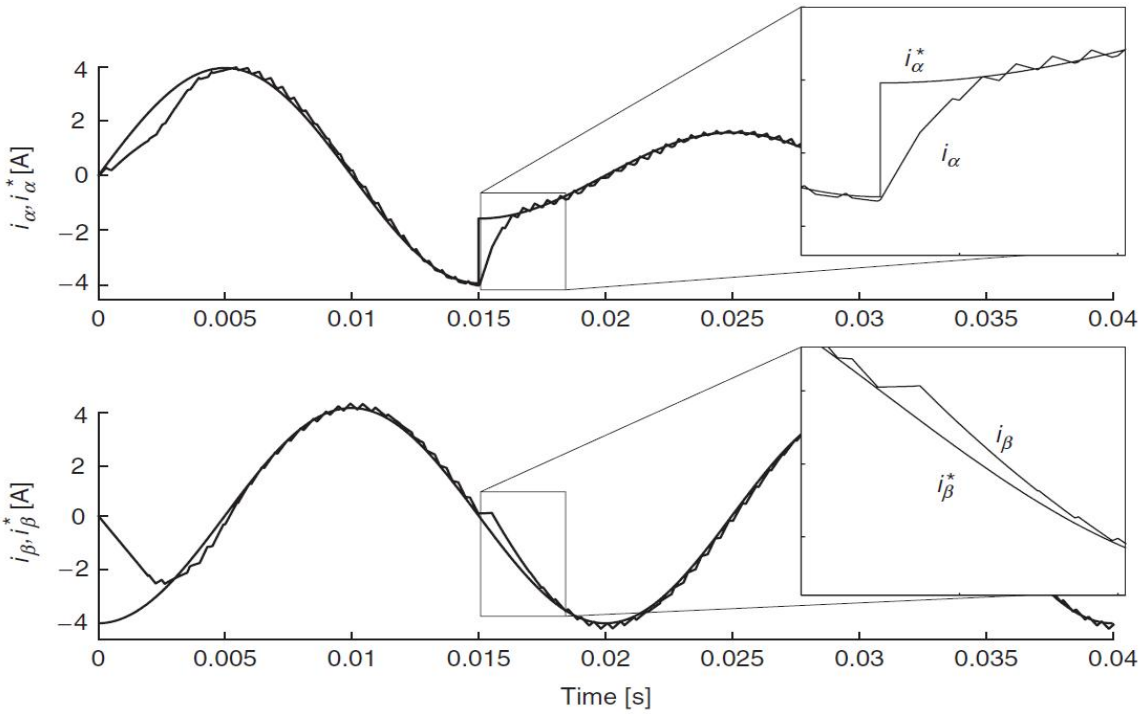

Figure 4.15: Results for a step in the reference current i_α^* using classical current control with PWM

(Permitted/adapted from Rodríguez & Cortés 2012)

4.5.3.3 Square waveform reference

In this simulation, the control algorithm was tested with a square waveform in orthogonal coordinates as a reference current. The result for square waveform in the amplitude of the references i_α and i_β was set to 2 A with T_S= 100 µs, and is shown in Figure 4.16. The i_α and i_β currents correctly followed the reference, and the remaining current ripple in steady-state results from the finite switching and controller frequency.

This simulation demonstrates that the predictive control method has a fast dynamic response, and once again, the algorithm shows excellent tracking behaviour.

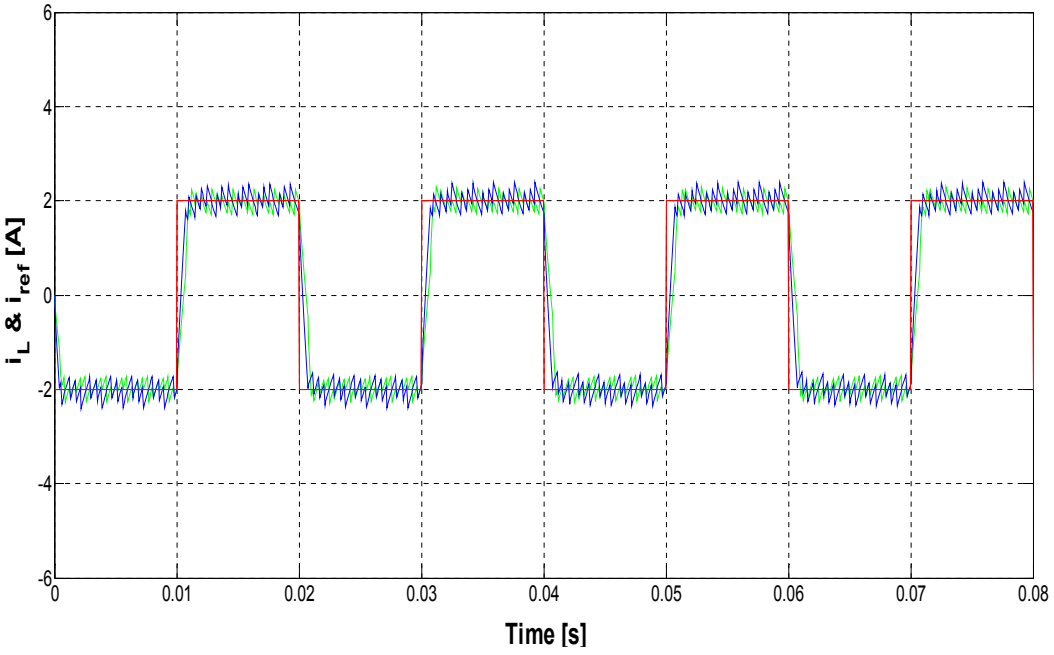

Figure 4.16: Square waveform reference for load current

4.5.3.4 Constant reference steps

In this simulation the performance of the control strategy using constant reference steps, was assessed. The simulation shows the control result for constant reference steps values, when a step change in the amplitude of the reference i_α and i_β were changed from 0 A to 4 A and 0 A to -3 A respectively at 0.02 s; this is shown in Figure 4.17. It can be seen in Figure 4.17 how the load currents reach their reference values with a fast dynamic response. Also, the current ripple exhibits a steady state that results from the finite switching and controller frequency.

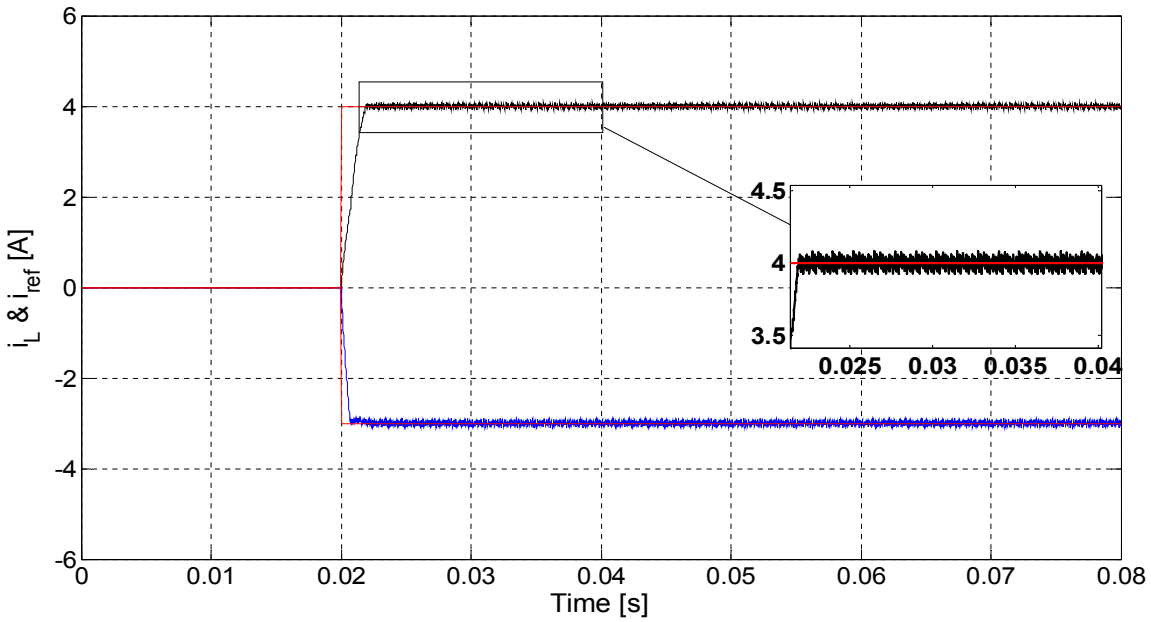

Figure 4.17: Constant reference steps for load current

4.5.4 Comparison of the model and actual system parameters

In nearly all systems, the parameters can change or are, to a degree, indeterminate. For example, the stator and rotor resistances and inductances of an induction machine can be changed due to temperature changes or saturation phenomena respectively. In the last evaluation, a mismatch between selected model parameters and the corresponding system parameters was considered. Different values were used for the load resistor and inductor. These values were estimated in order to evaluate the parameter sensitivity of the proposed control algorithm and to determine how stably the system could track the reference signal and the variation of the THD. The investigation in this section focused on the effect of parameter uncertainty in the system model under consideration.

The actual inductance was estimated to be 50% higher and lower than the parameter used in the model for sampling times T_S=25 µs and T_S=100 µs. In the other case, the inductance was increased to 100% for T_S= 25 µs and T_S= 100 µs. The actual resistance was estimated to be 40% higher and lower than the parameter used in the model for T_S= 25 µs.

It was noted in Figure 4.18(a) and (c) that when the load inductance was estimated to be +50% (THD= 1.02%) and +100% (THD= 1.09%) respectively for T_S= 25 µs, the control algorithm showed excellent reference tracking behaviour. When the sampling time, T_S, was increased to 100 µs, the current ripple on the load current increased; this is shown in Figure 4.18(b) where THD= 4.19%, and in Figure 4.18(d) where THD= 3.16%.

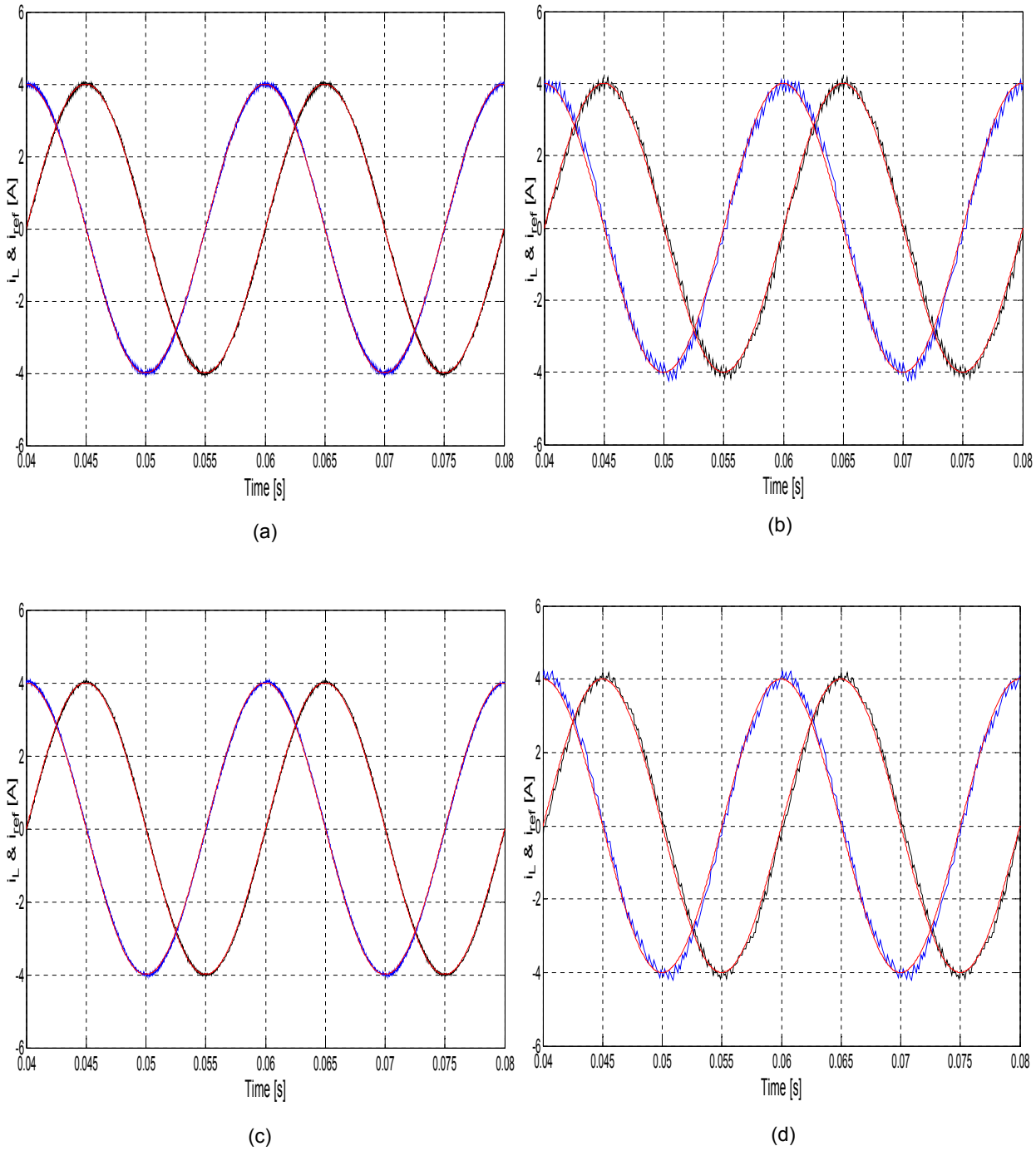

Figure 4.18: Inductance sensitivity for load current when estimated to be (a) +50% for 25 µs, (b) +50% for 100 µs, (c) +100% for 25 µs and (d) +100% for 100 µs

If, however, the inductance was estimated to be 50% lower than the parameter used in the model for T_S= 25 µs, the load current ripple increased a little, compared to the model inductance value (THD= 3.44%); for T_S= 100 µs, the current ripple increased (THD= 14.28%); this is shown in Figure 4.19.

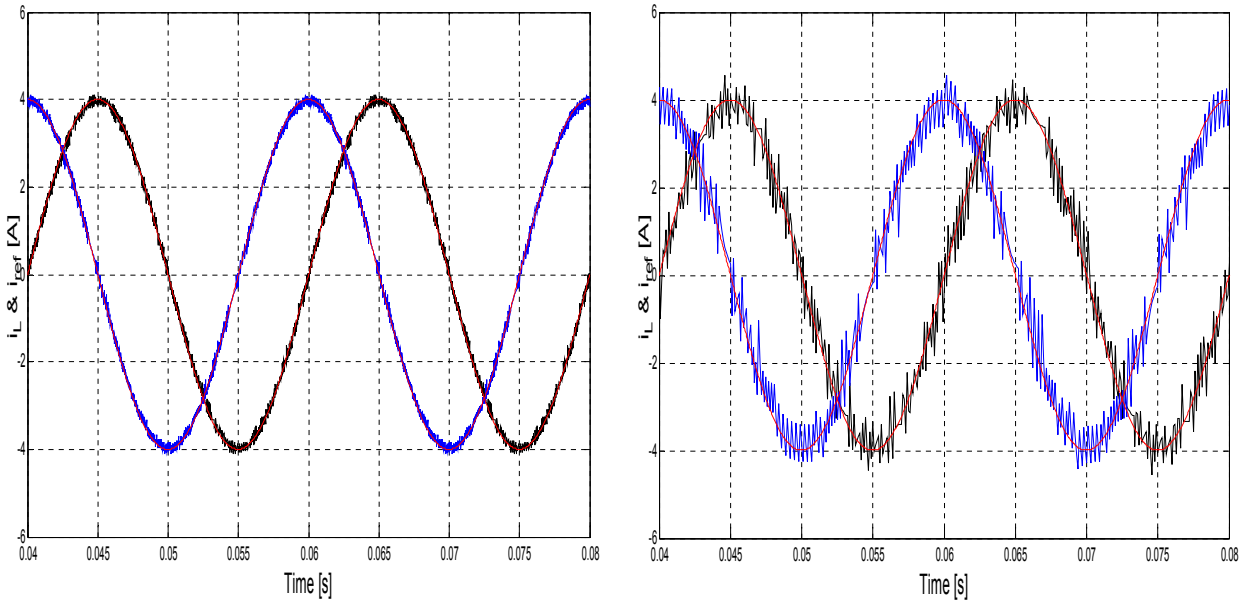

Figure 4.19: Inductance sensitivity for load current when estimated to be (a) -50% for 25 µs and (b) -50% for 100 µs

Figure 4.20 shows the simulation results when the actual resistance was estimated to be 40% higher as well as 40% lower than the parameter used in the model for T_S= 25 µs. In both cases, the predictive control method performed better in tracking the load current references. When the load resistance was estimated to be -40%, the load current was lower than its reference value (THD= 1.45%); when the load resistance was estimated to be +40%, the load current was higher than its reference value (THD= 1.53%).

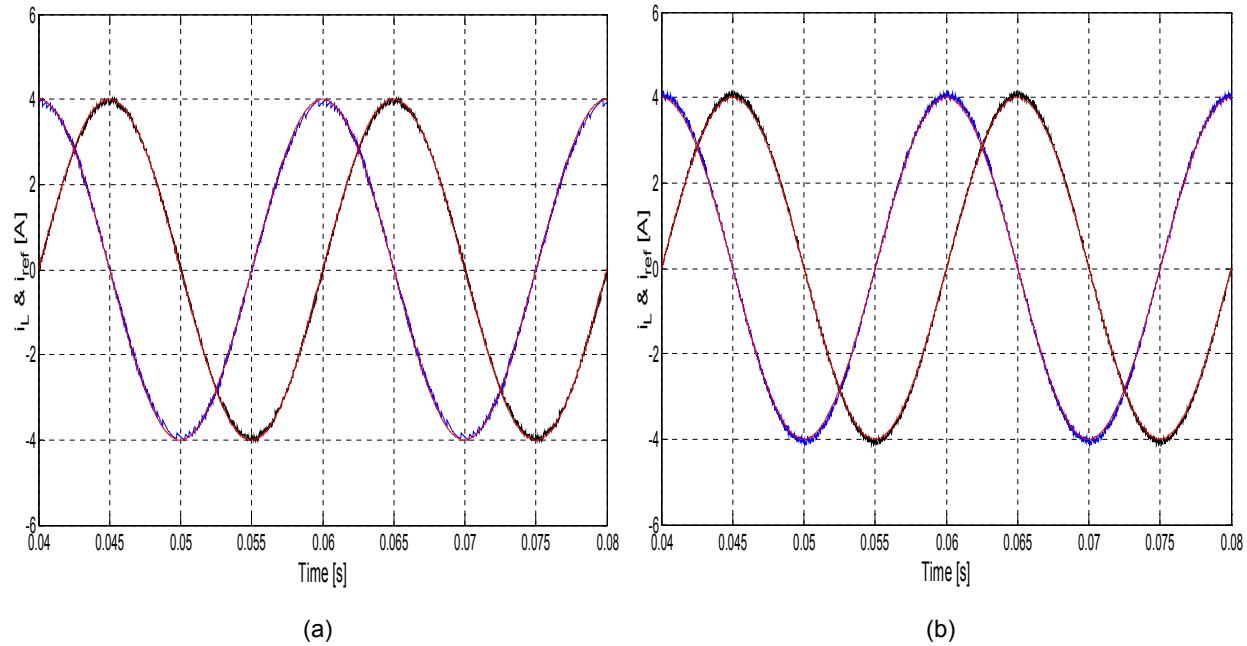

Figure 4.20: Resistance sensitivity for load current when estimated to be (a) -40% and (b) +40%

4.6 Summary

This chapter presented the FS-MPCC strategy with one-step prediction time to control the three-level DCC inverter. The RES model was used in this study to investigate the system performance when power is supplied to an RL-load. The best one of the 19 different voltage vectors was selected and applied to the inverter, although there were 27 different switching combinations.

In this chapter, as part of the DCC case study, the effectiveness of SSI technique was presented. The SimCoupler module enables MATLAB/Simulink users to implement and simulate power circuits in their original circuit form; this significantly shortens the time required to set up and simulate a system that includes electronic circuits. The important step in the SSI technique is the time synchronization of the two independent software platforms used, in this case: PSIM and MATLAB/Simulink.
The minimization of the current and voltage errors in the cost function provides rapid, dynamic response for load current control and guarantees capacitor voltage balance. The two main advantages of using FS-MPCC are that there is no need for modulation of any kind, nor for a linear controller, and the designer has the option of adjusting the weighting factor, λ_{DC}, within the cost function (*g*). Having this option permits the manipulation of the relationship between the terms dedicated to reference tracking, and those dedicated to voltage balancing in the DC-link.

The FS-MPCC algorithm was evaluated by means of co-simulation, and results were obtained for four different cases. Firstly, the DC-link capacitor voltage was balanced. The control algorithm provided excellent current tracking behaviour and the capacitor voltages were very well balanced with minimal error. The balancing of the DC-link capacitor voltages of the DCC was done with λ_{DC} = 0.02. The selected weighting factor provided the best performance in terms of the DC-link capacitor voltage balance, excellent current reference tracking and the lowest harmonics content in the load current. Secondly, the assessment of the stability of the control strategy subjected to a variable DC-link RES application was done in terms of the THD. The results showed that the predictive control method has the ability to track sinusoidal reference currents and perform exceptional tracking behaviour with all DC-link voltage values. Thirdly, sinusoidal waveform reference tracking was investigated. The control algorithm was tested by applying the following reference currents: a sinusoidal waveform and step changes in the amplitude of the sinusoidal waveform reference current, a step function waveform, and a square waveform in orthogonal coordinates. Results showed that the predictive control algorithm has a fast dynamic response and gives perfect tracking behaviour with inherent decoupling between i_α and i_β currents. Lastly, the performance of the proposed control was assessed by mismatching

selected model parameters and the corresponding actual system parameters. The results obtained showed that an FS-MPCC strategy gives very good performance under these conditions. All the assessments revealed that the FS-MPCC has flexibility under these conditions.

The results of the assessments of the FS-MPCC strategy applied in this research, have demonstrated that this strategy is a powerful tool when compared to the conventional method using modulation techniques. The FS-MPCC concept can be extended to any power converter system.

CHAPTER FIVE

PREDICTIVE CURRENT CONTROL TECHNIQUES FOR AN FCC INVERTER USED IN RESs APPLICATIONS

5.1 Introduction

The increase in the use of power from RESs, has led to the need for research on both new control strategies and better topologies for high-power converters; this is necessary to provide in the dual demand for performance and efficiency. In the last couple of decades, the multitude of applications of MLCs found in most industrial domains, have been intensively researched. By reflecting upon the increasing worldwide energy needs and the requirements for improved power quality and better efficiency, it is clear that control and power conversion by means of power electronics are becoming increasingly vital issues in renewable energy system applications in the present. The flying capacitor multilevel converter was presented by Meynard and Foch in the early 1990s as an alternative to diode-clamped inverters (Meynard & Foch 1992). The advantages of the FCC topology over other multilevel topologies such as diode-clamped converters and cascaded converters (Fazel et al. 2007; Lai & Peng 2002; Nami et al. 2008), has of late featured prominently in the literature (Defay et al. 2010; Escalante et al. 2002; Fazel et al. 2007; Feng et al. 2007; Hotait et al. 2010; Lai & Peng 2002; Lezana et al. 2009; McGrath & Holmes 2008; Meynard et al. 1997; Thielemans et al. 2010).

Many studies have been concluded in which an FS-MPCC scheme for three-phase multilevel inverters and drive applications has successfully been incorporated (Almaktoof et al. 2014; Li et al. 2009; Rodríguez & Cortés 2012; Vargas et al. 2007; Yaramasu et al. 2013). For RESs applications, the robustness and power of the FS-MPCC technique for a MLI, has been assessed when subjected to variable DC-link voltages, and variations in specific model parameters (Almaktoof et al. 2013; 2014a). The results indicated that FS-MPCC gives excellent performance under these conditions.

For MPC with a flying capacitor multilevel inverter, the two foremost control objectives are reference current tracking and balancing the voltages of the flying capacitor. These objectives are achieved concurrently by the multivariable control scheme. The MPC algorithm inputs are the measured currents and flying capacitor voltages, as well as the reference currents. The algorithm output corresponds to one of the switch states of the converter, without the application of a modulation scheme. A flying capacitor voltage algorithm based on predictive control, is presented to balance the flying capacitor voltage, because the natural balancing of the capacitor voltages of FCCs fails in certain circumstances, as in the case with PWM (Defay et al. 2010; Feng et al. 2007; Hotait et al. 2010; Khazraei et al. 2012).

This chapter presents a new direct model predictive control strategy for a three-phase, three-level FCC. Additionally, a hysteresis-based algorithm is presented which interacts with the FS-MPCC algorithm in a complimentary manner, to resolve the issue of balancing the flying capacitor voltages. There is no need for internal current control loops, and no modulators are required as the gate drive signals are generated directly by the proposed control method. Section 5.2 discusses the predictive current control technique for an FCC inverter. The control scheme used to control the flying capacitors is developed in the section 5.3. The results and a discussion of the performance of the algorithm, taking into account the RL-load are presented in Section 5.4. Section 5.5 contains the conclusion.

5.2. Predictive control techniques for an FCC inverter

For a directly controlled, three-phase, three-level FCC inverter, the calculation effort rises with the number of possible switching states. This kind of inverter would normally require 64 possible switching states if the best switching state for the next sampling cycle is to be determined in only one prediction step.

The proposed algorithm, however, needs to consider only 19 of those 64 switching states to select the correct voltage vector in one step. By using the 19 voltage vectors for two prediction steps, only 19^2 = 321 possibilities would have to be evaluated; this is an enormous reduction of the calculation power required. Additionally, a weighting factor would have to be added to the cost function in order to keep a good balance between the original control task as well as keep the flying capacitor voltages within the prescribed bounds around their reference values. The task of finding the correct weighting factor can sometimes be elaborate and has to be done with care. In the first task, only the optimum voltage vector from 19 possibilities is chosen; thereafter, the best switching state for balancing the voltages of the flying capacitors is selected and applied to the inverter by means of a hysteresis-based predictive control system.

5.2.1 System model

The topology of the three-level flying capacitor converter was discussed in detail in Chapter two and is depicted in Figure 5.1. With only one flying capacitor per phase, this is one of the less complicated converters, and it is for this reason that it was chosen for the MPC analysis; it was not expected to add any complications. The three-level FCC uses two pairs of complementary controlled switches, (S_1, S'_1) and (S_2, S'_2). These switches enable the connection of the flying capacitors, C_{1x}, where $x = a, b$ and c—the capacitors are in a series with the RL-load, as depicted in Figure 5.1. A summary of the different switch states and the corresponding output voltages is presented in Table 5.1. Consider the switch pair, S_{ix} where i =1 or 2: with the upper

switch of the switch pair is closed, S_{ix} is 1; with the lower switch is closed, S_{ix} is zero. When the load is coupled in a series with a flying capacitor, the voltage associated with the current flowing through the capacitor, changes. In a three-level FCC the voltage of the flying capacitor, C_{1x} must always be maintained at $v_{DC}/2$.

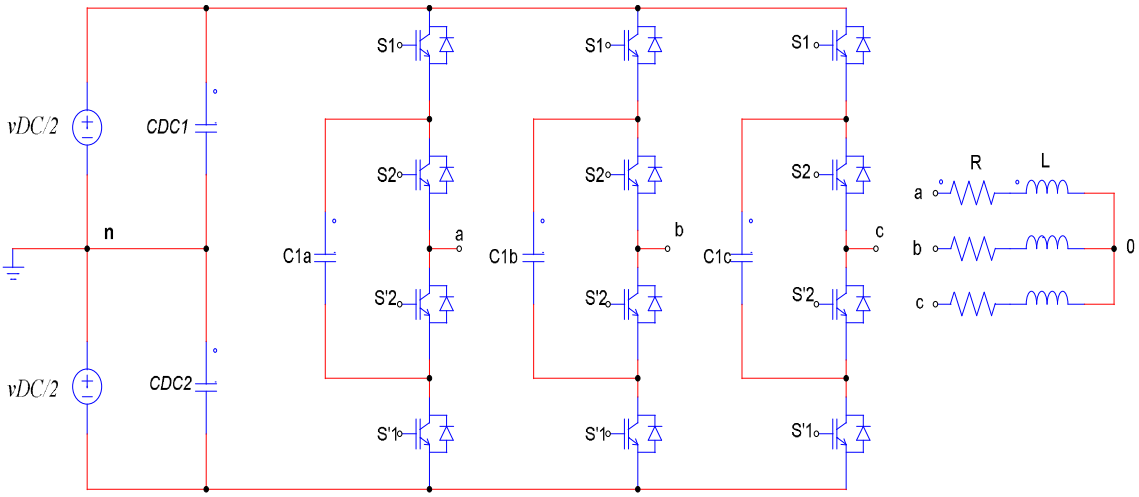

Figure 5.1: Three-phase, three-level FCC inverter with RL-load

Table 5.1: Switching states in one leg of the three-level FCC

Voltage Level	complementary pair no. 1		complementary pair no. 2		Leg voltage (v_{an})
	S_1	S'_1	S_2	S'_2	
1	1	0	1	0	$v_{DC}/_2$
2	1	0	1	0	0
	0	1	0	1	
3	0	1	0	1	$-v_{DC}/_2$

Because the maximum voltage stress occurs at $v_{DC}/2$, this requirement provides an optimal voltage rating for the switches. The transitional output voltage is generated by the two conditions of each phase; this allows a correction of the voltage of the capacitor for every possible direction, and it furthermore presents a way of controlling the capacitor voltage. The current paths for positive and negative phase currents are depicted in Figure 5.2, and all the circuit topologies for each possible switching state for a one leg, three-level FCC are depicted in Figure 5.3.

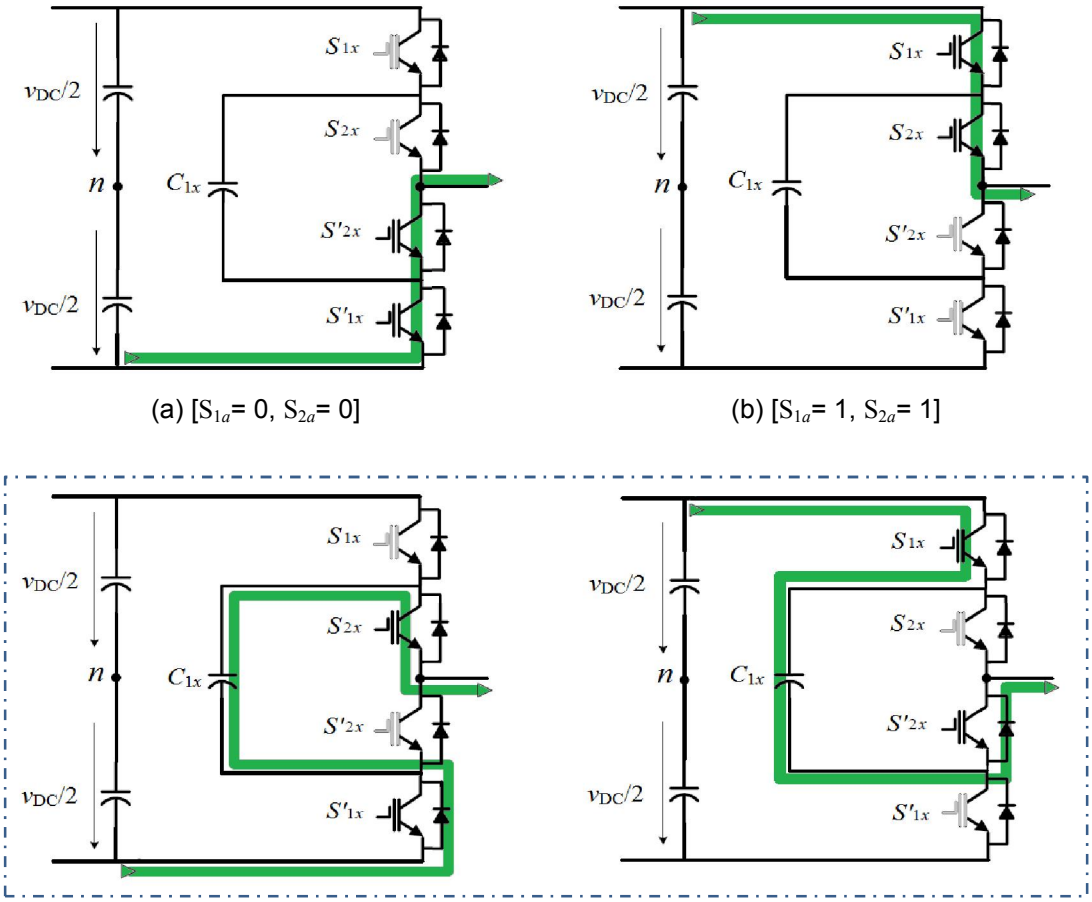

(a) [S_{1a}= 0, S_{2a}= 0] (b) [S_{1a}= 1, S_{2a}= 1]

(c) [S_{1a}= 0, S_{2a}= 1] (d) [S_{1a}= 1, S_{2a}= 0]

Figure 5.2: Conduction paths of the three-level FCC

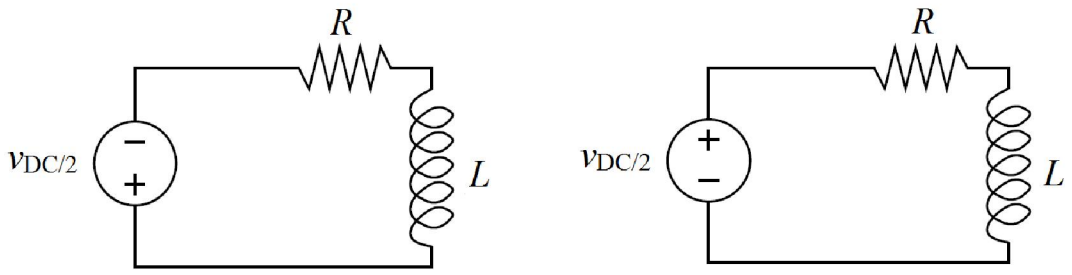

(a) Load voltage = $-v_{DC}/2$, [S_{1a}= 0, S_{2a}= 0] (b) Load voltage = $v_{DC}/2$, [S_{1a}= 1, S_{2a}= 1]

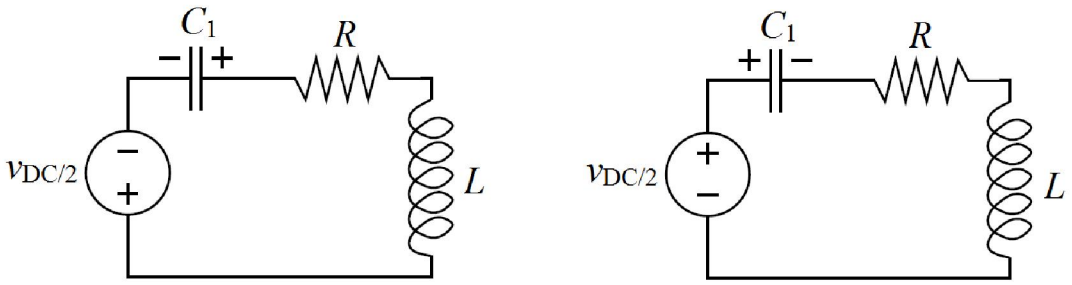

(c) Load voltage = 0 v, [S_{1a}= 0, S_{2a}= 1] (d) Load voltage = 0 v, [S_{1a}= 1, S_{2a}= 0]

Figure 5.3: Circuit topologies for available switching states for one leg, three-level FCC

5.2.2 Finite Set-Model Predictive Control of Flying Capacitor MLC

As described in Chapter three, an FS-MPCC strategy is a method to control the selected state by optimization of future switch states. For this application, a controller operating in discrete time and with a fixed update frequency is considered. If a switch state defined by the controller in the preceding update period is applied at time instant, k, the effect on the system states can be observed at time instant $(k + N1)$. Over the time interval $[\, k,\ k + N1\,]$, the controller can no longer change the outcome of the states at $(k + N1)$. Thus, the control algorithm starts by calculating the system states at time instant $(k + N1)$, from the prevailing system model as defined by the measurements taken at time k. This is called the estimation phase.

From $(k + N1)$ onwards, the controller uses an optimization algorithm to define the optimal sequence of a future switch state. In the predictive step, the controller calculates all possible control sequences over the time span from $(k + N1)$ to $(k + N2)$, based on the estimation at time, $(k + N1)$. Once the future states for all possible control sequences have been predicted, the optimal sequence can be selected. The optimal sequence amongst the permitted sequences is found by evaluating all sequences in a cost function, g, during the optimization step. The sequence which makes the cost function a minimum, is selected and the first switch state of this sequence in the prediction horizon, is applied by the controller at the time instant $(k + 1)$. At that update instant, a new measurement sample starts a new iteration of the MPC algorithm, resulting in a so-called receding horizon. The following discussion of an FS-MPCC is directly applied to a three-phase, three-level FCC inverter with RL-load, which is depicted in Figure 5.1.

A three-phase, three-level FCC can only deliver 64 possible switching states, of which 45 are redundant; this leaves 19 different voltage vectors (see Figure 5.4). Some switching states are redundant, generating the same voltage vector. For example, the innermost vector, V_0, shown in Figure 5.4, can be generated by three different switching states: (+, +, +), (0, 0, 0) and (−, −, −); see Appendix B. With this redundancy, a finite set-model predictive control with more than one prediction step can be implemented. The effort of calculation increases exponentially with the prediction horizon if the optimum inverter switching state is determined directly with a model-predictive control algorithm. For this reason the control task would not be feasible for prediction horizons greater than one prediction step. A complete enumeration of all switching states would already lead to 64^2 = 4 096 possible combinations for two prediction steps. By only using 19 voltage vectors for two prediction steps, only 19^2 = 321 possibilities need to be evaluated—an enormous reduction of the calculation power required.

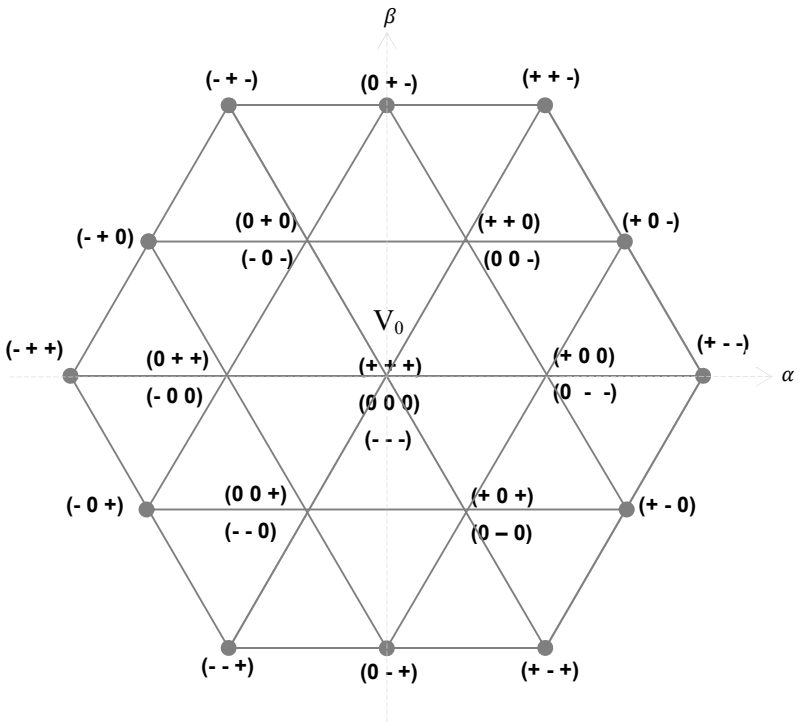

Figure 5.4: Voltage vectors and switching possibilities generated by a three-level inverter

In this study, the selection of the most suitable voltage vector of the 19 delivered was done with a prediction horizon of one, and two prediction steps. This facilitates a marked decrease in the amount of calculation required, as compared to carrying out the calculations for all 64 switching possibilities in one prediction step. Hence, the task is split into two different control algorithms based on the MPC. For these algorithms, a simple cost function (L1-norm) was used. The voltage balancing algorithm for choosing the best switching state regarding the voltage balance was performed by a hysteresis controller. In the implementation stage of FS-MPCC of a three-phase, three-level FCC for RL-Load, the following steps were performed:

1. An estimation step
2. A predictive step
3. An optimization step

5.2.2.1 Estimation step

For the three-phase, three-level FCC system, Nx is the number of update periods. It has been assigned as 1 because the goal is to finish all calculations in one update period and apply the selected switch state at the end of the update period. This means that when a measurement sample is taken at time instant k, it is possible to do all the calculations required by the MPC algorithm and to apply a newly defined

switch state at time instant $(k+1)$. To enable prediction of the impact of future possible switch states, an estimate of the state variables at $(k+1)$ is required.

The measurements of the phase currents, $i_x(k)$, and the flying capacitor voltage, $v_{1x}(k)$ with $x = a, b, c$, are taken at time, k. These measurements in combination with the applied switch states, $S_{ix}(k)$, are used as inputs for the system model, so as to obtain an estimation of the state variables at $(k+1)$. The switch states, $S_{ix}(k)$, remain unaltered throughout the update period, and any change in the capacitor voltage is taken to be sufficiently small for it to be neglected when the output voltage is calculated. With the aforementioned assumptions, the equations below have been derived for the voltage, v_{xn}, between the output pole, x, and the neutral point, n, of the power supply of a three-level FCC:

$$v_{xn}(k+1) = \left(S_{2x}(k) - {}^{1}/_{2}\right) v_{DC} - \left(S_{2x}(k) - S_{1x}(k)\right) v_{1x}(k) \tag{5.1}$$

where: the DC-link voltage, v_{DC}, is obtained by measurement.

The load phase voltage, v_{xo} (between the output pole and the neutral point), is determined from:

$$v_{on}(k+1) = \frac{v_{an}(k+1)+v_{bn}(k+1)+v_{cn}(k+1)}{3} \tag{5.2}$$

and

$$v_{xo}(k+1) = v_{xn}(k+1) + v_{on}(k+1) \tag{5.3}$$

where: v_{on} is the star-point voltage.

The flying capacitor voltages and output currents at time, $(k+1)$, have to be estimated.

Estimation of the output current:

At time, $(k+1)$, the expression for the current can be determined by means of the Euler forward method, which yields a discrete-time equation that can be used to find the future load current. To derive the continuous-time, state-space equations for the load of each phase, consider the differential equation of the load current:

$$v_{DC}(t) = R.i(t) + L\frac{di}{dt} \tag{5.4}$$

With the Clarke transformation applied to the load model, the load currents can be stated in relation to a simplified coordinate system having linearly independent axes, α and β. The values of α and β are defined as

$$v_\alpha = \frac{2}{3}(v_a - 0.5v_b - 0.5v_c) \tag{5.5}$$

$$v_\beta = \frac{2}{3}(0.5\sqrt{3}\, v_b - 0.5\sqrt{3}\, v_c) \tag{5.6}$$

After applying the transformation, the continuous-time, state-space equation of the load takes on the following form:

$$\begin{bmatrix} i_\alpha \\ \\ i_\beta \end{bmatrix} = \begin{bmatrix} -\frac{R}{L} & 0 \\ \\ 0 & -\frac{R}{L} \end{bmatrix} \begin{bmatrix} i_\alpha \\ \\ i_\beta \end{bmatrix} + \begin{bmatrix} \frac{1}{L} & 0 \\ \\ 0 & \frac{1}{L} \end{bmatrix} \begin{bmatrix} v_\alpha \\ \\ v_\beta \end{bmatrix} \tag{5.7}$$

The Euler forward equation (see Equation 5.8) is used to derive a discrete-time equation system representation for the future load current, which is required to obtain a discrete-time system representation. The derived approximation is given by

$$\dot{x} \approx \frac{x(k+1) - x(k)}{\mathrm{T_S}} \tag{5.8}$$

where: $\mathrm{T_S}$ is the sampling time; k is the current sampling instant; and x is the state variable.

The equation of the discrete-time load model is then expressed by

$$\begin{bmatrix} i_\alpha(k+1) \\ \\ i_\beta\,(k+1) \end{bmatrix} = \begin{bmatrix} 1 - \mathrm{T_S}\frac{R}{L} & 0 \\ \\ 0 & 1 - \mathrm{T_S}\frac{R}{L} \end{bmatrix} \begin{bmatrix} i_\alpha(k) \\ \\ i_\beta(k) \end{bmatrix} + \begin{bmatrix} \frac{\mathrm{T_S}}{L} & 0 \\ \\ 0 & \frac{\mathrm{T_S}}{L} \end{bmatrix} \begin{bmatrix} v_\alpha(k) \\ \\ v_\beta(k) \end{bmatrix} \tag{5.9}$$

Estimation of the flying capacitor voltage:

At the end of time, $(k+1)$, the flying capacitor voltages have to be estimated. The switch state determines whether, and in which sense, the load current passes through the capacitors; this is given by $(\mathrm{S}_{2x}(k) - \mathrm{S}_{1x}(k))$ in Equation 5.10.

$$v_{1x}(k+1) = v_{1x}(k) - \frac{\mathrm{T_S}}{2C}\,(i_x(k) + i_x(k+1))\,(\mathrm{S}_{2x}(k) - \mathrm{S}_{1x}(k)) \tag{5.10}$$

where *C* is the capacitance of the flying capacitor and x is a, b, c.

Equations 5.9 and 5.10 are used to predict the load current and flying capacitor voltage for each switching likelihood. For determining the subsequent values of the load currents and flying capacitor voltages, the cost function, g, is calculated for every one of the 19 possible voltage vectors produced by the inverter. The voltage vector that results in a minimum cost function is chosen and implemented during the sampling instance that follows. This is because the current and flying capacitor voltage will always be on or outside the hysteresis band. The switching state, therefore will be changed constantly.

5.2.2.2 Predictive step

Starting at time, $(k + N1)$, the controller has the capability to process any information it is fed during every update period, in order to bring the controlled variables closer to their desired values. Therefore, on the basis of estimates at time, $(k + N1)$, the controller is able to forecast the result of all feasible switch states, over the whole prediction horizon between $(k + N1)$ and $(k + N2)$. The overall forecast horizon is defined by

$$Np = N2 - N1 \tag{5.11}$$

In essence, the prediction equations are the same as the estimation equations except that they are evaluated $N1$ sample periods later (for the first prediction step, k and $(k + 1)$ in the estimation equations are augmented to $(k + N1)$ and $(k + N1 + 1)$ respectively for the prediction equations).

Also, the output current and flying capacitor voltage are not determined by measurement because the values estimated or forecasted from the preceding step are applied. This leads to the subsequent group of equations being assessed for all feasible switching states for $i \in [N_1, N_2]$. In the case of the three-level converter, the output voltages are

$$v_{xn}(k+i+1) = \left(S_{2x}(k+i) - {}^{1}/_{2}\right) v_{DC} - \left(S_{2x}(k+i) - S_{1x}(k+i)\right) v_{1x}(k+i) \tag{5.12}$$

the star point voltage is

$$v_{on}(k+i+1) = \frac{v_{an}(k+i+1) + v_{bn}(k+i+1) + v_{cn}(k+i+1)}{3} \tag{5.13}$$

and the yielding phase voltages are

$$v_{xo}(k+i+1) = v_{xn}(k+i+1) + v_{on}(k+i+1) \tag{5.14}$$

To bring the controlled currents that much closer to their reference, the controller can, from $i(k+1)$ onwards, process any possible output. In the next step, the controlled current is $i(k+2)$. The controller thus calculates the measured currents at $(k+2)$ for all possible switch states achieved at $(k+1)$. The output current with the RL-load can be expressed as

$$\begin{bmatrix} i_\alpha(k+2) \\ i_\beta\,(k+2) \end{bmatrix} = \begin{bmatrix} 1 - T_S\frac{R}{L} & 0 \\ 0 & 1 - T_S\frac{R}{L} \end{bmatrix} \begin{bmatrix} i_\alpha(k+1) \\ i_\beta(k+1) \end{bmatrix} + \begin{bmatrix} \frac{T_S}{L} & 0 \\ 0 & \frac{T_S}{L} \end{bmatrix} \begin{bmatrix} v_\alpha(k+1) \\ v_\beta(k+1) \end{bmatrix} \tag{5.15}$$

And with a long prediction horizon, the result of the output currents in $\alpha\beta$ frame is

$$\begin{bmatrix} i_\alpha(k+n) \\ i_\beta\ (k+n) \end{bmatrix} = \begin{bmatrix} 1-\mathrm{T_S}\frac{R}{L} & 0 \\ 0 & 1-\mathrm{T_S}\frac{R}{L} \end{bmatrix} \begin{bmatrix} i_\alpha(k+n-1) \\ i_\beta(k+n-1) \end{bmatrix} + \begin{bmatrix} \frac{\mathrm{T_S}}{L} & 0 \\ 0 & \frac{\mathrm{T_S}}{L} \end{bmatrix} \begin{bmatrix} v_\alpha(k+n-1) \\ v_\beta(k+n-1) \end{bmatrix} \quad (5.16)$$

Using this particular solution, the result of the output currents in the a, b, c frame is

$$i_x(k+i+1) = e^{-\mathrm{T_s}\frac{R}{L}} i_x(k+i) + \frac{1-e^{-\mathrm{T_S}\frac{R}{L}}}{R} v_{xo}(k+i+1) \quad (5.17)$$

These currents influence the capacitor voltages, as given by

$$v_{1x}(k+i+1) = v_{1x}(k+i) - \frac{\mathrm{T_S}}{2C}\left(i_x(k+i) + i_x(k+i+1)\right)\left(\mathrm{S}_{2x}(k+i) - \mathrm{S}_{1x}(k+i)\right) \quad (5.18)$$

From Equations 5.13 and 5.14, it is apparent that in the system model the phase output voltages of all phases determine the phase voltage of the load. The outcome is a set of equations that are convincingly linked. The results of all the switch state combinations are determined and applied in the optimization step; this is similar to the prediction phase where all the control actions have to be evaluated.

5.2.2.3 Optimization step

By assessing a cost function, g, the best sequence can be chosen; however, this can only happen after the paths of the prescribed variables for all possible control sequences have been computed. The sequence with the minimum cost is chosen, the first switch state is initiated by the controller at time, $(k+N_1)$, and the algorithm is re-started, producing what is called a receding horizon. The cost function assigns a cost to a deviation of state variables from their desired values, which are the reference values. In general, the cost is defined by the difference between the predicted variables and their references. When adding all the cost functions for each predicted future state, the total cost function is obtained. For a three-phase, three-level FCC inverter, a straightforward cost function can be expressed as an absolute value term with a single prediction step, as given in the following equation:

$$g = \left|i_{refx}(k+1) - i_x(k+1)\right| + \lambda_{DC}\left|v_{1xref}(k+1) - v_{1x}(k+1)\right| \quad (5.19)$$

The reference value is i_{refx} for the phase current and v_{1xref} for the voltage of capacitor C_{1x}. The weighting factor λ_{DC}, expresses the relative importance of an error in the flying capacitor voltage compared to an error in the output current. The optimal

switching operation is found when the total cost function is minimized and the cost function for a future predicted step, n, is

$$g = \sum_{n=1}^{N} \left| i_{refx}(k+n) - i_{\alpha}(k+n) \right| + \lambda_{DC} \left| v_{1xref}(k+n) - v_{1x}(k+n) \right| \quad (5.20)$$

The total cost function is the sum of the cost function for each converter phase.

To simplify calculations in this study, the following approximation is taken into account: the reference current is considered to remain constant when the prediction horizon has a short sampling time, T_S; this is shown in the following equation:

$$i_{ref}(k+n) \approx i_{ref}(k) \quad (5.21)$$

For a more exact estimate, the values of the reference current, $[i_{ref}(k+1)]$, for the a, b, and c axes are needed for Equations 5.18 and 5.19. These values have to be predicted from the existing current and previous values of the reference current, by applying the following second-order extrapolation:

$$i_{ref}(k+1) = 3i_{ref}(k) - 3i_{ref}(k-1) + i_{ref}(k-2) \quad (5.22)$$

Equation 5.22 is derived using the quadratic Lagrange extrapolation formula (Kukrer 1996; Rodríguez et al. 2007).

5.3 Hysteresis-based predictive control of flying capacitor voltages

To balance the flying capacitor voltages in a complimentary way when using the FS-MPCC scheme, a hysteresis algorithm, based on predictive control is presented. It must be noted that to enable the inverter to switch to zero voltages, the flying capacitors, C_1, C_2 and C_3 have to be charged to a voltage of $v_{DC}/2$. If in a phase, one of the zero switching states is selected, it will cause the corresponding flying capacitor voltage to either increase or decrease. The voltage change—increase or decrease—will be established by the direction of the current in the phase being considered and by the possibility that the voltage selected will be zero. Therefore, regardless of the switching states selected, the flying capacitor voltages must at all times remain balanced. After the determination of the most suitable voltage vector for the sampling cycle to follow, the corresponding optimum switching state generating this voltage vector must be identified. The voltage of each of the three flying capacitors has to remain within the tolerance set by a hysteresis band which straddles the reference voltage, $v_{DC}/2$. For the control algorithm presented, natural voltage balancing effects are insufficient for maintaining the flying capacitor voltages within the specified proximity to their reference values, making it necessary for an additional voltage balancing algorithm to be incorporated (Defay et al. 2010; Feng et

al. 2007; Khazraei et al. 2012; Hotait et al. 2010; Wilkinson et al. 2006). This algorithm selects the switching state which gives the derived optimum voltage vector and maintains the flying capacitor voltages inside their hysteresis bands. Provided that the flying capacitor voltage remains within its limits, either of the switching state combinations leading to a voltage of zero are allowed for this situation, and the switching state corresponding to zero that can be assigned with the lowest number of transitions is chosen. However, if the flying capacitor voltage drifts outside the boundaries of the hysteresis band straddling the reference voltage, only the switching state which forces the voltage back into the limits of that band, is allowed. The selection of the zero switching state to be used is made by taking the direction of the current in that phase into consideration. In this study, the width of the hysteresis band is the result of selecting a tolerance of 0.1% of the v_{DC} value. This allows a finite set-model predictive control with a prediction step greater than one to be implemented. A block diagram of the entire control algorithm of an FCC inverter with an RL-load is given in Figure 5.5.

The flowchart of a hysteresis-based voltage balancing algorithm is depicted in Figure 5.6. If an FCC is controlled directly, the switching states can only be changed at the beginning of a sampling cycle, which is different to conventional PWM. As a result, the flying capacitors have to be dimensioned with care as a zero voltage will be applied for a whole sampling cycle; this is in contrast to modulator-controlled inverters. A worst-case estimation of the necessary capacitor size can be done easily (see Equation 5.23) on the assumption that the maximum allowed current per phase, i_{max}, is drawn for the whole sampling cycle, T_S, and that the maximum flying capacitor voltage ripple, ΔV is defined as:

$$C_f = \frac{i_{max} T_S}{\Delta V} \tag{5.23}$$

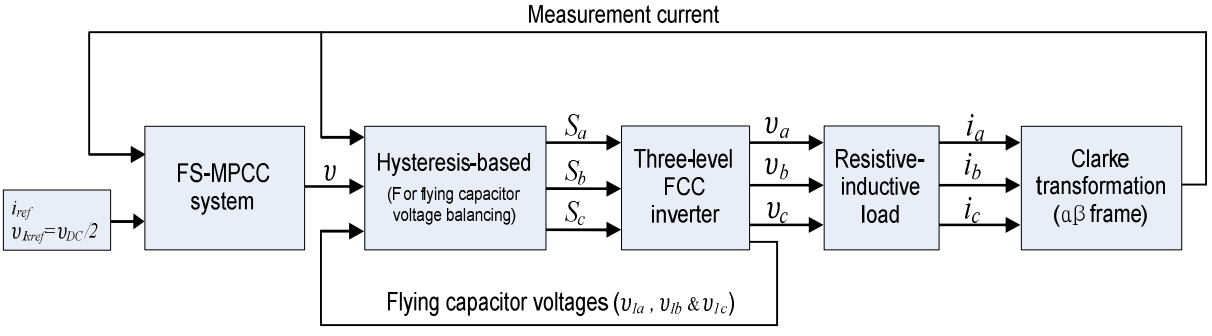

Figure 5.5: Block diagram of the proposed control algorithm of an FCC inverter connected to an RL-load

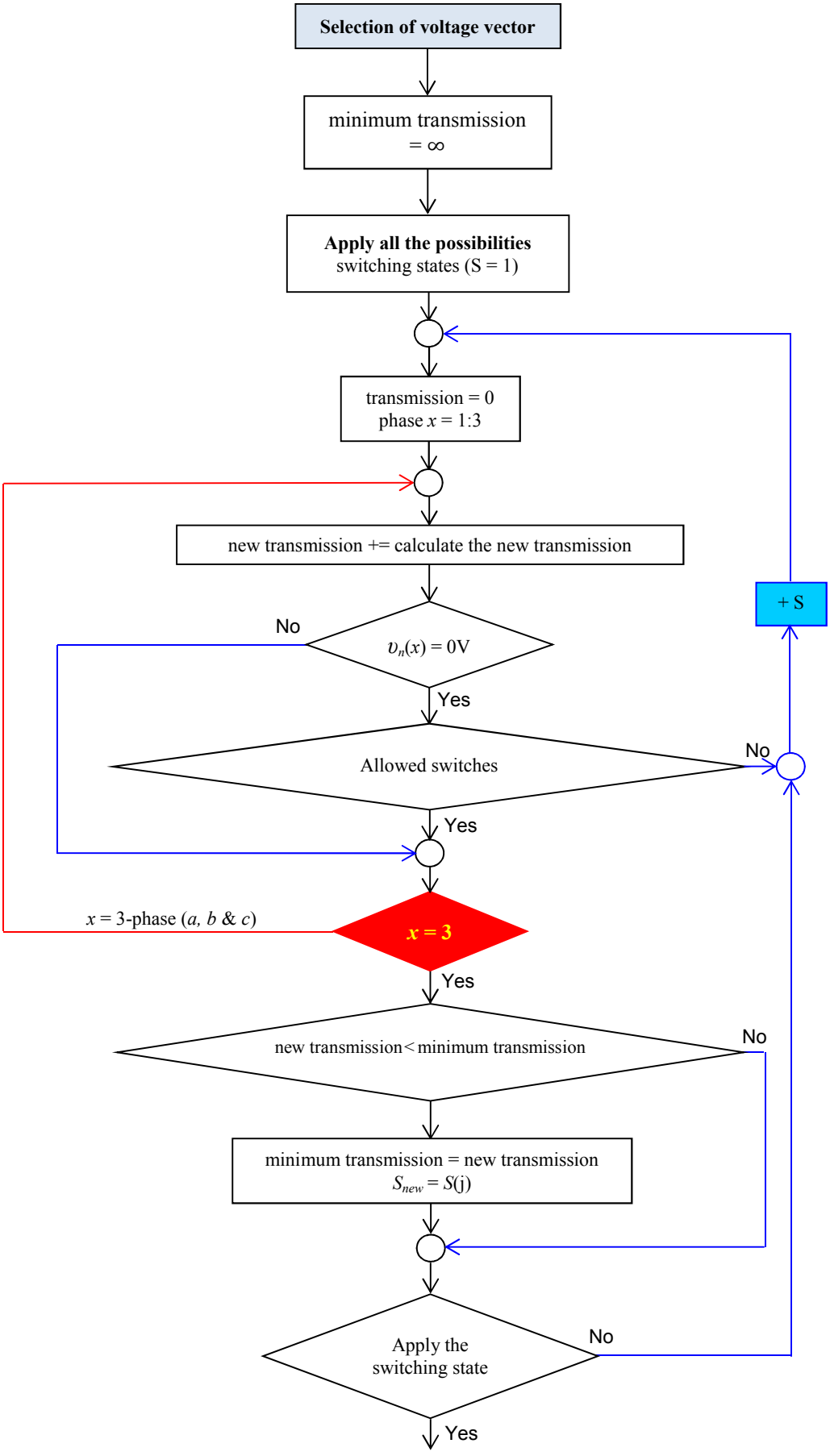

Figure 5.6: Hysteresis-based voltage balancing algorithm

5.4 Results and discussion

The FS-MPCC strategy for a three-phase, three-level FCC was co-simulated using MATLAB/Simulink together with PSIM; this was done to evaluate the performance of the proposed control algorithm and to check the performance and robustness of the proposed control method. The FS-MPCC algorithm was evaluated with regard to three performance indicators: the effectiveness of reference current tracking, the ability to balance the flying capacitor voltages and the THD. Table 5.2 shows the parameters and their values, as used for the co-simulations.

Table 5.2: Parameters used for the co-simulations

Parameter	Value
Load resistance, R	15 Ω
Load inductance, L	10 mH
Flying capacitor	560 µF
DC-link voltage, v_{DC}	400 V
Amplitude of the reference current, i_{ref}	10 & 14 A
Hysteresis-band limits relative to v_{DC}	0.1%
Sampling time, Ts	25 and 100 µs

5.4.1 Control strategy robustness under variable DC-link of three-level FCC

This simulation demonstrated the stability of the proposed control method under conditions of variable DC-link voltages; in particular when the DC-link voltage was changed from 350 to 450 V with T_S = 25 µs. Figure 5.7 shows the output currents for different values of DC-link voltages. It can be observed that the proposed control algorithm has the ability to follow sinusoidal reference currents despite substantially changing the DC-link voltage from the desired voltage. These results of the simulation are in Table 5.3.

Table 5.3: THD and output current for variable DC-link voltages

DC-Link value [V]	**Fundamental current at** 50 Hz, [A]	**THD** [%]
350	13.63	2.49
360	13.89	1.21
370	14.01	0.78
380	14	0.82
390	14	0.82
400	14	0.84
410	14	0.86
420	14	0.88
430	14	0.89
440	14	0.91
450	14	0.93

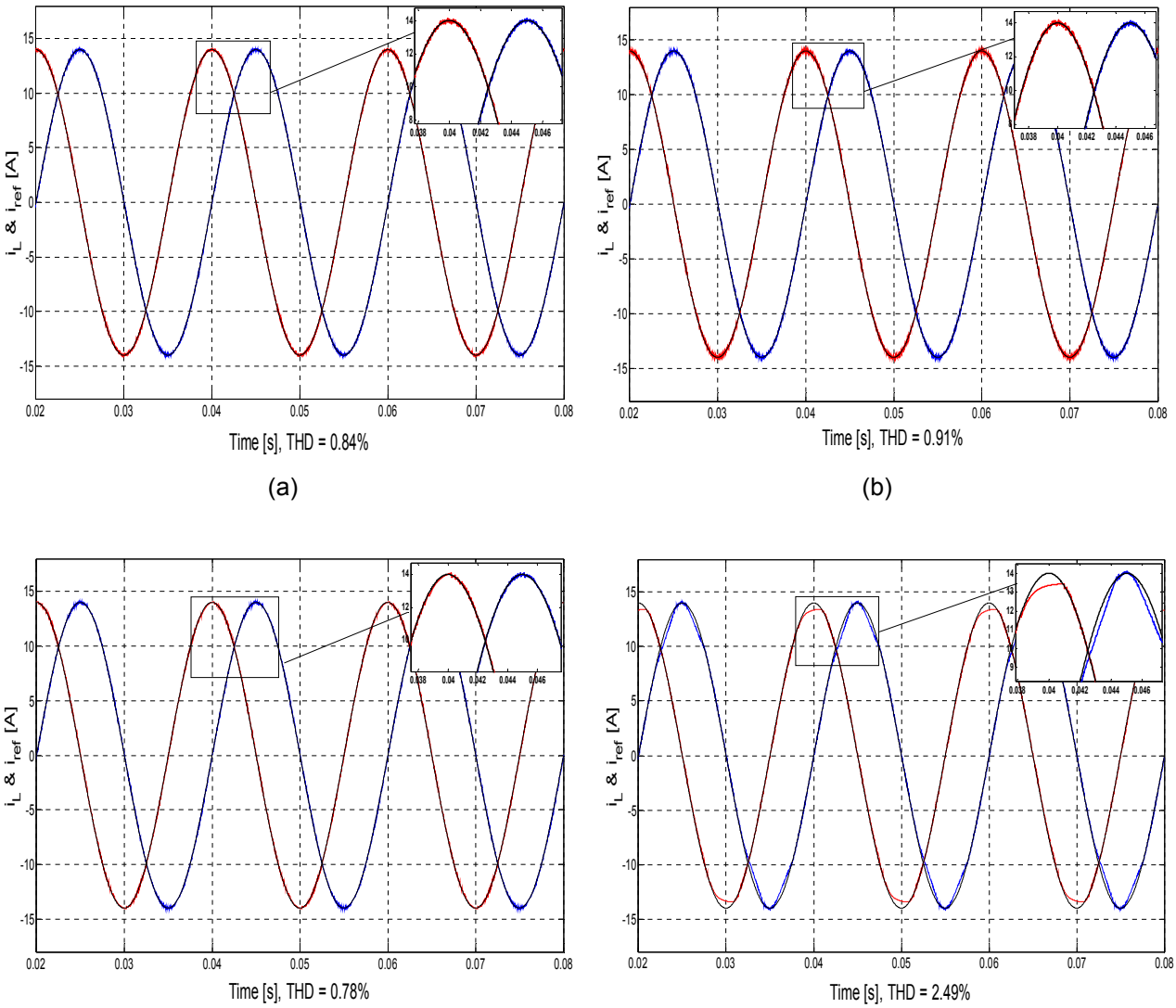

Figure 5.7: Output currents for different values of DC-link voltage

In Figure 5.7(a) are shown, the results of the DC-link when it was set to the designed voltage value of 400 V and the THD was 0.84%. Compare these results to those shown in Figure 5.7(b) when the DC-link was set to 440 V and the THD was increased to 0.91%, as well as those shown in Figures 5.7(c) and (d) when the DC-links were set to 370 V and 350 V and the THDs were decreased to 0.78% and increased to 2.49% respectively.

It is notable that voltages higher than the designed DC-link voltage value of 400 V produced a lower THD, while the amplitude of the output current was kept constant and tracked the reference current with a very small error. On the other hand, for DC-link voltage values smaller than the designed value, a higher THD with a relatively small amplitude error was produced.

5.4.2 Reference tracking

The second co-simulation run demonstrated the performance of the system for one and two prediction steps with an amplitude step change in the reference current and the current reference tracking when the weighting factor was set to 0.02 for T_S = 25 µs.

5.4.2.1 Sinusoidal reference steps

From the simulation, the control results for sinusoidal reference values were obtained; the load currents and load voltages are respectively shown in Figures 5.8(a) and (b). The flying capacitor voltages can be seen in Figure 5.9. The outcome of step changes in the amplitude of the reference currents is as follows: for i_α at time 0.035s, the amplitude changed from 14 A to 12 A and for i_β at time 0.04 s, the amplitude changed from 14 A to 10 A (see Figure 5.8(a)). Over the intervening time between the step change in the amplitude of currents i_α and i_β respectively, the load voltage, v_β, was kept at its maximum value until the reference current, i_β, was achieved.

The voltage balancing algorithm demonstrated that it has the ability to maintain the voltages of the flying capacitors within the band created by their hysteresis boundaries, as shown in Figure 5.9. The fact that the hysteresis boundaries were exceeded at some points where the voltage strayed outside the band, as depicted in Figure 5.9, was due to corrective action by the control algorithm. Where these transgressions occurred, a positive or negative switching state command was issued in the corresponding phase. The flying capacitor voltages can only be influenced if a zero switching state command is issued in that phase, and only then can the flying capacitor voltage be changed.

The ability of the proposed control algorithm to monitor sinusoidal reference currents was clearly demonstrated by the simulation. The predictive control method, as can be seen from this simulation, has a fast, dynamic response with built-in decoupling between i_α and i_β. Again, the algorithm showed exceptional monitoring performance, and the voltage balancing algorithm managed to keep the flying capacitor voltages within the proximity of their reference values.

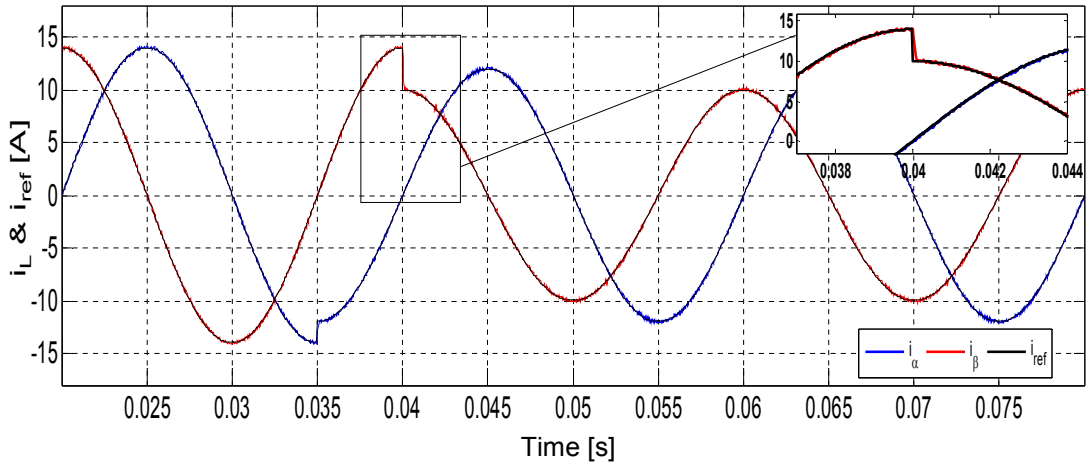

(a)

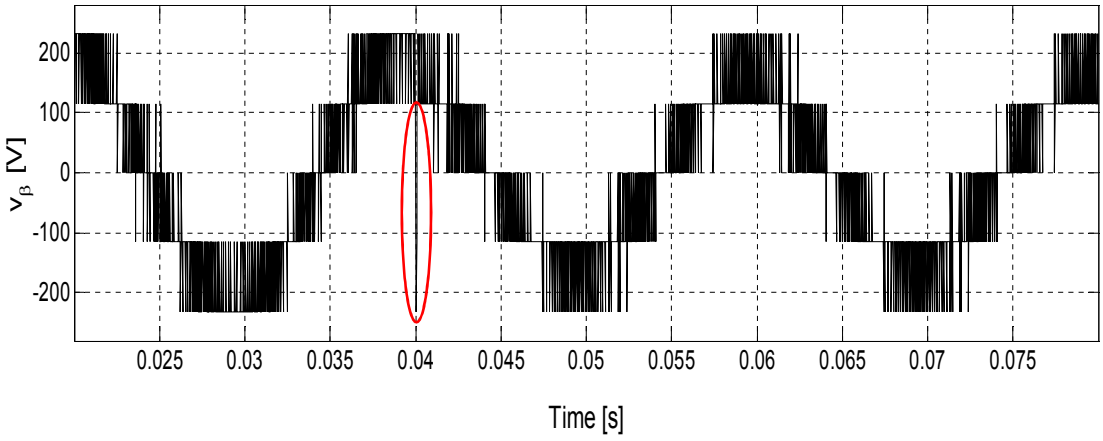

(b)

Figure 5.8: Sinusoidal reference steps for (a) load currents and (b) load voltage υ_β

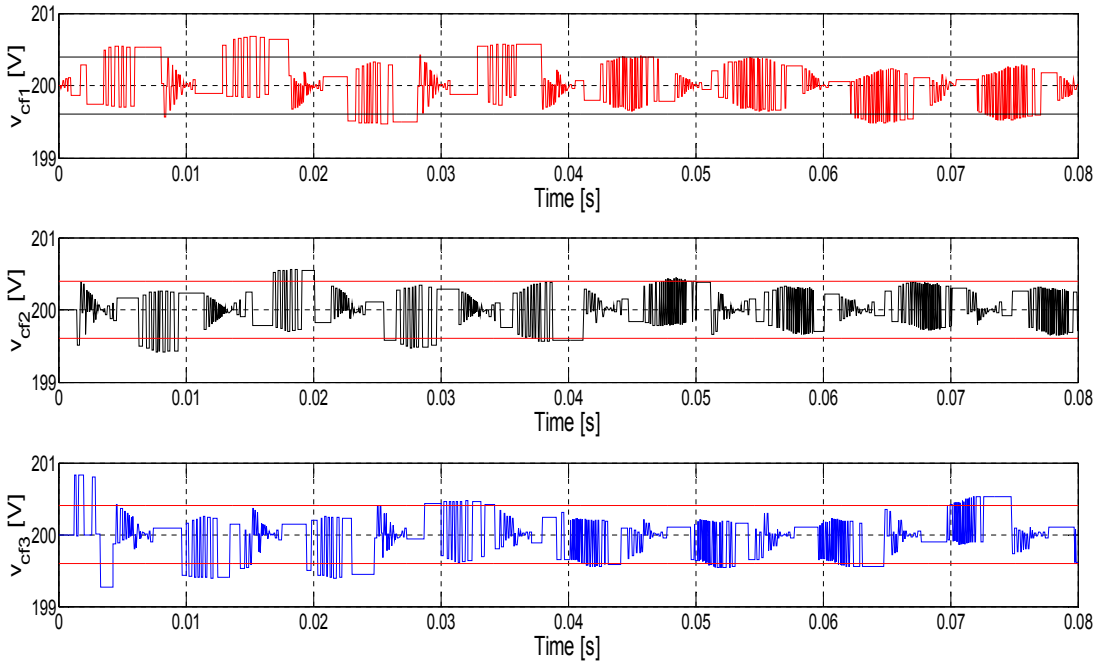

Figure 5.9: Flying capacitor voltages during an RL-load step

5.4.2.2 Sinusoidal reference tracking with two prediction steps

The robustness of the proposed control method was tested with two prediction steps. In Figures 5.10 and 5.11, the currents and load voltage are shown respectively. In Figure 5.10 is shown how the output currents track their references; this illustrates the excellent tracking behaviour of the control algorithm.

For the prediction horizon of two prediction steps, the error between the reference and actual current was evaluated to check the influence of the prediction horizon; this is shown in Figure 5.12.

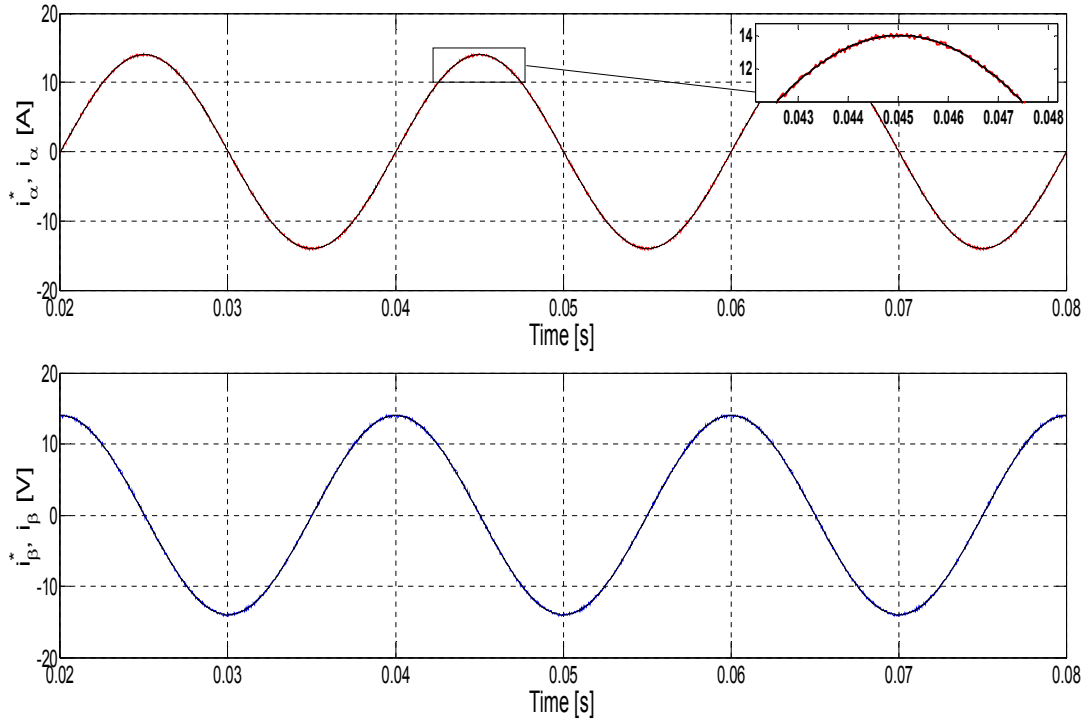

Figure 5.10: Output load currents for a two-step prediction horizon

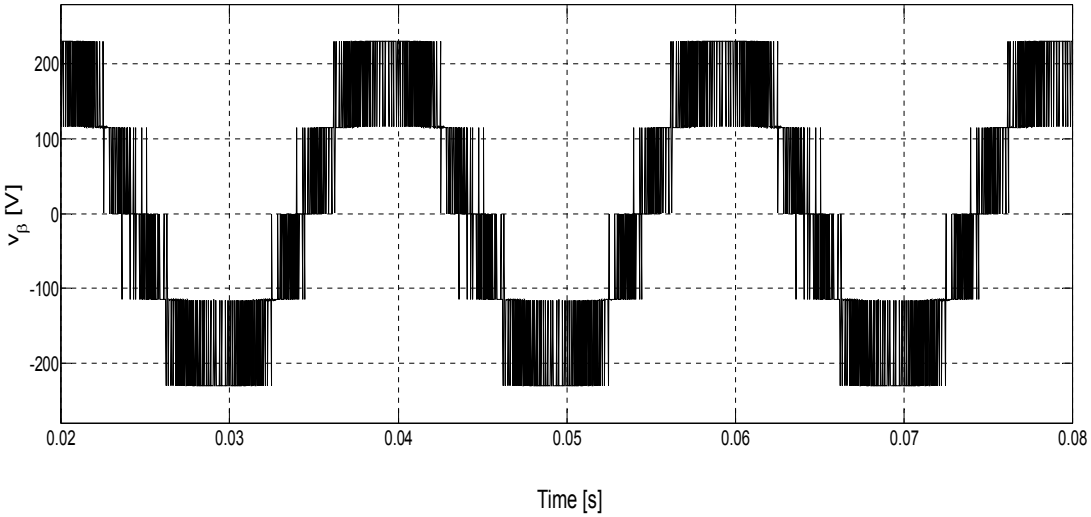

Figure 5.11: Load voltage for a two-step prediction horizon

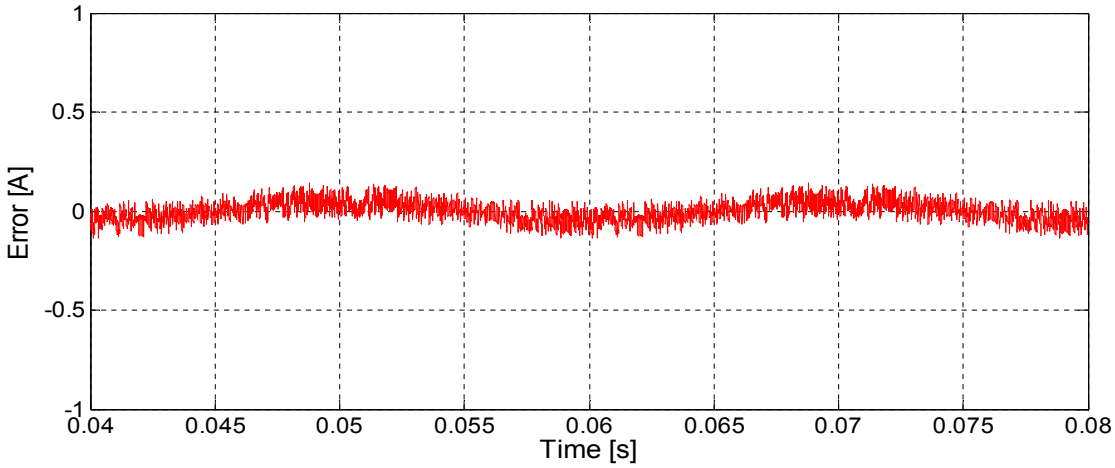

Figure 5.12: Error between the reference and load current for a two-step prediction horizon with a sampling time T_S = 25 µs

The flying capacitor voltages, as shown in Figure 5.13 were kept within the hysteresis band. The figure indicates that there were some points where the flying capacitor voltage output fell outside the band, but this situation was remedied by the operation of the control algorithm that brought the voltage back within the confines of the hysteresis band. In these cases where the voltage went out of bounds, a positive or negative switching state command was issued in the corresponding phase. The flying capacitor voltages can only be influenced if a zero switching state command is issued in that phase, and only then can the flying capacitor voltage be changed.

This simulation clearly demonstrated the ability of the proposed control algorithm to track sinusoidal reference currents while the flying capacitor voltages were kept within the hysteresis band straddling their reference voltages.

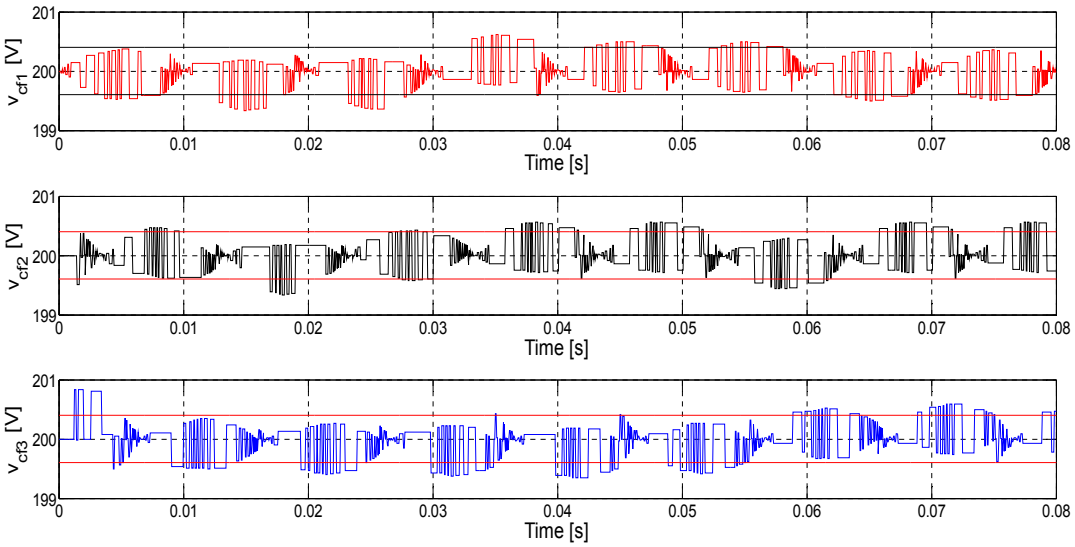

Figure 5.13: Flying capacitor voltages for a two-step prediction horizon

5.4.2.3 Square waveform reference

One of the applications of a square waveform is in a stepper motor driver where two things are normally required: a controller to create step and directional signals and that which the MPC does. A square waveform in orthogonal coordinates was applied as a reference current in order to assess the control algorithm of the model developed in this study. The resultant amplitude of the square waveform of the references, i_α and i_β set to 3 A and with T_S = 100 µs is shown in Figure 5.14. The flying capacitor voltages, also with T_S = 100 µs are shown in Figure 5.15. The currents, i_α and i_β correctly followed the reference, while the current ripple, which remained in a steady state, was affected by the controller frequency and finite switching. The flying capacitor voltages were maintained within the bounds of their reference voltages by the voltage balancing algorithm (see Figure 5.15).

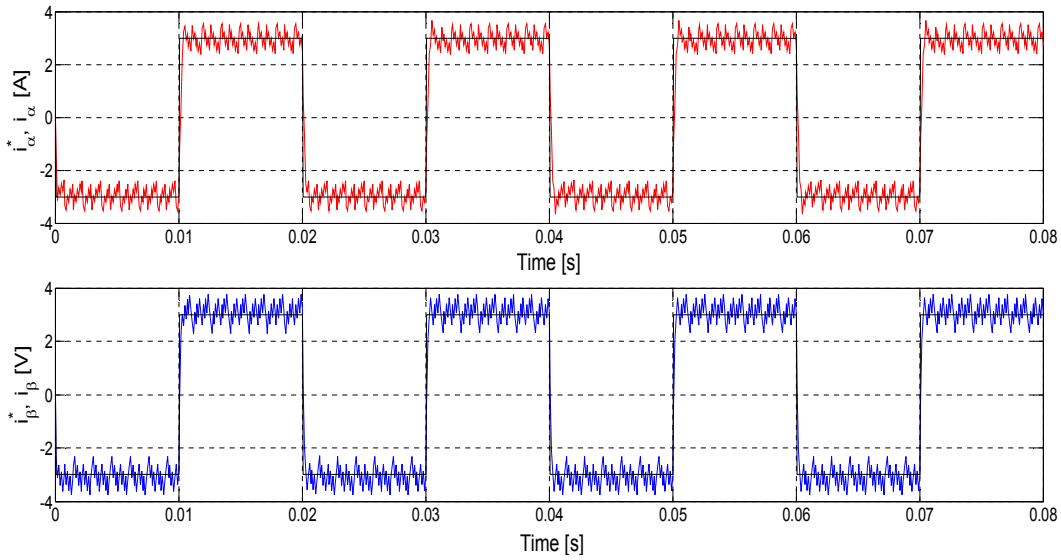

Figure 5.14: Square waveform reference for load current with T_S = 100 µs

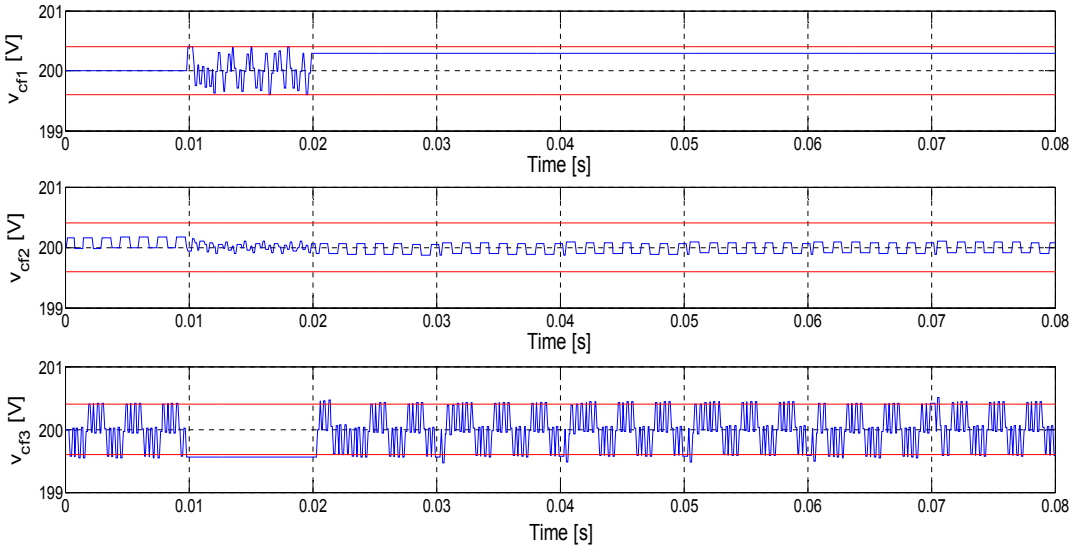

Figure 5.15: Flying capacitor voltages with a sampling time T_S = 100 µs

The result for the square waveform reference, i_α and i_β with amplitude 3 A and T_S = 25 µs is shown in Figure 5.16, and the result of the flying capacitor voltages with T_S = 25 µs is shown in Figure 5.17. The currents i_α and i_β correctly followed the reference with less ripple when compared to the results where T_S = 100 μs was used. The hysteresis-based voltage balancing algorithm ensures that the flying capacitor voltages are kept within the hysteresis band, as shown in Figure 5.17. At points where the hysteresis boundaries were breached, the voltage was pulled back into the band by the operation of the control algorithm. Like in the other cases, to coerce the voltage back into the band, a positive or negative switching state command was issued in the corresponding phase. The flying capacitor voltages can only be influenced if a zero switching state command is issued that phase and only then can the flying capacitor voltage be changed.

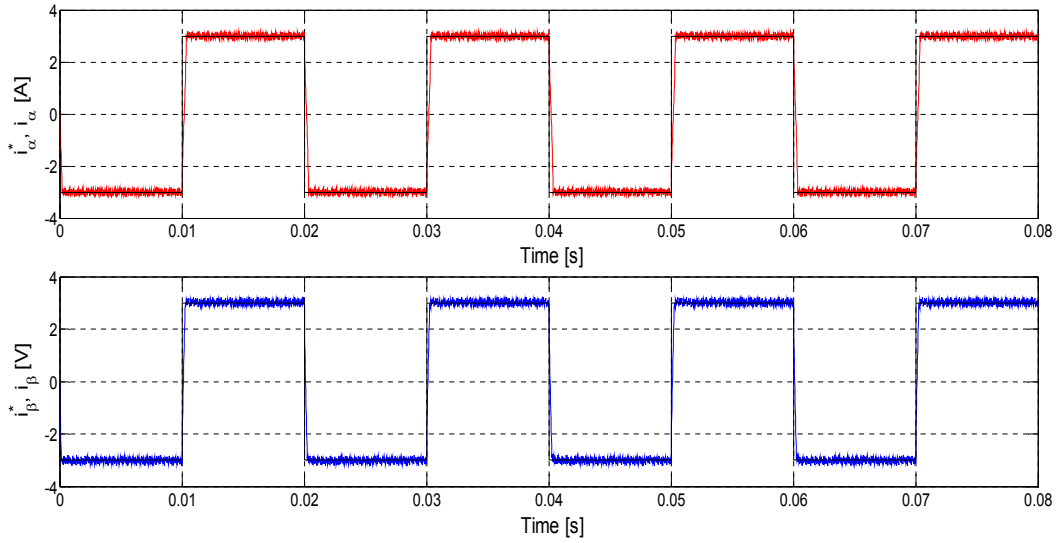

Figure 5.16: Square waveform reference for load current for T_S = 25 µs

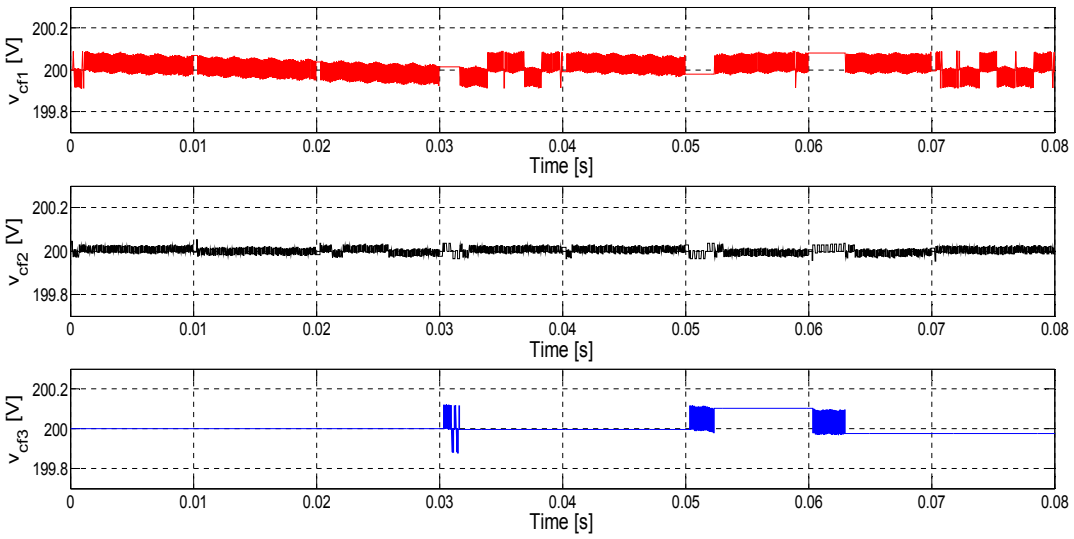

Figure 5.17: Flying capacitor voltages with a sampling time T_S = 25 µs

5.4.2.4 Constant reference steps

In this simulation, the performance of the control strategy using constant reference steps was tested. The resulting load currents with constant reference steps are shown in Figure 5.18. The simulation displayed the control result for constant reference steps values, when a step change in the amplitude of the references, i_α and i_β from 0 A to 10 A occurred at 0.02 s; this is shown in Figure 5.18. As can be seen, the load currents reach their reference with a fast, dynamic response; the current ripple that is caused by the finite switching and controller frequency, can be seen in a steady state.

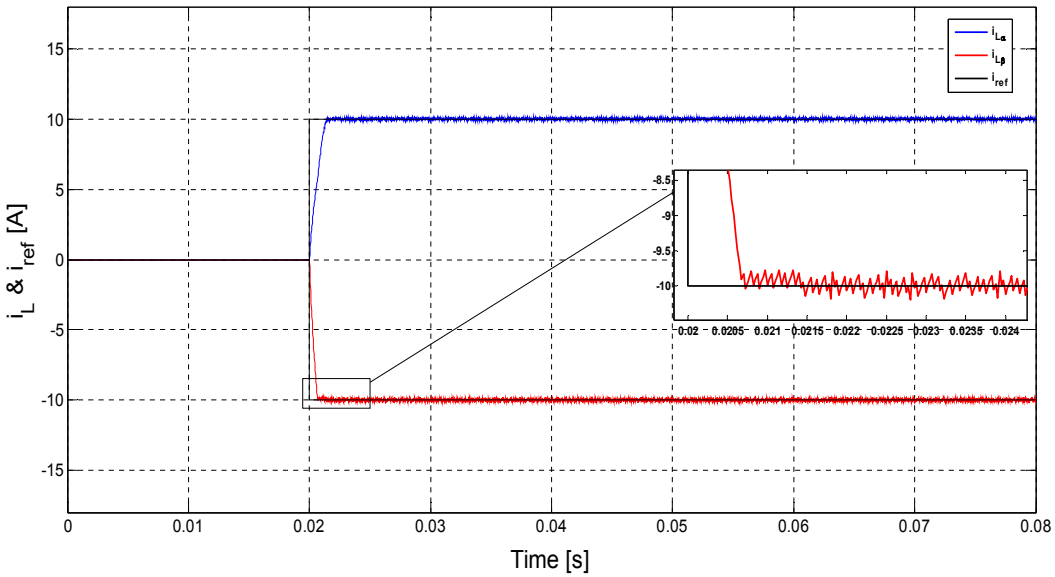

Figure 5.18: Constant reference steps for load current when amplitude current changed to 10 A

5.4.2.5 Sawtooth waveform reference

The control algorithm was tested with a sawtooth waveform in orthogonal coordinates as a reference current. The result for sawtooth waveform with the amplitude of the references, i_α and i_β set to 10 A, and T_S= 25 µs, are shown in Figure 5.19. The corresponding flying capacitor voltages are shown in Figures 5.19 and 5.20.

In this simulation, the currents, i_α and i_β correctly followed the reference. The remaining current ripple, having a steady state, resulted from the finite switching and controller frequency. The voltage balancing algorithm was able to keep the flying capacitor voltages within their hysteresis boundaries, as is shown in Figure 5.20. A violation of the boundaries can be noticed in the bottom graph of Figure 5.20; this is attributed to the long sampling time of the control algorithm. A hysteresis controller can only detect a violation of the hysteresis boundaries at the sampling instances.

This simulation demonstrated that the predictive control method has a fast, dynamic response. Again, the algorithm showed excellent tracking behaviour, and the flying capacitor voltages were kept within the hysteresis band by the hysteresis-based voltage balancing algorithm.

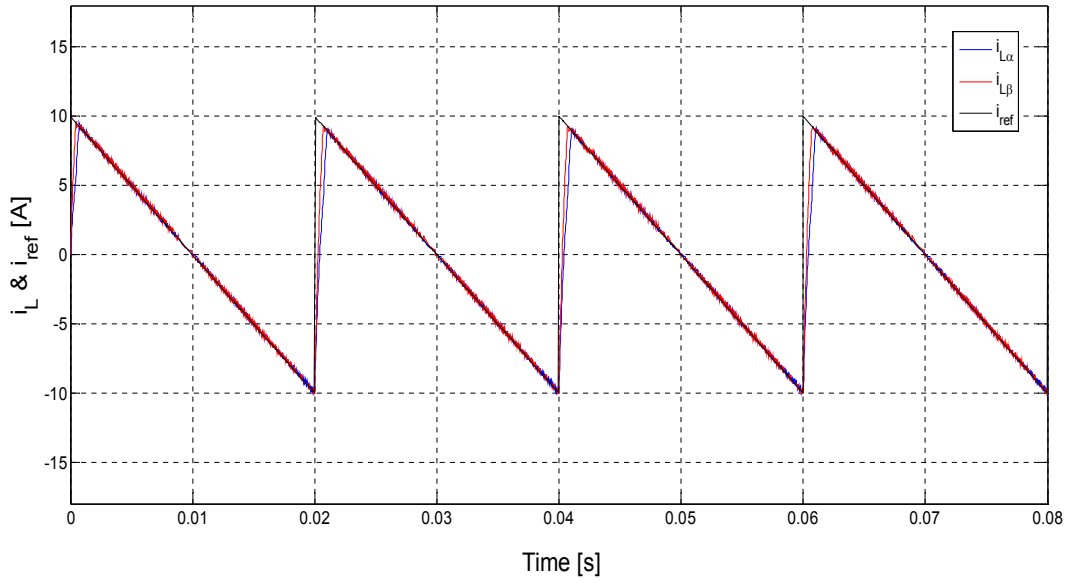

Figure 5.19: Sawtooth waveform reference for load current when amplitude current was set to 10 A with T_S= 25 µs

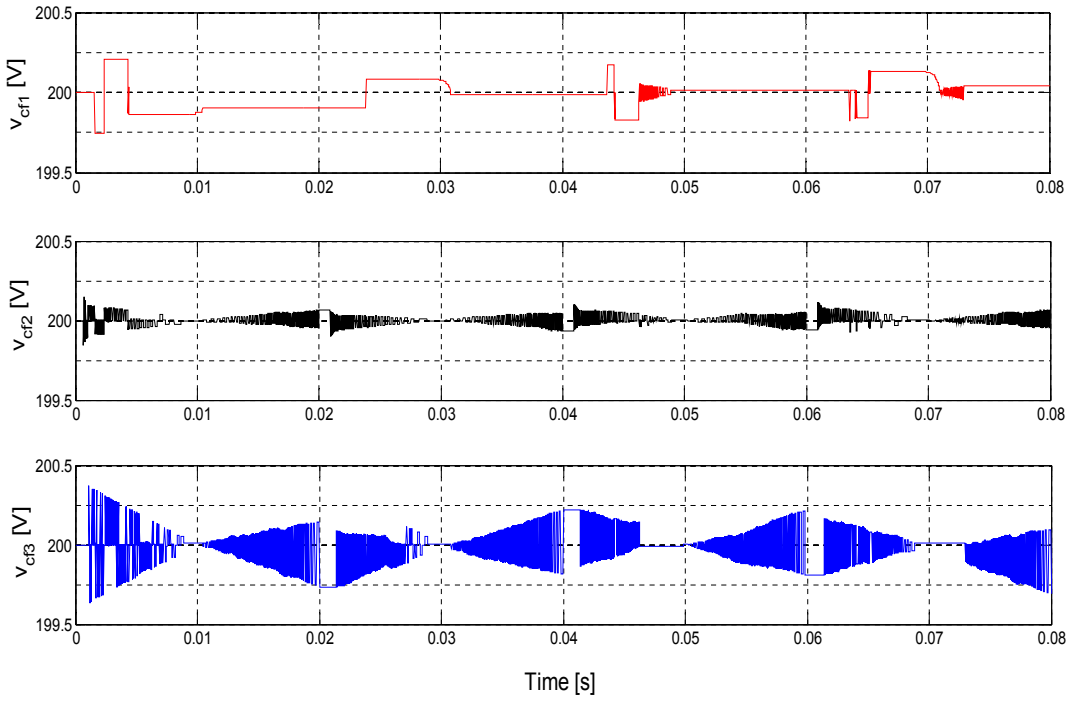

Figure 5.20: Flying capacitor voltages with T_S= 25 µs

5.4.3 Comparison of the model and actual system parameters

In the last evaluation, a mismatch between the selected model and the corresponding system parameter was considered. To evaluate the parameter sensitivity of the proposed control algorithm, different values for the load resistor and inductor were used. These values were estimated in order to determine how robustly the system could track the reference signal, balance the flying capacitor voltages and control the THD. The investigation in this section was designed to study the effect of parameter uncertainty on the system model under consideration.

The actual inductance was estimated both 50% higher and 50% lower, than the parameter used in the model, with sampling times, T_S= 25 μs and T_S= 100 μs. In another case, the inductance was increased to 100% with T_S= 25 μs and T_S= 100 μs. The actual resistance was estimated at 40% higher and 40% lower than the parameter used in the model, with T_S= 25 μs.

As indicated in Figure 5.21(a), when the load inductance was estimated at +50% with T_S= 25 μs (THD = 0.63%), the control algorithm showed excellent reference tracking behaviour. However, when T_S was increased to 100 μs, the current ripple on the load current increased (THD = 2.43%); this is depicted in Figure 5.21(b).

Comparatively, when the load inductance was estimated at +100% for T_S= 25 μs (THD=1.97%), the control algorithm demonstrated excellent reference tracking behaviour as shown in Figure 5.21(c). In Figure 5.2(d) the effect of increasing the sampling time to 100 μs, on the current ripple of the load current (THD = 2.16%), is shown.

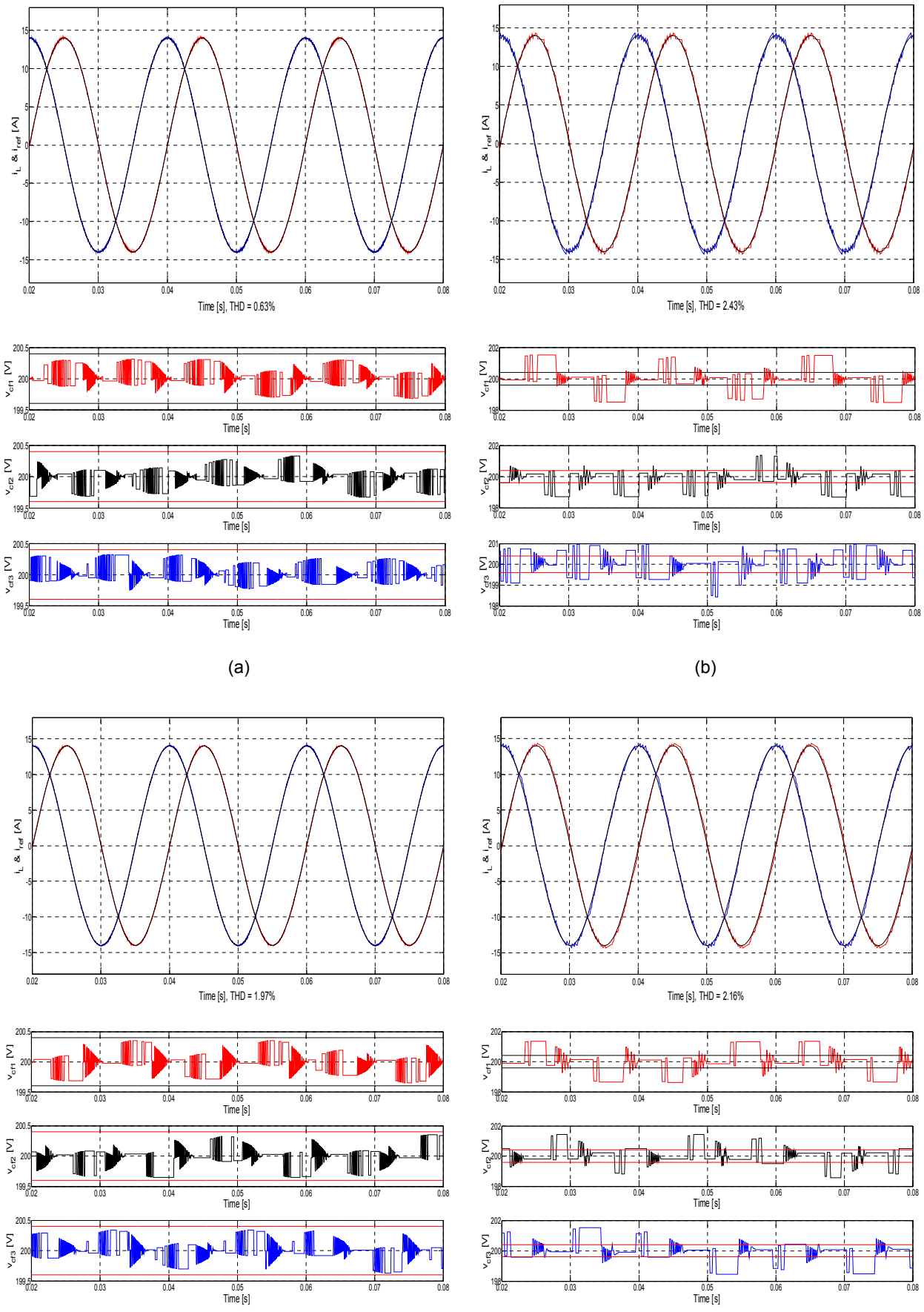

Figure 5.21: Inductance sensitivity for load current and flying capacitor voltage when estimated at +50%

If, however, the inductance was estimated at 50% lower than the parameter used in the model and with T_S= 25 µs, the load current ripple increased marginally, compared to the model inductance value (THD = 2.36%). On the other hand, with T_S= 100 µs, the current ripple increased substantially (THD = 10.23%), as seen in Figure 5.22.

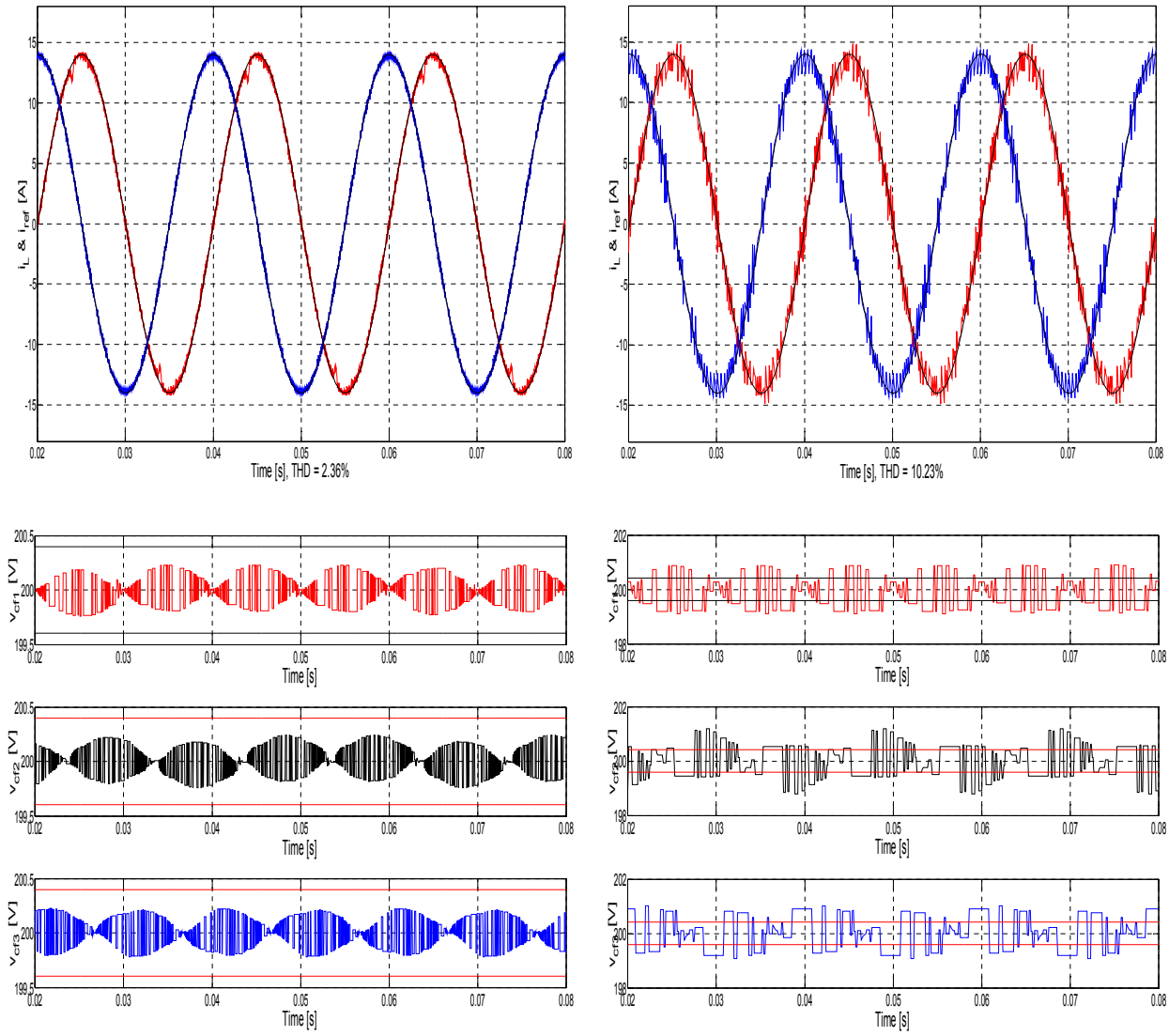

Figure 5.22: Inductance sensitivity for load current and flying capacitor voltage when estimated at -50% for (a) 25 µs and (b) 100 µs

Figures 5.23 and 5.24 show the simulation results respectively when: the actual resistance was estimated at 40% lower than the parameter used in the model with T_S= 25 µs and T_S= 100 µs and at 40% higher than the parameter used in the model with T_S= 25 µs and T_S=100 µs. In the case where the actual resistance was estimated at -40% with T_S= 25 µs (see Figure 5.23(a)), the predictive control method performed

better, both in tracking the load current references and flying capacitor voltage balancing, than when the actual resistance was estimated at +40% with T_S= 25 µs (see Figure 24(a)). In both situations where the load resistance was estimated at -40%, the load currents were higher than their reference values with THD = 0.82% when T_S = 25 µs (see Figure 5.23(a)) and TDH = 3.14% when T_S = 100 µs (see Figure 5.23(b)).

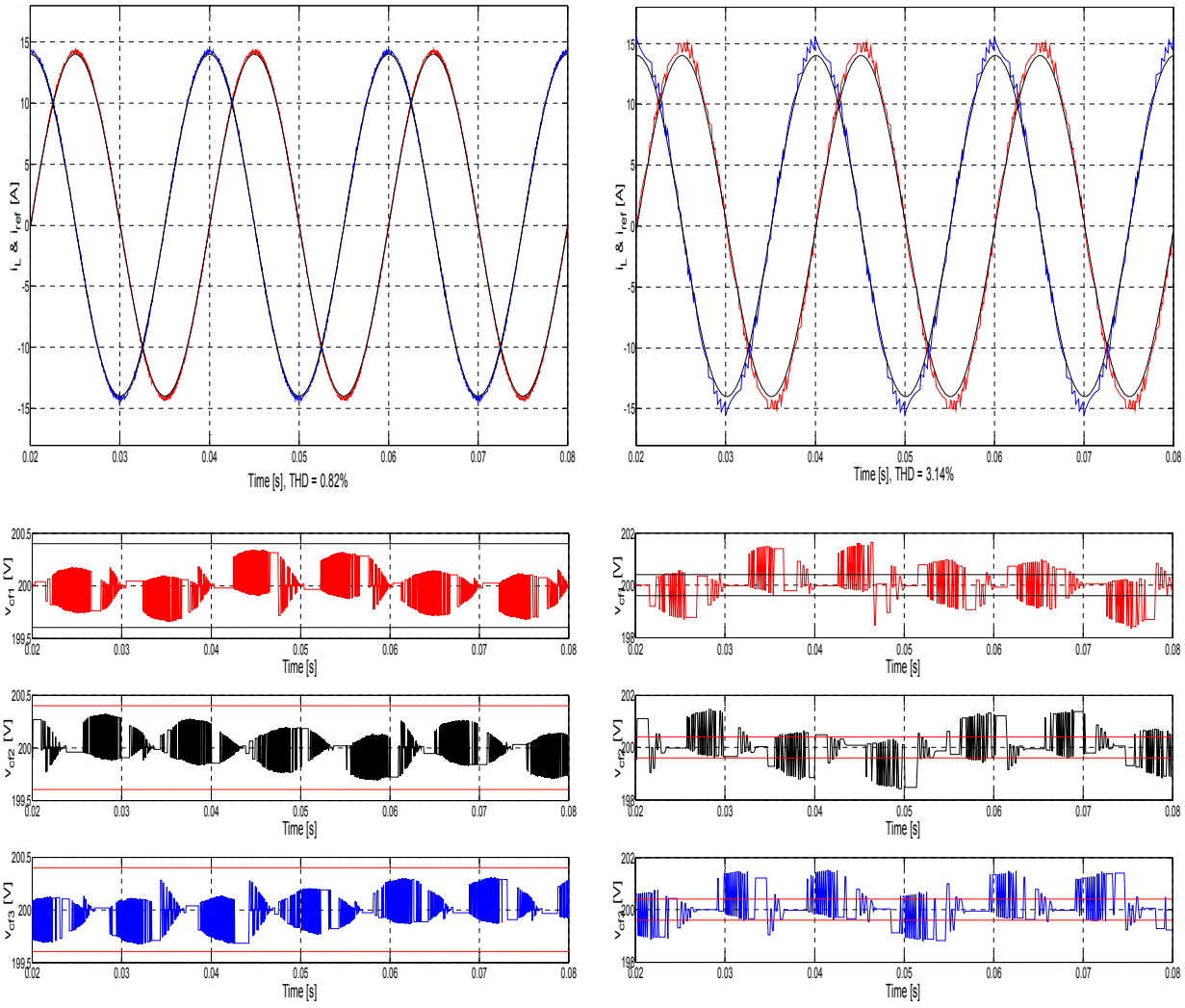

(a) (b)

Figure 5.23: Resistance sensitivity for load current when estimated at -40% for (a) T_S= 25 µs (b) T_S= 100 µs

With the actual resistance estimated at +40% higher with T_S= 25 µs (see Figure 5.24(a)), the predictive control method produced a better result with regard to tracking the load current references and in balancing the flying capacitor voltages than with T_S= 100 µs (see Figure 5.24 (b)). With the estimated load resistance at +40%,

however, the load currents were lower than their reference values, and with THD = 1.73% when T_S= 25 µs and THD = 3.09% for T_S= 100 µs.

The results obtained in mismatching the model and the actual system parameters are tabulated in Table 5.4 in terms of fundamental output current, THD and sampling period.

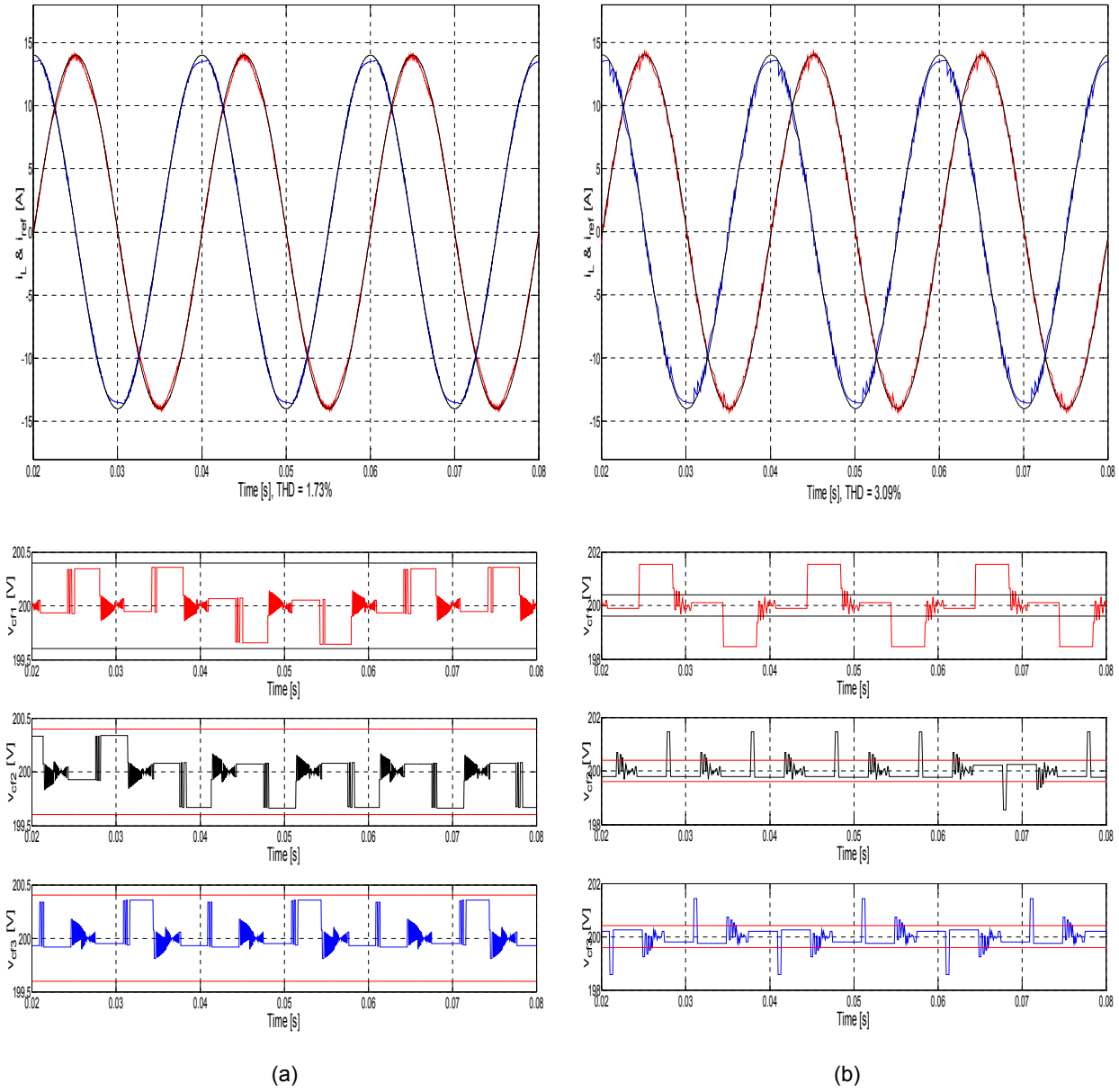

Figure 5.24: Resistance sensitivity for load current when estimated at +40% (a) T_S = 25 µs (b) T_S = 100 µs

Table 5.4: A mismatching between the model and the actual system parameters

Sampling time T_S, [µs]	Inductance, L		Resistance, R		Fundamental output current at 50 Hz, [A]	THD [%]
	%	Value, [mH]	[%]	Value, [Ω]		
25	+50	15	-	-	14.02	0.63
25	+100	20	-	-	13.96	1.97
100	+50	15	-	-	14.12	2.43
100	+100	20	-	-	14.13	2.16
25	-50	5	-	-	13.9	2.36
100	-50	5	-	-	13.65	10.23
25	-	-	+40	21	13.73	1.73
25	-	-	-40	9	14.21	0.82
100	-	-	-40	9	14.83	3.14
100	-	-	+40	21	13.75	3.09

5.5 Summary

The FS-MPCC strategy with one- and two-step prediction times to control the three-level FCC was presented. The RES model was used in this study to investigate the system performance, when power was supplied to an RL-load. The best 19 unique voltage vectors out of a possible 64 were selected and applied to the inverter.

The work presented in this chapter demonstrated the effectiveness of the SSI technique as shown by its application in the FCC case study presented. The SimCoupler Module enables MATLAB/Simulink users to implement and simulate power circuits in the original circuit form, thus greatly shortening the time to set up and simulate a system that includes electronic circuits. The important step in the SSI technique is the time synchronization of the two independent software platforms that are used, in this case PSIM and MATLAB/ Simulink.

The minimization of the current and capacitor voltage errors by using a cost function provides a fast, dynamic response for load current control and guarantees balanced flying capacitor voltages. The proposed control strategy does not require a linear controller or the application of a modulation technique. Additionally it affords the designer the freedom to adjust the weighting factor λ_{DC} in order to fulfil the requirements in terms of reference current tracking and flying capacitor voltage balance. The presented hysteresis-based voltage balancing algorithm has the ability to keep the flying capacitor voltages within the required proximity of their reference values.

The FS-MPCC algorithm was subjected to three different conditions and evaluated in terms of reference current tracking and flying capacitor voltage balance; this

evaluation was done by processing the results obtained through co-simulation. The first condition relates to the robustness of the control strategy being dependant on a variable DC-link as used in RESs applications, and this was assessed in terms of the THD. The results demonstrated that the predictive control method has the ability to track sinusoidal reference currents and exhibits excellent tracking behaviour with all DC-link voltage values. Furthermore, it was established that the capacitor voltages remained well balanced with minimal error. For the second condition, the sinusoidal waveform current reference tracking and sinusoidal waveform with a step change in the amplitude of the reference were investigated. The control algorithm was subsequently tested with different current waveforms in order to check the dynamic response; these reference currents were a square waveform in orthogonal coordinates, constant reference steps and a sawtooth waveform. For all four waveforms, the results showed that the algorithm displayed excellent tracking behaviour and a fast dynamic response with inherent decoupling between i_α and i_β at the step changes. Moreover, the voltage balancing algorithm, based on predictive control, was able to keep the flying capacitor voltages within the bounds of their reference values. Finally, the performance of the proposed control was assessed by creating a mismatch between the model parameter and the actual, corresponding system parameter. These results indicated that the FS-MPCC approach gives excellent results under these conditions. In general, when the sampling time was increased, the load current ripple increased while the flying capacitor voltages at some points exceeded the hysteresis boundaries for a longer time. This situation was remedied by the operation of the control algorithm which, brought the voltage back within the confines of the hysteresis band.

The FS-MPCC strategy applied in this research has demonstrated how powerful the tool is when compared to the conventional method of using modulation techniques. This concept can be extended to any power converter system, and the developed hysteresis-based voltage balancing algorithm will be able to keep the flying capacitor voltages within the bounds of their reference values.

CHAPTER SIX

CONCLUSION AND RECOMMENDATIONS

6.1 Conclusion

6.2 Further work and recommendations

6.1 Conclusion

An MPC is based largely on fast microprocessor calculations. This thesis successfully addressed and solved the reduction of the enormous amount of calculations required in the direct control of an inverter without a modulator. In such a case, the calculation cycles usually rise exponentially with an increase in the prediction horizon. This has been a major problem to overcome in MPC as the control task is not feasible for predicting horizons greater than one prediction step.

The flying capacitor voltage and DC-link capacitor voltage balance problems was also resolved. The main challenge was to ensure that proper functioning of the inverter kept the correct voltage across the flying capacitors and DC-link voltages at all times during the operation of the converters. In this thesis, both of the above-mentioned problems were overcome, along with the reduction of the THD in the output stage of the inverters.

In Chapter two of this thesis, the state-of-the-art of MLC technology and its applications was discussed. This chapter started with an introduction to power electronic converters. The fundamentals and concept of MLC structures were presented, as along with the advantages and disadvantages of each converter type. Next, a comparison of the most promising multilevel topologies was presented, based on the number of components and isolated DC sources required. Following this section, voltage balancing problems depending on the MLC topology were highlighted. Most of the focus in this chapter addressed modern and more practical industrial applications of MLCs as used in RESs installations where MLCs can be used to interface with a PV system and/or wind turbine resources. It should be noted that not all multilevel power converter-related applications could be covered; however, the basic principles of different MLCs have been discussed methodically.

Chapter three introduced various predictive control methods. The literature made it clear that predictive control is widely used for the control of power electronic converters and motor drives. This chapter presented an examination of the terminology used in predictive control and described the modelling of the proposed system and the approximations for the derivatives of differential equations. The cost function classifications in terms of weighting factors, delay compensation procedure, and reference frames were also presented. This chapter further detailed different compensating procedures which can be included in a wide variety of cost function equations and weighting factors. Examples of the presented procedures are provided for a wide variety of cost functions, and examples of adjustments for the weighting factors of several predictive control applications are also provided. Finally, simulation results of a three-phase VSI using a finite set-model predictive current control were

obtained in order to show the influence on the load current and load voltage of some system parameters used in predictive control.

Chapter four presented the FS-MPCC strategy with one-step prediction time to control the three-level DCC inverter. The RES model was used in this study to investigate the system performance when power is supplied to an RL-load. The best 19 different voltage vectors were selected and applied to the inverter, even though there are 27 different switching combinations.

This chapter demonstrated the effectiveness of the SSI technique, as shown in the presented DCC case study. The SimCoupler Module enables MATLAB/Simulink users to implement and simulate power circuits in the original circuit form, greatly shortening the time required to set up and simulate a system that includes electronic circuits. The important step in the SSI technique is the time synchronization of the two independent software platforms used, in this case: PSIM and MATLAB/Simulink.

Minimization of the current and voltage errors in the cost function provides rapid dynamic response for the load current control, and guarantees the DC-link capacitor voltage balance. The two main advantages of using an FS-MPCC are firstly that there is no need for modulation of any kind, nor for a linear controller. Secondly, the designer has the option of adjusting the weighting factor, λ_{DC}, within the cost function, *g*; this permits manipulation of the relationship between the terms dedicated to reference tracking and those dedicated to voltage balancing in the DC-link.

The FS-MPCC algorithm was evaluated for four different cases using co-simulation results. Firstly, the DC-link capacitor voltages were balanced. The control algorithm provided very good current tracking behaviour and the capacitor voltages were very well balanced with very little error. In the DCC, the balancing of the DC-link capacitor voltages was achieved by setting $\lambda_{DC} = 0.02$. The selected weighting factor provided the best performance in balancing the DC-link capacitor voltages, excellent current reference tracking and the lowest harmonics content in the load current.

Secondly, the robustness of the control strategy under variable DC-link voltages was assessed in terms of the THD. The results showed that the predictive control method has the ability to track sinusoidal reference currents and perform excellent tracking behaviour with all DC-link voltage values.

Thirdly, the control algorithm was tested with reference currents representing a sinusoidal waveform (with and without a step change), a constant steps waveform and a square waveform in orthogonal coordinates. Results showed that the predictive control algorithm has a fast dynamic response and gives excellent tracking behaviour with inherent decoupling between i_α and i_β currents.

Lastly, the performance of the proposed control algorithm was assessed by mismatching selected, corresponding parameters of the model and the actual system.

These final results showed that the FS-MPCC strategy gives very good performance under these conditions, and all the assessments revealed that the FS-MPCC has flexibility under these conditions.
The FS-MPCC strategy as applied in this research demonstrated how powerful the tool is when compared to the conventional method of using modulation techniques. This concept can be extended to any power converter system.

Chapter five presented the FS-MPCC strategy as used in RESs applications with one- and two-step prediction times to control the three-level FCC. The RES model was used in this study to investigate the system performance when power is supplied to an RL-load. The best 19 different voltage vectors were selected and applied to the inverter.
This chapter demonstrated the effectiveness of the SSI technique as was shown in the presented FCC case study as well as the time synchronization of the two independent software platforms. The SimCoupler Module enables MATLAB/Simulink users to implement and simulate power circuits in the original circuit form, thus, greatly shortening the time to set up and simulate a system that includes electronic circuits.
The minimization of the current and capacitor voltage errors in the cost function provides a fast dynamic response for the load current control and guarantees balanced flying capacitor voltages. An FS-MPCC affords the designer the opportunity of adjusting the weighting factor λ_{DC}, thus, influencing the relationship within the cost function, *g*, between the reference tracking term and voltage balancing term. A hysteresis-based voltage balancing algorithm was developed and presented; this algorithm, applied to flying capacitors, ensures that the voltages are kept within the limits of their reference values.
The FS-MPCC algorithm was tested by co-simulation; three different conditions were imposed, and the effect of each condition was evaluated by the resulting deviations in terms of reference current tracking and balancing of flying capacitor voltages.
Firstly, the robustness of the control strategy under a variable DC-link voltage was assessed in terms of the THD. These results showed that the predictive control method has the ability to track sinusoidal reference currents and showed excellent tracking behaviour with all DC-link voltage values. Furthermore, the capacitor voltages were very well balanced with an insignificant error.
Secondly, the tracking of the sinusoidal waveform reference current and step changes in the amplitude of the reference current were investigated. The control algorithm was also tested with different reference current waveforms: a square waveform in orthogonal coordinates, constant reference steps and a sawtooth waveform. The results showed that the algorithm exhibits excellent tracking behaviour

and a fast dynamic response with inherent decoupling between i_α and i_β at the step changes. Moreover, based on predictive control, the hysteresis voltage balancing algorithm was able to keep the flying capacitor voltages within the bounds of their reference values. Lastly, the performance of the proposed control was assessed by a mismatch of corresponding, selected parameters of the model and the actual system. The results demonstrated that the FS-MPCC strategy gives very good performance under these conditions. All the assessments showed that the FS-MPCC has flexibility under these conditions.

The FS-MPCC strategy applied in the research demonstrated how powerful the tool is as compared to the conventional method of using modulation techniques. This concept can be extended to any power converter system, and the hysteresis-based voltage balancing algorithm ensures that the flying capacitor voltages are kept within the hysteresis band.

This thesis has contributed a novel approach by using the FS-MPCC and hysteresis based on MPC in a single cost function to control a power electronics converter. The technical and theoretical issues regarding the use of the FS-MPCC in power electronics have been thoroughly explored and improved upon. The study illustrated and provided a benchmark on how to implement predictive control techniques to improve the performance in some classes of power converters; these improvements relate to power quality and dynamic response. This implementation has huge benefits to future micro-power generation and improved efficiency in power electronic drives and electronic vehicle developments. In particular, two algorithms have been developed. The purpose of the first algorithm is to reduce the calculation effort for the MPC and to increase the prediction horizon, making longer prediction horizons possible. The second algorithm balances the DC-link capacitor voltages in the DCC and flying capacitor voltages in the FCC; this algorithm keeps the DC-link capacitor voltages and flying capacitor voltages within the hysteresis band.

These two algorithms, operating together in one cost function, offer the following contributions to the research area:

1. It is in fact, the use of FS-MPCC which affords the possibility not to use the PWM circuits.
2. They can be applied to different kinds of MLIs and, thus, to a wide variety of power electronic circuit applications.
3. They are suitable for any type of loads and, therefore, applicable to variable speed used in induction machines, as well as high-torque DC machines.
4. They are suitable for RESs applications and, thus, appropriate in UPS, Grid-Tie and Smart Grid applications.

5. They can be applied to different voltage levels without significantly changing the control circuit.
6. The designer has the freedom of adjusting the weighting factor λ_{DC}.

6.2 Further work and recommendations

The results of this thesis have the potential to be extended in several directions, namely: extension of the prediction horizon, estimating online RL-load values in the system, improving the selection of weighting factors and finding a general solution for multi-level and multi-phase systems. These issues are briefly discussed below.

Extending prediction horizon:

It is well known that choosing longer prediction horizons, in general, gives better closed-loop performance than when shorter ones are chosen. Unfortunately, to find the optimal input sequence for an FS-MPCC requires the solution of a complex optimization problem; this limits the use of longer horizons in practical applications.

To overcome this shortcoming, it would be useful if a suboptimal solution based on the stability results presented in this thesis could be found. Therefore, one can develop more efficient algorithms that would allow the use of longer horizons in solving the optimization problem.

Estimation of online RL-load values in the system:

The effect of mismatched parameter values in the RL-load resulted in increased THD. To further improve the quality of the output currents, online estimation of the RL-load parameters is suggested. Such an online estimation system provides the parameters of the connected load for updating the model.

Weighting factors design:

Another key element in the performance of the resulting closed-loop system is the selection of suitable weighting factors. Unfortunately, there are no analytical methods, numerical methods or control design theories available for adjusting these parameters, and currently they are determined by trial-and-error procedures. Although this limitation has not hindered MPC from being used productively in several power converters, it could be beneficial if an accurate analytical procedure could be found; deriving some basic procedures would reduce the uncertainty and improve the efficiency of the final-adjustment stage.

A general solution for multi-level and multi-phase systems:

There is an exponential increase in the number of possible switching states when the number of levels and/or phases increases—this directly impacts on the number of permitted states. To solve the optimization problem without substantially increasing the number of the calculations, a better algorithm needs to be developed.

And last but not the least, some important aspects of MPC for power electronic converters can be further investigated. For instance, prediction equations for higher order systems and loss mechanisms such as the switching losses can be implemented in the cost function to optimize the control of the converter.

REFERENCES

Aaltonen, M., Tiitinen, P., Lalu, J. & Heikkila, S. 1995. Direct Torque Control of Three-Phase Drives, *ABB Technik*, No. 3, 1995, pp. 19–24.

Abu-Rub, H., Guzinski, J., Krzeminski, Z. & Toliyat, H. A. 2004. Predictive current control of voltage source inverters, *IEEE Trans. on Ind. Electron.*, vol. 51 no. 3, pp. 585–593.

Agelidis, V. G. Calais, M. 1998. Application Specific Harmonic Performance Evaluation of Multicarrier PWM Techniques. *IEEE PESC*, 1998, pp. 172–178.

Aguilera, R., Quevedo, D. & Lezana, P. 2010. Predictive control of an asymmetric multicell converter with floating cells, in *Proc. IEEE Int Ind. Electron. (ISIE) Symp.*, 2010, pp. 3165–3170.

Alepuz, S., Busquets-Monge, S., Bordonau, J., Cortés, P. & Kouro, S. 2009. Control methods for low voltage ride-through compliance in grid-connected NPC converter based wind power systems using predictive control, in *Proc. IEEE Energy Convers. Congr. Exposition, 2009. ECCE 2009*, pp. 363–369.

Alepuz, S., Busquets-Monge, S., Bordonau, J., Gago, J., González, D. & Balcells, J. 2006. Interfacing renewable energy sources to the utility grid using a three-level inverter. *IEEE Transactions on Industrial Electronics,* 53 (5), pp. 1504–1511.

Almaktoof A. M., Raji A. K., & Kahn M. T. 2014. Finite-Set Model Predictive Control and DC-Link Capacitor Voltages Balancing for Three-Level NPC Inverters, Proceeding of the *16th International Power Electronics and Motion Control Conference and Exposition (PEMC 2014),* pp. 305–310, on 21–24 September, 2014, Antalya-Turkey.

Almaktoof, A. M., Raji, A. K. Kahn, M. T. E. 2014. Finite Set-Model Predictive Current control of three-phase voltage source inverter for Renewable Energy Systems (RES) applications, *Journal of Energy and Power Engineering*, USA, 8 (2014), pp. 748–755.

Almaktoof, A. M., Raji, A., & Kahn, M. T. 2013. Performance Evaluation and Improvement of an FS-MPC for Two-Level VSI, in *Proceeding of the International Conference on Electrical and Electronics Engineering, Clean Energy and Green Computing (EEECEGC 2013),* United Arab Emirates, pp. 120–126. December 11–13, 2013.

Alonso, O., Sanchis, P., Gubia, E. & Marroyo, L. 2003. Cascaded H-bridge Multilevel Converter for Grid Connected Photovoltaic Generators with Independent Maximum Power Point Tracking of each Solar Array, *IEEE Power Electronics Specialist Conference*, 15–19 June 2003, pp. 731–735.

Antoniewicz, P. & Kazmierkowski, M. P. 2008. Virtual-flux-based predictive direct power control of AC/DC converters with online inductance estimation, *IEEE Trans. Ind. Electron.*, vol. 55, no. 12, pp. 4381–4390.

Antoniewicz, P., Kazmierkowski, M. P., Aurtenechea, S. & Rodríguez, M. A. 2007. Comparative study of two predictive direct power control algorithms for three-phase AC/DC converters, in *Proc. Eur. Conf. Power Electron. Applicat.*, 2007, pp. 1–10.

Antwerp, J. G. V. & Braatz, R. D. 2000. Model predictive control of large scale processes, *in Proc. Control*, vol. 10, no. 1, pp. 1–8.

Arahal, M., Barrero, F., Toral, S., Duran, M. & Gregor, R. 2009. Multi-phase current control using finite-state model-predictive control, *Control Engineering Practice*, vol. 17, no. 5, pp. 579–587.

Asher, G.M., Sumner, M., Cupertino, F. & Lattanzi, A. 2001. Direct Flux Control of Induction Motor Drives, *European Conference on Power Electronics and Applications EPE 2001*, Graz, 2001.

Barrero, F., Arahal, M., Gregor, R., Toral, S. & Duran, M. 2009. A proof of concept study of predictive current control for VSI-driven asymmetrical dual three-phase AC machines, *IEEE Transactions on Industrial Electronics*, vol. 56, no. 6, pp. 1937–1954.

Bendre, A. Venkataramanan, G. Rosene, D. and Srinivasan, V. 2006. Modeling and design of a neutral-point voltage regulator for a three-level diode-clamped inverter using multiple-carrier modulation, *IEEE Trans. Ind. Electron*., 53 (3), pp. 718–726.

Blaabjerg, F., Teodorescu, R., Liserre, M. & Timbus, A. V. 2006. Overview of control and grid synchronization for distributed power generation systems, *IEEE Transactions on Industrial Electronics*, vol. 53, no. 5, pp. 1398–1409.

Boscaino, V. & Capponi, G. 2011. High Accuracy Modelling of Hybrid Power Supplies, MATLAB for Engineers - Applications in Control, Electrical Engineering, IT and Robotics, Dr. Karel Perutka (Ed.), ISBN: 978-953-307-914-1, InTech, Available from: http://cdn.intechopen.com/pdfs-wm/21224.pdf.

Bose B.K., (editor). 1997. *Power Electronics Variable Frequency Drives*, IEEE Press, New York, 1997, pp.400–453.

Bose, B. 2009. Power Electronics and Motor Drives Recent Progress and Perspective. *Industrial Electronics, IEEE Transactions on*, vol. 56, no. 2, pp. 581–588, 2009.

Bose, B. K. 2000. Fuzzy logic and neural networks in power electronics and drives. *Industry Applications Magazine, IEEE*, vol. 6, no. 3, pp. 57–63, 2000.

Bose, B. K. 2007. Neural Network Applications in Power Electronics and Motor Drives-An Introduction and Perspective. *Industrial Electronics, IEEE Transactions on*, vol. 54, no. 1, pp. 14–33, 2007.

Bueno, E.J., Cobreces, S., Rodríguez, F.J., Hernandez, A. & Espinosa, F. 2008. Design of a back-to-back NPC converter interface for wind turbines with squirrel-cage induction generator, *IEEE Trans. on Energy Conversion*, Vol. 23 No.3, pp.932–45.

Bum-Seok, S., Sinha G., Manjrekar, M. & Lipo, T., 1998. Multilevel Power Conversion - An Overview Of Topologies And Modulation Strategies, *Proceedings Of The 6th International Conference on Optimization of Electrical and Electronic Equipments*, vol. 2, pp. 11–24, May 1998.

Buso, S., Fasolo, S. & Mattavelli, P. 2001. Uninterruptible power supply multi-loop control employing digital predictive voltage and current regulators, *in IEEE Transactions on Industry Applications*, vol. 37, no. 6, pp. 1846–1854.

Busquets-Monge, S., Rocabert, J. Rodríguez, P. Alepuz, S. & Bordonau, J. 2008. Multilevel diode-clamped converter for photovoltaic generators with independent voltage control of each solar array. *IEEE Transactions on Industrial Electronics*, vol 55, no. 7, pp. 2713–2723.

Camacho, E. F. & Bordons, C. 1999. *Model Predictive Control*. NY: Springer-Verlag, 1999.

Carrara, G. Casini, D. Gardella, S. Salutari, R. 1993. Optimal PWM for the Control of Multilevel Voltage Source Inverter. *Fifth Annual European Conference on Power Electronics*, vol. 4, 1993, pp. 255–259.

Carrara, G. Gardella, S. Marchesoni, M. Salutari, R. Sciutto, G. 1992. A New Multilevel PWM Method: A Theoretical Analysis. *IEEE Trans. Power Electronics*, vol. 7, no. 3, July 1992, pp. 497–505.

Carrasco, J.M., Franquelo, L.G, Bialasiewicz, J.T., Galvan, E., PortilloGuisado, R.C., Prats, M.A.M., Leon, J.I. & Moreno-Alfonso N. 2006. Power-Electronic Systems for the Grid Integration of Renewable Energy Sources: A Survey. *IEEE Trans. on Industrial Electronics*, vol. 53, no. 4, pp. 1002–1016.

Catucci, M., Clare, J. & Wheeler, P. 2005. Predictive control strategies for ZCS direct converter HV power supply, *in European Conference on Power Electronics and Applications*, Sep. 2005.

Catucci, M., Clare, J. & Wheeler, P. 2006. Predective control strategy for ZCS single stage resonant converter, *in IEEE Annual Conference on Industrial Electronics*, Nov. 2006, pp. 2905–2910.

Celanovic, N., & Boroyevich, D. 2001. A fast space-vector modulation algorithm for multilevel three-phase converters, *IEEE Transactions on Industry Applications*, 37 (2), pp. 637–641.

Celanovic, N., & Boroyevich, D. 2001. A fast space-vector modulation algorithm for multilevel three-phase converters, *IEEE Transactions on Industry Applications*, 37 (2), pp. 637–641.

Cengelci, E., Sulistijo, S. U., Woom, B. O., Enjeti, P., Teodorescu, R. & Blaabjerg, F. 1998. A New Medium Voltage PWM Inverter Topology for Adjustable Speed Drives, in *Conf. Rec. IEEE-IAS Annu. Meeting*, St. Louis, MO, Oct. 1998, pp. 1416–1423.

Chen, J., Prodic, A., Erickson, R. & Maksimovic, D. 2003. Predictive digital current programmed control, *in IEEE Transactions on Power Electronics*, vol. 18, no. 1, pp. 411–419.

Chen, Y. Mwinyiwiwa, B. Wolanski, Z. Ooi, B. 1997. Regulating and Equalizing DC Capacitance Voltages in Multilevel STATCOM. *IEEE Trans. Power Delivery*, vol. 12, no. 2, April 1997, pp. 901–907.

Chen, Y., Mwinyiwiwa, B., Wolanski, Z. & Ooi, B. 1997(a). Unified Power Flow Controller (UPFC) Based on Chopper Stabilized Multilevel Converter, *IEEE Power Electronics Specialists Conference*, 1997, pp. 331–337.

Chiasson, J.N., Tolbert, L.M., McKenzie, K.J. & Zhong D. 2005. Elimination of harmonics in a multilevel converter using the theory of symmetric polynomials and resultants, *IEEE Transactions on Control Systems Technology*, Volume 13, Issue 2, Mar 2005 pp. 216–223.

Choi, N. S. Cho, G. C. Cho, G. H. 1993. Modeling and Analysis of a Static Var Compensator Using Multilevel Voltage Source Inverter. *IEEE IAS Annual Meeting*, 1993, pp. 901–908.

Choi, N. S. Cho, J. G. Cho, G. H. 1991. A General Circuit Topology of Multilevel Inverter. *IEEE PESC,* 1991, pp. 96–103.

Clarke, D. W., Mohtadi, C. & Tuffs, P. S. 1987. Generalized Predictive Control—Part I. The Basic Algorithm, *Automatica*, Vol. 23, No. 2, 1987, pp. 137–148.

Clos, G. Schindele, L. Franke, T. and Gartner. S. 2005. Simple direct capacitor voltage balancing of a flying capacitor converter. European Conference on Power Electronics and Applications (EPE 2005), pp. 11–14, September 2005.

Correa, P., Pacas, M. & Rodríguez, J. 2007. Predictive torque control for inverter-fed induction machines, *in IEEE Transactions on Industrial Electronics*, vol. 54, no. 2, pp. 1073–1079.

Correa, P., Rodríguez, J., Lizama, I. & D.Andler, 2009. A predictive control scheme for current-source rectifiers, *IEEE Trans. Ind. Electron.*, vol. 56, no. 5, pp. 1813–1815.

Cortés, P., Kazmierkowski, M., Kennel, R., Quevedo, D. & Rodríguez, J. 2008. Predictive control in power electronics and drives, *in IEEE Transactions on Industrial Electronics*, vol. 55, no. 12, pp. 4312–4324.

Cortés, P., Ortiz, G., Yuz J. I., et al., 2009. Model predictive control of an inverter with output LC filter for UPS applications, *IEEE Transactions on Industrial Electronics*, vol. 56, no. 6, pp. 1875–1883.

Cortés, P., Rodríguez, J., Antoniewicz, P. & Kazmierkowski, M. 2008(a). Direct power control of an AFE using predictive control, *IEEE Transactions on Power Electronics*, vol. 23, no. 5, pp. 2516–2523.

Cortés, P., Rodríguez, J., Quevedo, D. E. & Silva, C. 2008(b). Predictive current control strategy with imposed load current spectrum, *IEEE Transactions on Power Electronics*, vol. 23, no. 2, pp. 612–618.

Cortés, P., Rodríguez, J., Silva, C. & Flores, A. 2012. Delay compensation in model predictive current control of a three-phase inverter, *IEEE Trans. Ind. Electron.*, vol. 59, no. 2, pp. 1323–1325.

Cortés, P., Vattuone, L., Rodríguez, J. & Duran, M. 2009(a). A method of predictive current control with reduced number of calculations for five-phase voltage source inverters, *in 35th IEEE Annual Conference on Electronics IECON '09*, November 2009, pp. 53–58.

D. W. Clarke, C. Mohtadi, P. S. Tuffs, Generalized Predictive Control— Part II. Extensions and Interpretations, Automatica, Vol. 23, No. 2, 1987, pp. 149–160.

Dang, H., Wheeler, P. & Clare, J. 2006. A control analysis and implementation of high voltage, high frequency direct power converter, *in IEEE Annual Conference on Industrial Electronics*, Nov. 2006, pp. 2096–2102.

Defay F., Llor A. M., & Fadel M. 2010. Direct Control Strategy for a Four-Level Three-Phase Flying-Capacitor Inverter, *Industrial Electronics, IEEE Transactions on*, vol. 57, no. 7, pp. 2240–2248.

Defay, F. Llor, A. M. & Fadel, M. 2008. A predictive control with flying capacitor balancing of a multicell active power filter, *IEEE Trans. Ind. Electron.*, vol. 55, no. 9, pp. 3212–3220.

Depenbrock, M. 1985. Direct Self Control for Inverter Supplied High Dynamic AC Drives, *etzArchiv*, Vol. 7, 1985, pp. 211–218.

Depenbrock, M. 1988. Direct self-control (DSC) of inverter-fed induction machine, *in IEEE Transactions on Power Electronics*, vol. 3, no. 4, pp. 420–429.

Ding, K., Zou, Y., Wang, Z., Wu, Z. & Zhang, Y. 2004. A novel hybrid diode-clamp cascade multilevel converter for high power application; Industry Applications Conference, *39th IAS Annual Meeting. Conference Record of the 2004 IEEE*, Volume 2, 3–7 Oct. 2004, pp. 820–827 vol.2.

Du, Z., Tolbert, L.M. & Chiasson, J.N. 2006. Active Harmonic Elimination for Multilevel Converters, *IEEE Transactions on Power Electronics,* Volume 21, Issue 2, pp. 459–469.

Duran, M. J., Prieto, J., Barrero, F. & Toral, S. 2011. Predictive current control of dual three-phase drives using restrained search techniques, *IEEE Transactions on Industrial Electronics*, vol. 58, no. 8, pp. 3253–3263.

Eaton, J. W. & Rawlings, J. B. 1992. Model-predictive control of chemical processes, *in Chemical Engineering Science*, vol. 47, no. 4, pp. 705–720.

Emeljanov, S.V. 1969. Automatic Control Systems with Variable Structure, Munich, Vienna: R. Oldenbourg Verlag, 1969.

Enslin, J. H. R., Zhao, J. & Spee, R. 1996. Operation of the Unified Power Flow Controller as Harmonic Isolator, *IEEE Transactions on Power Electronics*, vol. 11, no. 6, pp. 776–784.

Escalante M. F., Vannier J. C., & Arzande A. 2002. Flying capacitor multilevel inverters and DTC motor drive applications, *Industrial Electronics, IEEE Transactions on*, vol. 49, no. 4, pp. 809–815.

Fazel S. S., Bernet S., Krug D., & Jalili K. 2007. Design and comparison of 4-kV neutral-point-clamped, flying capacitor, and series-connected H-bridge multilevel converters, *Industry Applications, IEEE Transactions on*, vol. 43, no. 4, pp. 1032–1040.

Feng, C. Liang, J. and Agelidis, V. G. 2007. Modified Phase-Shifted PWM Control for Flying Capacitor Multilevel Converters. *IEEE Transactions on Power Electronics*, 22(1), pp. 178–185.

Flach, E. 1999. Direct Control of the Mean Torque Value of an Induction Machine, Dissertation, Darmstadt: Technical University Darmstadt, 1999.

Fracchia, M. Ghiara, T. Marchesoni, M. Mazzucchelli, M. 1992. Optimized Modulation Techniques for the Generalized N-Level Converter. *IEEE PESC*, 1992, pp. 1205–1213.

Franquelo, L. G., Rodríguez, Leon, J., Kouro, J. I. S., Portillo, R. & Prats, M. A. M. 2008. The age of multilevel converters arrives, *IEEE Industrial Electronics Magazine*, vol. 2(2), pp. 28–39.

Fujita, H. & Akagi, H. 1998. The Unified Power Quality Conditioner: The Integration of Series- and Shunt-Active Filters, *IEEE Transactions on Power Electronics*, vol. 13, no. 2, pp. 315–322.

Fujita, H., Watanabe, Y. & Akagi, H. 1998. Control and Analysis of a Unified Power Flow Controller, *IEEE Power Electronics Specialists Conference*, 1998, pp. 805–811.

Gamboa, P., Silva, J. F., Pinto, S. F. & Margato, E. 2009. Predictive optimal matrix converter control for a dynamic voltage restorer with flywheel energy storage, in *Proc. 35th Annu. Conf. IEEE Ind. Electron. IECON '09*, 2009, pp. 759–764.

Garcia, C., Prett, D. & Morari, M. 1989. Model predictvie control: Theory and practice-a survey, *in Automatica*, pp. 335–348.

Geyer, T. 2011. A Comparison of Control and Modulation Schemes for Medium-Voltage Drives: Emerging Predictive Control Concepts Versus PWM-Based Schemes. *Industry Applications, IEEE Transactions on*, vol. 47, no. 3, pp. 1380–1389.

Geyer, T. Papafotiou, G. & Morari, M. 2009. Model Predictive Direct Torque Control–Part I: Concept, Algorithm, and Analysis. *IEEE Transactions on Industrial Electronics*, vol. 56, no. 6, pp. 1894–1905, June 2009.

Geyer, T., Papafotiou, G., Frasca, R. & Morari, M. 2008. Constrained optimal control of the step-down DC-DC converter, *IEEE Trans. Power Electron.*, vol. 23, no. 5, pp. 2454–2464.

Ghias, A.M.Y.M. Pou, J. Ciobotaru, M. Agelidis, V.G. 2012. Voltage balancing strategy for a five-level flying capacitor converter using phase disposition PWM with sawtooth-shaped carriers. *IECON 2012 - 38th Annual Conference on IEEE Industrial Electronics Society,* pp. 5013–5019

Goodwin, G. C., Seron, M. M. & Dona, J. A. D. 2005. *Constrained Control and Estimation – An Optimization Perspective*. Springer Verlag, 2005.

Grzesiak, L. & Tomasik, J. 2007. Novel DC link balancing scheme in generic n-level back-to-back converter system, *in International Conference on Power Electronics*, Oct. 2007, pp. 1044–1049.

Gyugyi, L. 1994. Dynamic Compensation of AC Transmission Lines by Solid-State Synchronous Voltage Sources, *IEEE Transactions on Power Delivery*, vol. 9, no. 2, pp. 904–911.

Gyugyi, L., Schauder, C. D., Williams, S. L., Reitman, T. R., Torgerson, D. R. & Edris, A. 1995. The Unified Power Flow Controller: A New Approach to Power Transmission Control, IEEE *Transactions on Power Delivery*, vol. 10, no. 2, pp. 1085–1093.

Hill, W. A. & Harbourt, C. D. 1999. Performance of Medium Voltage Multilevel Converters, in *Conf. Rec. IEEE-IAS Annu. Meeting*, Oct. 1999, Phoenix, AZ, pp. 1186–1192.

Holmes, G., & Lipo, T. 2003. *Pulse width modulation for power converters: Principles and practice*, IEEE Press Series on Power Engineering, Wiley-Inter science.

Holtz, J. & Schwellenberg, U. 1982. A new Fast-Response Current Control Scheme for Line Controlled Converters, *International Semiconductor Power Converter Conference*, pp. 175–183, Orlando, 1982.

Holtz, J. & Stadtfeld, S. 1983. A Predictive Controller for the Stator Current Vector of AC-Machines fed from a Switched Voltage Source, *International Power Electronics Conference IPEC*, Vol. 2, pp. 1665–1675, Tokio.

Holtz, J. 1994. Pulsewidth modulation for electronic power conversion, *in Proceedings of the IEEE*, vol. 82, no. 8, Aug. 1994, pp. 1194–1214.

Holtz, J. 2011. Power Electronics-A Continuing Challenge. *Industrial Electronics Magazine, IEEE*, vol. 5, no. 2, pp. 6–15, 2011.

Hotait H. A., Massoud A. M., Finney S. J., & Williams B. W. 2010. Capacitor voltage balancing using redundant states of space vector modulation for five-level diode clamped inverters, *Power Electronics, IET*, vol. 3, no. 2, pp. 292–313.

Huang, J. & Corzine, K. A. 2006. Extended operation of flying capacitor multilevel inverters, *IEEE Trans. Power Electron*., vol. 21(1), pp. 140 – 147, Jan. 2006.

Jeon, S. & Cho, G. 1997. A Series-Parallel Compensated Uninterruptible Power Supply with Sinusoidal Input Current and Sinusoidal Output Voltage, *IEEE Power Electronics Specialists Conference*, 1997, pp. 297–303.

Jeong, S.-G. & Woo, M.-H. 1997. DSP-based active power filter with predictive current control, *in IEEE Transactions on Industrial Electronic*, vol. 44, no. 3, pp. 329–336.

Jingang, H. Peng, Y. Liwei, Z. Xinyuan, T. Tianhao, T. 2007. Selective Harmonic Elimination for an Asymmetrical Multilevel Converter. *Industrial Electronics, 2007. ISIE 2007. IEEE International Symposium on*, vol., no., pp.993-997, on 4–7 June 2007.

Kamran, F. & Habetler, T. G. 1995. A Novel On-Line UPS with Universal Filtering Capabilities, *IEEE Power Electronics Specialists Conference*, 1995, pp. 500–506.

Kamran, F. & Habetler, T. G. 1998. Combined Deadbeat Control of a Series-Parallel Converter Combination Used as a Universal Power Filter, *IEEE Transactions on Power Electronics*, vol. 13, no. 1, pp. 160–168.

Kazmierkowski, M. P. Krishnan, R. and Blaabjerg, F. 2002. *Control in Power Electronics*. New York: Academic, 2002.

Kennel, R. & Schroeder, D. 1983. Predictive control strategy for converters, *Proc. of the third IFAC Symposium*, Lausanne, 1983, pp. 415 – 422, Lausanne.

Kennel, R. 1984. Pradiktives Fuhrungsverfahren fur Stromrichter (Predictive Control Strategy for Inverters), Dissertation, Kaiserslautern: Kaiserslautern University, 1984.

Kennel, R., Linder, A. & Linke, M. 2001. Generalized Predictive Control (GPC)—Ready for Use in Drive Applications?, *32nd IEEE Power Electronics Specialists Conference pesc2001*, Vol. 4, pp. 1839–1844, Vancouver.

Khazraei, M., Sepahvand, H., Corzine, K. & Ferdowsi. M. 2010. A generalized capacitor voltage balancing scheme for flying capacitor multilevel converters. *25th Annual IEEE Applied Power Electronics Conference and Exposition (APEC 2010),* pp. 58–62, February 2010.

Khazraei, M., Sepahvand, H., Corzine, K.A. & Ferdowsi. M. 2012. Active Capacitor Voltage Balancing in Single-Phase Flying-Capacitor Multilevel Power Converters. *IEEE Transactions on Industrial Electronics*, 59(2), pp. 769–778.

Kimura, N., Kouno, A., Morizan, T. & Taniguchi, K. 2002. Suppression of harmonics of multi-level converter applied for back-to-back HVDC link, Proceedings of the Power Conversion Conference. PCC Osaka 2002, Volume 3, on 2–5 April 2002,pp.1132–1137 vol.3.

Konstantinou, G. Ciobotaru, M. Agelidis, V. 2013. Selective harmonic elimination pulse-width modulation of modular multilevel converters. *Power Electronics, IET*, vol.6, no.1, pp.96–107, Jan. 2013.

Kouro, S. Cortés, P. Vargas, R. Ammann, U. and Rodríguez, J. 2009. Model Predictive Control A Simple and Powerful Method to Control Power Converters. *Industrial Electronics, IEEE Transactions on*, vol. 56, no. 6, pp. 1826–1838, Jun. 2009.

Kouro, S. Malinowski, M. Gopakumar, K. Pou, J. Franquelo, L. Wu, B. Rodríguez, J. Pérez, M. A. and Leon J. 2010. Recent Advances and Industrial Applications of Multilevel Converters. *Industrial Electronics, IEEE Transactions on*, vol. 57, no. 8, pp. 2553–2580.

Kukrer, O. 1996. Discrete-time current control of voltage-fed three-phase PWM inverters, *in IEEE Transactions on Power Electronics*, vol. 11, no. 2, pp. 260–269.

Lai J. S. & Peng F. Z. 2002. Multilevel converters-a new breed of power converters, *Industry Applications, IEEE Transactions on*, vol. 32, no. 3, pp. 509–517.

Lai, J. S. & Peng, F. Z. 1996. Multilevel Converters-A new breed of Power converters, *IEEE Transactions of Industry Applications,* Vol. 32, No. 3, pp. 509–517.

Lee, S. G. Kang, D. W. Lee Y. H. and Hyun, D. S. 2001. The Carrier-Based PWM method for Voltage Balancing of Flying Capacitor Multilevel Inverter. *IEEE Power Electron. Spec. Conf.*, vol. 1, pp. 126–131, 2001.

Le-Huy, H., Slimani, K. & Viarouge, P. 1994. Analysis and implementation of a realtime predictive current controller for permanent-magnet synchronous servo drives, *in IEEE Transactions on Industrial Electronics*, vol. 41, no. 1, pp. 110-117.

Lezana, P., Aguilera R., & Quevedo D. E. 2009. Model predictive control of an asymmetric flying capacitor converter, *Industrial Electronics, IEEE Transactions on*, vol. 56, no. 6, pp. 1839–1846.

Li, J., Zhuo, F., Wang, X., Wang, L., & Ni, S. 2009. A grid-connected PV system with power quality improvement based on boost + dual-level fourleg inverter, *in Proc. IEEE Int. Power Electron. and Motion Control Conf.*, Wuhan, China, pp. 436–440.

Lie, Xu. Agelidis, V.G. 2005. A VSC transmission system using flying capacitor multilevel converters and selective harmonic elimination PWM control. *Power Engineering Conference, 2005. IPEC 2005. The 7th International*, Vol. 2, pp.1176–1181, Nov. 29–Dec. 2 2005.

Linder, A. & Kennel, R. 2005. Model predictive control for electrical drives, *in IEEE Power Electronics Specialists Conference*, 2005, pp. 1793-1799.

Linder, A. 2005. Modellbasierte Prädiktivregelung in Der Antriebstechnik, Ph.D. dissertation, Wuppertal Univ., Wuppertal, Germany, 2005.

Linder, A., Kanchan, R., Kennel, R. & Stolze, P. 2010. *Model-Based Predictive Control of Electric Drives*. Cuvillier Verlag, Gottingen, 2010.

Liu, H. L. Cho, G. H. 1994. Three-Level Space Vector PWM in Low Index Modulation Region Avoiding Narrow Pulse Problem. *IEEE Trans. Power Electronics,* vol. 9, no. 5, Sept. 1994, pp. 481–486.

Lizama, I., Rodríguez, J., Wu, B., Correa, P., Rivera, M. & Perez, M. 2009. Predictive control for current source rectifiers operating at low switching frequency, in *Proc. IEEE 6th Int. Power Electron. Motion Control Conf. IPEMC '09*, 2009, pp. 1630–1633.

Lopez, O., Teodorescu, R. & Gandoy, JD. 2006. Multilevel Transformerless Topologies for Single-Phase Grid-Connected Converters. in *Proceedings of 32nd Annual Conference of the IEEE Industrial Electronics Society*. pp. 5191–5196.

Luo, F. L. &Hong, Y. 2013. Renewable Energy Systems: Advanced Conversion Technologies and Applications. Taylor & Francis Group, LLC. CRC Press is an imprint of Taylor & Francis Group, an Informal business. International Standard Book Number-13: 978-1-4398-9110-0.

Maciejowski, J. M. 2002. *Predictive Control with Constraints*. Englewood Cliffs, NJ: Prentice Hall, 2002.

Malesani, L., Mattavelli, P. & Buso, S. 1999. Robust dead-beat current control for PWM rectifiers and active filters, *in IEEE Transactions on Industry Applications*, vol. 35, no. 3, pp. 613–620.

Mariethoz, S., Almer, S., Baja, M., Beccuti, A. G., Patino, D., Wernrud, A., Buisson, J., Cormerais, H., Geyer, T., Fujioka, H., Jonsson, U. T., Kao, C.-Y., Morari, M., Papafotiou, G., Rantzer, A. & Riedinger, P. 2010. Comparison of hybrid control techniques for buck and boost DC-DC converters, *IEEE Trans. Contr. Syst. Tech.*, vol. 18, no. 5, pp. 1126–1145.

Mattavelli, P. 2005. An improved deadbeat control for UPS using disturbance observers, *in IEEE Transactions on Industrial Electronics*, vol. 52, no. 1, pp. 206–212.

Mayer, H. R. & Pfaff, G. 1985. Direct Control of Induction Motor Currents—Design and Experimental Results, *European Conference on Power Electronics and Applications EPE 1985*, Vol. 2, pp. 3.7–3.12, Brussel, 1985.

Mayne, D., Rawlings, J., Rao, C. & Scokaert, P. 2000. Constrained model predictive control: Optimality and stability, *in Automatica*, pp. 789–814.

McGrath B. P. & Holmes D. G. 2008. Analytical modelling of voltage balance dynamics for a flying capacitor multilevel converter, *Power Electronics, IEEE Transactions on*, vol. 23, no. 2, pp. 543–550.

McGrath, B. P., & Holmes, D. G. 2002. Multicarrier PWM strategies for multilevel inverters, *IEEE Transactions on Industrial Electronics*, 49 (4), pp. 858–867.

Menzies, R. W. & Zhuang, Y. 1995. Advanced Static Compensation Using a Multilevel GTO Thyristor Inverter. *IEEE Trans. Power Delivery*, April 1995, pp. 732–738.

Menzies, R. W. Steimer, P. Steinke, J. K. 1994. Five-Level GTO Inverters for Large Induction Motor Drives. *IEEE Trans. Industry Applications,* vol. 30, no. 4, July 1994, pp. 938–944.

Menzies, R. W. Steimer, P. Steinke, J. K. 1994. Five-Level GTO Inverters for Large Induction Motor Drives. *IEEE Trans. Industry Applications,* vol. 30, no. 4, July 1994, pp. 938–944.

Meynard, T., Fadel M., & Aouda N. 1997. Modeling of multilevel converters, *Industrial Electronics, IEEE Transactions on*, vol. 44, no. 3, pp. 356–364.

Meynard, T.A. & Foch, H. 1992. Multilevel conversion: High voltage choppers and voltage source inverters, *in IEEE PESC Conf. Rec*., 397–403.

Miranda, H., Cortés, P., Yuz, J. I. & Rodríguez, J. 2009. Predictive torque control of induction machines based on state-space models, *IEEE Transactions on Industrial Electronics*, vol. 56, no. 6, pp. 1916–1924.

Mohan, N. Undeland, T. M. and Robbins, W. P. 1995. *Power Electronics*, 2nd ed. Hoboken, NJ: Wiley, 1995.

Moran, L. & Joos, G. 1998. Principles of Active Power Filters, *IEEE Industry Applications Society Annual Meeting*, Oct. 1998, Tutorial Course Notes.

Mossoba, J. & Lehn, P. 2003. A controller architecture for high bandwidth active power filters, *in IEEE Transactions on Power Electronics*, vol. 18, no. 1, pp. 317–325.

Muller, S., Ammann, U. & Rees, S. 2005. New time-discrete modulation scheme for matrix converters, *in IEEE Transactions on Industrial Electronics*, vol. 52, no. 6, pp. 1607–1615.

Muthu, S. & Kim, J. M. S. 1997. Steady-State Operating Characteristics of Unified Active Power Filters, *IEEE Applied Power Electronics Conference*, 1997, pp. 199–205.

Mutschler, P. 1998. A new speed-control method for induction motors, *in Power Conversion Intelligent Motion*, pp. 131–136.

Myrzik, J. & Calais, M. 2003. String and module integrated inverters for single phase grid connected photovoltaic systems – a review. *Proceeding of IEEE Power Tech Conference Bologna*, June 23–26, vol. 2. 2003, Bologna.

Nabae, A., Takahashi, I. & Akagi. H. 1981. A new neutral-point-clamped PWM inverter, *IEEE Trans. Ind. Applicat*., IA (17), pp. 518–523.

Najmi, V., Ebrahimi, S. & Oraee, H. 2012. Output voltage quality intensification of diode clamped multilevel inverters using FM PWM technique, *Power Electronics and Drive Systems Technology (PEDSTC), 2012 3rd*, pp.98–102.

Nami A. & Zare F. 2009. Multilevel Converters in Renewable Energy Systems, Renewable Energy, T J Hammons (Ed.), ISBN: 978-953-7619-52-7, InTech, Available from: http://www.intechopen.com/books/renewable-energy/multilevel-converters-in-renewable-energy-systems.

Nami, A., Zare, F., Ledwich, G., Ghosh, A. & Blaabjerg, F. 2008. Comparison between Symmetrical and Asymmetrical Single Phase Multilevel Inverter with Diode-Clamped Topology. Proceeding in *39th IEEE Power Electronics Specialists Conference (PESC08)*, June 2008, pp. 2921–2926. Rhodes, Greece.

Nasiri, A. 2007. Digital control of three-phase series-parallel uninterruptible power supply systems, *in IEEE Transactions on Power Electronics*, vol. 22, no. 4, pp. 1116–1127.

Naumanen, V. Luukko, J. Silventoinen, P. Pyrho andnen, J. Sareandn, H. and Rauma K. 2010. Compensation of DC link voltage variation of a multilevel series-connected H-bridge inverter. IET Power Electronics, 3(5), pp. 793–803, September 2010.

Ohsato, M. H. Kimura, G. Shioya, M. 1991. Five-Stepped PWM Inverter Used in Photovoltaic Systems. *IEEE Trans. Industrial Electronics*, vol. 38, no. 5, Oct. 1991, pp. 393–397.

Pan, Z. & Peng, F. Z. 2009. A sinusoidal PWM method with voltage balancing capability for diode-clamped five-level converters, *in IEEE Transactions on Industry Applications*, vol. 45, no. 3, pp. 1028–1034.

Pan, Z., Peng, F. Z., Corzine, K., Stefanovic, V., Leuthen, J. & Gataric, S. 2005. Voltage balancing control of diode-clamped multilevel rectifier/inverter systems, *in IEEE Transactions on Industry Applications*, vol. 41, no. 6, pp. 1698–1706.

Peng, F. Z. 2001. A Generalized Multilevel Converter Topology with Self Voltage Balancing, *IEEE Transactions on Industry Applications*, vol. 37, Mar./Apr. 2001, pp. 611–618.

Peng, F. Z., Lai, J.-S., McKeever, J. & VanCoevering, J. 1995. A multilevel voltage-source converter system with balanced DC voltages, *in IEEE Power Electronics Specialists Conference*, vol. 2, Jun. 1995, pp. 1144–1150.

Peng, F.Z. & Lai, J.S. 1995. A multilevel voltage-source inverter with separate dc sources, *in Conf. Rec. IEEE/IAS Annu. Meeting*, 2541–2548, 1995.

Perantzakis, G., Xepapas, F. & Manias, S. 2005. Efficient predictive current control technique for multilevel voltage source inverters, *in European Conference on Power Electronics and Applications*, Sep. 2005.

Perantzakis, G., Xepapas, F., Papathanassiou, S. & Manias, S. 2005(a). A predictive current control technique for three-level NPC voltage source inverters, *in IEEE Power Electronics Specialists Conference*, Jun. 2005, pp. 1241–1246.

Pérez, M., Lizana, R. & Rodríguez, J. 2011. Predictive control of DC-link voltage in an active-front-end rectifier, in *Proc. IEEE Int Ind. Electron. (ISIE) Symp.*, 2011, pp. 1811–1816.

Pérez, M., Rodríguez, J. & Coccia, A. 2009. Predictive current control in a single phase PFC boost rectifier, in *Proc. IEEE Int. Conf. Ind. Technol. ICIT 2009*, 2009, pp. 1–6.

Pérez, M., Rodríguez, J., Fuentes, E. & Kammerer, F. 2012. Predictive control of AC-AC modular multilevel converters, *IEEE Trans. Ind. Electron.*, vol. 59, no. 7, p. 28–39.

Peyrl, H., Papafotiou, G. & Morari, M. 2009. Model predictive torque control of a switched reluctance motor, in *Proc. 2009 IEEE Int. Conf. Ind. Technol.*, Feb. 2009, pp. 1–6.

PSIM Software, “Tutorial on How to Use the SimCoupler Module”. Powersim Inc. April 2006. www.psim-europe.com/openload2.php?doc=tutorialSimcoupler.pdf. [30 March 2014].

PSIM® User’s Guide, Powersim Inc., PSIM 9.3, June 2014.

PSPICE, *Microsim Reference Manual*, Version 7.1, October 1996.

Pulikanti, S. R. Muttaqi K. & Suntanto, D. 2012. Control of five-level flying capacitor based active-neutral-pointclamped converter for grid connected wind energy applications, *in Industry Applications Society Annual Meeting (IAS),* 2012 IEEE, 2012, pp. 1–9.

Purcell, A. & Acarnley, P.P. 1998. Multilevel hysteresis comparator forms for direct torque control schemes, Electronic Letters, Vol. 34, No. 6, 1998, pp. 601–603.

Raviraj, V. & Sen, P. 1997. Comparative study of proportional-integral, sliding mode, and fuzzy logic controllers for power converters. *Industry Applications, IEEE Transactions on*, vol. 33, no. 2, pp. 518–524.

Richardeau, F. Baudesson, P. & Meynard, T. A. 2002. Failures-tolerance and remedial strategies of a PWM multicell inverter, *IEEE Transactions on Power Electronics*, vol. 17, no. 6, pp. 905–912.

Rivera, M., Elizondo, J. L., Macias, M. E., Probst, O. M., Micheloud, O. M., Rodríguez, J., Rojas, C. & Wilson, A. 2010. Model predictive control of a doubly fed induction generator with an indirect matrix converter, in *Proc. IECON 2010—36th Annu. Conf. IEEE Ind. Electron. Soc.*, 2010, pp. 2959–2965.

Rivera, M., Rodríguez, J., Espinoza, J. & Abu-Rub, H. 2012. Instantaneous reactive power minimization and current control for an indirect matrix converter under a distorted AC-supply, *IEEE Trans. Ind. Inf.*, vol. 8, no. 3, pp. 482–490.

Rivera, M., Rojas, C., Rodríguez, J., Wheeler, P., Wu, B. & Espinoza, J. 2011. Predictive current control with input filter resonance mitigation for a direct matrix converter, *IEEE Trans. Power Electron.*, vol. 26 , no. 10, pp. 2794 - 2803.

Rodríguez, J. & Cortés, C. 2012. *Predictive control of Power Converters and Electrical Drives,* (UK: A Johan Wiley & Sons, Ltd., 2012).

Rodríguez, J., Lai, J. S. & Peng, F. Z. 2002. Multilevel Inverters: Survey of Topologies, Controls, and Applications, *IEEE Transactions on Industry Applications*, vol. 49, no. 4, Aug. 2002, pp. 724–738.

Rodríguez, J., Pontt, J. Silva, C. A., Correa, P. Lezana, P., Cortés, P. & Ammann, U. 2007. Predictive current control of a voltage source inverter, *in IEEE Transactions on Industrial Electronics*, vol. 54, no. 1, Feb. 2007, pp. 495–503.

Rodríguez, J., Pontt, J. Silva, C., Cortés, P., Rees, S. & U. Ammann, 2004. Predictive direct torque control of an induction machine, in *Proc. Power Electron. Motion Control Conf.*, Sep. 2–4, 2004, Riga, Latvia,

Rodríguez, J., Pontt, J., Correa, P., Lezana, P. & P. Cortés, 2005. Predictive power control of an AC/DC/AC converter, *in Conference Record of the Industry Applications Conference*, vol. 2, Oct. 2005, pp. 934–939.

Rodríguez, J., Pontt, J., Silva, C., Salgado, M., Rees, S., Ammann, U., Lezana, P., Huerta, R. & Cortés, P. 2004(a). Predictive control of three-phase inverter, *in Electronics Letters*, vol. 40, no. 9, pp. 561–563.

Rossiter, J. 2003. Model-based Predictive Control: A Practical Approach. United States of America: CRC Press, 2003.

Ruderman, A. & Reznikov, B. 2009. Five-level single-leg flying capacitor converter voltage balance dynamics analysis, in *Industrial Electronics, 2009. IECON '09. 35th Annual Conference of IEEE*, 2009, pp. 486–491.

Saggini, S., Stefanutti, W., Tedeschi, E. & Mattavelli, P. 2007. Digital deadbeat control tuning for DC-DC converters using error correlation, *in IEEE Transactions on Power Electronics*, vol. 22, no. 4, pp. 1566–1570.

sędłak, M., styński, S., Kaźmierkowski, M., P. & Malinowski, M. 2012. Three-level four-leg flying capacitor converter for renewable energy sources, Przegląd Elektrotechniczny, vol. 2012(12a), pp. 6–11, 2012.

Shakweh, Y. 2001. MV inverter stack topologies, *IEE Power Engineering Journal*, pp. 139–149.

Sharma, R. & Gao, H. 2006. A new dc-dc converter for fuel cell powered distributed residential power generation systems, *in Proc. IEEE APEC*, Mar. 2006, pp. 1014–1018.

Shukla, A., Ghosh, A. & Joshi, A. 2007. Capacitor voltage balancing schemes in flying capacitor multilevel inverters, *in IEEE Power Electronics Specialists Conference*, Jun. 2007, pp. 2367–2372.

Shukla, A., Ghosh, A. & Joshi, A. 2008. Improved multilevel hysteresis current regulation and capacitor voltage balancing schemes for flying capacitor multilevel inverter, *in IEEE Transactions on Power Electronics*, vol. 23, no. 2, pp. 518–529.

Siemens, 2012. Energy Sector 2012, Erlangen (Germany), www.siemens.com/energy [17 February 2014].

Silva, E., McGrath, B., Quevedo, D. & Goodwin, G. 2007. Predictive control of a flying capacitor converter, *in American Control Conference*, Jul. 2007, pp. 3763–3768.

Sinha, G. Lipo, T. A. 1996. A Four Level Rectifier-Inverter System for Drive Applications. *IEEE IAS Annual Meeting,* 1996, pp. 980–987.

Song, B. M. & Lai, J. S. 2001. A Multilevel Soft-switching Inverter with Inductor Coupling, *IEEE Transactions on Industry. Applications*, vol. 37, pp. 628–636.

Springob, L. & Holtz, J. 1998. High-bandwidth current control for torque-ripple compensation in PM synchronous machines, *in IEEE Transactions on Industrial Electronics*, vol. 45, no. 5, pp. 713–721.

Srikanthan, S. Mishra, M.K. and Rao. R.K.V. 2009. Improved hysteresis current control of three-level inverter for distribution static compensator application. IET Power Electronics, 2(5), pp. 517–526, September 2009.

Steinke, J. K. 1988. Control Strategy for a Three Phase AC Traction Drive with a 3-Level GTO PWM Inverter," *IEEE PESC*, pp. 431–438.

Stolze, P., du Toit, D., Tomlinson, M., Kennel, R. & Mouton, T. 2011. Model Predictive Control of a Flying Capacitor Converter with Output LC Filter for UPS Applications, IEEE Africon 2011 - The Falls Resort and Conference Centre, Sep. 2011.

Takahashi, I. & Noguchi, T. 1985. A New Quick Response and High Efficiency Control Strategy of an Induction Motor, *IEEE IAS Annual Meeting*, pp. 496–502, Toronto.

Takahashi, I. & Noguchi, T. 1986. A new quick-response and high-efficiency control strategy of an induction motor, *in IEEE Transactions on Industry Applications*, vol. IA-22, no. 5, pp. 820–827.

Tallam, R., Naik, R., & Nondahl, T. 2005. A carrier-based PWM scheme for neutral-point voltage balancing in three-level inverters, *IEEE Trans. Ind. Appl.*, 41 (6), pp. 1734–1743.

Tan, S. Lai, Y. and Tse, C. 2006. A unified approach to the design of PWM-based sliding-mode voltage controllers for basic DC-DC converters in continuous conduction mode. *Circuits and Systems I: Regular Papers, IEEE Transactions on*, vol. 53, no. 8, pp. 1816–1827, 2006.

Teodorescu, R., Blaabjerg, F., Pedersen, J.K., Cengelci, E., Sulistijo, S.U., Woo, B.W. & Enjeti, P. 1999. Multilevel converters - a survey, *Proceedings of EPE '99, 8th European Conference on Power Electronics and Applications*, 7–9 September 1999, CD-ROM paper.

Texas Instruments. Designer and supplier of digital signal processing solutions and semiconductor products, 1995. www.ti.com [10 February 2014].

Thielemans S., Ruderman A., Reznikov B. & Melkebeek J. A. A. 2010. Self-precharge for single-leg odd-level multilevel converter, in *Power Electronics, Machines and Drives (PEMD 2010), 5th IET International Conference on*. IET, 2010, pp. 1–6.

Thielemans, S. Ruderman, A. Reznikov, B. Melkebeek, J. 2012. Improved Natural Balancing With Modified Phase-Shifted PWM for Single-Leg Five-Level Flying-Capacitor Converters. *Power Electronics, IEEE Transactions on*, vol.27, no.4, pp.1658–1667, April 2012

Thielemans, S., Vyncke, T. J. & Melkebeek, J. A. A. 2011. Voltage quality analysis of a three-level flying capacitor inverter with model based predictive control, in *Proc. IEEE 8th Int Power Electron. ECCE Asia (ICPE and ECCE) Conf.*, 2011, pp. 124–131.

Tolbert, L. M. & Peng, F. Z. 2000. Multilevel Converters as a Utility Interface for Renewable Energy Systems, *IEEE Power Engineering Society Summer Meeting*, IEEE, Volume 2, 16–20 pp. 1271-1274. Seattle, Washington.

Townsend, C., Summers, T. & Betz, R. 2012. Multigoal heuristic model predictive control technique applied to a cascaded H-bridge statcom, *IEEE Trans. Power Electron.*, vol. 27, no. 3, pp. 1191–1200.

Trzynadlowski, A.M., Bech, M.M., Blaabjerg, F., Pedersen, J.K., 1999. An Integral Space-Vector PWM Technique for DSP-Controlled Voltage-Source Inverters, *IEEE Transactions on Industry Applications*, Vol. 35, No. 5, 1999, pp. 1091–1097.

Tsirukis, A. & Morari, M.1992.Controller design with actuator constraints, *in IEEE Conference on Decision and Control*, vol. 3, 1992, pp. 2623–2628.

Turpin, C., Baudesson, P., Richardeau, F., Forest, F. & Meynard, T. A. 2002. Fault management of multicell converters, *IEEE Transactions on Industrial Electronics*, vol. 49, no. 5, pp. 988–997.

van Zyl, A. Enslin, J. H. R. & Spee, R. 1996. A New Unified Approach to Power Quality Management, *IEEE Transactions on Power Electronics*, vol. 11, no. 5, pp. 691–697.

Vargas, R. Ammann, U. Rodríguez, J. & Pontt, J. 2008. Predictive strategy to control common-mode voltage in loads fed by matrix converters, *IEEE Transactions on Industrial Electronics*, vol. 55, no. 12, pp. 4372–4380.

Vargas, R., Ammann, U., Hudoffsky, B., Rodríguez, J. & Wheeler, P. 2010. Predictive torque control of an induction machine fed by amatrix converter with reactive input power control, *IEEE Trans. Power Electron.*, vol. 25, no. 6, pp. 1426–1438.

Vargas, R., Cortés, P., Ammann, U., Rodríguez, J. & Pontt, J. 2007. Predictive control of a three-phase neutral-point-clamped inverter, *in IEEE Transactions on Industrial Electronics*, vol. 54, no. 5, Oct. 2007, pp. 2697-2705.

Vargas, R., Rodríguez, J., Ammann, U. & Wheeler, P. W. 2008(a). Predictive current control of an induction machine fed by a matrix converter with reactive power control, *IEEE Transactions on Industrial Electronics*, vol. 55, no. 12, pp. 4362–4371.

Vassallo, J., Clare, J.C. & Wheeler, P.W. 2003. A power-equalized harmonic-elimination scheme for utility-connected cascaded H-bridge multilevel converters; Industrial Electronics Society, 2003. *IECON '03. The 29th Annual Conference of the IEEE*, Volume 2, 2-6 Nov. 2003, pp.1185–1190.

Vazquez, S. Montero, C. Bordons, C. Franquelo, L.G., 2011. Model predictive control of a VSI with long prediction horizon. *Industrial Electronics (ISIE), 2011 IEEE International Symposium on*, pp.1805–1810, 27–30 June 2011

Villegas, J., Vazquez, S., Carrasco, J. M. & Gil, I. 2010. Model predictive control of a switched reluctance machine using discrete space vector modulation, in *Proc. IEEE Int Ind. Electron. (ISIE) Symp.*, 2010, pp. 3139–3144.

Wilkinson, R. H., Meynard, T. A. & Mouton, H. 2006. Natural balance of multicell converters: The general case, *IEEE Transactions on Power Electronics*, vol. 21, pp. 1658–1666.

Xiaoming, Y. & Barbi, I. 2000. Fundamentals of a new diode clamping multilevel inverter, IEEE Transactions on Power Electronics, Volume 15, Issue 4, pp. 711–718.

Xilinx: The programmable logic company, 2014. www.xilinx.com [02 March 2014].

Yaramasu, V. Wu, B. Rivera, M. and Rodríguez, J. 2013. Predictive current control and DC-link capacitor voltages balancing for four-leg NPC inverters, Industrial Electronics (ISIE), *2013 IEEE International Symposium on*, Tehran, pp.1–6.

Yaramasu, V., Rivera, M., Wu, B. & Rodríguez, J. 2013(a). Model Predictive Current Control of Two-Level Four-Leg Inverters—Part I: Concept, Algorithm, and Simulation Analysis, *IEEE Transactions on Industrial Electronics,* vol. 28 no. 7. July 2013, pp. 3459–3468.

Zare, F. & Ledwich, G. 2008. A new predictive current control technique for multilevel converters. *Australian Journal of Electrical and Electronic Engineering*, 4(1), pp. 25–35.

Zhang, W., Feng, G. & Liu, Y. F. 2003. Analysis and implementation of a new PFC digital control method, *in Proc. IEEE PESC*, Acapulco, Mexico, 2003, pp. 335–340.

Zhiguo, P., Peng, F.Z., Stefanovic, V. & Leuthen, M. 2004. A diode-clamped multilevel converter with reduced number of clamping diodes; *Applied Power Electronics Conference and Exposition, 2004. APEC '04. Nineteenth Annual IEEE*, Volume 2, vol.2, pp. 820–824.

Zhong, D., Tolbert, L.M., Chiasson, J.N. & Hui L. 2005. Low switching frequency active harmonic elimination in multilevel converters with unequal DC voltages; Industry Applications Conference, 2005. Fourtieth IAS Annual Meeting. Conference Record of the 2005, Volume 1, 2–6 Oct. 2005 pp. 92–98.

Zill, D. & Cullen, M. 2000. *Advanced Engineering Mathematics*. Sudbury, Massachusetts: ones and Bartlett, 2000.

APPENDICES

Appendix A: Coordinate transformations

Appendix B: Switching states and voltage vectors

Appendix C: Total harmonic distortion factor

Appendix D: Modeling and co-simulation models

Appendix A: Coordinate transformations

For a three-phase system, the voltages and currents can be described in different reference frames, also called coordinate systems. In many applications it is useful to present the system model either in a static $\alpha\beta$ reference frame using the well-known Clarke transformation, or a rotating dq reference frame, using Park transformation. The relation between the Clarke's and Park's reference frames is depicted in Figure A.1.

Clarke direct $abc/\alpha\beta0$ and inverse $\alpha\beta0/abc$ transformations:

$$\begin{bmatrix} X_\alpha \\ X_\beta \\ X_0 \end{bmatrix} = \frac{2}{3}\begin{bmatrix} 1 & -\frac{1}{2} & -\frac{1}{2} \\ 0 & \frac{\sqrt{3}}{2} & -\frac{\sqrt{3}}{2} \\ \frac{1}{2} & \frac{1}{2} & \frac{1}{2} \end{bmatrix}.\begin{bmatrix} X_a \\ X_b \\ X_c \end{bmatrix} \tag{A.1}$$

$$\begin{bmatrix} X_a \\ X_b \\ X_c \end{bmatrix} = \frac{2}{3}\begin{bmatrix} 1 & 0 & 1 \\ -\frac{1}{2} & \frac{\sqrt{3}}{2} & 1 \\ -\frac{1}{2} & -\frac{\sqrt{3}}{2} & 1 \end{bmatrix}.\begin{bmatrix} X_a \\ X_b \\ X_c \end{bmatrix} \tag{A.2}$$

Park direct $dq0/abc$ and inverse $abc/dq0$ transformations:

$$\begin{bmatrix} X_d \\ X_q \\ X_0 \end{bmatrix} = \frac{2}{3}\begin{bmatrix} \sin(\omega t) & \sin(\omega t - \frac{2\pi}{3}) & \sin(\omega t + \frac{2\pi}{3}) \\ \cos(\omega t) & \cos(\omega t - \frac{2\pi}{3}) & \cos(\omega t + \frac{2\pi}{3}) \\ \frac{1}{2} & \frac{1}{2} & \frac{1}{2} \end{bmatrix}.\begin{bmatrix} X_a \\ X_b \\ X_c \end{bmatrix} \tag{A.3}$$

$$\begin{bmatrix} X_a \\ X_b \\ X_c \end{bmatrix} = \frac{2}{3}\begin{bmatrix} \sin(\omega t) & \cos(\omega t) & 1 \\ \sin(\omega t - \frac{2\pi}{3}) & \cos(\omega t - \frac{2\pi}{3}) & 1 \\ \sin(\omega t + \frac{2\pi}{3}) & \cos(\omega t + \frac{2\pi}{3}) & 1 \end{bmatrix}.\begin{bmatrix} X_d \\ X_q \\ X_0 \end{bmatrix} \tag{A.4}$$

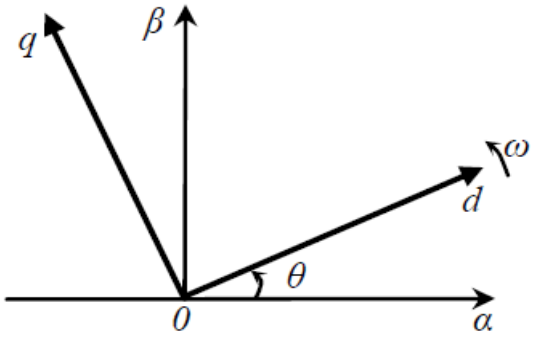

Figure A.1: Relationship between the Park's and Clarke's reference frames

Appendix B: Switching states and voltage vectors

In a three-phase, three-level inverter there are 27 possible switching states, of which 19 produce different voltage vectors; this depicted in Figure B.1. Note that some of the possible switching states are redundant, generating the same voltage vector. For example, the innermost vector, V_0 , can be generated by three switching states, namely: (+, +, +), (0, 0, 0) and (−, −, −); the corresponding load configurations generated are shown in Figure B.2, and by applying these three states in the equation for the space vector definition of the output voltage:

$$V = \frac{2}{3}\left(v_{a0} + a v_{b0} + a^2 v_{c0}\right) \tag{B.1}$$

Each of these switching states for the innermost generates V_0:

$$V_0 = \frac{2}{3}\left(\frac{v_{DC}}{2} + a\frac{v_{DC}}{2} + a^2\frac{v_{DC}}{2}\right) = 0 \tag{B.2}$$

$$V_0 = \frac{2}{3}\left(0 + a0 + a^2 0\right) = 0 \tag{B.3}$$

$$V_0 = \frac{2}{3}\left(-\frac{v_{DC}}{2} - a\frac{v_{DC}}{2} - a^2\frac{v_{DC}}{2}\right) = 0 \tag{B.4}$$

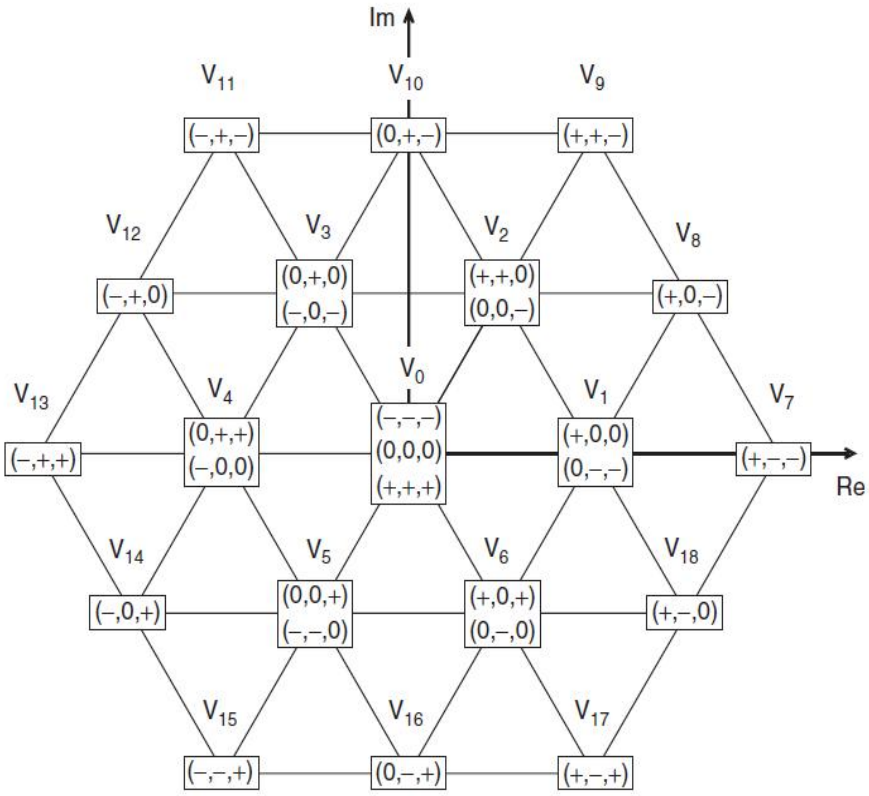

Figure B.1: Possible voltage vectors and switching states generated by a three-level inverter

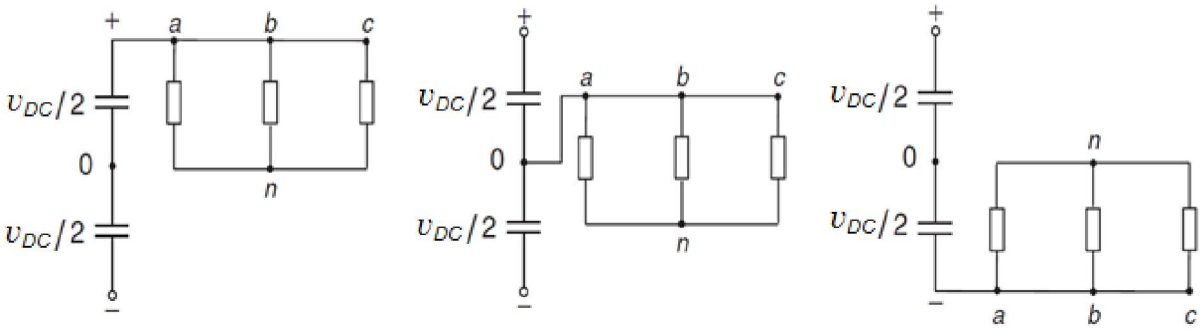

(a) (b) (c)

Figure B.2: Different switching states that generate the zero vector V_0.
(a) (+, +, +) (b) (0, 0, 0) (c) (−, −, −)

All the inner voltage vectors V_1 to V_6 can be generated by two different switching states, which means that if one of two is used, the other one will be redundant. In Figure B.3 the switching states that generate V_1 are shown. Switching state (+, 0, 0) yields:

$$V_1 = \frac{2}{3}\left(\frac{v_{DC}}{2} + a0 + a^2 0\right) = \frac{v_{DC}}{3} \tag{B.5}$$

and switching state (0, −, −) generates the same vector:

$$V_1 = \frac{2}{3}\left(0 - a\frac{v_{DC}}{2} - a^2\frac{v_{DC}}{2}\right) = \frac{v_{DC}}{3} \tag{B.6}$$

From Figure B.1 it can be seen that despite both switching states generating the same voltage vector, they affect the DC-link capacitors differently with regard charging and discharging.

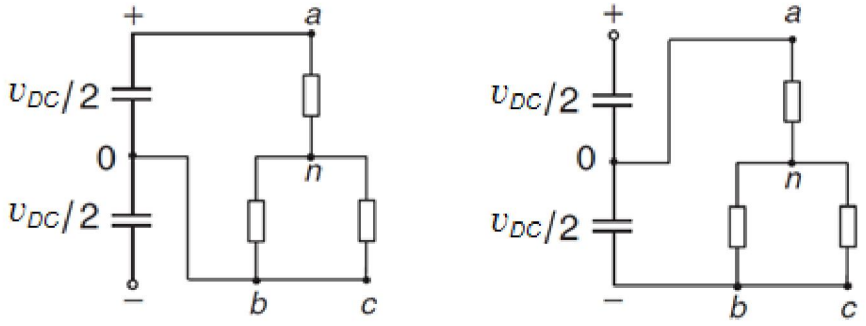

(a) (b)

Figure B.3: Different switching states that generate vector V1. (a) (+, 0, 0), (b) (0, −, −)

Outer vectors present no redundancies. Figure B.4 shows switching state (+, 0, −) that generates vector V_8, calculated as:

$$V_8 = \frac{2}{3}\left(\frac{v_{DC}}{2} + a0 - a^2\frac{v_{DC}}{2}\right) = \frac{v_{DC}}{3}(1 - a^2) = \frac{v_{DC}}{\sqrt{3}}e^{j\pi/6} \quad \text{(B.7)}$$

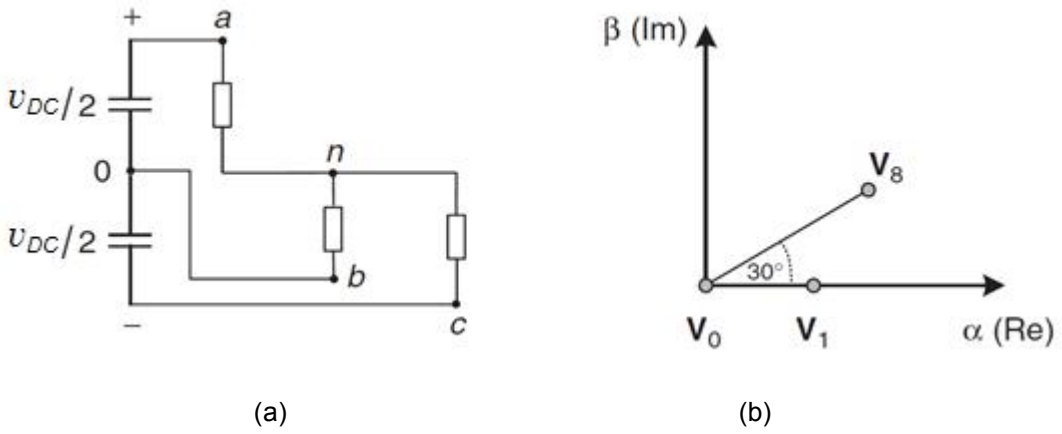

(a) (b)

Figure B.4: Generation of voltage vector V_8. (a) Switching configuration (+, 0, −) (b) Vector V_8 in the complex plane

Appendix C: Total harmonic distortion (THD) factor

Total harmonic distortion is most commonly used factor to characterize the magnitude of the distorted signals. It gives the ratio between the rms of the harmonics and the rms of fundamental component. It is a measure of the quality of the synthesized waveforms that shows to what deviation is the produced waveform from a perfect sinusoidal waveform.

$$\mathrm{THD} = \frac{\sqrt{\sum_{n=2}^{\infty} X_n^2}}{X_1} \qquad \text{(C.1)}$$

Appendix D: Modeling and Co-simulation models

D.1 MATLAB/Simulink environment

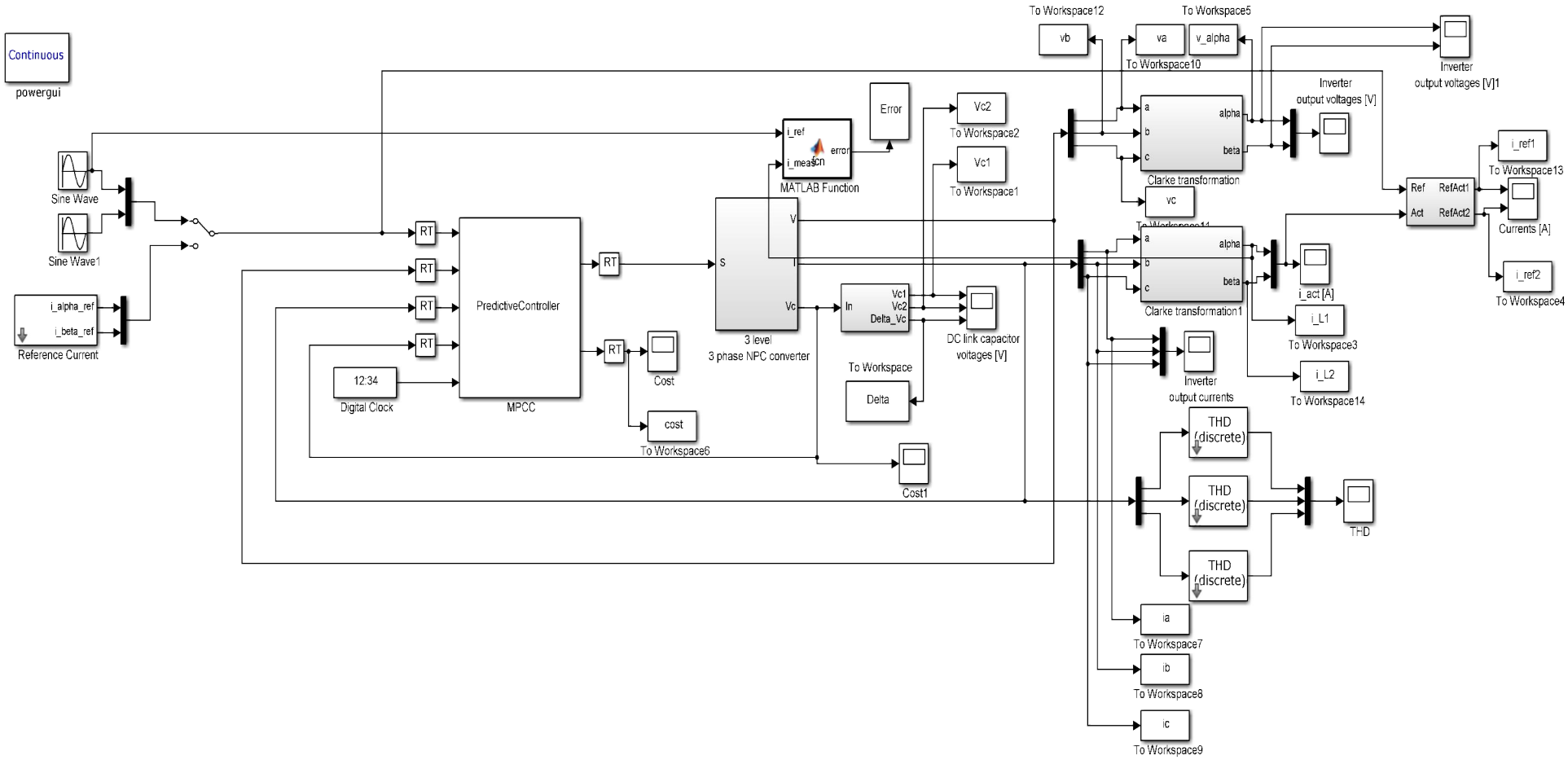

Figure D.1: Predictive current control techniques for DCC inverter

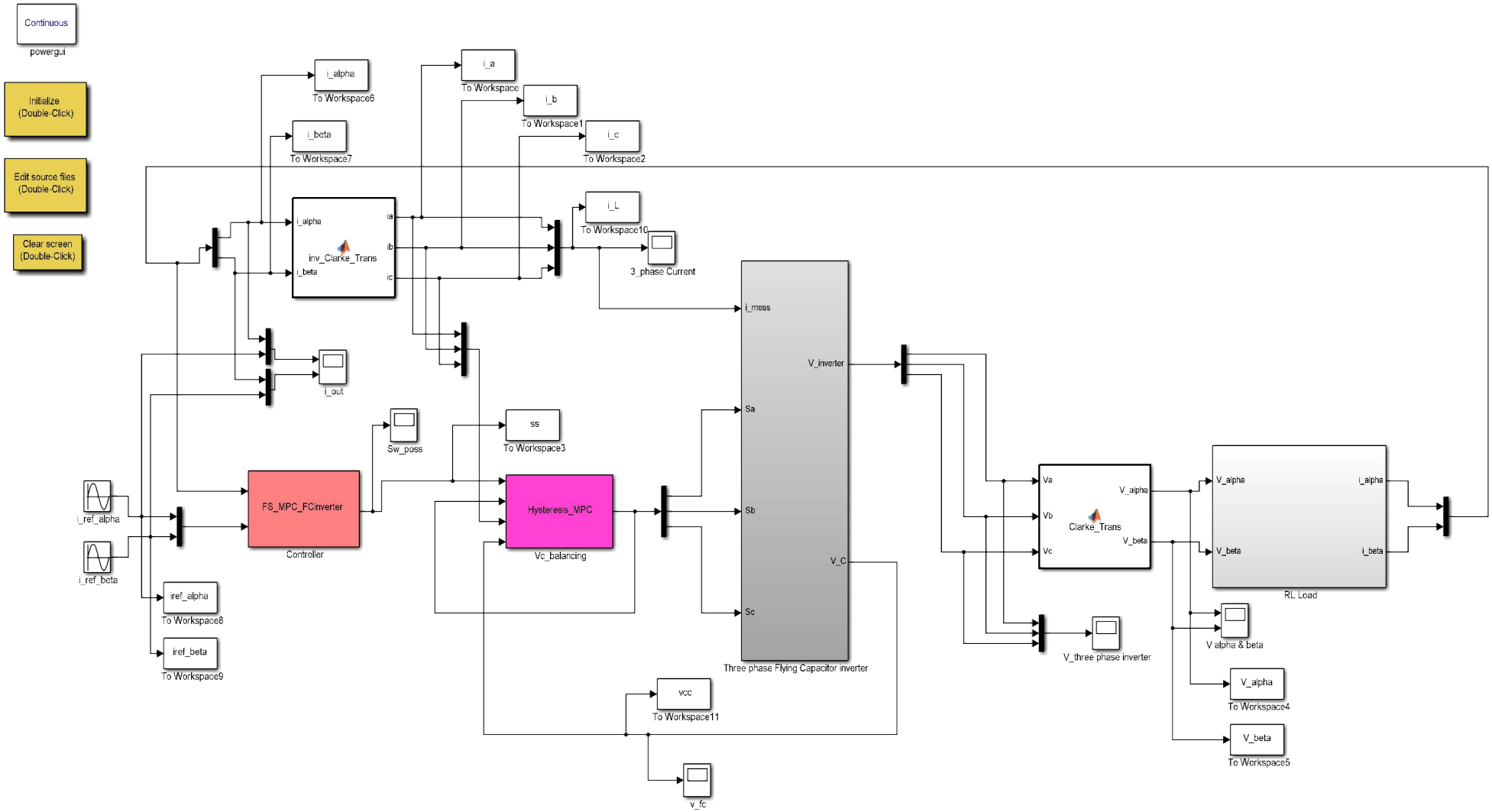

Figure D.2: Predictive current control techniques for FCC inverter using SSI

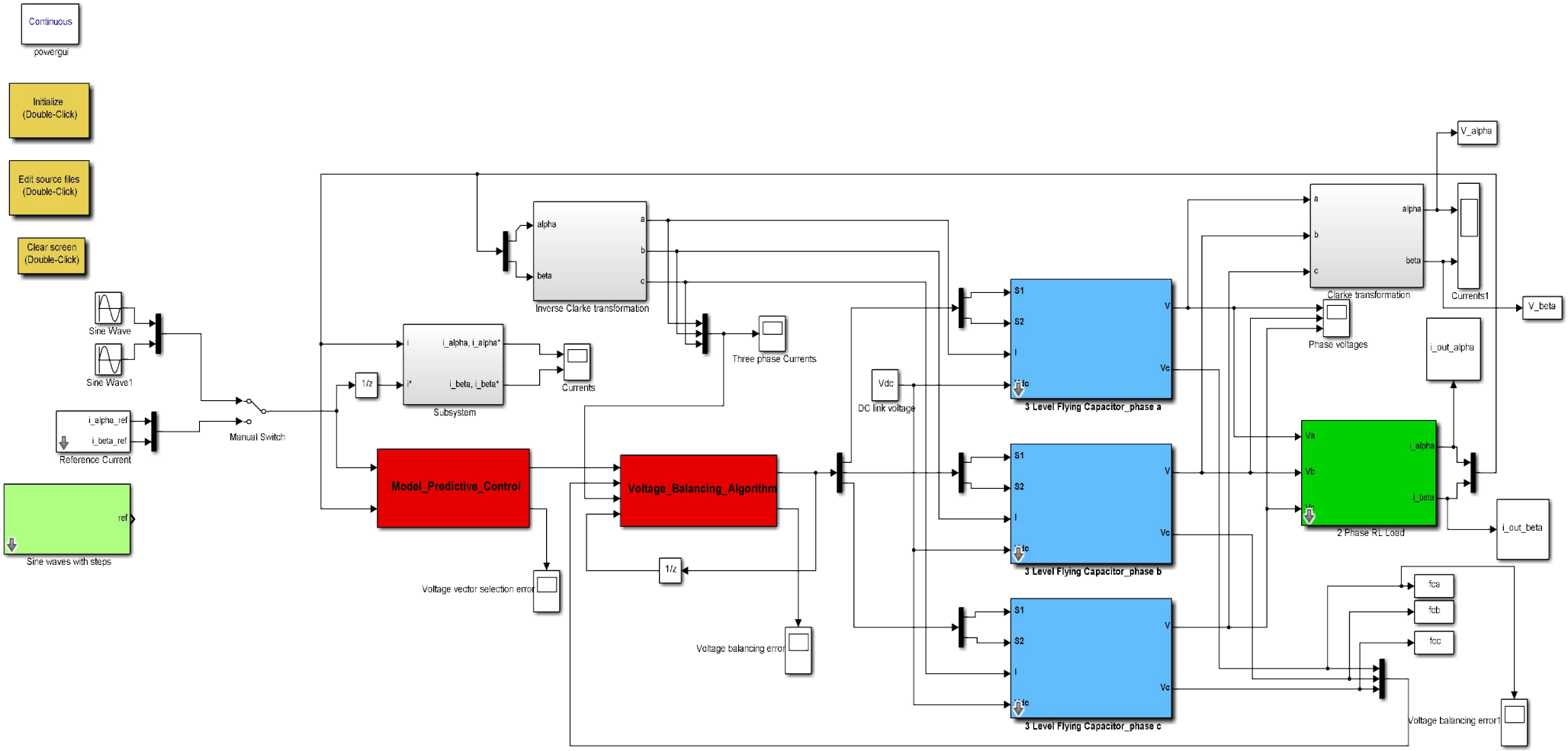

Figure D.3: Predictive current control techniques for FCC inverter using MATLAB

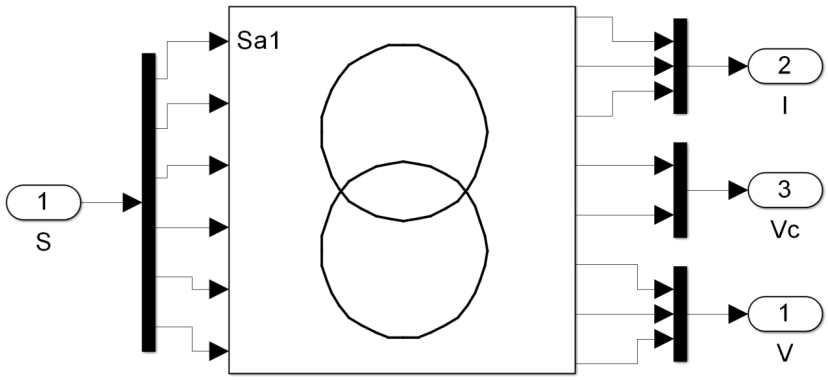

Figure D.4: The SimCoupler Module for co-simulation PSIM with MATLAB/Simulink

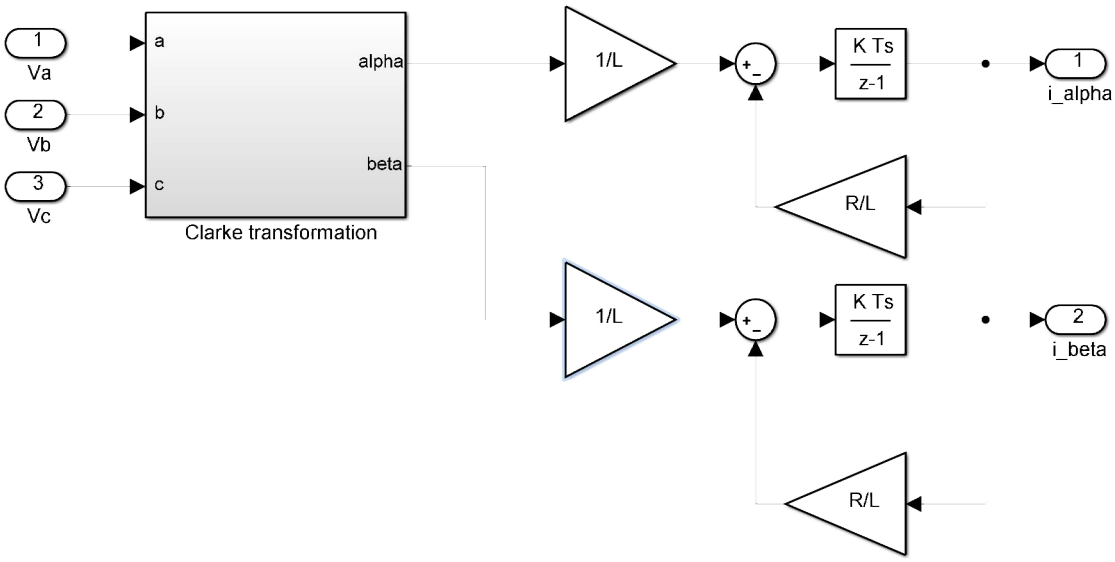

Figure D.5: Simulink model for RL-Load in $\alpha\beta$ coordinates using Clarke transformations

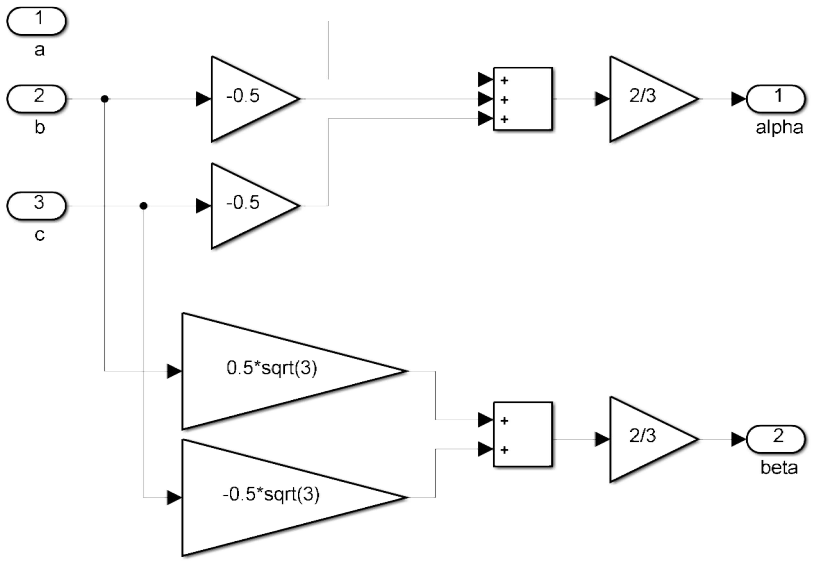

Figure D.6: Transformation from *abc* to *αβ* coordinates

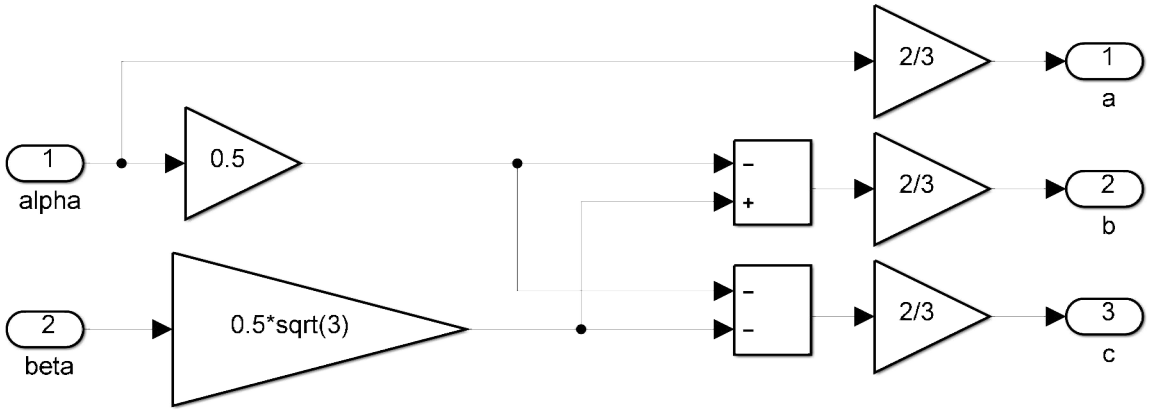

Figure D.7: Transformation from *αβ* to *abc* coordinates

D.2 PSIM Software environment

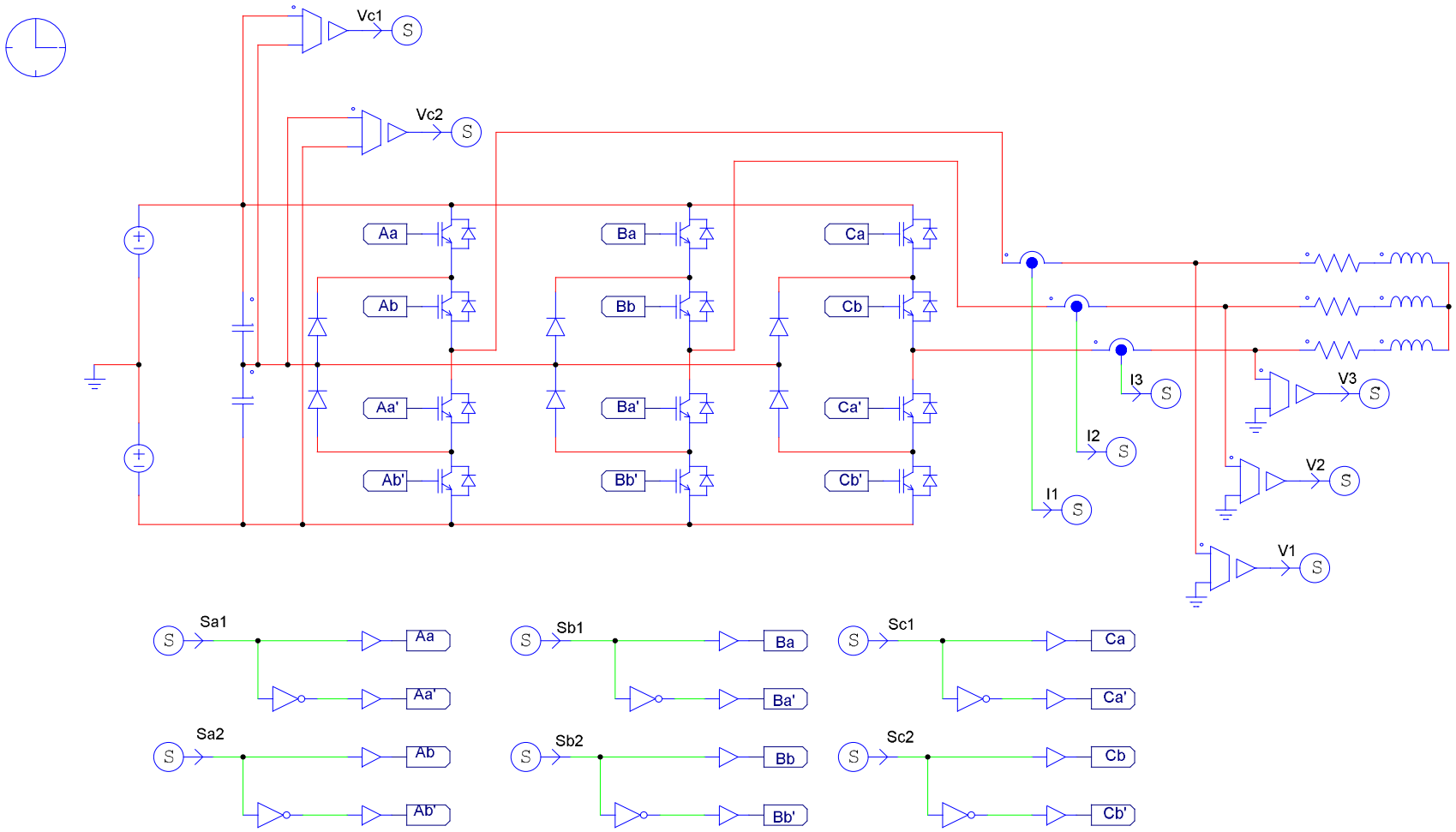

Figure D.8: Three-phase, three-level DCC inverter with RL-load implemented in PSIM

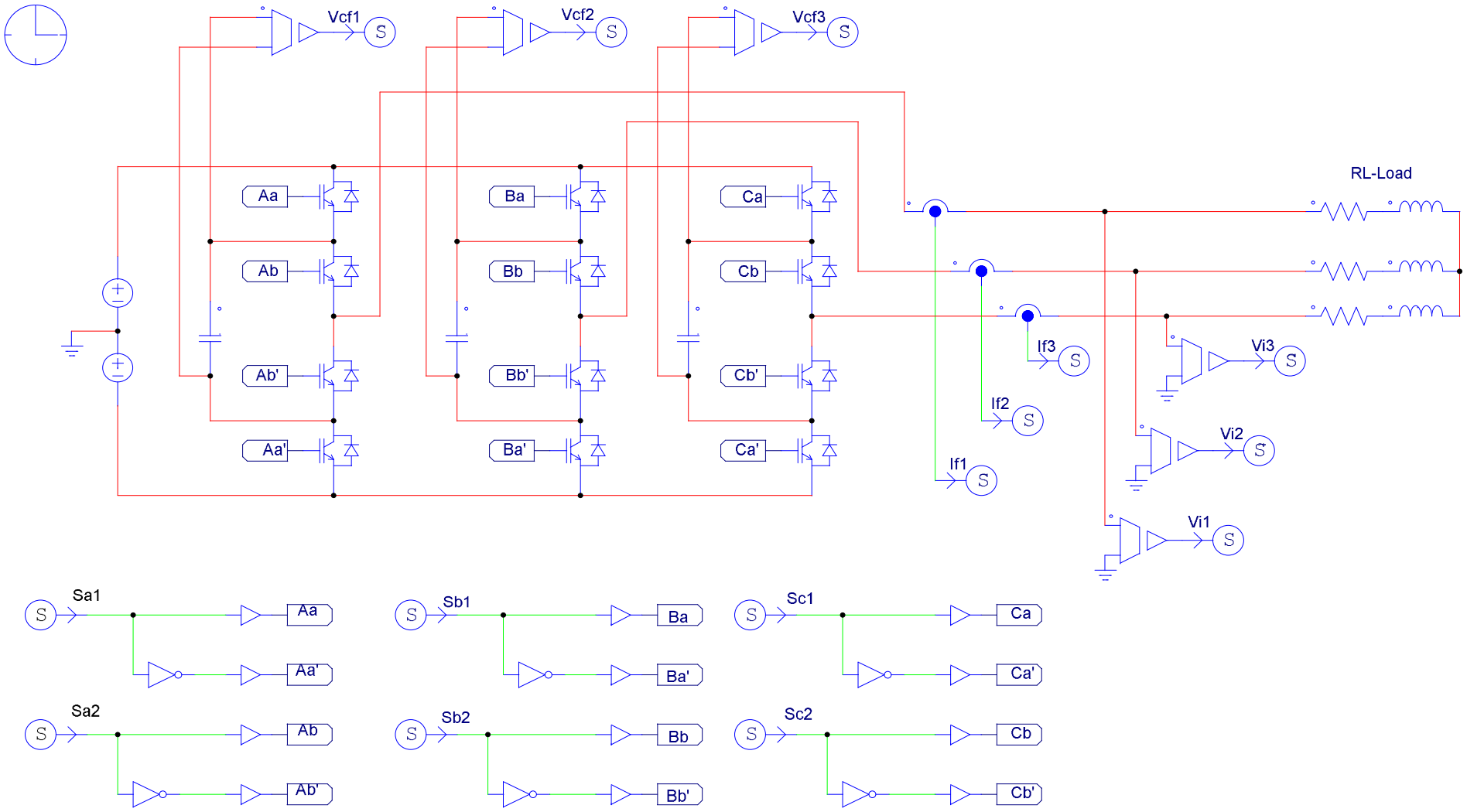

Figure D.9: Three-phase, three-level FCC inverter with RL-load implemented in PSIM

D.3 Three-phase, two-level VSI with long prediction horizon

An FS-MPCC strategy for a three-phase, two-level VSI was simulated with MATLAB/Simulink; this was done to evaluate the performance of the proposed control algorithm, and check the performance and robustness of the proposed predictive control method subject to four prediction horizons. A sinusoidal reference current was applied to the system, the amplitude of the reference current was set to 4 A and the frequency to 50 Hz per phase, and an RL-load was connected to the output of the VSI; this is shown in Figure D.10. In Table D.1 the parameters used for the simulations are shown.

Table D.1: Parameters used for the simulations

Parameter	Value
Load resistor, R	10 Ω
Load inductor, L	10 mH
AC Filter, L	10 mH
DC link voltage, υ_{DC}	100 V
Reference amplitude current, i_{ref}	4 A
Sampling time, T_S	50 μs

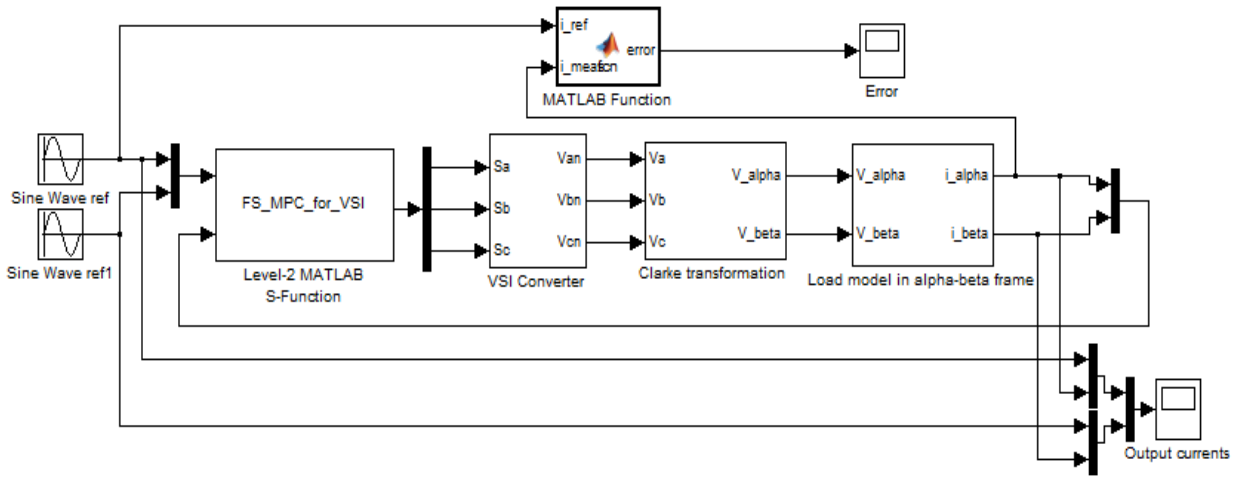

Figure D.10: Modeling an FS-MPC of VSI using MATLAB /Simulink

The robustness of the proposed control method was tested with four prediction steps; it can be seen in Figure D.11 how the output currents track their references with four prediction steps, and it can also be seen that the control algorithm shows excellent tracking behaviour.

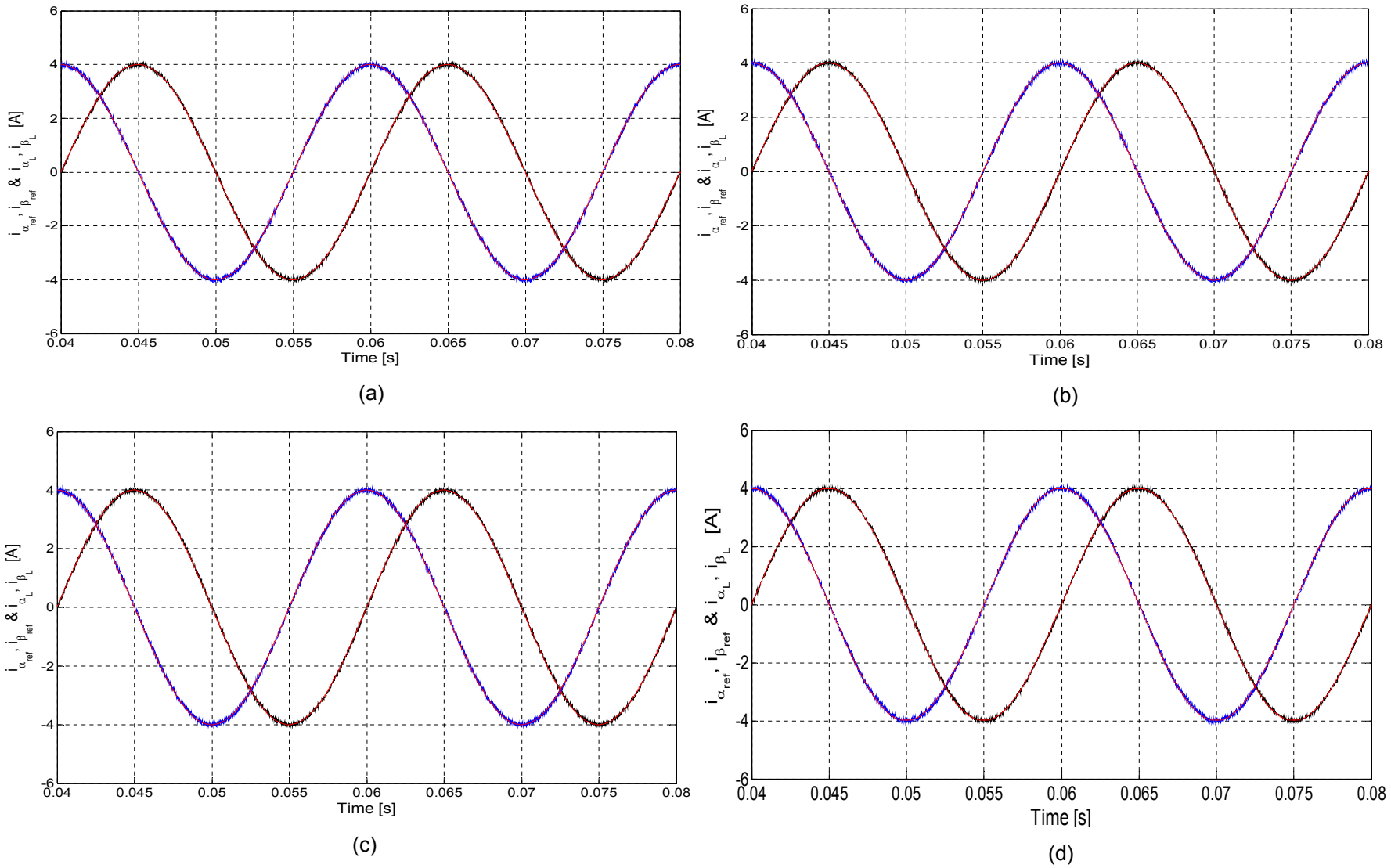

Figure D.11: The load current with RL-load for different values of prediction horizon for a sampling time T_S = 25 µs: a) n = 1 b) n = 2 c) n = 3 d) n = 4